Pertanika Journal of

SCIENCE & TECHNOLOGY

JST

VOL. 24 (2) JUL. 2016

PERTANIKA JOURNALS

A scientific journal published by Universiti Putra Malaysia Press

Journal of Science & Technology

Journal of Science & Technology

Journal of Science & Technology

About the Journal

Overview

Pertanika Journal of Science & Technology (JST) is the official journal of Universiti Putra Malaysia published by UPM Press. It is an open-access online scientific journal which is free of charge. It publishes the scientific outputs. It neither accepts nor commissions third party content.

Recognized internationally as the leading peer-reviewed interdisciplinary journal devoted to the publication of original papers, it serves as a forum for practical approaches to improving quality in issues pertaining to science and engineering and its related fields.

JST is a **biannual** (January and July) periodical that considers for publication original articles as per its scope. The journal publishes in **English** and it is open to authors around the world regardless of the nationality.

The Journal is available world-wide.

Aims and scope

Pertanika Journal of Science and Technology aims to provide a forum for high quality research related to science and engineering research. Areas relevant to the scope of the journal include: bioinformatics, bioscience, biotechnology and bio-molecular sciences, chemistry, computer science, ecology, engineering, engineering design, environmental control and management, mathematics and statistics, medicine and health sciences, nanotechnology, physics, safety and emergency management, and related fields of study.

History

Pertanika was founded in 1978. A decision was made in 1992 to streamline Pertanika into three journals as Journal of Tropical Agricultural Science, Journal of Science & Technology, and Journal of Social Sciences & Humanities to meet the need for specialised journals in areas of study aligned with the interdisciplinary strengths of the university.

After almost 25 years, as an interdisciplinary Journal of Science & Technology, the revamped journal now focuses on research in science and engineering and its related fields.

Goal of *Pertanika*

Our goal is to bring the highest quality research to the widest possible audience.

Quality

We aim for excellence, sustained by a responsible and professional approach to journal publishing. Submissions are guaranteed to receive a decision within 14 weeks. The elapsed time from submission to publication for the articles averages 5-6 months.

Abstracting and indexing of *Pertanika*

Pertanika is almost 40 years old; this accumulated knowledge has resulted in Pertanika JST being abstracted and indexed in SCOPUS (Elsevier), Thomson (ISI) Web of Knowledge [BIOSIS & CAB Abstracts], EBSCO & EBSCOhost, DOAJ, ERA, Cabell's Directories, Google Scholar, MyAIS, ISC & Rubriq (Journal Guide).

Future vision

We are continuously improving access to our journal archives, content, and research services. We have the drive to realise exciting new horizons that will benefit not only the academic community, but society itself.

Citing journal articles

The abbreviation for Pertanika Journal of Science & Technology is *Pertanika J. Sci. Technol.*

Publication policy

Pertanika policy prohibits an author from submitting the same manuscript for concurrent consideration by two or more publications. It prohibits as well publication of any manuscript that has already been published either in whole or substantial part elsewhere. It also does not permit publication of manuscript that has been published in full in Proceedings.

Code of Ethics

The Pertanika Journals and Universiti Putra Malaysia takes seriously the responsibility of all of its journal publications to reflect the highest in publication ethics. Thus all journals and journal editors are expected to abide by the Journal's codes of ethics. Refer to Pertanika's **Code of Ethics** for full details, or visit the Journal's web link at http://www.pertanika.upm.edu.my/code_of_ethics.php

International Standard Serial Number (ISSN)

An ISSN is an 8-digit code used to identify periodicals such as journals of all kinds and on all media–print and electronic. All Pertanika journals have ISSN as well as an e-ISSN.

Journal of Science & Technology: ISSN 0128-7680 (*Print*); ISSN 2231-8526 (*Online*).

Lag time

A decision on acceptance or rejection of a manuscript is reached in 3 to 4 months (average 14 weeks). The elapsed time from submission to publication for the articles averages 5-6 months.

Authorship

Authors are not permitted to add or remove any names from the authorship provided at the time of initial submission without the consent of the Journal's Chief Executive Editor.

Manuscript preparation

Refer to Pertanika's **INSTRUCTIONS TO AUTHORS** at the back of this journal.

Most scientific papers are prepared according to a format called IMRAD. The term represents the first letters of the words **I**ntroduction, **M**aterials and Methods, **R**esults, **A**nd, **D**iscussion. IMRAD is simply a more 'defined' version of the "IBC" [Introduction, Body, Conclusion] format used for all academic writing. IMRAD indicates a pattern or format rather than a complete list of headings or components of research papers; the missing parts of a paper are: *Title, Authors, Keywords, Abstract, Conclusions*, and *References*. Additionally, some papers include Acknowledgments and Appendices.

The *Introduction* explains the scope and objective of the study in the light of current knowledge on the subject; the *Materials and Methods* describes how the study was conducted; the *Results* section reports what was found in the study; and the *Discussion* section explains meaning and significance of the results and provides suggestions for future directions of research. The manuscript must be prepared according to the Journal's **INSTRUCTIONS TO AUTHORS**.

Editorial process

Authors are notified with an acknowledgement containing a *Manuscript ID* on receipt of a manuscript, and upon the editorial decision regarding publication.

Journal of Science & Technology
Journal of Science & Technology

Pertanika follows a **double-blind peer-review** process. Manuscripts deemed suitable for publication are usually sent to reviewers. Authors are encouraged to suggest names of at least three potential reviewers at the time of submission of their manuscript to Pertanika, but the editors will make the final choice. The editors are not, however, bound by these suggestions.

Notification of the editorial decision is usually provided within ten to fourteen weeks from the receipt of manuscript. Publication of solicited manuscripts is not guaranteed. In most cases, manuscripts are accepted conditionally, pending an author's revision of the material.

As articles are double-blind reviewed, material that might identify authorship of the paper should be placed only on page 2 as described in the first-4 page format in Pertanika's **INSTRUCTIONS TO AUTHORS** given at the back of this journal.

The Journal's peer-review

In the peer-review process, three referees independently evaluate the scientific quality of the submitted manuscripts.

Peer reviewers are experts chosen by journal editors to provide written assessment of the **strengths** and **weaknesses** of written research, with the aim of improving the reporting of research and identifying the most appropriate and highest quality material for the journal.

Operating and review process

What happens to a manuscript once it is submitted to *Pertanika*? Typically, there are seven steps to the editorial review process:

1. The Journal's chief executive editor and the editorial board examine the paper to determine whether it is appropriate for the journal and should be reviewed. If not appropriate, the manuscript is rejected outright and the author is informed.

2. The chief executive editor sends the article-identifying information having been removed, to three reviewers. Typically, one of these is from the Journal's editorial board. Others are specialists in the subject matter represented by the article. The chief executive editor asks them to complete the review in three weeks.

   Comments to authors are about the appropriateness and adequacy of the theoretical or conceptual framework, literature review, method, results and discussion, and conclusions. Reviewers often include suggestions for strengthening of the manuscript. Comments to the editor are in the nature of the significance of the work and its potential contribution to the literature.

3. The chief executive editor, in consultation with the editor-in-chief, examines the reviews and decides whether to reject the manuscript, invite the author(s) to revise and resubmit the manuscript, or seek additional reviews. Final acceptance or rejection rests with the Edito-in-Chief, who reserves the right to refuse any material for publication. In rare instances, the manuscript is accepted with almost no revision. Almost without exception, reviewers' comments (to the author) are forwarded to the author. If a revision is indicated, the editor provides guidelines for attending to the reviewers' suggestions and perhaps additional advice about revising the manuscript.

4. The authors decide whether and how to address the reviewers' comments and criticisms and the editor's concerns. The authors return a revised version of the paper to the chief executive editor along with specific information describing how they have answered' the concerns of the reviewers and the editor, usually in a tabular form. The author(s) may also submit a rebuttal if there is a need especially when the author disagrees with certain comments provided by reviewer(s).

5. The chief executive editor sends the revised paper out for re-review. Typically, at least one of the original reviewers will be asked to examine the article.

6. When the reviewers have completed their work, the chief executive editor in consultation with the editorial board and the editor-in-chief examine their comments and decide whether the paper is ready to be published, needs another round of revisions, or should be rejected.

7. If the decision is to accept, an acceptance letter is sent to all the author(s), the paper is sent to the Press. The article should appear in print in approximately three months.

   The Publisher ensures that the paper adheres to the correct style (in-text citations, the reference list, and tables are typical areas of concern, clarity, and grammar). The authors are asked to respond to any minor queries by the Publisher. Following these corrections, page proofs are mailed to the corresponding authors for their final approval. At this point, **only essential changes are accepted**. Finally, the article appears in the pages of the Journal and is posted on-line.

JST
Journal of Science & Technology
AN INTERNATIONAL PEER-REVIEWED JOURNAL

EDITORIAL OFFICE
JOURNAL DIVISION
Office of the Deputy Vice Chancellor (R&I)
1st Floor, IDEA Tower II
UPM-MTDC Technology Centre
Universiti Putra Malaysia
43400 Serdang, Selangor Malaysia.
Gen Enq.: +603 8947 1622 | 1619 | 1616
E-mail: executive_editor.pertanika@upm.my
URL: www.journals-jd.upm.edu.my

PUBLISHER
Kamariah Mohd Saidin
UPM Press
Universiti Putra Malaysia
43400 UPM, Serdang, Selangor, Malaysia.
Tel: +603 8946 8855, 8946 8854
Fax: +603 8941 6172
E-mail: penerbit@putra.upm.edu.my
URL: http://penerbit.upm.edu.my

ABSTRACTING/INDEXING

Pertanika is now over 35 years old; this accumulated knowledge has resulted the journals being indexed in SCOPUS (Elsevier), Thomson (ISI) Web of Knowledge [BIOSIS & CAB Abstracts], EBSCO, DOAJ, Google Scholar, AGRICOLA, ISC, Citefactor, Rubriq and MyAIS. JST is also indexed in ERA.

Pertanika Journal of Science & Technology
Vol. 24 (2) Jul. 2016

Contents

Case Studies

Selected Papers from the International Conference on Computational Methods in Engineering and Health Sciences 2015 (ICCMEH 2015)

Selected Papers from the International Conference on Innovations, Shifts and Challenges (ICISC 2015)

Foreword

Welcome to the **Second Issue 2016** of the Journal of Science and Technology (JST)!

JST is an open-access journal for studies in science and technology published by Universiti Putra Malaysia Press. It is independently owned and managed by the university and is run on a non-profit basis for the benefit of the world-wide science community.

In this issue, **24 articles** are published; **two** are review articles, **nine** are regular articles and **two** are case studies. This issue also features **seven** selected papers from the International Conference on Computational Methods in Engineering and Health Sciences 2015 (ICCMEH 2015) and **four** selected papers from the International Conference on Innovations, Shifts and Challenges (ICISC 2015). The authors of these articles vary in country of origin, coming from **Malaysia**, **India**, **Thailand**, **Australia**, **Algeria**, **Palestine**, **Taiwan** and **Indonesia**.

The first review article in this issue discusses the flow modification around a circular cylinder applying splitter plates, where it was found that the length ratio was a more important factor compared with the gap ratio in the case of vortex suppression (*Babak Mahjoub, Kamarul Arifin Ahmad* and *Surjatin Wiriadidjaja*). The second review article is a comprehensive and comparative study on online testability for reversible logic (*Hari Mohan Gaur, Ashutosh Kumar Singh* and *Umesh Ghanekar*).

The first regular article in this issue is on the seismic response of a light rail transit station equipped with braced viscous damper (*Fateh, A., Hejazi, F., Ramanathan, R. A.* and *Jaffar, M. S.*). The following articles look at: the path analysis of mental health among Thai elderly with Diabetes Mellitus (*Chonticha Kaewanuchit*); data clustering using differential search algorithm (*Vijay Kumar, Jitender Kumar Chhabra* and *Dinesh Kumar*); the effect of silica fillers on viscosity, peel strength, shear strength and tack of a styrene-butadiene rubber-based adhesive (*Poh, B. T.* and *Loh, W. S.*); an artificial neural network for modelling rainfall runoff (*Aida Tayebiyan, Thamer Ahmad Mohammad, Abdul Halim Ghazali* and *Syamsiah Mashohor*); modified levels of parallel Odd-Even Transposition Sorting Network (OETSN) with GPU computing using CUDA (*Neetu Faujdar* and *SP Ghrera*); identification, characterisation and phylogenetic analysis of commensal bacteria isolated from human breast milk in Malaysia (*Zubaida Hassan, Shuhaimi Mustafa, Raha Abdul Rahim* and *Nurulfiza Mat Isa*); coverage and lifetime optimisation of WSN using evolutionary algorithms and collision-free nearest neighbour assertion (*Vinodh P. Vijayan* and *N. Kumar*); and data gathering protocol for reducing energy utilisation in a qireless sensor network (*Biju Paul* and *N. Kumar*).

The two case studies featured in this issue highlight the 18F-FDG-PET CT features of colo-colic intussusceptions in patient with colonic carcinoma (*Fathinul Fikri, A. S., Noraini Sarina, A., Shahrin, S.* and *Abdul Jalil, N.*) and the pattern of calcification on CT and FDG-

PET of a rare perineural mantle cell lymphoma, with a potential as a non-histological imaging marker (*Fathinul Fikri, A. S., Ramdave Shakher* and *Abdul Jalil, N.*)

I conclude this issue with 11 articles arising from the ICCMEH 2015 and ICISC 2015 international conferences: a combined meshless RBF-FDTD method for the analysis of transient electromagnetic fields (*Khalef, R., Benkhawa, L., Grine, F., Benhabiles, M. T.* and *Riabi, M. L.*); high capacity video steganography technique in a transform domain (*Hemalatha, S., U. Dinesh Acharya* and *Renuka, A.*); the heat transfer performance of gold/water nanofluid flows in a minitube using the thermal lattice boltzmann method (*Ahmed A. Hussien, Mohd Z. Abdullah, Mohd A. Al-Nimr, N. M. Yusop, C. Nuntadusit* and *M. H. Elnaggar*); flapping membrane wing as a prediction towards inter-domain flight (*Abas, M. F., Aftab, S. M. A., Rafie, A. S. M., Yusoff, H.* and *Ahmad, K. A.*); CFD investigation of transonic axial compressor rotor blades in various off-design conditions (*Pauline Epsipha, Mohammad, Z.* and *Kamarul, A. A.*); on the extension of moving particle method for flow computation in irregular flow domain (*Ng, K. C., Sheu, T. W. H.* and *Hwang, Y. H.*); split-disk properties of kenaf yarn fibre-reinforced unsaturated polyester composites using the filament winding method (*Misri, S., Ishak, M. R., Sapuan, S. M.* and *Leman, Z.*); using Tracker to engage students' learning and research in physics (*Eddy Yusuf*); automatic tag generation in folksonomy for learning resources reuse and sharing (*Ching Chieh Kiu*); a case study on utilising a mobile application to teach Malaysian governance to international students (*Azizan Yatim*); and an investigation into the impact of E-learning implementation on change management in Malaysian private higher education institutions (*Sheiladevi, S.* and *Rahman, A.*).

I anticipate that you will find the evidence presented in this issue to be intriguing, thought-provoking, and, hopefully, useful in setting up new milestones. Please recommend the journal to your colleagues and students to make this endeavour meaningful.

I would also like to express my gratitude to all the contributors, namely, the authors, reviewers and editors for their professional contribution towards making this issue feasible. Last but not least, the editorial assistance of the journal division staff is fully appreciated.

JST is currently accepting manuscripts for upcoming issues based on original qualitative or quantitative research that opens new areas of inquiry and investigation.

Chief Executive Editor
Nayan Deep S. KANWAL, FRSA, ABIM, AMIS, Ph.D.
nayan@upm.my

Pertanika J. Sci. & Technol. 24 (2): 231 - 244 (2016)

SCIENCE & TECHNOLOGY

Journal homepage: http://www.pertanika.upm.edu.my/

Review Article

Flow Modification around a Circular Cylinder Applying Splitter Plates

Babak Mahjoub, Kamarul Arifin Ahmad* and Surjatin Wiriadidjaja

Department of Aerospace, Engineering Faculty, Universiti Putra Malaysia, 43400 UPM Serdang, Selangor, Malaysia

ABSTRACT

A number of different studies were reviewed to investigate the functionality of splitter plates for the purpose of drag reduction and vortex elimination behind a circular cylinder. The studies were carried out numerically or experimentally in different combinations of Reynolds range, 2D or 3D dimensions, with intention of drag reduction, vortex suppression or both. Results were compared to discover the generalities of a splitter plate's applications and its performance in drag reduction and vortex control. The reduction of 12% up to 38.6% in drag coefficient suggests that all reviewed studies verified the effectiveness of upstream plate in drag reduction. Varied upstream plate's gap ratios (gap between the plate and cylinder) were tested and the optimum position was obtained. For the finite cylinder case, however, the studies discovered that the effectiveness of upstream plate decreased severely and thus, are barely considered as a drag reductive tool for shorter cylinders. Although downstream plate influences drag force, its prominent application is found to be vortex shedding elimination (up to 14.7%). The length ratio and gap ratio of downstream plate were varied in these studies and it was found that the length ratio was a more important factor compared with the gap ratio in the case of vortex suppression.

Keywords: Circular cylinder, Drag reduction, Flow control, Vortex shedding, Vortex suppression, pressure coefficient, Strouhal number, Aspect ratio

INTRODUCTION

BLUFF bodies which are immersed in a flow field endure high drag forces due to their non-streamlined shapes. These drag forces cause many undesirable consequences such as energy loss. As flow passes a bluff body, depending on the Reynolds number and

Article history:
Received: 17 February 2016
Accepted: 22 April 2016

E-mail addresses:
Babak.mahjoub@gmail.com (Babak Mahjoub),
aekamarul@upm.edu.my (Kamarul Arifin Ahmad),
surjatin@upm.edu.my (Surjatin Wiriadidjaja)
*Corresponding Author

ISSN: 0128-7680

corresponding flow regime, various regions, such as separated flow, wake and periodic vortex shedding regions form behind the body. Each of these formations can be considered as either a desirable phenomenon (turbulence vortex shedding in heat transfer applications) or an unwanted occurrence. The aim of preventing those undesirable excitations has made the topic of flow control more significant among scientists in the past three decades. The purpose of reducing drag forces, delaying separation and suppressing vortex shedding in order to overcome erosion problem and reducing undesirable vibrations have motivated researchers to conduct various methods to achieve these goals in the field of flow control.

Flow over circular cylinders recently has become a matter of consideration due to its applications in industries. Bridge pillars and industrial stacks are examples which demand flow enhancement in order to increase their lifespan. There have been several methods to control the flow over these bodies; however, they are all categorised as active and passive flow control. As the presence of external energy is demanded in an active flow control, this type of flow control requires a more complex structure compared with passive control. Electric motors, pumps and speakers are some devices used in an active flow control to generate blow, suction and sound wave exertion. Endeavours of researchers in flow modification applying acoustic perturbation (Okamoto et al., 1981), cylinder oscillation (Suryanarayana et al, 1993;) Nakano & Rockwell, 1991), heating cylinder (Wang et al., 2000), applying electromagnetic forces (Kim & Lee, 2001), and blowing and suction (Bearman, 1965) are some of the examples within the scope of active flow control. Alternatively, applying changes to the body shape, attaching extra elements, changing the surface roughness, creating grooves or bumps on the surface are cheaper and easier ways to control and enhance the flow which are all considered as passive control method. Some typical examples of studies on passive control are controlling the separation of shear layers, effect of surface roughness (Buresti, 1981), applying different arrangements between two cylinders (Zdravkovich, 1977), controlling induced vibration among tandem cylinders (Assi et al., 2010), using small control cylinders (Kuo et al., 2007), (Bouak & Lemay, 1998), and utilising splitter plates downstream and upstream of a cylinder (Cimbala & Leon, 1996; Kwon & Choi, 1996; Anderson & Szewczyk, 1997; Hwang & Yang, 2007; Shukla et al., 2009).

Ensuring various effective influences on flow control over cylinders and application of splitter plates have recently become a focus among researchers. They have been used in the form of attached (Cimbala & Leon, 1996; Shukla et al., 2009) and detached (Hwang & Yang, 2007; Igbalajobi et al., 2013) upstream and downstream of the circular cylinder for the purpose of drag reduction, separation delay, vortex suppression and fluctuating lift assuagement. Apelt and West (1973) studied the effect of adding splitter plate by investigating pressure distribution (Apelt et al., 1973). Their research demonstrated the high level of dependency of drag force, base pressure and wake area to the presence of splitter plate. Zdravkovich researched on various aerodynamically control methods and mentioned splitter plate as a device to stabilise the wake (Zdravkovich, 1981). Kwon & Choi studied vortex shedding behind a circular cylinder numerically and discovered how the attached splitter plate affects it. In their research, it was shown that the Strouhal number is dependent on the length of plate. The presence of splitter plate is effective as long as it is completely positioned on the cylinder stream line, so it must be aligned with the mean flow direction (Kwon & Choi, 1996). This fact convinced some

researchers to apply hinged plates to the cylinder as demonstrated by Cimbala & Leon (year of publication) who conducted their experiments using attached hinged plates, so plates were able to rotate in some pre-defined angles (Cimbala & Leon, 1996). Anderson & Szewczyk (year of publication) carried out an experiment for a variety of splitter plate lengths and found out that there was a reverse relation between base pressure and formation length. In their experiments, different plates with different length ratio (L/D =0-1.5) were tested (Anderson & Szewczyk, 1997). Ozono's study illustrated that in certain range of spacing between the cylinder and plate, the Strouhal number exceeds the natural vortex shedding frequency of the cylinder (Ozono, 1999). Shukla et al. (year of publication) also used hinged splitter plate behind the cylinder; likewise, the effect of plate on the vortex shedding suppression was observed (Shukla et al., 2009). Alam et al. (year of publication) applied tripping rods to reduce fluctuation fluid forces in two side-by-side and tandem cylinders (Alam, Sakamoto, & Moriya, 2003). Akilli et al. showed in their experiments that the plate thickness has no effect on the flow characteristic. They experimentally tested the effect of detached plate on the vortex shedding suppression in the shallow water using PIV techniques (Akilli, Sahin, & Filiz Tumen, 2005). In order to achieve more drag reduction using splitter plates, Hwang & Yang (year of publication) placed dual detached splitter plates, one upstream and the other downstream, on (or behind?) the cylinder. In their experiment, the position of the splitter plates were a matter of consideration (Hwang & Yang, 2007). Recently, many studies have been conducted considering the cylinder as a finite object with regards to its aspect ratio- the ratio of its height to its diameter (Uematsu & Yamada, 1995; Sumner, Heseltine, & Dansereau, 2004; Cimbala & Çengel, 2008; Igbalajobi et al., 2013; H. F. Wang, Zhou, & Mi, 2012). The current review attempts to compile the results of those studies on the application of upstream, downstream and dual plate, and make a comparison between the results of finite and infinite (2D and 3D) analysis. Table 1 summarises the specifications of these studies which will be compared and discussed in this review article.

Table 1
List of selected studies and their test details

Study	Test Method	Re Range	Dim.	Plates used
Apelt & West 1973	Experimental	$1X10^4 – 5X10^4$	2D	Downstream
Apelt et al. 1975	Experimental	$1X10^4 – 5X10^4$	2D	Downstream
Hwang et al. 2003	Numerical	30 – 100 – 160	2D	Upstream + Downstream
Hwang & Yang 2007	Numerical	30 – 100 – 160	2D	Upstream + Downstream
Igbalajobi et al. 2013	Experimental	$7.4 X 10^4$	3D	Downstream

DRAG REDUCTION

Pressure distribution around a circular cylinder is the reason for drag formation on the cylinder. The non-streamlined shape of the cylinder causes significant differences between the stagnation pressure (P_s) and the base pressure (P_b). The higher pressure on the stagnation point results in generating a drag force on the opposite direction of the body movement (in case the body is moving) or on the direction of the fluid flow (in case the fluid is moving over the body). Pressure drag is the most dominant type of drag on the cylindrical shaped bodies in the laminar

flow, thus modifying the flow in a way that diminishes the pressure difference between those two points resulting in drag reduction. Figure 1 demonstrates the distribution of pressure coefficient along the circumferential direction of an isolated circular cylinder (Apelt & West, 1975; Hwang et al., 2003). Pressure coefficient for cylinder stagnation point is shown at θ=0o while the cylinder stagnation point is shown at θ=180^o.

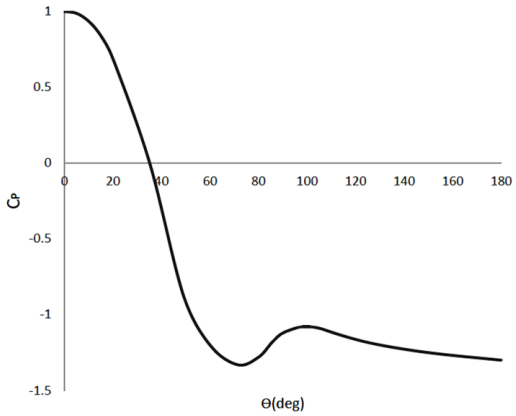

Figure 1. Distribution of pressure coefficient along the circumferential direction of the circular cylinder (Apelt & West, 1975).

In a referred study, a wake splitter plate was placed along the centreline of the cylinder to augment the pressure coefficient on the cylinder base (C_{pb}). Based on the cylinder diameter (D), length ratio of splitter plates was defined as (L/D) varying from 2 to 7. It was found that the pressure drag coefficient was independent of Reynolds number as C_p values were identical for all the velocities corresponding to 10^4<Re<$5x10^4$. Figure 2 illustrates how drag coefficient (C_D) varies as C_{pb} changes in different plate's L/D. C_D follows a descending order until it reaches L/D=1.5, then the trend changes direction in L/D=2 where a relative maximum is observed in C_D diagram. For length ratio longer than 5, no significant changes in C_D have been noted. The length ratio of wake splitter plates is a dominant factor in vortex shedding elimination which will be discussed later. Therefore, a more serious consideration has been given to L/D>2. A study on the effect of splitter plates L/D≤2 was conducted by Apelt et al. (year of publication) and it was ascertained that the presence of splitter plate increases the base pressure and subsequently reduces pressure drag. It was also observed that even shorter splitter plates made remarkable changes in C_{pb} and C_D (Apelt et al., 1973). Increasing L/D however, proved to have improved modification in vortex suppression resulting in the author continuing investigation on splitter plates as long as L/D≥2. The maximum drag reduction obtained was 33% based on Apelt's study (year of publication) which was acquired by implementing splitter plates longer than 5D. Applying splitter plates with L/D≥5 has no significant changes in drag reduction (Apelt & West, 1975). Based on visualisation studies downstream of the cylinder, for very large splitter plates, the flow reattaches on the plate at the L/D=5 regardless of the length of the plates.

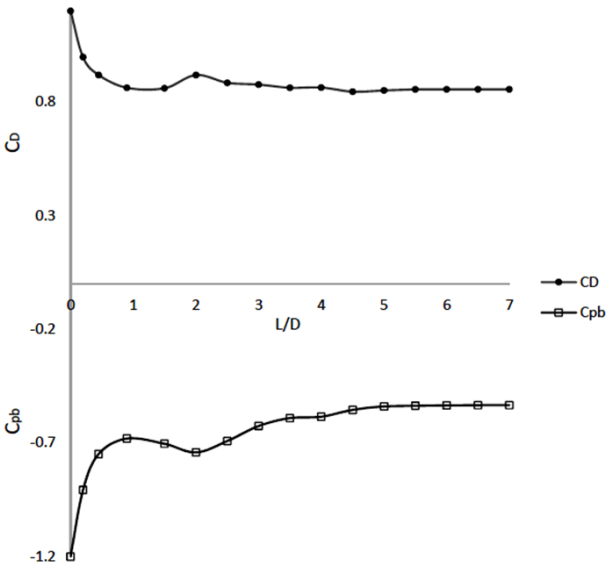

Figure 2. Variation of C_{pb} and C_D with downstream plate's length ratio. L/D≤2 (Apelt et al., 1973), 2≤L/D≤7 (Apelt & West, 1975).

Hwang (year of publication) had studied the use of splitter plates as C_P modifier) in order to reduce drag on the circular cylinder. The study was conducted numerically at laminar flow with Re=30,100 and 160 and the upstream plate was settled in front of the cylinder centreline without relative angle (Hwang & Yang, 2007). The mechanism of drag reduction differs from what was used in Apelt's (year of publication) study as pressure coefficient at cylinder stagnation point (C_{Ps}) was the varying parameter. By decreasing C_{ps} the difference between C_{ps} and C_{pb} is reduced which in turn diminished the drag force. The two controlling parameters were the plate's length ratio to the cylinder diameter (L_1/D) and the gap between the plate's trailing edge and cylinder stagnation point measured relatively to the cylinder diameter (G_1/D).

As seen in Figure 3, there is a minimum value for C_D and the upstream plate's position varies along the cylinder centreline. Hwang's justification vindicates this phenomenon using pressure distribution in fluid along the cylinder centreline shown in Figure 4. The dashed-dotted line represents the distribution of C_P without a splitter plate while the solid line denotes the case with upstream plate. The solid line is not continuous and is intercepted in a position of x which corresponds to place in which the plate is implemented. That's where the line becomes dashed-double dot and represents the C_p on the plate's surface. The mechanism of drag reduction using upstream splitter plate differs from what a downstream splitter plate does. They even act independently in the case of applying dual splitter plates (one upstream and one downstream). Upstream plates cause a sudden reduction in the flow's momentum energy while the flow reaches the plate's leading edge. At that point, pressure escalates drastically due to the conservation of energy. By moving along the plate, the flow's energy is converted to momentum energy gradually, thus a sudden fall is observed for the pressure until the flow attains the trailing edge of the plate. The flow continues its path recovering the kinetic energy till

it gets to the cylinder stagnation point. Once more, energy conversion happens and momentum turns into pressure due to the blockage of the cylinder. Compared with an isolated cylinder, this pressure at stagnation has a lower value, and this fact is legitimatised by considering energy loss via friction and blockage during the flow passage over the plate.

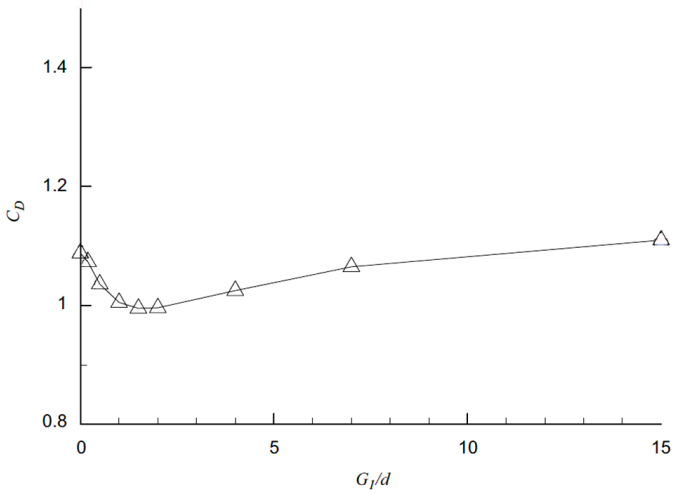

Figure 3. Drag coefficient in different upstream plate's gap ratios. Re=160 (Hwang & Yang, 2007).

The minimum drag coefficient is obtained by locating the plate in a proper position which causes the flow to have its minimum possible pressure magnitude at the vicinity of the cylinder. The variation of C_p along cylinder centreline is demonstrated for three different gap ratios of 0.5, 1.5 and 4 in Fig. 4 a, b, and c respectively. It is noticed that by moving the plate further to the cylinder, a lower pressure flow comes out of the trailing edge of the plate, which is promising to obtaining lower C_D on the plate. Additionally, the wider the distance of the plate from the cylinder, the more time it takes for the flow to recover its energy and consequently the higher value it has in the vicinity of the cylinder. Therefore, there is an optimum position where the value of C_P is minimum at the stagnation point of the cylinder which is at G_1=1.5D.

To enhance the flow characteristics around the cylinder, Hwang (year of publication) also applied an additional downstream splitter plate while the upstream plate was fixed in its proper position. Although employing a splitter plate behind the cylinder follows the primary objective of vortex shedding elimination, it has a positive effect on the reduction of drag force over the cylinder. The length ratio was defined as G_2/D and L_2/D corresponds to the distance between cylinder stagnation point and the downstream plate's leading edge. Figure 5 represents the variation of C_D for two cases - G_2/D varies when only downstream plate is implemented (Δ) and when dual plates are applied (□). The value for drag coefficient reaches its minimum at G_2/D=2.5 regardless of the presence of upstream plate. The figure also indicates the same pattern of C_D response to the variation of G_2/D in both cases. This similarity indicates that the mechanism of drag reduction for downstream splitter plate is completely independent of the upstream plate's performance.

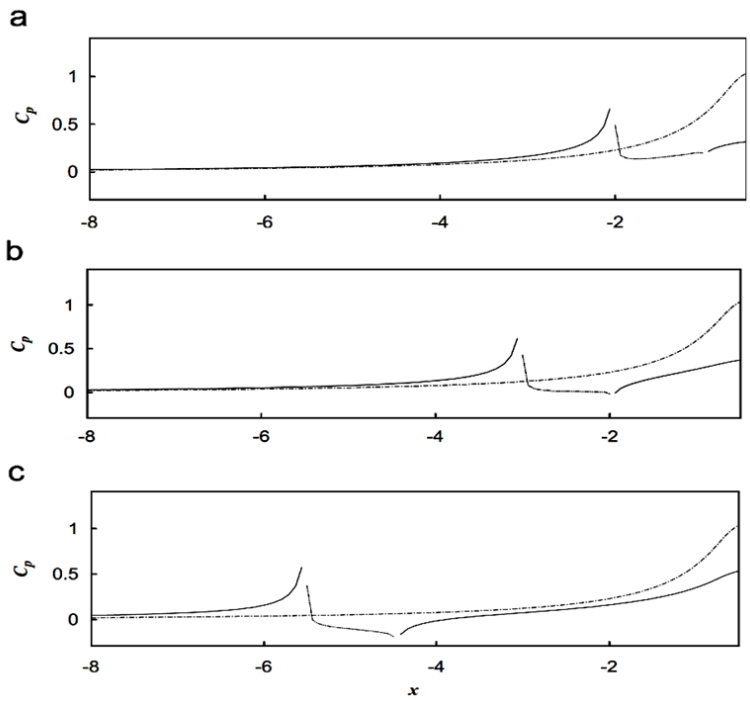

Figure 4. Variation of C_p along the upstream centreline for three different upstream gap ratios. (a) $G_1/D = 0.5$, (b) $G_1/D = 1.5$, (c) $G_1/D = 4$ (Hwang & Yang, 2007).

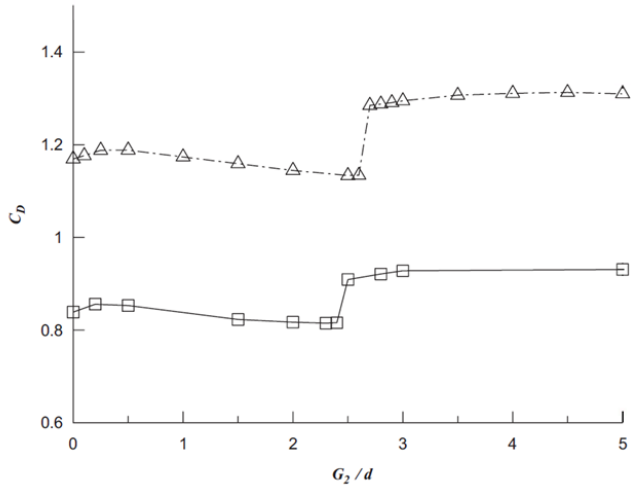

Figure 5. C_D distribution for different downstream gap ratios, $G_1/D = 1.5$. (Δ) Downstream plate (Hwang et al. 2003), (□) Dual plate (Hwang & Yang, 2007)

The effect of downstream plate in its optimum position ($G_2/D = 2.4$) was reported at 14.7% in Hwang et al.'s study (2003). The reason for this effect is that when a downstream plate is settled, C_{pb} increases and lessens the difference between C_{pb} and C_{ps} as shown in Figure 6.

The time-averaged distribution of pressure along the circumferential direction of the cylinder coefficient for other cases is plotted in Figure 6. The reason for C_{pb} augmentation due to the implementation of upstream plate solely (even a very small effect) is that it affects vortex shedding indirectly by generating free shear layers. The maximum drag reduction happened when both plates were applied and caused C_{ps} to decrease (upstream) and C_{pb} to increase (upstream and downstream), and since its maximum obtained value was 38.6%, it was found out that the upstream plate plays a more important role for this purpose (compared with a value of 14.7% which was caused by using the downstream plate only). Apelt and West (1975) had reported a 33% of drag reduction by only applying a plate behind the cylinder/ They discovered that unlike for the upstream plate, the determinant factor for downstream plate is the length ratio of the plate. As discussed later, longer plates are more applicable for vortex shedding suppression, thus, implementing short plates behind the cylinder would not be a rational choice for any purpose of drag reduction or vortex shedding elimination.

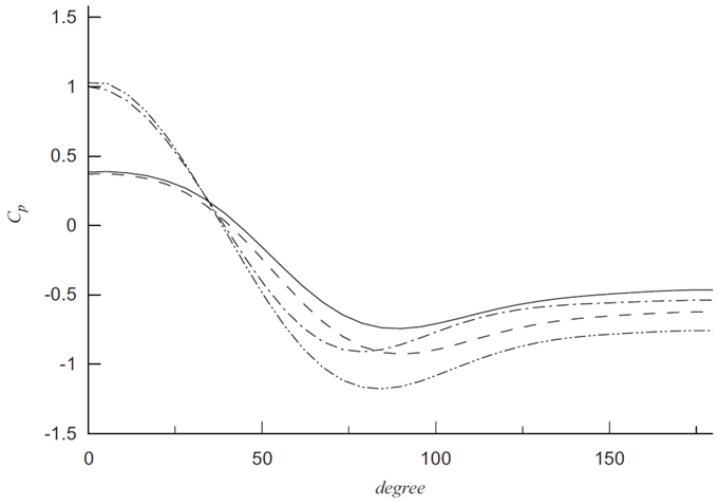

Fig. 6. Distribution of C_p along the circumferential direction of cylinder. (Dashed) upstream only, (Dashed-dotted) downstream only, (Solid line) dual plate, (Dashed-double dotted) no plate (Hwang & Yang, 2007)

Igbalajobi et al. (2013) looked at a broader application of downstream splitter plate as he experimentally applied the same plates as Apelt and West (correct?) to investigate their effectiveness in cylinders with aspect ratio (the ratio of cylinder height to its diameter). The experiment was conducted in a low-speed wind tunnel at a Reynolds number of $7.4x10^4$[17]. Figure 7 contains data for different aspect ratios of AR=9, 7, 5, and 3 in plate's length ratio varying from 1 to 7. Unlike certain studies (Apelt et al., 1973; Apelt & West, 1975) the plate is not attached to the cylinder; (note that the data presented for mean drag coefficients concern total cylinder drag (pressure and skin friction drag) and the drag generated by the plate is not considered in the calculations). Based on Figure 7, for the shorter cylinders, the effect of downstream splitter plate in drag reduction is less compared with the infinite cylinder (data for infinite cylinder are from Apelt & West, 1975). The bulkier the cylinders gets, the less effective the plate becomes; in the case AR≤7 this effect is negligible (maximum 3%). The

difference between two trend lines of infinite and AR=3 proves this statement. Even for the case AR=9 for which the maximum effect reaches up to 12%, the pattern for C_D behaviour to the L/D changes is different from what was observed for the infinite cylinder in Apelt's study. The reason relates s to the effect of tip vortex structure. For shorter cylinders, this structure absorbs a greater portion of the wake and becomes the leading aspect which determines wake behaviour. Thus, the drag is no longer influenced by the plate behind the cylinder.

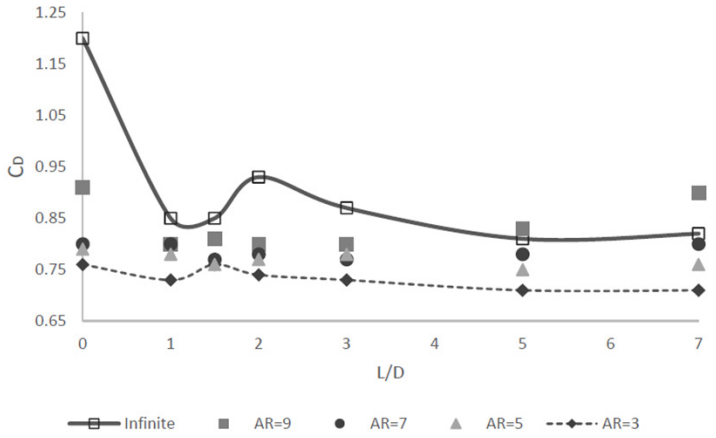

Figure 7. Mean C_D in different downstream plate's length ratio. Infinite cylinder (Apelt & West, 1975), Finite cylinder (Igbalajobi et al., 2013).

VORTEX SHEDDING SUPPRESSION

Power spectra graph for vortex frequencies behind a circular cylinder experience a peak at a frequency corresponding a specific Strouhal number (Igbalajobi et al., 2013). This peak reduces in its amplitude as the downstream plate is placed behind the cylinder till the peak decays and the power spectrum follows a steady trend. Figure8 shows a power spectrum for a cylinder with AR=9. For splitter plates above 3D, no peak is observed which shows the shedding suppression by the mean of plates longer than 3D. The frequency where the peak occurs corresponds to the Strouhal number where vortices are shed behind the cylinder. This occurrence which is based on instabilities of shear layer (Nakamura, 1996) can be neutralised by implementation of splitter plates downstream of the cylinder. Splitter plates if placed in a proper gap relative to cylinder diameter are able to extend upwards the shear layer to its trailing edge and barricade the free-stream flow to be carried along into the base region (Akilli et al., 2005). This is categorised as a direct wake modification based on the classification of flow control into 2 major types of boundary-layer controls and direct-wake modifications (Choi et al., 2008). Altering a downstream splitter plate's length ratio (L_2/D) (Apelt & West, 1975; Igbalajobi et al., 2013), gap ratio (G_2/D) (Akilli et al., 2005; Hwang & Yang, 2007) or picking a suitable combination between them results in vortex shedding suppression behind the cylinder. Table 2 lists four different studies with information about the state in which vortex shedding suppression has occurred.

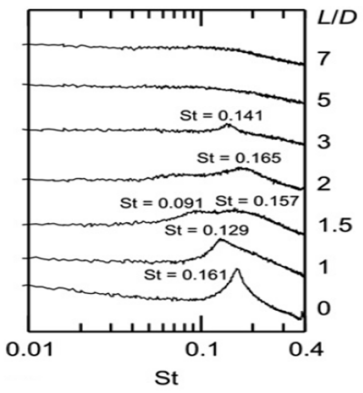

Figure 8. Power spectrum of vortex frequency for different L_2/D behind a finite circular cylinder with AR=9 (Igbalajobi et al., 2013).

Table 2
States in which suppression of shedding happens in four different studies

Study	Re	L_2/D	G_2/D	St	Dimension
Hwang et al. (2007)	100	Cte = 1	2.4	0.122	Infinite
Apelt et al. (1975)	1-5 X10^4	≥3	Cte = 0	0.165	Infinite
Akilli et al. (2005)	5 x 10^3	Cte = 1	1.75	0.163	Infinite
Igbalajobi et al. (2013)	7.4 x 10^4	≥3	Cte = negligible	0.141	AR=9

In a similar situation, Strouhal number for infinite cylinder is higher than the finite one. Looking deeper in a finite case , shorter cylinders possess lower value of Strouhal number as base pressure is higher and vortex formation length becomes longer (Igbalajobi et al., 2013). In the study by Igbalajobi et al. the length ratio was the altering parameter of the splitter plate with a constant gap ratio relative to the cylinder diameter (G_2/D=1). Splitter plates with length ratio of 1-7 were examined to determine the minimum length to eliminate shedding for each cylinder aspect ratio. It was discovered that as the cylinder gets bulkier, a shorter plate is needed to attenuate the shedding. The behaviour of cylinders with AR=7, 9 was found to be similar to the infinite as the vortices were not shed with a same pattern along the height of the cylinder. In fact, there is no shedding at the tip and near the ground plane. Unlike for the long cylinder, a uniform shape of vortices covers along the whole downstream from the ground plane to the tip. This is justified by the prominence of tip structure in bulkier cylinders compared with longer cylinders. This phenomenon makes shedding control easier in short cylinders even by using shorter plates (Igbalajobi et al., 2013).

Both Hwang (2007) and Akilli (2005) considered constant length for the downstream plate and the varying parameter is determined to be the gap ratio. The differences between their studies were the range of Reynolds number and the presence of upstream plate, which was implemented in Hwang's study but not in Alilli's. The critical G_2/D was 2.4 in Hwang's case as the vortex shedding was effectively suppressed. By moving the plate to the position

of 2.5D this effect is no longer stable and vortices start to shed behind the trailing edge of the plate as it is seen in Fig. 9. The significant rise in Strouhal number (St = 0.122 at $G_2/D = 2.4$ to 0.146 at $G_2/D = 2.5$) also confirms this fact. The effectiveness of the upstream plate in the reduction of Strouhal number was reported at10% (Hwang & Yang, 2007), and that's why the critical state in Akilli's study (with no upstream plate) experienced a higher Strouhal number compared with Hwang's study despite the same configuration of the cylinder and plate. Figure 10 shows how the splitter plate loses its functionality as it exceeds the critical gap which was obtained in Akilli's study and was reported to be $G_2/D = 1.75$. The Strouhal number however, continues to diminish as the gap gets bigger until it reaches the value of 2.7D (Akilli et al., 2005) unlike Hwang's study in which the shedding suppression and Strouhal number reduction stop after achieving a same gap ratio.

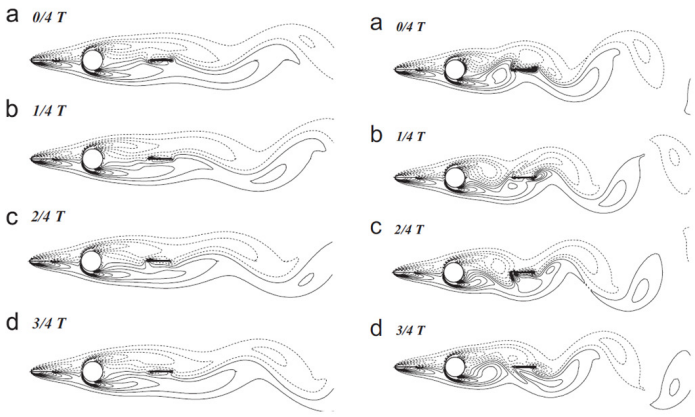

Figure 9. Vorticity contour in 4 intervals of a period. Left: G_2/D=2.4 (critical), Right: G_2/D=2.5 (supercritical) (Hwang & Yang, 2007)

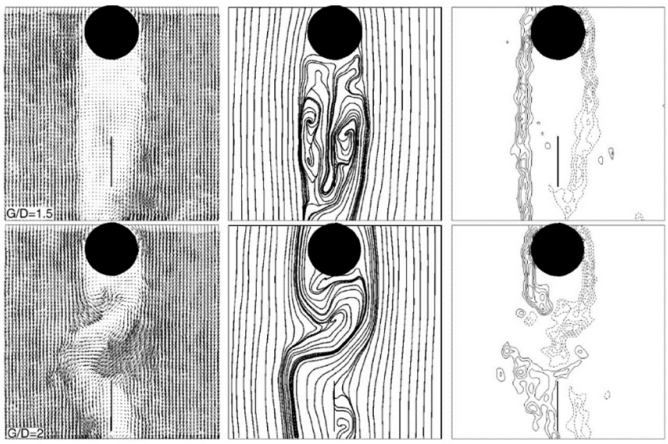

Figure 10. Velocity vector field, streamlines and vorticity contour for two gap ratios. G_2/D subcritical, G_2/D supercritical. Shedding appears when G_2/D exceed the critical value of 1.75 (Akilli et al., 2005).

It is deduced in Akilli's study that the peak is observed in the power spectra and vortices are even shed in low frequencies. Low Reynolds number in this study may be the reason for this phenomenon. The unclear state and lack of a precise setting for splitter plates make this topic open for further investigations. Besides, applying plates with a height similar to the cylinder may not be practical especially in large structures. This consideration necessitates a new scope for future experiments concerning 3D analysis to investigate whether or not shorter plates (in height) have the same functionality in drag reduction and vortex shedding suppression.

SUMMARY

A review of the effectiveness of splitter plate in drag reduction and vortex suppression of a circular cylinder was conducted. All the reviewed studies verified that the presence of upstream plates has a significant influence on drag reduction since they lessen the pressure at the stagnation point and partly augment the base pressure behind the cylinder. The important parameter of the upstream plate is discovered to be its position to the cylinder, relative to the cylinder diameter. This plate has no impact on the vortex shedding behind the cylinder. Downstream plate has less effect on the drag compared with the upstream one and this fact was confirmed in all studies. The main use of a downstream plate is vortex shedding suppression which can be optimised through altering the combination of its relative position and length to the cylinder. Regarding the 3-dimensional analysis, bulkier cylinders sustain less drag force and experience lower frequency of vortices. However, the effect of plates in drag reduction were observed less when compared with the infinite case. Yet, it was easier to achieve the elimination of shedding behind the finite cases and which required shorter plates. In case of failure of suppression, downstream plates cause a significant reduction in the frequency of remaining vortices.

ACKNOWLEDGEMENTS

The authors would like to acknowledge Universiti Putra Malaysia for awarding the FRGS grant 03-02-13-1301FR that enabled the writing of this review article.

REFERENCES

Akilli, H., Sahin, B., & Filiz Tumen, N. (2005). Suppression of vortex shedding of circular cylinder in shallow water by a splitter plate. *Flow Measurement and Instrumentation, 16*(4), 211-219. doi:10.1016/j.flowmeasinst.2005.04.004

Alam, M. M., Sakamoto, H., & Moriya, M. (2003). Reduction of fluid forces acting on a single circular cylinder and two circular cylinders by using tripping rods. *Journal of Fluids and Structures, 18*(3-4), 347-366.doi:10.1016/j.jfluidstructs.2003.07.011

Anderson, E., & Szewczyk, A. (1997). Effects of a splitter plate on the near wake of a circular cylinder in 2 and 3-dimensional flow configurations. *Experiments in Fluids, 23*(2), 161-174.

Apelt, C., & West, G. (1975). The effects of wake splitter plates on bluff-body flow in the range 10 4< R< 5× 10 4. Part 2. *Journal of Fluid Mechanics, 71*(1), 145-160.

Apelt, C., West, G., & Szewczyk, A. A. (1973). The effects of wake splitter plates on the flow past a circular cylinder in the range 10 4< R< 5× 10 4. *Journal of Fluid Mechanics, 61*(01), 187-198.

Assi, G., Bearman, P., & Meneghini, J. R. (2010). On the wake-induced vibration of tandem circular cylinders: the vortex interaction excitation mechanism. *Journal of Fluid Mechanics, 661*, 365-401.

Bearman, P. (1965). Investigation of the flow behind a two-dimensional model with a blunt trailing edge and fitted with splitter plates. *Journal of Fluid Mechanics, 21*(02), 241-255.

Bouak, F., & Lemay, J. (1998). Passive control of the aerodynamic forces acting on a circular cylinder. *Experimental Thermal and Fluid Science, 16*(1), 112-121.

Buresti, G. (1981). The effect of surface roughness on the flow regime around circular cylinders. *Journal of Wind Engineering and Industrial Aerodynamics, 8*(1), 105-114.

Choi, H., Jeon, W.-P., & Kim, J. (2008). Control of Flow Over a Bluff Body. *Annual Review of Fluid Mechanics, 40*(1), 113-139. doi:10.1146/annurev.fluid.39.050905.110149

Cimbala, J. M., & Çengel, Y. A. (2008). *Essentials of fluid mechanics: fundamentals and applications*: McGraw-Hill Higher Education.

Cimbala, J. M., & Leon, J. (1996). Drag of freely rotatable cylinder/splitter-plate body at subcritical Reynolds number. *AIAA journal, 34*(11), 2446-2448.

Hwang, J.-Y., & Yang, K.-S. (2007). Drag reduction on a circular cylinder using dual detached splitter plates. *Journal of Wind Engineering and Industrial Aerodynamics, 95*(7), 551-564. doi:10.1016/j.jweia.2006.11.003

Hwang, J.-Y., Yang, K.-S., & Sun, S.-H. (2003). Reduction of flow-induced forces on a circular cylinder using a detached splitter plate. *Physics of Fluids (1994-present), 15*(8), 2433-2436.

Igbalajobi, A., McClean, J. F., Sumner, D., & Bergstrom, D. J. (2013). The effect of a wake-mounted splitter plate on the flow around a surface-mounted finite-height circular cylinder. *Journal of Fluids and Structures, 37*, 185-200. doi:10.1016/j.jfluidstructs.2012.10.001

Kim, S.-J., & Lee, C. M. (2001). Control of flows around a circular cylinder: suppression of oscillatory lift force. *Fluid Dynamics Research, 29*(1), 47-63.

Kuo, C. H., Chiou, L. C., & Chen, C. C. (2007). Wake flow pattern modified by small control cylinders at low Reynolds number. *Journal of Fluids and Structures, 23*(6), 938-956. doi:10.1016/j.jfluidstructs.2007.01.002

Kwon, K., & Choi, H. (1996). Control of laminar vortex shedding behind a circular cylinder using splitter plates. *Physics of Fluids (1994-present), 8*(2), 479-486.

Nakamura, Y. (1996). Vortex shedding from bluff bodies with splitter plates. *Journal of Fluids and Structures, 10*(2), 147-158.

Nakano, M., & Rockwell, D. (1991). Destabilization of the Karman vortex street by frequency□modulated excitation. *Physics of Fluids A: Fluid Dynamics (1989-1993), 3*(5), 723-725.

OKAMOTO, S., HIROSE, T., & ADACHI, T. (1981). The Effect of Sound on the Vortex-shedding from a Circular Cylinder: Acoustical Vibrations Directed along Axis of Cylinder. *Bulletin of JSME, 24*(187), 45-53.

Ozono, S. (1999). Flow control of vortex shedding by a short splitter plate asymmetrically arranged downstream of a cylinder. *Physics of Fluids, 11*, 2928-2934.

Shukla, S., Govardhan, R. N., & Arakeri, J. H. (2009). Flow over a cylinder with a hinged-splitter plate. *Journal of Fluids and Structures, 25*(4), 713-720. doi:10.1016/j.jfluidstructs.2008.11.004

Sumner, D., Heseltine, J. L., & Dansereau, O. J. P. (2004). Wake structure of a finite circular cylinder of small aspect ratio. *Experiments in Fluids, 37*(5), 720-730. doi:10.1007/s00348-004-0862-7

Suryanarayana, G., Pauer, H., & Meier, G. (1993). Bluff-body drag reduction by passive ventilation. *Experiments in Fluids, 16*(2), 73-81.

Uematsu, Y., & Yamada, M. (1995). Effects of aspect ratio and surface roughness on the time-averaged aerodynamic forces on cantilevered circular cylinders at high Reynolds numbers. *Journal of Wind Engineering and Industrial Aerodynamics, 54*, 301-312.

Wang, A.-B., Trávníček, Z., & Chia, K.-C. (2000). On the relationship of effective Reynolds number and Strouhal number for the laminar vortex shedding of a heated circular cylinder. *Physics of Fluids (1994-present), 12*(6), 1401-1410.

Wang, H. F., Zhou, Y., & Mi, J. (2012). Effects of aspect ratio on the drag of a wall-mounted finite-length cylinder in subcritical and critical regimes. *Experiments in Fluids, 53*(2), 423-436. doi:10.1007/s00348-012-1299-z

Zdravkovich, M. (1977). Review—review of flow interference between two circular cylinders in various arrangements. *Journal of Fluids Engineering, 99*(4), 618-633.

Zdravkovich, M. (1981). Review and classification of various aerodynamic and hydrodynamic means for suppressing vortex shedding. *Journal of Wind Engineering and Industrial Aerodynamics, 7*(2), 145-189.

Pertanika J. Sci. & Technol. 24 (2): 245 - 271 (2016)

PERTANIKA JOURNALS

SCIENCE & TECHNOLOGY

Journal homepage: http://www.pertanika.upm.edu.my/

Review Article

A Comprehensive and Comparative Study on Online Testability for Reversible Logic

Hari Mohan Gaur[1]*, Ashutosh Kumar Singh[2] and Umesh Ghanekar[1]

[1]*Department of Electronics and Communication Engineering, National Institute of Technology, Kurukshetra, Haryana, India*

[2]*Department of Computer Applications, National Institute of Technology, Kurukshetra, Haryana, India*

ABSTRACT

Reversible logic is one of the rising fields for low-power electronic devices. Testing of these devices is a significant issue where the researchers are at par with the latest innovations in the field. However, new technology gives birth to new challenges, and in this field too, several fault models have arisen. Several online testing methods have been proposed for their detection, which are scaled on various performance parameters. This paper provides a comparative study of online testability for reversible logic. We bring together a review of fault models, performance parameters and online testing strategies from the literature with the aim of obtaining a near optimal solution by efficiently exploring the entire search space. We critically analyze a range of online testing strategies reported by researchers using parity preservation and generation, dual-rail coding and concurrent error detection schemes. These strategies are presented in two broad classifications, namely designing with novel gates and designing with existing circuits. All the techniques are explained in detail with a brief mathematical illustration. A comparison of experimental results based on the available number of benchmarks and combinational logic circuits is presented. The best possible strategy is highlighted on behalf of performance parameters.

Keywords: Reversible logic, online testing, fault models, performance parameters, comparative study

INTRODUCTION

Testing of irreversible circuits has been extensively studied in the 70s; however, reversible logic has been studied by researchers only to some extent. More attention is required to meet the demand of high-speed low-power electronic devices. Reversible logic ensures nearly energy-free computation by preventing

Article history:
Received: 14 September 2015
Accepted: 15 March 2016

E-mail addresses:
leoharimohan84@gmail.com (Hari Mohan Gaur),
ashutosh@nitkkr.ac.in (Ashutosh Kumar Singh),
ugnitk@nitkkr.ac.in (Umesh Ghanekar)
*Corresponding Author

ISSN: 0128-7680

loss of information in the form of heat as in irreversible operations (Bennett, 1973; Landauer, 1961). Since testing guarantees the true functioning of these devices, it is very important to attain the desired results. Testing of reversible logic circuits is achieved at the cost of an increase in gate count, quantum cost, ancilla inputs and garbage output. Although gate count and quantum cost have improved over the years, the argument for ancilla inputs and garbage output persists. One resembles an extra input bit and the other an extra output bit; both are sources of power loss in reversible circuits.

Reversible logic performs bijective functions, where a unique output state is obtained from every input state and therefore, the number of inputs should be the same as the number of outputs. The outcome is fully controllable and observable operations, which, in turn make the testing of reversible logic circuits easier than that of irreversible logic circuits. Also, some challenges have arisen as a consequence of new technology that should be considered during the entire testable design process. Some major challenges pertaining to online testability include:

- Design complexity due to high density of gates,
- A variety of new fault models; the maximum number of faults should be covered in one design,
- Garbage and ancilla input minimization, the outcomes of implementing a reversible function from an irreversible function,
- Very low signal levels as compared to that of irreversible logic circuits (Polian et al., 2005) and
- Fanout and feedback, a technology problem which is not permitted in reversible circuits.

There are two possible approaches of testing for any system, and in reversible logic, the first is online testing and the other is offline testing. A circuit is said to be online testable if it is able to find a fault within the circuit during its operation. In the case of offline testing, a number of test vectors are applied after taking out the circuit from its usual operation, for which correct output values are known. All the existing reversible logic-testing approaches that have been proposed previously are divided into these two major categories as shown in Figure 1. Further classification is given on the basis of different methodology of testing reversible logic circuits. Designing with novel gates and designing with the existing circuit are two methods in case of online testing. Test-set generation and compaction ATPG (Patel et al., 2004, Polian et al., 2005 & Tabei et al., 2005) and DFT methodology (Rahman et al., 2007, & Rahman et al., 2011) are found prominent in case of offline testing. We are concerned here with online testing approaches as online testing is gaining ground over offline testing. The latter approach entails utmost 2^n test vectors to test a circuit with n number of inputs, which probably becomes hugely time consuming and places the emphasis on categorizing various strategies on the basis of quantum cost, gate count, ancilla input and garbage output. Quantum cost is not reported by most researchers, but gate count has a proportional relationship with it.

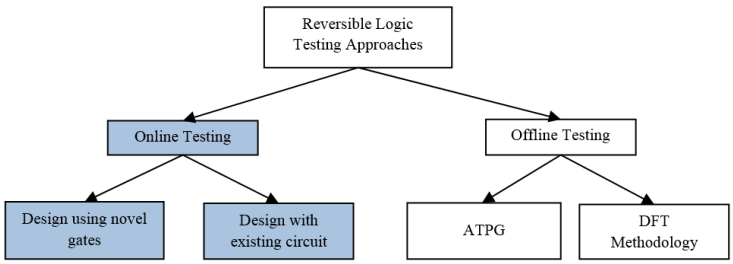

Figure 1. Classification of testing approaches.

In this paper, we first consider some background details, which include the basics of reversible logic, fault, fault models and performance parameters pertaining to online testing of reversible logic. Then, we demonstrate various testing approaches in online testing of reversible logic circuits from the literature by differentiating them into two categories. These approaches are then summarized and compared in a table based on their features, highlighting the optimum among them on behalf of performance parameters in two consecutive sections. Finally, the last section provides a comparative study of all the approaches on available work and future directions related to performance parameters with fault models.

BACKGROUND

Reversible Functions and Reversible Gates

A logic function with n Boolean variables is a reversible function if it maps distinct input to distinct output. There should be $n \times n$ bijective function mapping between input and output. In general, a truth table or a permutation can be used to represent a reversible function (Chua & Singh, 2014) as shown in the example in Table 1, where each output (x,y) is assigned to a unique input (a,b) without any replication.

Table 1
Reversible Function

Input		Output	
a b	Permutation	x y	Permutation
0 0	0	0 0	0
0 1	1	0 1	1
1 0	2	1 1	3
1 1	3	1 0	2

A reversible gate realizes a reversible function. A k input k output gate that produces k distinct output from its k distinct input functions is called a $k \times k$ reversible gate. There is one-to-one mapping between input and output vectors and therefore, the input state can be reconstructed from its output state. Various reversible gates are given in the literature, which is used for synthesizing reversible circuits using different algorithms (Shende et al., 2003).

Some of the commonly used are the NOT (Feynman, 1985), CNOT (Feynman, 1985), Toffoli (Toffoli, 1980), Fredkin (Fredkin & Toffoli, 1982) and Peres (Peres, 1985) gates, which are demonstrated in Figure 2**,** with inputs *a*, *b* and *c* and their respective response *x*, *y* and *z* shown in Table 2.

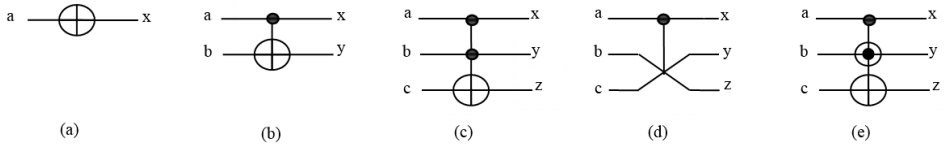

Figure 2. Reversible gates (a) NOT, (b) CNOT, (c) Toffoli, (d) Fredkin and (e) Peres.

Table 2
Responses of Reversible Gates for Their Corresponding Inputs

	x	y	z
NOT	a'	-	-
C-NOT	a	ab	-
Toffoli	a	b	c⊕ab
Fredkin	a	a'b+ac	ab+a'c
Peres	a	a⊕b	ab⊕c

Fault and Fault Models

Faults are any kind of imperfection in a circuit that affects the functional behavior of a system. They are classified into two main categories (Hurst, 1998). The first category includes permanent faults that affect the functional behavior of a system due to incorrect interconnections, designing and masking, breakage etc. The second includes non-permanent faults that affect the functional behavior of a system for a finite period of time. Non-permanent faults occur due to environmental conditions like temperature, humidity, dust etc., which are called transient faults or are due to non-environmental conditions like ageing, loose connections, critical timing (hazards and race) etc. which are called intermittent faults. The online approach finds its application to detect permanent as well as non-permanent faults. In this review paper, we focused only on non-permanent faults that occurred only once during the operation of a circuit.

A fault model describes the type of fault that occurs in a circuit. It identifies the target of testing. There are several fault models proposed in the literature. In this paper, we focused only on structural fault models in reversible logic circuits. The following is a detailed discussion of fault models as depicted in Figure 3 from the left to the right.

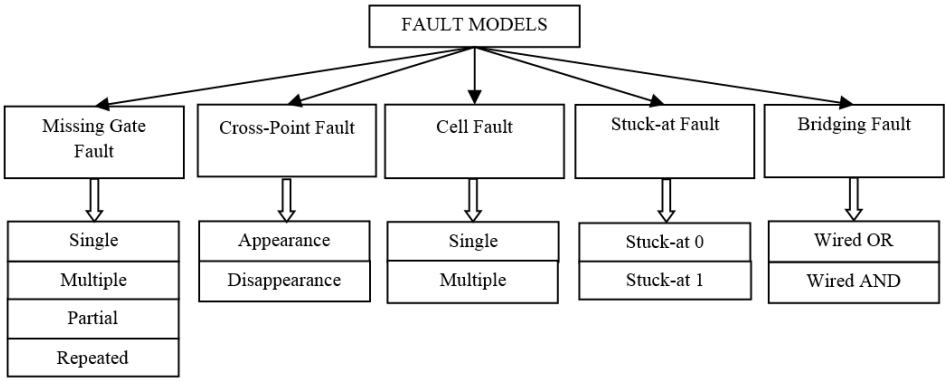

Figure 3. Fault models in reversible circuits.

Missing gate fault. A missing gate fault is defined as complete disappearance of a reversible gate from a circuit. If a single gate disappears from a circuit, it is called a 'single missing gate fault'. If two or more consecutive gates disappear, the fault is called a 'multiple missing gate fault'. Figure 4a shows that the first gate is missing and Figure 4b shows the first two consecutive gates missing. These faults are transient fault models that appear in a circuit due to short or mistuned input pulses (Polian, Hayes, Fiehn, & Becker, 2005).The un-faulty/ faulty value is written on the wire at each stage where the value is likely to be changed.

Missing gate faults may also occur as repeated gate faults when any gate replicates its functionality in certain instances, for instance, in a reversible circuit as shown in Figure 4c, where the second gate repeated its functionality twice. If the number of instances is even, it affects the circuit in a similar way as in the case of a single missing gate fault and if the instances are odd in number, then there is no change in the functionality of the circuit and a partial missing gate fault occurs when any control point loses its control from a gate in a reversible circuit as shown in Figure 5b.This fault model appears in a circuit due to long or duplicated input pulses.

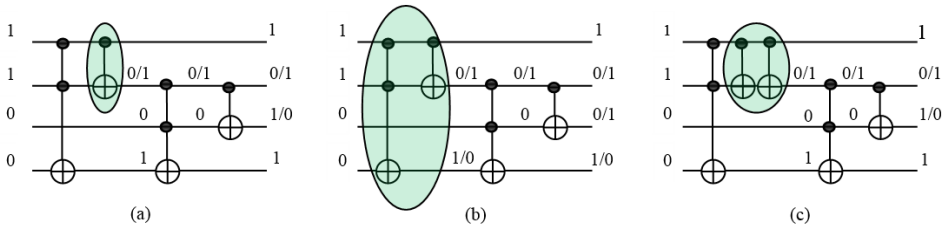

Figure 4. Illustration of fault models (a) Single missing gate fault (b) Single missing gate fault and (c) Repeated gate fault.

Cross-point fault. This fault model is related to the missing or extra connection at the cross-point or control point of a gate in a reversible circuit (Zhong, & Muzio, 2009). There are two types of cross-point faults that may occur in a circuit. They are the appearance fault,

which occurs when an extra control point is added on a gate, as shown in Figure 5a and the disappearance fault, which occurs when one or more control points are missing from a gate as shown in Figure 5b, similar to a partial missing gate fault.

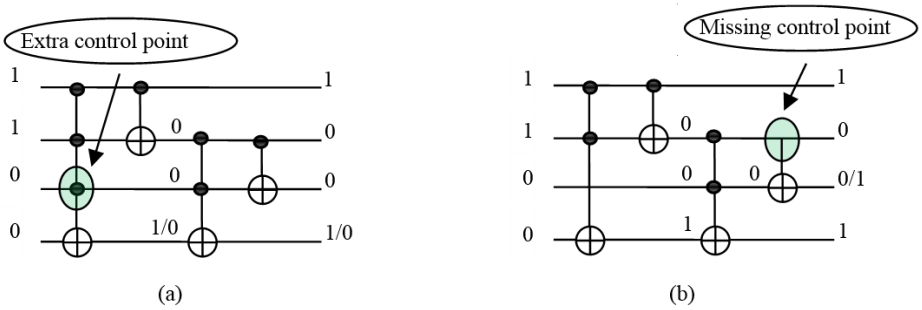

Figure 5. Illustration of fault models (a) Appearance fault and (b) Partial missing gate fault/ Disappearance fault.

Cell fault. This type of fault occurs due to malfunctioning of any gate in a reversible circuit such that it produces an incorrect output (Hayes et al., 2004). These faults may appear in a circuit in any form as in the case of repeated gate faults, where the output becomes faulty due to the repeated operation of a gate or a cell. These faults are based on the fault modeling of cellular logic arrays (Kautz, 1967) and that is why they are called cell faults.

Stuck-at fault. Like the traditional stuck-at fault model, this type of fault occurs in a circuit when a wire gets stuck or is fixed on a single value 0 or 1; these are called the stuck-at 0 or stuck-at 1 faults, respectively (Peres, 1985). The possible nine sites for the occurrence of this type of fault are represented by small circles shown in Figure 6a.

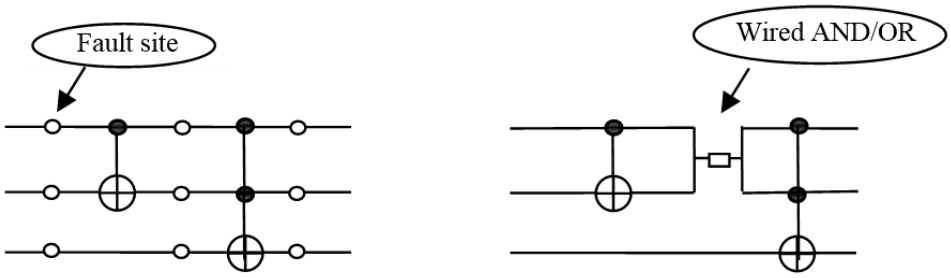

Figure 6. Illustration of fault models (a) Stuck-at fault (b) Bridging fault.

Bridging fault. Again, similar to the traditional fault model, this type of fault takes place when two adjacent wires in a circuit get physically bridged or shorted by means of wired AND/ OR interconnections. As a result, the response comes to an erroneous value (Hurst, 1998), as shown in Figure 6b.

Whenever any type of fault occurs in a circuit, the result is a change of single or multiple values of bits on any wire. This is referred to as a bit fault. When the value of a single line is changed, the fault is called a 'single bit fault' and if the values of two or more lines are changed,

the fault is called a 'multiple bit fault'. Figure 7a and Figure 7b demonstrate the respective faults where the propagation stuck-at-0 fault is shown by the highlighted box.

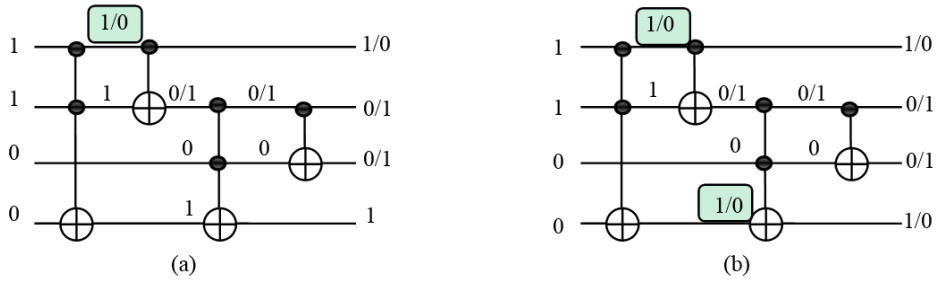

Figure 7. Illustration of fault models (a) Single bit fault and (b) Multiple bit fault.

Hence, the bit fault model is exclusively meant for online testing of reversible logic circuits as the detection of bit faults will detect all other fault models (Gaur et al., 2015). As a result, the complexity of designing for online testability reduces. In the case of offline testability, a separate algorithm is required for each fault.

Performance Metrics

It has been pointed out in the literature that the proposed testable design techniques in reversible logic circuits are justified by means of certain parameters. These parameters illustrate different performance measures for a testable design and on the basis of these measures; quality and performance can be evaluated. These performance measures are defined below:

Gate count. The total number of reversible gates required to realize a reversible circuit is its gate count. It is the straightforward function to find the cost of a reversible circuit, often called the logic cost (Golubitsky & Maslov, 2012). Figure 8a shows the rd32 benchmark circuit (Maslov et al., 2015) as an example where the gate count is 4. Sometimes, a gate count is analyzed on the basis of basic building blocks used to realize a reversible circuit as shown in Figure 8b where three *R* gates (Vasudevan et al., 2004) are required to implement an NOR function.

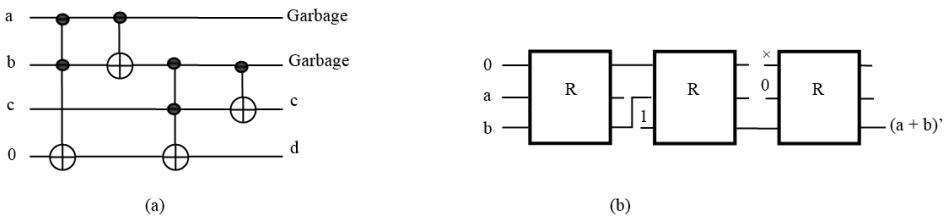

Figure 8. Example circuits (a) rd32 benchmark and (b) Implementation of NOR function using R gate.

Quantum cost. The majority of researchers use quantum cost to evaluate the quality of their design. The quantum cost of a quantum circuit is defined as the sum of elementary quantum gates (1×1, 2×2, Controlled-V and Controlled-V+ quantum gates) used to realize a circuit. In the case of circuits consisting of larger gates, one can substitute them with their equivalent elementary quantum implementation (Barenco et al., 1995; Golubitsky & Maslov, 2012). The quantum cost of some common reversible gates can be found in Table 3; for more information please refer to Maslov and Dueck (2015). The rd32 circuit in Figure 8a can be realized by eight elementary gates; hence, the quantum cost is 8.

Table 3
Quantum Cost of Common Reversible Gates

Name	Size	Quantum Cost
NOT	1×1	1
CNOT	2×2	1
Swap	2×2	3
Toffoli	3×3	5
Fredkin	3×3	3
Peres	3×3	4

Garbage. In order to make a function reversible, some additional output is added to the circuit to maintain equality between the number of outputs and inputs. The values of these additional outputs are not important in the realization of a circuit (Maslov & Dueck, 2015). There are two unused additional outputs in the rd32 benchmark in Figure 8a (marked garbage against them), which are referred to as garbage of garbage output. They are one of the causes of power loss in reversible circuits in the form of information loss, which should be minimized.

Ancilla inputs/Constant inputs. In the designing of a reversible circuit from an irreversible function, certain constant inputs are required whose values are set to constant 0 or 1 (Mohammadi & Eshghi, 2009). In quantum computation these are extra qubits added to the quantum circuit that are set as a constant state that is affected by the quantum operators in order to realize a reversible function. The number of inputs increases the number of qubits in a reversible circuit that increases the area/size of the circuit. These inputs are also referred to as branch cost (Farazmand et al., 2010) as a new branch is added with the addition of an ancilla input.The value of the last line in the rd32 circuit in Figure 8a is set to constant 0 and is referred to as ancilla input. The total number of inputs (sum of variable and constant inputs) in a reversible circuit is also a measure of performance as both are directly related to the area/size of a circuit.

The above-mentioned parameters have a direct relationship with area/size. If these parameters increase, they raise the size of the design and hence, power dissipation increases. Consequently, they should be minimized and should be considered as a matter for concern throughout the development of test strategies. The quantum cost has a proportional relationship with gate count, while ancilla input is an extra source of input power and garbage represents power loss. There are some technology-dependent measures like input to output delay, which gives computation rapidity while the fault coverage shows the quality of design.

Delay can be calculated as the product of depth and number of unit delays of the circuit (Mohammadi & Eshghi, 2009), where depth is the number of stages in a quantum circuit and unit delay is the duration of each stage when all the gates present in the circuit are replaced by their equivalent elementary quantum gates. Fault coverage is the ratio of the number of faults detected to the total number of faults in the circuit (Jha & Gupta, 2003).

DESIGN USING NOVEL TESTABLE GATES

Testing of the reversible circuit came into existence a decade ago and researchers have been curious about the idea of testing in the emerging field of reversible logic. The smart way to achieve online testability is to design new online testable gates, keeping the minimum number of inputs, quantum cost and garbage output. Only a few researchers have proposed this as well. These new gates do have some additional input and output other than purely functional ones to achieve testability during their operation.

Designing with R_1 and R_2 Online Testable Gates

The very first online testable 4×4 reversible gates,R_1 & R_2, in addition to a new reversible gate *R*, were introduced in the year 2004 (Vasudevan et al., 2004) depicted in Figure 9. The method is meant for the detection of single bit faults inside a reversible circuit. The gate R_1 is used to produce logical functions with a parity output bit, and gate R_2 is used to pass the output of gate R_1 directly to its output in addition to one more output parity bit. Both the reversible gates combine to form a testable block TB, as can be seen in Figure 10. The input *p* is set to logic 1 and *r* is set to logic 0 in order to achieve online testability. Test output *q* and *s* of TB should resulting complementary values that can be checked using the proposed dual-rail checker circuit composed of eight reversible *R* gates. Non-complementary output of TB implies a fault within the reversible gates R_1 or R_2.

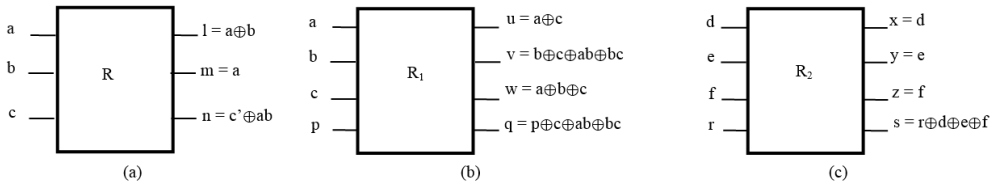

Figure 9. Schematic of proposed gates Gates (Vasudevan, 2004; Vasudevan et al., 2006) (a) R gate, (b) R_1 gate and (c) R_2gate.

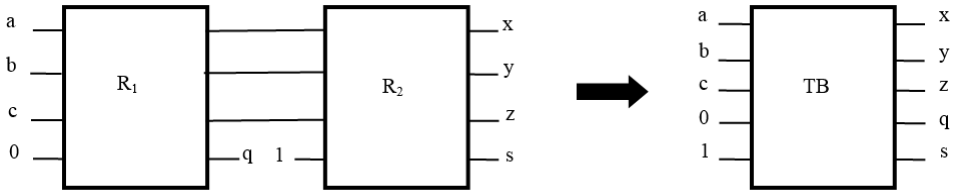

Figure 10. Construction of testable block (TB) (Vasudevan, 2004; Vasudevan et al. 2006)

Experiments were done using a set of benchmarks. Results were analyzed on the basis of the number gates used to synthesize a circuit, which includes a total number of TBs ($R_1$and R_2) and R gates (used to implement the required number of rail checker circuits) as gate count (GC) and garbage output (GO) as shown in Table 4. The quantum cost of TB and R is not indicated by the author; it would have been large as their output functions were complex. Also, the required number of checker circuits was equal to the number of TBs used to synthesize a circuit. Hence, the idea is better as far as GO is concerned. The idea was extended further and the authors implemented their proposed scheme in CMOS technology (Vasudevan et al., 2006) in VHDL using Xilinx ISE. The results showed the technology specific measures, power dissipation (PD) in microwatts and total number of transistors (NoT) required for realize a benchmark circuit.

Table 4
Operating Cost of Testable Design in Proposed Method (Vasudevan, 2004; Vasudevan et al., 2006)

Benchmark/Circuit	NoT	PD	GC	GO
xor5	81	69.35	4	8
t	81	54.21	8	16
b1	105	43.12	9	8
majority	129	62.12	11	13
con 1	285	93.42	24	36
clip	309	216.51	26	37
t481	3604	293.21	34	412
rd53	777	311.20	65	90
o64	1545	56.21	129	258
misex 1	1401	675.31	117	161
Full Adder without Propagate	-	59.32	4	3
Full Adder with Propagate	-	-	4	2

Illustration. The test bits q and s of TB shown in Figure 10 can be given as:

$$q = p \oplus c \oplus ab \oplus bc$$

$$\begin{aligned} s &= r \oplus d \oplus e \oplus f = r \oplus u \oplus v \oplus w \\ &= r \oplus a \oplus c \oplus b \oplus c \oplus ab \oplus bc \oplus a \oplus b \oplus c \\ &= r \oplus c \oplus ab \oplus bc \end{aligned}$$

$$\text{Let } x = c \oplus ab \oplus bc$$

This means that if $p = 0$ and $r = 1$, the value of q and s will be complementary values for correct operations.

Improved Rail-Check Circuit with R_1 and R_2

An efficient rail-check circuit, namely IRC (improved rail check), was proposed (Hasan et al., 2009) in the advancement of the former approach for the detection of a single bit fault. The method proved competent in terms of reduction in quantum cost and garbage output. The design consisted of only a Fredkin gate and a Feynman gate (Chua & Singh, 2014) shown in Figure 11 rather than using *R* gates, where x_1 and x_2 are test inputs. Test output *d* produces a high state for a faulty operation and *G* represents garbage value. Hence, quantum cost decreases as the quantum cost of IRC is only 5, regardless of the number of gates used to synthesize a circuit.

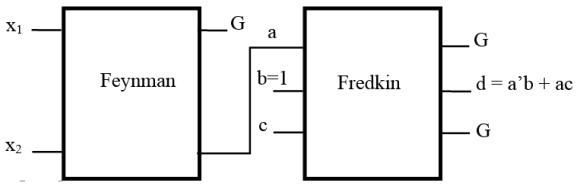

Figure 11. Schematic of IRC (Hasan et al., 2009)

A set of benchmark circuits and some sequential logic blocks like SR, D, JK and T flip flops were realized and performance was evaluated on the basis of the total number of gates, GC, and garbage output, GO. This is depicted in Table 5.

Illustration. In Figure 11, if $x_1 = x_2 = 1$ or $x_1 = x_2 = 0$ then output of the Feynman gate

$a = x_1 \oplus x_2 = 0$

This implies the output of the Fredkin gate:

$d = 1$ for $b = 1$ and $d = 0$ for $b = 0$

Table 5
Operating Cost of Testable Design in Proposed Method (Hasan et al., 2009)

Sequential Circuit	GO	GC
RS FF	28	24
JK FF	36	32
D FF	33	28
T FF	41	36
Master Slave FF	73	64

Benchmarks	GO	GC
xor5	20	16
rd53	180	156
hwb4	101	92
mod5adder	285	248
ham7	214	196
4mod5	42	36
rd32	51	44
5mod5	181	156
4 _49	139	124
hwb5	329	292
2or5	172	148
ham3	39	36
3_17	63	56

This shows that output *d* is the decision parameter to check whether the input to the IRC circuit is complementary or not.

Designing with OTG

Thapliyal and Vinod (2007) proposed a 4×4 reversible online testable gate (OTG) shown in Figure 12, which can perform all Boolean functions. The OTG seems better with respect to the earlier proposed R_1 gate in terms of computational complexity. In view of online testability, OTG is used in combination with the 4×4 Feynman gate to form a testable block CTSG for the detection of a single bit fault, as mentioned in Figure 13. The output *R* and *W* of CTSG should give complementary logic values for the correct operation; otherwise, there will be a fault in OTG or in the Feynman gate. The value of *E* is set in accordance to the necessity of any logical function implementation.

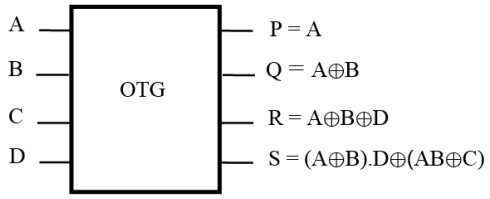

Figure 12. Schematic of OTG (Thapliyal & Vinod, 2007).

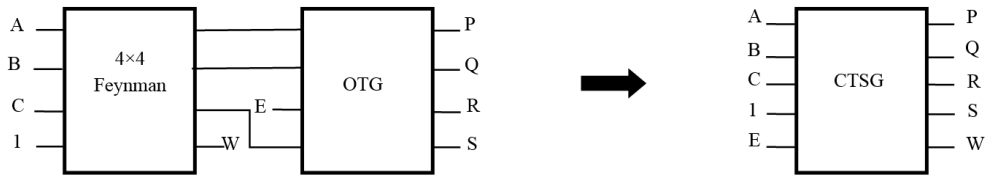

Figure 13. Construction of CTSG (Thapliyal & Vinod, 2007).

A number of testable combinational logic circuits like full adder, ripple carry adder and carry skip adder were synthesized using CTSG. The complementary values for *W* and *R* can be verified using the proposed improved two-pair two-rail checker per CTSG. The implementation was justified in terms of number of OTG used as GC, garbage output GO and unit delay (D). This is shown in Table 6. The quantum cost is high as the output functions of OTG are again complex as that of TB regardless of gate count.

Table 6
Operating Cost for Testable Design in Proposed Method (Thapliyal & Vinod, 2007)

Circuit	GO	GC	D
Full Adder with propagate	2	2	2
4-bit ripple carry adder	8	4	4
4-bit carry skip adder	17	22	-

Illustration. Output *W* and *R* of CTSG can be given as:

$$W = A \oplus B \oplus C \oplus 1 = (A \oplus B \oplus C)'$$

$R = (A \oplus B \oplus C)$; $D = C$ (connections shown in Figure 13)

This proves that *W* and *R* will hold complementary values that can be detected by the proposed dual rail-checker circuit to attain online testability.

Designing with Dual Rail-Coding-Scheme-Based Reversible Gates

In 2010 Farazmand et al. proposed an idea to reduce design complexity by eliminating the necessity of separate rail checker circuits. They projected two self-testable reversible gates by means of a dual-rail coding scheme for the detection of single bit faults. The schematic representation of the proposed gates as NAND gate and fanout branch is shown in Figure 14. The dual rail NAND gate was used to implement Boolean functions and the dual rail fanout was used to provide branching capability as they did not use reversible logic, which may require synthesizing a circuit.

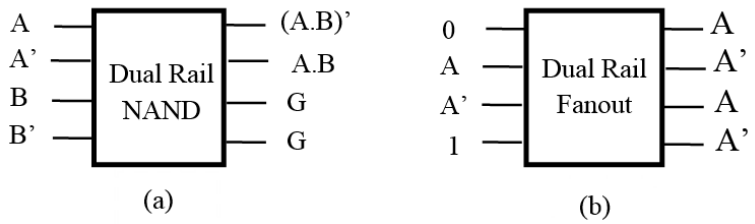

Figure 14. Schematic of dual rail reversible gates Farazmand et al., 2010 (a) as NAND gate and (b) as fanout branch.

Experiments were done on a set of benchmarks where the rail-checker circuit was used only at the final output stage. As a result, there was a large reduction of area in terms of branch cost/ancilla input (AI) and number of inputs (NoI), as seen in Table 7. The method was more efficient in terms of fault coverage and claims 100% coverage of single bit faults.

Table 7
Operating Cost of Testable Design in Proposed Method (Farazmand et al., 2010)

Benchmarks	GO	NoI	AI
xor5	112	224	116
t	48	96	40
b1	30	60	24
Majority	18	36	20
con 1	44	88	48
clip	1250	2500	800
t481	9534	19068	958

Benchmarks	GO	NoI	AI
rd53	212	424	220
misex 1	134	268	118
o64	258	516	0

Illustration. The dual rail-coding scheme in reversible logic empowers self-testability in the gate itself. The outputs of a reversible circuit implemented using these gates will always be complementary, which can be detected using a dual rail- checker circuit only at the final output stage as illustrated in the schematic of NAND gate realization in Figure 14.

Designing with LG, FIG and DCG

Further, in 2011 Zamani and Tahoori introduced an idea of development of gates in such a manner that they produced the necessary information at the output rather. This was an alternative to the parity generation method. In this approach, a detection line was added to gates whose value was inverted at every gate stage. The error can be detected by knowing the number of stages present in a circuit for the detection of missing gate faults and repeated gate faults. The proposed reversible gates are Logic Gate LG, Fanout/Inversion Gate FIG and Decision Collector Gate DCG as shown in Figure 15. The 4×4 LG gate is used to implement a Boolean function with target inputs A and B and outputs F_1 and F_2 where C is the control input, D is the detection line and G is garbage. The 3×3 FIG gate is used to make the fanout/inversion branch since a fanout is not allowed with reversible circuits. The control input is C set to logic 0/1 such that input A appears as A'/A at outputs F_1 and F_2 of FIG and D is again treated as the detection line. The error can be detected on the basis of the output at detection line D, which is collected by DCG. The value of D will be different for both even and odd numbers of stages in a circuit synthesized using LG and FIG. During any operation, initially all input D values were set to 0, the output value of D (say D_{odd}) was 1 for odd numbers of stages and the output value of D (say D_{even}) was 0 for even numbers of stages in a fault-free circuit. For a circuit consisting of both even and odd numbers of stages, the fault can be analyzed using the 3×3 DCG gate with inputs D_{even} and D_{odd} for even and odd numbers of stages, respectively, where C is the control input. The erroneous output is identified by the *Alarm* output of DCG.

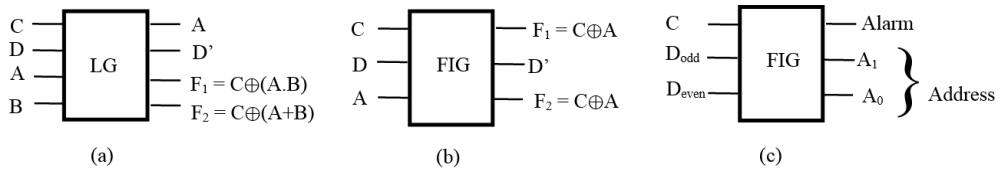

Figure 15. Schematic of proposed gates (Zamani et al., 2011) (a) LG, (b) FIG and (c) DCG.

The benchmark circuit made use of this approach and performance was analyzed on the basis of gate count (LG/FIG/DCG), garbage and delay as seen in Table 8. The method is more suitable in terms of delay, but is faulty because of an increase in design complexity, gate count and garbage output. The method was only meant for the detection of single missing and repeated gate faults.

Table 8
Operating Cost of Testable Design in Proposed Method (Zamani et al., 2011)

Benchmarks	GO	GC	D
Majority	25	17	6
t481	9712	7283	22
b9	815	587	13
alu2	1859	1385	18
term1	3835	2882	17
vda	2653	1948	17
x4	5203	3887	16

Illustration. In the example shown in Figure 16, the upper sub-circuit contains three stages (odd in number) and the lower contains two stages (even in number). For testability, initially the detection line *D* was set to value 0, hence $D_{odd} = 1$ and $D_{even} = 0$. For non-erroneous output the output on *Alarm* was 0, keeping $C = 1$. For other than these values of D_{odd} and D_{even}, a high signal value appeared at the *Alarm* output of DCG, revealing a fault.

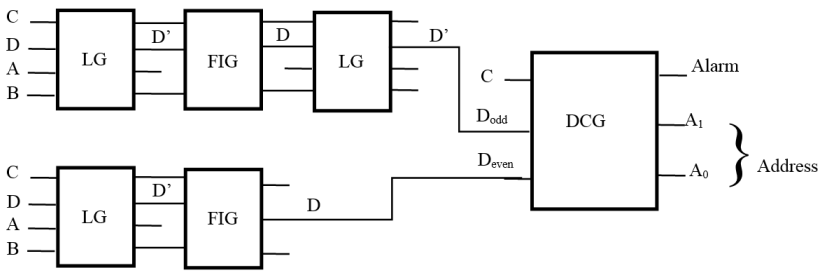

Figure 16. Illustration of method of online testing using LG, FIG and DCG.

Concurrent Error Detection Approach

Reversible functions are bijective functions where the input and output have a one-to-one relationship. Also, the inputs can be regenerated at the outputs if the output signal is re-applied at the inputs of a reversible gate/circuit. The problem of testing can be resolved by the comparison of original inputs and regenerated inputs by comparing these values. This scheme is termed 'concurrent error detection' of a reversible circuit.

Thapliyal and Ranganathan (2004) exploited the idea of concurrent error detection for online testing of reversible logic circuits and established the detection of multi-bit error at the outputs of a reversible circuit in a method called inverse and compare. As a result, the reduction on power dissipation could be achieved by minimizing the requirement of excessive garbage output in design for testability. The technique is illustrated in Figure 17a. The problem of fanout was avoided by the use of intermediate Feynman gate(s). The implementation of the concurrently testable full adder was proposed using OTG (Thapliyal & Vinod, 2007) and its inverse gate IOTG, which can be seen in Figure 17b. The fault can be detected by comparing primary inputs to OTG and outputs of IOTG. This results in zero garbage and a delay of 3

units using only three gates with a quantum cost of 20. The application of the concurrent error detection technique for quantum dot cellular automata QCA was also explained by Thapliyal and Vinod. Their method reduced the design complexity, but the quantum cost and garbage were much higher for bigger circuits as the number of gates used to synthesize a circuit was more than double. The ancilla input would be much higher with the addition of a Feynman gate for dealing with the output. Also, it is very complicated to insert a comparator circuit after each block in an electronic device.

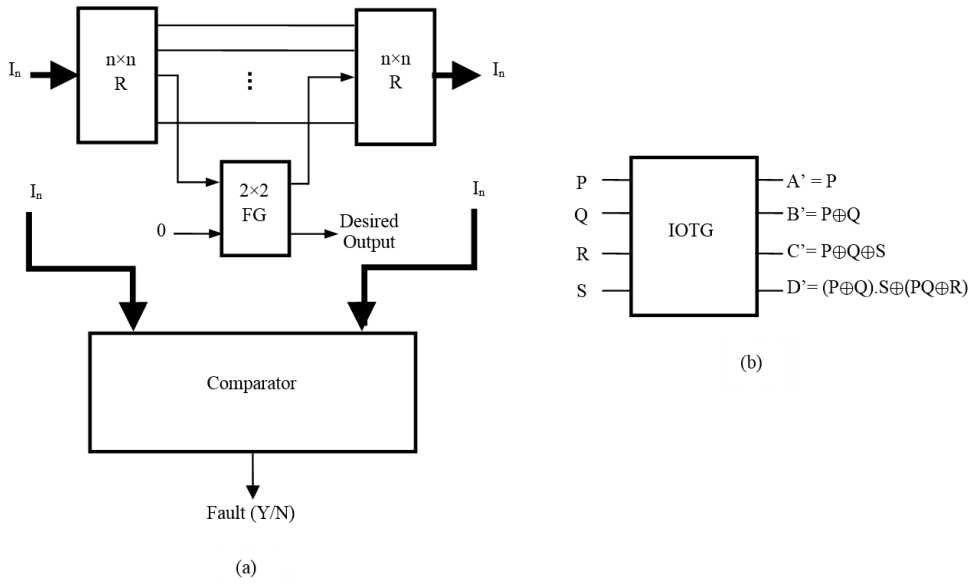

Figure 17. Concurrent error detection (a) Block diagram representation and (b) Schematic of IOTG.

Illustration. It is already proven that reversible gates produce input functions. The output functions can be seen in the equations given below for IOTG as shown in Figure 17b. The output of IOTG can be given as:

$$A' = P = A$$

$$B' = P \oplus \mathrm{Q} = \mathrm{A} \oplus (\mathrm{A} \oplus \mathrm{B}) = \mathrm{B}$$

Similarly, $C' = C$ and $D' = D$

Hence, one can detect faults in a reversible circuit by comparing primary inputs and regenerated inputs as shown in the block diagram representation in Figure 17a.

Attributes of Designing with Novel Gates Methods

Extracted attributes of all the testing methods explained in this section are depicted in Table 9. These attributes appropriately compare all these methods. Comparison tables are also given. By comparison, it is found that the method by Vasudevan et. al., 2006 and Hasan et. al., 2009

proved better in performance in terms of minimum garbage output. The later approach has lower quantum cost and garbage than the first method.

Table 9
Attributes of Designing with Novel Gates Methods

Testing Method	Features	Tables for comparison
(Vasudevan et al., 2004 and Vasudevan et al., 2006)	Large GC (i.e. QC high), GO is comparatively small.	4,5,7 and 8
(M.Hasan et al., 2009)	QC and GO both are high	4,5,7 and 8
(Thapliyal et al., 2007)	QC is high and GO is comparatively small	4,6
(Farzamand et al., 2010)	QC , GO and NoI are high	4,5,7 and 8
(Zamani et al., 2011)	QC and GO both are high	4,5,7 and 8
(Thapliyal et al., 2004)	GC, QC, AI and GO all are high	-

DESIGNING WITH EXISTING CIRCUIT

Another way of achieving online testability in reversible logic circuits is to design with any existing standard circuits. In this approach, the original circuit is modified by adding a number of reversible gates and wires with constant inputs in order to attain online testability.

Designing with Derived Reversible Gates

In this regard Mahammad and Veezhinathan (2010) proposed a two-step procedure of conversion of a reversible gate in its testable form to detect single bit faults. A reversible gate URG was also proposed that used four basic logic functions efficiently in terms of quantum cost. In the first step a reversible gate R was converted into a deduced reversible gate DR_a such that for a $n \times n$ reversible gate with input vector I_{ia} and output vector O_{ia} was changed into $(n+1) \times (n+1)$ reversible gate with input vector I_{ia+1} and output vector O_{ia+1} without changing the original functionality of the circuit as depicted in Figure 18a.

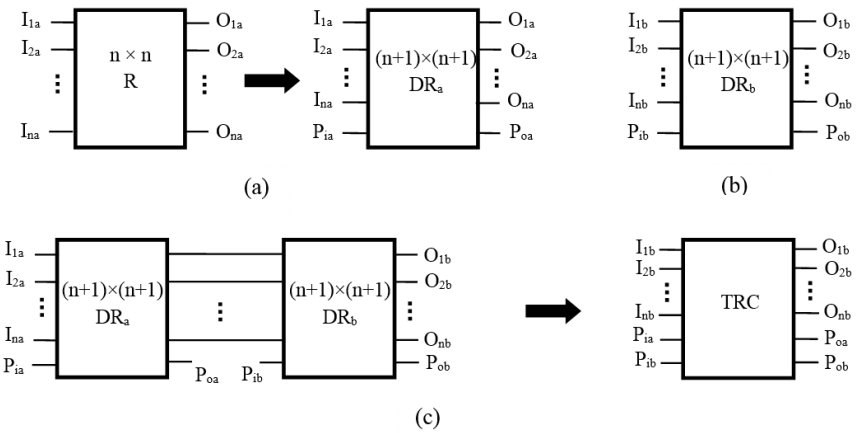

Figure 18. Basic fundamental used in proposed scheme (Mahammad et al., 2010) (a) Conversion of DR_a from reversible gate R, (b) Schematic of identity gate DR_b and (c) Construction of TRC.

If, I_{ia}= (I_{1a}, I_{2a}...I_{na}) *and* O_{ia} = (O_{1a}, O_{2a}...O_{na}), then I_{ia+1} = (I_{1a}, I_{2a}... $I_{na,}$ P_{ia}) *and* O_{ia+1} = (O_{1a}, O_{2a}...$O_{na,}$ P_{oa}) *w*here P_{ia} and P_{oa} are the input and output parity bit corresponding to the first step, respectively and P_{oa}=[$O_{1a}\oplus O_{2a}\oplus ...O_{na}\oplus P_{ia}$].

In the second step DR_a was cascaded with (n+1) × (n+1) identity reversible gate DR_b as shown in Figure 18b to form (n+2) × (n+2) testable reversible cell TRC as can be seen in Figure18c. The unity reversible gate passes the output of DR_a directly to its output except parity P_{oa} and generates another parity bit P_{ob} with respect to the input parity bit P_{ib} such that for a (n+1) × (n+1) identity gate, the input vector and output vector are given by I_{ib+1} = (I_{1b}, I_{2b}… $I_{nb,}$ P_{ib}) and O_{ib+1} = (O_{1b}, O_{2b}…$O_{nb,}$ P_{ob}), respectively, where (O_{1a}, O_{2a}…O_{na}) = (I_{1b}, I_{2b}… I_{nb}) = (O_{1b}, O_{2b}…O_{nb}) and P_{ob} = [$O_{1b}\oplus O_{2b}\oplus ... O_{nb}\oplus P_{ib}$].

The detection of faults can be done by assigning logic values to the input parity bits and checking the corresponding output parity bit. If P_{ia} and P_{ib} are assigned the same logic values, then P_{oa} and P_{ob} should be same or if P_{ia} and P_{ib} are assigned complementary logic values, then P_{oa} and P_{ob} should be complementary to prevent an erroneous result. Moreover, a testable cell TC is also proposed to detect faults consisting of multiple TRCs. The illustration below is based on implementing a testable Fredkin based 2×4 decoder. The results are given in terms of CMOS characteristics 2.249×10^{-9}μW dynamic power using 1496 numbers of transistors with a delay of 13.2ns. The method is efficient in terms of quantum cost, but the number of ancilla inputs increases to twice the number of TRC used to synthesize a circuit.

Illustration. Using Figure 18c, if P_{oa} = 0 and P_{ob} = 1, then P_{oa} = [$O_{1a}\oplus O_{2a}\oplus …O_{na}\oplus 0$] = $F_{oa}\oplus 0 = F_{oa}$and P_{ob} = [$O_{1b}\oplus O_{2b}\oplus …O_{nb}\oplus 1$] = $F_{ob}\oplus 1$ = ~F_{oa}. Since $F_{ob} = F_{oa}$, this implies Poa= ~P_{ob}. Hence, for a complementary input parity bit, output will always be complementary for correct operation of any circuit that can be checked using a dual-rail-checker circuit or proposed testable circuit called TC.

Design Using ETG for ESOP-Based Toffoli Circuits

Another idea for a testable design with existing circuit was proposed by Nayeem and Rice in 2011 for the detection of single and multiple bit faults. The idea is valid for the exclusive sum-of-product (ESOP)-based Toffoli circuits, which ensure a negligible increment in garbage on the cost of small increase quantum cost. The process of conversion of an ESOP circuit in its testable form unfolds in three steps. In the first step every n-bit Toffoli gate in the circuit is converted into (n+1)-bit ETG (Extended Toffoli Gate) (Chen et al., 2008) using an additional parity line without disturbing the original circuit. In the second step, CNOT gates are included from all the output lines to the parity line. In the third step, CNOT gates are again added from each input line to the parity line ahead and behind the complete circuit. This requires the addition of twice the number of CNOT gates as the number of input lines plus the number of outputs, which enhance quantum cost, but garbage output remains the same as in the original circuit. The steps of conversion of a given circuit in its testable form are shown in Figure 19. The fault is detected if the value of the output parity bit changes from 0 to 1 during its operation. This method is also valid for the ESOP circuit consisting of the inverted-Toffoli gate. The performance of this method is predicted in terms of quantum cost (QC) and garbage output (GO) by performing experiments on some benchmark circuits, as can be seen in Table 10.

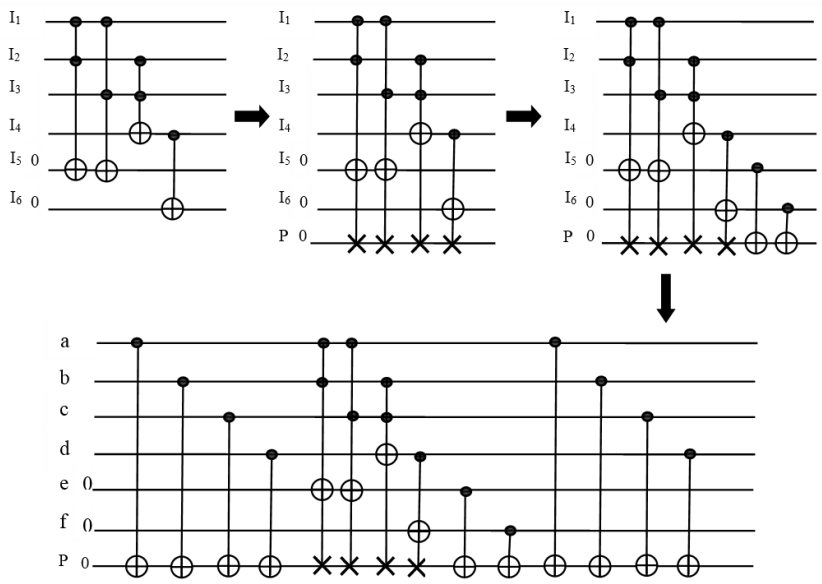

Figure 19. Conversion of ESOP-based circuit in its testable form (Nayeem & Rice, 2011).

Illustration. Mathematically, the output of the parity line *P* of build testable circuit shown in Figure 19 can be given as:

$$P \oplus a \oplus b \oplus c \oplus d \oplus ab \oplus ac \oplus bc \oplus (d \oplus bc) \oplus (e \oplus ab \oplus ac) \oplus (f \oplus d) \oplus a \oplus b \oplus c \oplus d$$

Since values of P, e and f are set logic 0 then,

$$a \oplus b \oplus c \oplus d \oplus ab \oplus ac \oplus bc \oplus (d \oplus bc) \oplus (ab \oplus ac) \oplus d \oplus a \oplus b \oplus c \oplus d$$

The solution gives the value of output of wire *P* as logic 0 if there are bit faults in the circuit or at the input and output of the circuit. If the value of output *P* changes to logic 1, a fault can be detected.

Design Using ETG for Toffoli-Based Circuits

The approach in previous section was extended by Nayeem and Rice (Vancouver, 2011) for any type of Toffoli circuit for the detection of single and multiple bit faults. An online testable circuit was constructed from a Toffoli circuit in similar manner except for the second step where, first a Toffoli gate was converted into an ETG connected to an additional parity line and then CNOT gates were inserted from all lines to parity lines before and after the original circuit. This required only double the number of lines as the number of additional CNOT gates compared to the previous method, as shown in Figure 20. The fault was also detected in the same manner by checking the logic value of output of parity line. Further, this technique was again extended for ternary Toffoli circuits (Nayeem & Rice, 2012). The detailed study was specified in Nayeem and Rice (2013), where a large number of benchmarks were used and a comparative study of proposed methods was given. Figures of merit are depicted in Table 10

in comparison to their previous approach.

The two methods in Nayeem and Rice (Canada, 2011; Vancouver, 2011) were efficient in terms of garbage output GO and ancilla input AI, but the quantum cost increased with the addition of CNOT gates. GO remained the same as that of the original circuit and only one AI was required to convert a circuit to its testable form. The basic difference between the respective methods was that the first was meant for ESOP-based circuits and the other was valid for all Toffoli circuits.

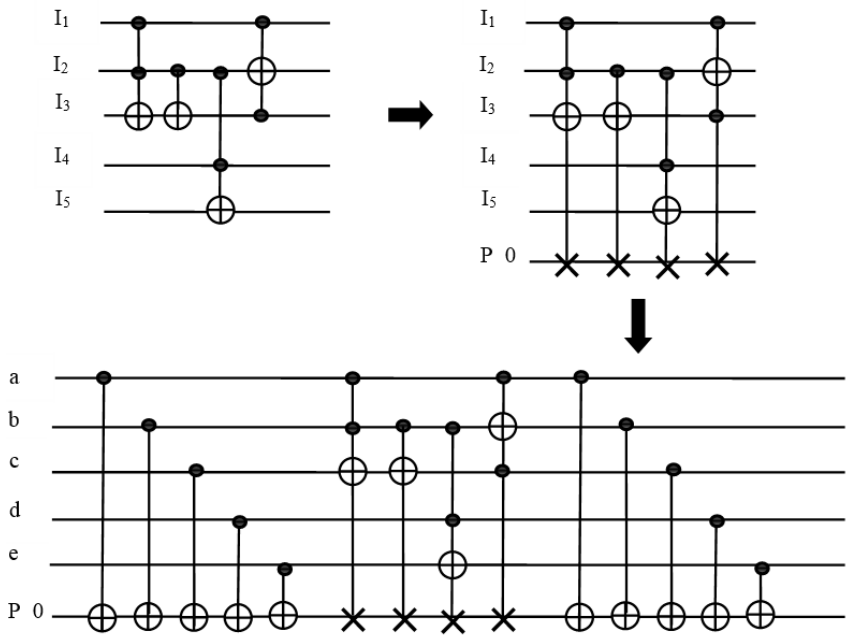

Figure 20. Conversion of a Toffoli-based circuit in its testable form Nayeem and Rice (Vancouver, 2011).

Table 10
Comparison and Operating Cost for Testable Design in Proposed Methods

Benchmarks	Nayeem et al. (Canada 2011; 2013)		Nayeem et al. (Vancouver 2011; 2013)	
	QC	GO	QC	GO
majority	154	5	154	5
con 1	184	7	184	7
misex 1	1040	8	439	8
ham7	259	7	162	7
rd32	49	3	45	3
alu2	4882	10	4551	10
9symml	11065	9	11066	9
alu4	48951	14	42071	14
nth prime3	607	7	575	7

Illustration. Mathematically, the output of the parity line *P* of the constructed testable circuit as shown in Figure 20 can be given as:

$$P \oplus a \oplus b \oplus c \oplus d \oplus e \oplus ab \oplus b \oplus bd \oplus a\,(c \oplus ab \oplus b) \oplus a \oplus [b \oplus a\,(c \oplus ab \oplus b)] \oplus (c \oplus ab \oplus b) \oplus d \oplus (bd \oplus e)$$

The solution gives a value of output of wire *P* as logic 0 when applying input logic 0 in the same manner if a bit fault had occurred in the circuit or at the input and output of the circuit. The value of output *P* changed to logic 1 from 0 and hence, a fault was detected.

Design Using Testable Toffoli and Peres

In this concern, Sen et al. (2012) also proposed a DFT methodology in which they demonstrated the idea of converting a reversible gate into its online testable form, ensuring detection of nearly all multiple bit faults. The authors introduced a DFT process algorithm based on parity generation using concurrent error detection. The algorithm renovated a reversible gate into its online testable form, and this resulted in three error detecting bits that were used to test a circuit. The testable 3×3 Toffoli gate was synthesized with input *A*, *B* and *C* and output *X*, *Y* and *Z* as shown in Figure 21. The fault can be noticed by error detecting bits P, Q and R. These bits should hold logic 0 values for a fault-free circuit operation. Similarly, a testable Peres gate was also proposed and the implementation of an online testable full adder was given for justification.

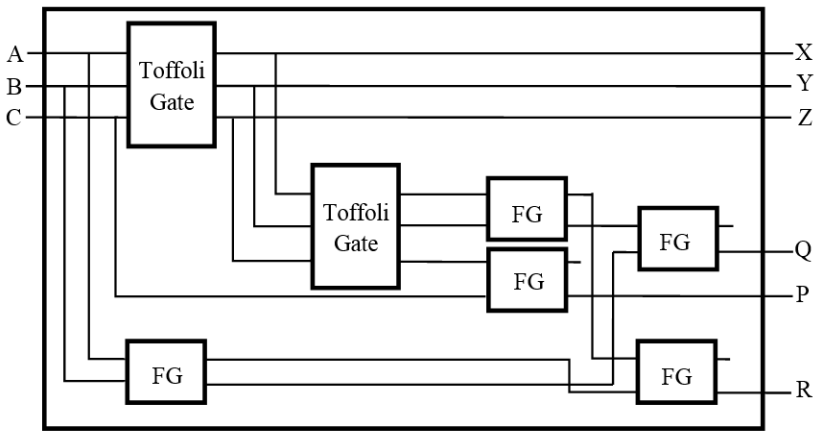

Figure 21. Online testable 3×3 Toffoli gate (Sen et al., 2012).

The performance of the proposed DFT was evaluated by performing experiments on the existing reversible gates, three benchmark circuits, full adder and full subtractor circuit, as shown in Table 11. The testable Toffoli gate had a quantum cost of 11 and a garbage output of 3. Hence, the quantum cost was much higher regardless of the lower gate count.

Table 11
Operating Cost of Testable Design in Proposed Method (Sen et al., 2012).

Benchmark circuit/Gate	GC
Peres gate	7
Toffoli gate	7
Fredkin gate	11
Full Adder with propagate	14
Full subtractor	21
ham3	21
3_17	49
Nth prime3	28

Illustration. Error detecting bits for a testable Toffoli gate as shown in Figure 21 can be calculated as:

$$P = (A \oplus B) \oplus (A \oplus B) = 0$$

$$Q = C \oplus C = 0$$

$$R = A \oplus A = 0$$

If single/multiple bit faults occur in any gate or at the wire, any values of error detecting bits flip to logic 1 and the fault can be detected.

Extracted Attributes of Designing with Existing Circuit

Extracted attributes of all the testing methods explained in this section are depicted in Table 12. These attributes appropriately compare all these methods. Comparison tables are also provided. It is found that the method suggested by Nayeem & Rice, Canada, 2011 and Nayeem & Rice, Vancouver, 2011 was better in performance in terms of minimum garbage output. Also, the first method was more efficient in terms of quantum cost and garbage output.

Table 12
Attributes of Designing with Existing Circuit Methods

Testing Method	Features	Demonstration table number
Mahammad et al., 2010	AI and GO are large due to TC, QC is comparatively small	-
Nayeem et al., Canada, 2011	QC large but minimum GO	10 and 11
Nayeem) et al., Vancouver, 2011	QC large but minimum GO	10 and 11
Sen et al., 2012	QC, NoI and GO are large per testable gate	10 and 11

DISCUSSION AND CONCLUSION

There are various methods in two broad classifications of designing with proposed gates and designing with existing circuits. These methods are claimed to cover all the faults in the new family of fault models. Detection is achieved by the detection of single and multiple bit faults. These methods are illustrated by performing experiments on benchmark circuits and evaluating results in terms of performance parameters. Final attribute tables in two respective sections suggest the pros and cons of each method, which can be used to determine the suitability for designing under online testability. The evaluation is summarized in Table 13 with testability technique, considered fault models and metrics that can well define their identity.

Table 13
Comparison Table of Discussed Online Testing Approaches

S No.	Author	Online Testability Approach	Fault model	Computed parameters
1	Vasudevan et al. (2004)	Propose testable Reversible Gates R1 & R2 and Parity Generation method for testing is used	Single Bit Fault	GC, GO
2	Vasudevan et al. (2006)	CMOS realization with previous testable technique is provided	Single Bit Fault	GC, GO
3	Thapliyal et al. (2007)	Parity Generation method for testing is used Proposed reversible gate OTG with Feynman gate	Single Bit Fault	GC, GO, D
4	Chowdhury et al. (2009)	Improved Rail-check circuit is proposed and R1 and R2 are used for parity generation	Single Bit Fault	GC, GO
5	Mahammad et al. (2010)	Reversible gate URG and testable design with existing circuit using parity generation	Single Bit Fault	-
6	Tahoori et al. (2010)	Reversible Gates with dual rail I/O	Single Bit Fault	NoI, GO, AI
7	Thapliyal et. al. (2010)	Concurrent error detection using OTG and majority voter scheme in QCA	Single/Multiple Bit Fault	GC, GO, QC, D
8	Nayeem et. al. (Canada, 2011)	Testable design with existing circuit for ESOP-based circuit	Single/Multiple Bit Fault	QC, GO
9	Nayeem et. al. (Vancouver, 2011)	Testable design with existing circuit for Toffoli-based reversible circuit	Single/Multiple Bit Fault	QC, GO
10	Tahoori et. al. (2011)	Reversible gates, namely FIG, DCG and LG for testability	MGF and RGF	GC, GO, D
11	Sen et. al. (2012)	Concurrent error detection technique based on parity	Single/Multiple Bit Fault	GC
12	Nayeem et. al. (2013)	Testable design with existing circuit for ESOP and non-ESOP-based Toffoli circuits	Single/Multiple Bit Fault	QC, GO

A comparison of implemented online testable combination circuits can be seen in Table 14 with performance measures. Table 4 presents CMOS-technology dependent measures like number of transistors and power dissipation. The online testable sequential circuits with performance measures can be seen in Table 5. Quantum cost is not reported by most researchers, but gate count is proportionally related to it. If the gate count is low, the quantum cost can be high; this depends on the complexity of the output function of the respective gates.

Table 14
Comparison Table for Online Testable Combinational Logic Circuits

Circuit	Vasudevan et al., 2004 & Vasudevan et al., 2006			Thapliyal et al., 2007			Thapliyal et al., 2010			Sen et al., 2012		
	QC	GO	GC	QC	GO	GC	QC	GO	GC	QC	GO	GC
Full adder without propagate	–	3	4	–	–	–	–	–	–	–	–	–
Full Adder with propagate	–	2	4	–	2	2	30	3	8	–	–	14
4-bit ripple carry adder	–	–	–	–	8	4	–	–	–	–	–	–
4-bit carry skip adder	–	–	–	–	17	22	–	–	–	–	–	–
Full subtractor	–	–	–	–	–	–	–	–	–	–	–	21

Table 15 summarizes all the covered benchmarking circuits (Maslov et al., 2015; Reversible benchmarks, 2015) with online testability along with the comparison of all discussed techniques on the basis of performance parameters (QC, GO, GC and AI). The comparison clearly points out differences in area/size and consequently, the increment and decrement of power dissipation in designing with testability for reversible logic. The method with the best possible results among the depicted two categories is shown in the highlighted blocks.

Table 15
Comparison Table for all Discussed Approaches

Benchmarks	Vasudevan et al.				Hasan et al.				Farazmand et al.				Nayeem et al. Can.2011				Nayeem et al. Van 2011				Zamani et al.				Sen et al.			
	QC	GO	NoG	AI	QC	GO	NoG	AI	QC	GO	NoG	AI	QC	GO	NoG	AI	QC	GO	NoG	AI	QC	GO	NoG	BrC	QC	GO	NoG	AI
xor5	_	8	81	_	_	20	16	_	_	112	_	116	_	_	_	_	_	_	_	_	_	_	_	_	_	_	_	_
t	_	16	81	_	_	_	_	_	_	48	_	40	_	_	_	_	_	_	_	_	_	_	_	_	_	_	_	_
b1	_	8	105	_	_	_	_	_	_	30	_	24	_	_	_	_	_	_	_	_	_	_	_	_	_	_	_	_
Majority	_	13	129	_	_	_	_	_	_	18	_	20	154	5	_	_	154	5	_	_		25	17	_	_	_	_	_
con 1	_	36	285	_	_	_	_	_	_	44	_	48	184	7	_	_	184	7	_	_	_	_	_	_	_	_	_	_
clip	_	37	309	_	_	_	_	_	_	1250	_	800	_	_	_	_	_	_	_	_	_	_	_	_	_	_	_	_
t481	_	412	3604	_	_	_	_	_	_	9534	_	958	_	_	_	_	_	_	_	_		9712	7283	_	_	_	_	_
rd53	_	90	777	_	_	180	156	_	_	212	_	220	_	_	_	_	_	_	_	_	_	_	_	_	_	_	_	_
misex 1	_	161	1401	_	_	_	_	_	_	134	_	118	1040	8	_	_	439	8	_	_	_	_	_	_	_	_	_	_
o64	_	258	1545	_	_	_	_	_	_	258	_	0	_	_	_	_	_	_	_	_	_	_	_	_	_	_	_	_
ham7	_	_	_	_	_	214	196	_	_	_	_	_	259	7	_	_	162	7	_	_	_	_	_	_	_	_	_	_
rd32	_	_	_	_	_	51	44	_	_	_	_	_	49	3	_	_	45	3	_	_	_	_	_	_	_	_	_	_
ham3	_	_	_	_	_	39	36	_	_	_	_	_	_	_	_	_	_	_	_	_	_	_	_	_	_	_	21	_
3_17	_	_	_	_	_	63	56	_	_	_	_	_	_	_	_	_	_	_	_	_	_	_	_	_	_	_	49	_
b9	_	_	_	_	_	_	_	_	_	_	_	_	_	_	_	_	_	_	_	_	_	815	587	_	_	_	_	_
alu2	_	_	_	_	_	_	_	_	_	_	_	_	4882	10	_	_	4551	10	_	_	_	1859	1385	_	_	_	_	_
nth prime3	_	_	_	_	_	_	_	_	_	_	_	_	607	7	_	_	575	7	_	_	_	_	_	_	_	_	28	_

It is observed that the bijective property in reversible logic is maximally utilised for online testability. One can easily generate or preserve information of input and output vectors in the form of parity. In reversible circuits TB (Vasudevan et al., 2004; Vasudevan et al. 2006) and CTSG (Thapliyal & Vinod, 2007), a fault was detected by generating two output parity bits. Sometimes, a reversible gate (Mahammad & Veezhinathan, 2010) or a circuit (Nayeem & Rice, Canada, 2011; Vancouver, 2011; 2013) was modified in order to generate parity bits by adding an extra wire and CNOT gates. Also, it was used along with a concurrent error detection technique (Sen et al., 2012) to generate error-detecting information. Moreover, the method of concurrent error detection in collaboration with parity generation was used in Thapliyal and Ranganathan (2004) and Sen et al. (2012). Dual-rail-coding (Farazmand et al., 2010) methods also utilised this fact for testability in reversible circuits. It was also observed that quantum cost was slightly improved, but the optimization of ancilla input and garbage output still required more effort by the researchers.

We have presented a comparative study of online testability in reversible logic circuits along with a brief illustration of each method by combining all possible fault models and performance metrics. The major challenges pertaining to online testability are presented. The paper also projects the role of garbage output and ancilla inputs in increasing power dissipation. Furthermore, the reliability of the method of parity preservation and generation, concurrent error detection and dual-rail coding techniques in designing for testability is discussed. Despite significant progress in online testability of reversible logic, new techniques will always arise to replace existing ones. This paper points out the considerable issues in this area and encourages the development of new strategies to face a new era of reversible logic because several challenges remain.

REFERENCES

Barenco, A., Bennett, C.H., Cleve, R., DiVincenzo, D. P., Margolus, N., Shor, P., Sleator, T., Smolin, J. A., Weinfurter, H. (1995). Elementary gates for quantum computation. *Journal Physical Review A.52*(5), 3457-3467.

Bennett, C. H. (1973). Logical reversibility of computation. *Journal of Research and Development - IBM, 17*(6), 525-532.

Chen, J., Zhang, X., Wang, L., Wei, X., & Zhao, W. (2008). Extended Toffoli gate implementation with photons.*Proceedings of 9th International Conference on Solid-State and Integrated-Circuit Technology* (p.575-578).

Chua, S. C., & Singh, A. K. (2014). Heuristic synthesis of reversible logic – A comparative study. *Advances in Electrical and Electronics Engineering, 12*(3), 210-225.

Farazmand N., Zamani M., & Tahoori M. B. (2010).Online fault testing of reversible logic using dual rail coding. *Proceedings of 16th IEEE International Symposium on On-Line Testing (IOLTS)*(pp. 204-205).

Feynman, R. P. (1985).Quantum mechanical computers. *Optics News, 11*, 11-20.

Fredkin, E., & Toffoli, T. (1982).Conservative logic. *International of Journal Theoritical Physics*, *21*(3-4), 219-253.

Gaur, H.M., Singh, A. K., & Ghanekar, U. (2015). A review on online testability for reversible logic. *Procedia Computer Science, 70,* 384-391.

Golubitsky, O., & Maslov, D. A.(2012). Study of optimal 4-bit reversible Toffoli circuits and their synthesis. *IEEE Transactions on Computers, 61*(9), 1341-1353.

Hasan, M., Tauhidul, Islam, A. K. M., & Chowdhury, A. R. (2009).Design and analysis of online testability of reversible sequential circuits. *Proceedings of 12th IEEE International Conference on Computer and Information Technology* (pp. 180-185).

Hayes, J. P., Polian, I., & Becker, B. (2004).Testing for missing gate faults in reversible circuits. *Proceedings of 13th IEEE Asian Test Symposium (ATS)*(pp. 100-105).

Hurst, S. L. (1998). *VLSI testing – Digital and mixed analogue/digital techniques*. London, United Kingdom: The Institution of Electrical Engineers.

Jha N. K., & Gupta S. (2003). *Testing of digital systems*. Cambridge University Press.

Kautz, W. H. (1967). Testing for faults in combinational cellular logic arrays. *Proceedings IEEE Conference on Record of the Eighth Annual Symposium on Switching and Automata Theory* (pp. 161-174).

Landauer, R. (1961). Irreversibility and heat generation in the computing process. *IBM Journal of Research and Development*, *5*(3), 183-219.

Mahammad, S. K. N., & Veezhinathan, K. (2010).Constructing online testable circuits usingreversible logic. *IEEE Transaction on Instrumentation & Meas*urement, *59*(1), 101-109.

Maslov, D., Dueck, G., & Scott, N. (2015, October). Reversible logic synthesis benchmark. Retrieved from http://www.cs.uvic.ca/~dmaslov.

Maslov, D., & Dueck, G. W. (2015, October). Garbage in reversible designs of multiple output functions. Available at http://cs.unb.ca/profs/gdueck/reversible/multiple.pdf.

Mohammadi M., & Eshghi M. (2009). On figures of merit in reversible logic design. *Springer Journal of Quantum Information Processing, 8*(4), 297-318.

Nayeem, N. M., & Rice, J. E. (2012). A new approach to online testing of TGFSOP-based Ternary Toffoli circuits. *42nd IEEE International Symposium on Multi-Valued Logic* (pp. 315-321).

Nayeem, N. M., & Rice, J. E. (2011). A shared-cube approach to ESOP-based synthesis of reversible logic. *Facta. Univ. Series. Electron Energetics, 24*(3), 385-402.

Nayeem N. M.,&Rice, J. E. (2011).A simple approach for designing testable reversible circuits. *Proceedings of IEEE Pacific Rim. Conference Comm. and Signal Processing (PACRIM)*(pp. 85-90). Victoria, Canada.

Nayeem, N. M., & Rice, J. E. (2011). Online fault detection in reversible logic.*Proceedings of IEEE SymposiumDefect and Fault Tolerance in VLSI and Nanotechnology system (DFT)*(pp. 426-434). Vancouver.

Nayeem, N. M., & Rice, J. E. (2013).Online testable approaches in reversible logic. *Journal of Electronic Testing, 29*(6), 763-778.

Patel, K. N., Hays, J. P., & Markov, I. L. (2004). Fault testing for reversible logic. *IEEE Transacton on CAD of Integrated Circuits and Systems, 23*(8), 1220-1230.

Peres, A. (1985).Reversible logic and quantum computers. *Physical Review A, 32*(6), 3266-3276.

Polian, I., Hayes, J. P., Fiehn, T., & Becker, B. (2005).A family of logical fault models for reversible circuits. *Proceedings of the 14th Asian Test Symposium (ATS)* (pp.422-427). Calcutta.

Rahaman, H., Kole, D., Das, D., & Bhattacharya, B. B. (2007).Optimum test set for bridging fault detection in reversible circuits. *Proceedings of 16th Asian Test Symposium* (p125-128).

Rahaman, H., Kole, D. K., Das, D. K., & Bhattacharya, B. B. (2011). Fault diagnosis in reversible circuits under missing-gate fault model. *Computers and Electrical Engineering, 37*(4), 475-485.

Sen, B., Das, J., & Sikdar, B. K. (2012). A DFT methodology targeting online testing of reversible circuit. *IEEE International Conference of Devices, Circuits and Systems,* pp.689-693.

Shende, V. V., Prasad, A. K., Markov, I. L., & Hayes, J. P. (2003). Synthesis of reversible logic circuits. *IEEE Transacton on CAD of Integrated Circuits and Systems 22*(6), 710-722.

Tabei, K., & Yamada, T. (2005). On generating test sets for reversible circuits. *Proceedings of 14th IEEE Asian Test Symposium* (p.422-427).

Thapliyal, H., & Vinod, A. P. (2007).Designing efficient online testable reversible adders with new reversible gate. *Proceedings of IEEE International Symposium on Circuits and Systems (ISCAS)* (pp.1085-1088). New Orleans.

Thapliyal, H., & Ranganathan, N. (2004). Reversible logic based concurrent error detection methodology for emerging nanocircuit. *Proceedings of 10th IEEE International Conferencence on Nano Technology* (pp.217-222).

Toffoli, T. (1980). Reversible computing. *Proceedings of Automata, Lang. Program Conference* (pp. 632-644).

Vasudevan, D. P., Lala, P. K., Jia, D., & Parkerson, J. P. (2006). Reversible logic design with online testability. *IEEE Transaction on Instrumentation & Measurement, 55*(2), 406-414.

Vasudevan, D. P., Lala, P. K., & Parkerson, J. P. (2004).Online testable reversible logic circuit design using NAND blocks. *Proceedings of 19th IEEE International Symposium on Defect Fault Tolerance on VLSI Systems.*(pp. 324-331).

Zamani, M., & Tahoori, M. B. (2011). Online missing/repeated gate faults detection in reversible circuits. *Proceedings of IEEE Int. Symp. Defect and Fault Tolerance in VLSI and Nanotechnology Systems* (pp. 435-442).

Zhong, J., & Muzio, J. C. (2006) Analyzing fault models for reversible logic circuits. *Proceedings of IEEE Congress on Evolutionary Computation (CEC)* (pp. 2422-2427).

Pertanika J. Sci. & Technol. 24 (2): 273 - 283 (2016)

PERTANIKA JOURNALS

SCIENCE & TECHNOLOGY

Journal homepage: http://www.pertanika.upm.edu.my/

Seismic Response of a Light Rail Transit Station Equipped with Braced Viscous Damper

Fateh, A., Hejazi, F.*, Ramanathan, R. A. and Jaffar, M. S.

Department of Civil Engineering, Faculty of Engineering, Universiti Putra Malaysia, 43400 Serdang, Selangor, Malaysia

ABSTRACT

The use of the Light Rail Transit (LRT) system is currently preferred because LRT is sustainable, improves travel options and facilitates swift mobility in urban areas. Hence, the structural stability and safety of this public transportation system against seismic occurrences are indispensable. Given that these structures cannot be considered conventional frames because of their complex architectural design, focussing meticulously on reliable seismic design codes and structural rehabilitation techniques is vital for the design of the lateral resistance system. One Malaysian LRT station is considered in this study, and the seismic response of this train station when equipped with supplementary viscous damper devices is evaluated. Thus, the LRT station is modelled through finite element simulation. The methods of seismic analysis are limited to linear seismic analyses, namely, response spectrum and time history analyses. Results derived in this study show a significant improvement in structural response when the station is fitted with dampers; approximately 40% reduction in displacement is observed at the top joint of the roof. Furthermore, the lateral base shears decrease by approximately 70%.

Keywords: Brace viscous damper, time history analysis, light rail transit, response spectra

INTRODUCTION

The general use of Light Rail Transit (LRT) is preferable because LRT is sustainable, improves travel options and facilitates swift mobility in urban areas. Hence, the safety of this type of public transportation against seismic occurrences is indispensable. Considering that LRT systems cannot be erected on conventional frames because of their architectural complexity, focussing meticulously on reliable seismic design codes

Article history:
Received: 8 January 2015
Accepted: 4 February 2016

E-mail addresses:
amirfateh.saze@yahoo.com (Fateh, A.),
farzad@fhejazi.com (Hejazi, F.),
ramesh-86@hotmail.com (Ramanathan, R. A.)
msj@upm.my (Jaffar, M. S.)
*Corresponding Author

ISSN: 0128-7680

and structural rehabilitation is vital. The misconception by Malaysians that the country is free from earthquake disasters has become the main concern of engineers in Malaysia in analysing and designing structures without accounting for the possibility of an earthquake and thereby, even going for retrofitting of the existing structures.

Peak Ground Acceleration (PGA) plays an important role in design and earthquake load determination. Given the fact Malaysia does not have any reliable and economic seismic code, local engineers utilise the specifications of available international codes to determine the seismic loads to be applied. The direct application of international standards, such as the Uniform Building Code UBC 1997 or the American Assocation of State Highway and Transport Officials Standard Specifications for Highway Bridges AASTHO 1996, to determine such loads has resulted in high construction costs because of the overestimation of PGA for Malaysia in the absence of sufficient seismic data for Malaysian conditions.

REVIEW OF LITERATURE AND STUDY SCOPE

The Lam stochastic model was introduced to simulate the elastic response spectra (5% critical damping) of large-magnitude long-distance earthquakes generated by the Sunda Arc subduction source in Indonesia (Lam et al., 2009). A new set of attenuation relationships for PGA, peak ground velocity and response spectrum analysis in rock sites caused by distant Sumatran-subduction earthquakes have been derived for Singapore and Peninsular Malaysia based on synthetic seismograms that account for source and path effects (Megawati et al., 2003; 2005). A previous study investigated potential effective factors, such as site ground response, variation in the water table and soil properties, in the response of a structure to multi-directional earthquake loading (Yang & Yan, 2009). The spatial effects on the seismic responses of large structures with two-line support were studied. The 3D variation in ground motion was modelled with an empirical coherency loss function. Numerical outcomes indicated that horizontal multi-support excitations have a large amplification effect on the seismic responses of the trussed arch (Su et al., 2006; 2007).

In the present study, the seismic response of an LRT station located in Kuala Lumpur, Malaysia was evaluated. Time history analysis was performed using the Structural Analysis Programme (i.e. SAP-2000) by modelling structures ‘with’ and ‘without’ the brace viscous damper. In other words, in this study the damper element was introduced as a supplementary energy dissipation device to the existing station’s frame and the seismic behaviour of the mentioned frame was assessed. The efficiency of deployment of SAP-2000 in dynamic analysis was established based on the results derived (Behnia et al., 2013).

MATERIALS AND METHODS

Detail of the Case Study

The structure of the study station is supported by three reinforced concrete (RC) column piers attached to the foundations located on the road shoulders. The spacing between the supporting column piers is orthogonal to the carriageway. The guide way structure varies between 13.0 and 16.5 m and is repeated every 12.0 m along the viaduct piers, as shown in Figure 1. The

station consists of steelwork, fabricated plated steel sections spanning continuously between the supporting RC piers and simply supported precast pre-stressed hollow core slabs with over 12 m spans. The steel girders are supported on laminated elastomeric bearing pads to reduce the risk of damage to the RC piers caused by the rotation of the beams being loaded. A series of one-way and two-way RC slab frameworks spanning onto in situ RC beams are in turn supported by RC columns. The design is independent of the viaduct structure to prevent dynamic loads from the rail from propagating into the station structure. The roof is pinned or fixed to a curved truss frame, stable on its own plane by virtue of moment continuity throughout, and exhibits 1 to 3 degrees of static indeterminacy. The resistance of the base is improved with the use of a continuous plate girder that effectively acts as the base tie. On-elevation lateral stability in the orthogonal direction to the plane of the frame is provided by tie-bracing or moment frame trusses or beams. Roof diaphragm action is ensured with the use of on-plan tie-bracing and roof sheeting. For the stations constructed with reinforced concrete, the rigid connection between the RC girders and piers ensures a portalised framing on-elevation lateral stability configuration. On-elevation lateral stability between the concourse level and the platform is provided by the inherent-moment connections between the in situ RC columns and beams. The building is founded on RC pile caps and in situ bored RC piles. Tie-beams between these pile caps are employed to resist the pile out-of-tolerance moments and ensure robustness and rigidity. These tie-beams also resist the bending action caused by vehicular impact loading. In order to evaluate the dynamic behaviour of LRT station time history as well as response spectrum analyses (RSA) was performed. Time history analysis shows the response of a structure over seismic time history record. Furthermore, the results were separated for each direction of motion to assess the seismic behaviour of structure with the existence of a damper. This study was performed for evaluation of an elevated light rail transit station. In the case of an underground station, a few design considerations and parameters such as soil pressure should be included during modelling. Therefore, the evaluation of seismic response of an underground station is out of this study scope.

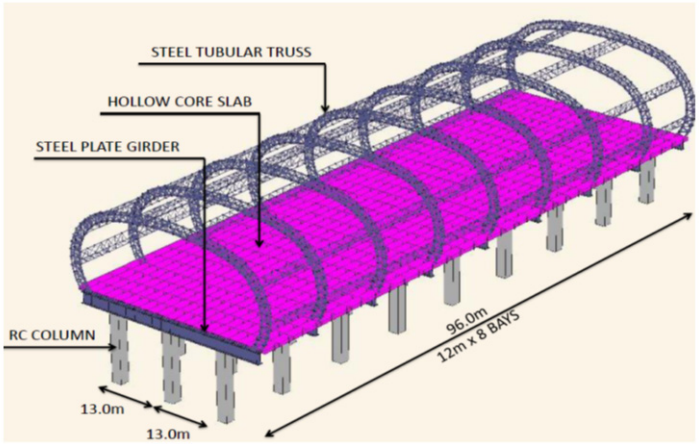

Figure 1. Structural layout of the LRT station.

Software Model Detail

This research was carried out by employing the modelling techniques and capabilities of SAP-2000. As illustrated in Figure 2, the model comprised a 3D space frame model founded on fixed supports. Two models were created to represent the station 'with' and 'without' dampers so as to analyse the different impact. The models were analysed through linear dynamic time history analysis.

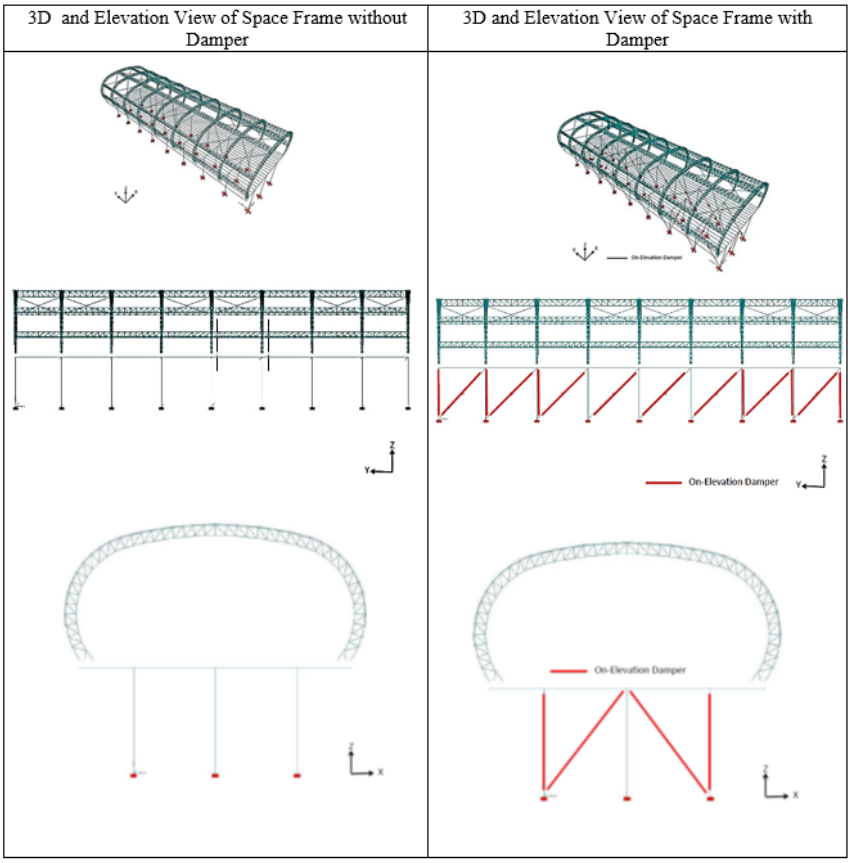

Figure 2. 3D space frame models 'with' and 'without' dampers.

Loading Details

The material densities adopted in the calculation of loads were based on British Standards, schedule of weights of building materials (BS 648:198). Live load reduction in accordance with loading for buildings, code of practice for dead and imposed loads (BS 6399-1:1995) was inapplicable because of the relative low-rise nature of the station buildings. Wind loads were calculated in accordance with Loading for buildings, Code of practice for wind loads (BS 6399-2) and Malaysian Standards, code of practice on wind loading for building structure (MS 1553:2002). Vehicular impact loads were considered in the design of the primary station piers over the vehicular trafficked roads according to British Standards, the design of highway

bridges for vehicle collision loads (BD 60), which stipulates an equivalent static load of 1000 kN at 3.0 m and 500 kN at 1.5 m above the carriageway level parallel to traffic direction and half of the above values for the orthogonal direction. All structures were designed for the worst combination of loading. Different load combinations were considered to fulfil the ultimate limit state and serviceability limit state criteria, which are based on structural use of concrete, Code of practice for design and construction, BS 8110 and structural use of steelwork in building, BS 5950. Since the station consisted of a variety of structural elements such as RC frame and steel girder and was subjected to the various types of load such as wind, earthquake and moving loads, use of different design codes was inevitable.

Construction Materials and Structural Control Specifications

In the reinforced concrete elements, longitudinal reinforcement bars (Type 2 deformed grade T460), that is, threaded rebar with minimum characteristic yield strength of 460 N/mm^2, were utilised. Shear links were of grade R250, that is, plain rebar with minimum yield strength of 250 N/mm^2. The mesh reinforcement, BRC, had minimum characteristic yield strength of 485 N/mm^2. The grades and properties of the hollow core slab were based on the specifications of the renowned prefabricator, Eastern Pretech (Malaysia) Sdn. Bhd. The properties of the damper are damping coefficient of 490 KN m/s, brace stiffness of 98066 KN/m and brace-damper mass of 1360 KNs^2/m; these properties were based on a previous study (Panah et al., 2008).

Seismic Analysis and Software Modelling Procedure

A general overview of different analysis methods is presented in Figure 3. Modal analyses were performed to determine the modes of vibration of the LRT station. The modes were utilised as the basis of modal superposition in the time history analysis. In the modal analyses, the structural system of the LRT station was relatively regular and suitable for either single-dominant modal response analysis or multi-modal response analysis. To evaluate the response of all modes of vibration with a significant contribution to the global response, the following conditions were considered and should be satisfied for each direction as stated in the Euro code EC8.

Firstly, the effective modal masses for the modes considered should be at least 90% of the total mass of the structure. Secondly, all modes with effective modal masses greater than 5% of the total mass must be considered. Modal analysis, which defines the fundamental modes inclusive of participating masses was established for both un-damped and damped structures. A linear time history analysis of the LRT station was performed with the El Centro 1940 earthquake as 3D excitation (X, Y and Z). The displacement and base reactions were the benchmark for the comparison. The process of seimic evaluation of LRT station is shown in Figure 3.

RESULTS AND DISCUSSION

Four parameters were compared to check the response of the proposed models in linear static and dynamic analyses. The three parameters are the three natural vibration periods of the sample buildings, participating mass ratios, displacements of the buildings and base shear

of the buildings. Understanding the modelling features is critical to obtaining an idea of the situation before viewing the results of all the analyses. Figure 4 shows the essential elements that pertain to the important features of the model.

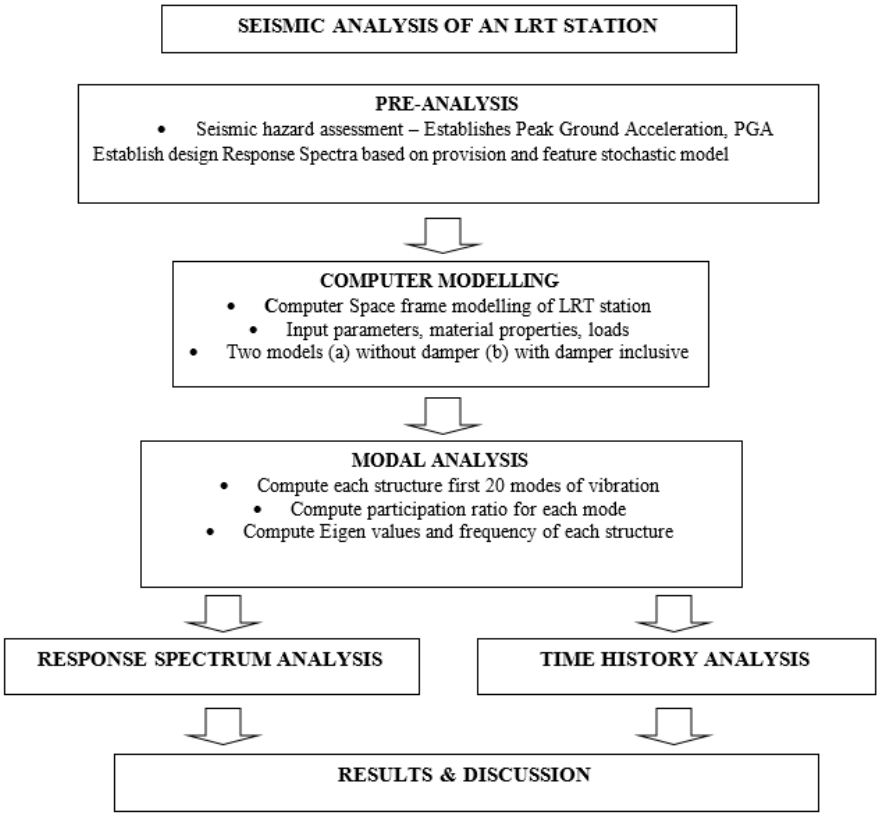

Figure 3. Seismic analysis procedure of the LRT station

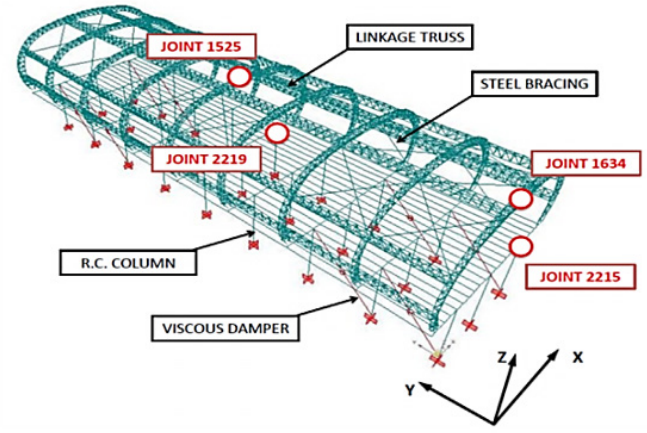

Figure 4. LRT station FE 3D model

Modal and Linear Time History Analyses

Twenty Eigen modes were selected during pre-analysis and their equivalent frequencies and periods were calculated. The dominant period for the un-damped case was 1.594 s, whereas for the damped case it was 0.938 s. Time history analysis was performed in X, Y and Z directions for the station building structures. The displacement and base shear results were evaluated for both models (damped and un-damped). The acceleration time record of the El Centro earthquake was applied directly to the base of the station building structure for both models in all the three directions. The excitation in the lateral directions (X and Y) produced significant responses. By contrast, the excitation in the vertical direction (Z) produced no significant change in the responses. The time history response at each joint was derived from the analysis. The results showed a limited response of the LRT station for 20 seconds of the entire duration of the earthquake, which was 50 s. However, the critical components of the earthquake fell within the first 20 s. Apart from the maximum responses, a time-dependent function was also obtained; hence, a dynamic response can be plotted with respect to time. Similarly, four joints were selected through Response Spectrum Analysis (RSA) to display the response to time history excitation. Figures 5 and 6 show the displacement response to earthquake excitation in X and Y directions in relation to the damped and un-damped models at different locations. The provision of viscous dampers caused a significant decrease in response. Two joints at the top of the tubular roof structure (Joints 1525 and 1634) exhibited approximately 40% reduction for the damped condition even though the damper was not physically connected to any part of the roof structure. Furthermore, two joints at the top of the RC column or piers (Joints 2219 and 2215) showed approximately 90% reduction for the damped condition. Contrary to the roof joints, the column at Joint 2215 was directly connected to the damper and thus allowed for high dissipation of energy, which in turn reduced the displacement significantly. Figure 7 shows the base shear time-dependent graphs obtained through time history analysis in X and Y directions for the two models, namely, the damped and un-damped structures. Comparison of the un-damped and damped structures indicated more than 60% reduction in Y direction and 71% in X direction in accordance with the overall base shear.

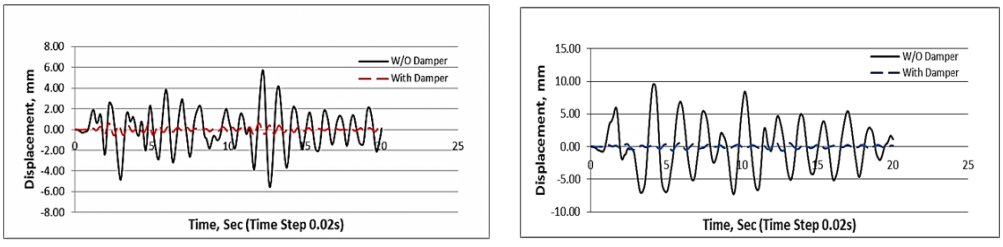

a) X direction displacement

b) Y direction displacement

Figure 5. Time history displacement for Joints 1525 and 1634, Roof Top Node

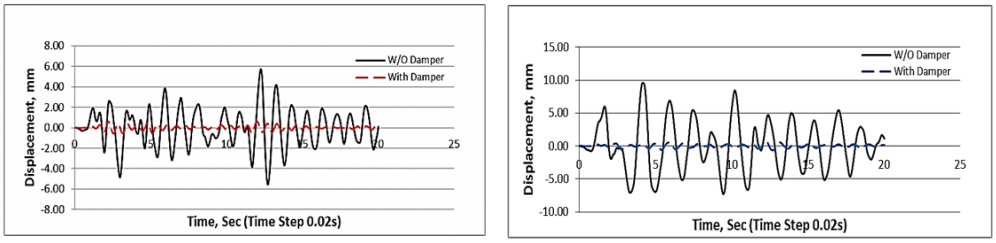

a) X direction displacement

b) Y direction displacement

Figure 6. Time history displacement for Joints 2215 and 2219, RC Column Top Node

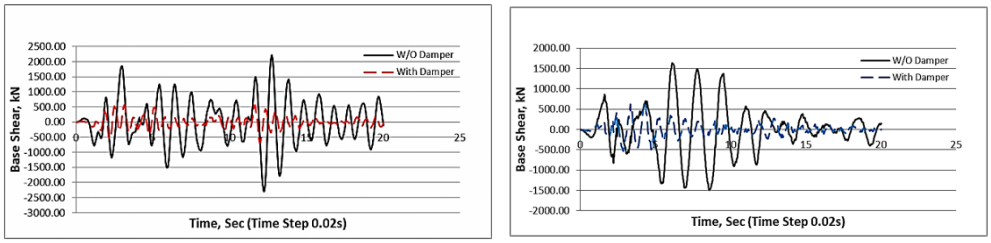

a) X direction base shear

b) (a) Y direction base shear

Figure 7. Time history of base shear

Modal Analysis

Modal analysis is a prerequisite for both analysis cases. Based on the abovementioned conditions, 20 Eigen modes were selected during pre-analysis. Their equivalent frequencies and periods were calculated. The dominant period for the un-damped case was 1.594 s whereas for the damped case it was 0.938 s.

Response Spectrum Analysis

The response spectrum curve is plotted in Figure 8. The RSA of the structure was performed for the un-damped and damped LRT station structures and the results were separated for each direction of motion. Differential displacements in all three global directions obtained from the comparison of the damped and un-damped structures are shown in Table 1 together with the corresponding percentage of reduction for ease of comparison.

The displacements were confined to four predefined joints within the model, which were used as the basis for discussion.

1. Two joints at the top of the tubular roof structure (Joints 1525 and 1634) exhibited more than 40% reduction for the damped condition even though the damper was not physically connected to any part of the roof structure.
2. Two joints at the topmost point of the RC column or piers (Joints 2219 and 2215), which were connected to the damper element (damped model), showed more than 80% reduction compared to the un-damped model.

Comparison of the four predefined design response spectra showed more than 75% reduction in overall base shear (Table 2). Generally, the introduction of dampers to the structure reduced the inherited frequency of the structure, which was inversely proportional to the natural period of vibration, and affected the overall equivalent static earthquake load applied to the structure, which in turn, reduced the base shear.

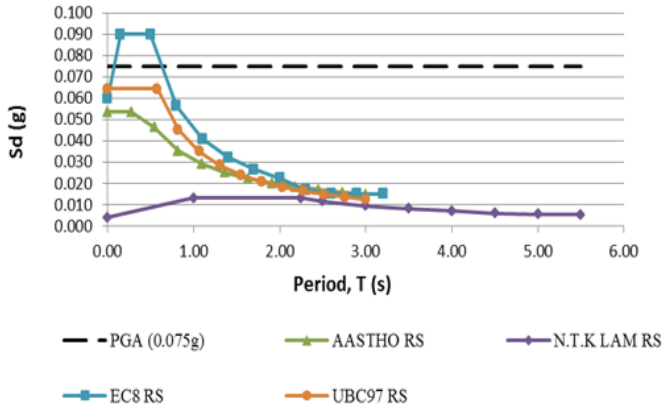

Figure 8. Summary of the Seismic Design Response Spectrum Curve

Table 1
Displacement in the Damped and Un-damped Structures

Response Spectrum Curve		Un-damped Structure			Damped Structure			Reduction (%)		
		dx (mm)	dy (mm)	dz (mm)	dx (mm)	dy (mm)	dz (mm)	dx	dy	dz
JOINT 1525	ASSHTO	1.463	2.171	0.563	0.691	0.971	0.555	52.77	55.27	1.42
	UBC97	1.769	2.274	0.742	0.968	1.202	0.732	45.28	47.14	1.35
	EC8	2.177	2.728	1.043	1.212	1.473	1.029	44.33	46.00	1.34
	LAM.S	0.613	1.248	0.095	0.158	0.373	0.093	74.23	70.11	2.11
JOINT 1634	ASSHTO	1.361	2.184	0.43	0.722	0.989	0.429	46.95	54.72	0.23
	UBC97	1.642	2.288	0.559	1.009	1.224	0.559	38.55	46.50	0.00
	EC8	2.017	2.745	0.778	1.261	1.499	0.772	37.48	45.39	0.77
	LAM.S	0.574	1.255	0.101	0.168	0.38	0.093	70.73	69.72	7.92
JOINT 2215	ASSHTO	0.626	1.36	0.006	0.031	0.016	0.002	95.05	98.82	50.87
	UBC97	0.753	1.419	0.007	0.043	0.02	0.003	94.29	98.59	43.61
	EC8	0.925	1.701	0.008	0.054	0.025	0.005	94.16	98.53	36.38
	LAM.S	0.265	0.786	0.002	0.007	0.006	0.001	97.32	99.20	61.35
JOINT 2219	ASSHTO	0.787	1.362	0.007	0.032	0.015	0.003	95.93	98.90	57.14
	UBC97	0.945	1.42	0.008	0.045	0.019	0.005	95.24	98.66	37.50
	EC8	1.16	1.703	0.011	0.056	0.023	0.006	95.17	98.65	45.45
	LAM.S	0.334	0.787	0.003	0.007	0.006	0.001	97.90	99.24	66.67

Table 2
Base Reaction for Damped and Un-damped Structures

Response Spectrum Curve	Un-damped Structure			Damped Structure			Reduction (%)		
	Fx (kN)	Fy (kN)	Fz (kN)	Fx (kN)	Fy (kN)	Fz (kN)	Fx	Fy	Fz
ASSHTO	251.84	190.42	44.73	54.29	32.39	44.92	78.44	82.99	0.43
UBC97	302.59	198.59	58.99	76.05	40.13	59.18	74.87	79.79	0.32
EC8	371.51	238.16	82.96	95.25	49.31	83.22	74.36	79.29	0.32
LAM.S	106.84	109.99	7.52	12.43	12.36	7.52	88.36	88.77	0.11

CONCLUSION

The seismic behaviour of a structure in terms of displacement and base shear was determined. The numerical results for the two models (un-damped and damped) clearly indicate that the dampers reduced the seismic response of structures in an extremely efficient manner. The horizontal displacements of the joint at the top of the structure were reduced by 40% for both the RSA and time history cases. Consequently, the horizontal displacements of the joint at the top of the column or pier were reduced by 80% and 90% for the RSA case and time history cases, respectively. Lastly, the lateral base shears were reduced by 75% and 65% for the RSA and time history cases, respectively. The benefits of damper application in the LRT station were demonstrated by the comparative data provided above. Therefore, it can be inferred that an improvement in the performance of the structure during earthquake excitation was observed from the modelling study.

ACKNOWLEDGEMENTS

This work received financial support from the Ministry of Higher Education of Malaysia under FRGS Research Project Nos. 5524254 and 5524256 and was further supported by University Putra Malaysia under Putra Grant No. 9415100. The support provided is gratefully acknowledged.

REFERENCES

AASHTO (1996). *American Association of State Highway and Transportation, Officials Standard Specifications for Highway Bridges* (16th ed.). AASHTO.

Behnia, A., Chai, H. K., Ranjbar, N., Behnia, N., Fateh, A., & Mehrabi, N. (2013). Effects of coordinated crowd motion on dynamic responses of composite floors in buildings. *The IES Journal Part A: Civil & Structural Engineering, 6*(1), 1-7.

British Standard. (1985). *BS 8110-1: 1985, Structural Use of Concrete: Part 1: Code of Practice for Design and Construction*. British Standard Institute.

British Standard. (1995). *BS 6399-2: 1995: Wind Loads.* British Standard Institute.

European Standard. (1998). EN 1998-1 Part 1: General rules, seismic actions and rules for building, *European Standard NF EN*, *1*.

Lam, N. T. K., Balendra, T., Wilson, J. L., & Venkatesan, S. (2009). Seismic load estimates of distant subduction earthquakes affecting Singapore. *Engineering Structures, 31*(5), 1230-1240.

Mayes, R. L., Buckle, I. G., Kelly, T. E., & Jones, L. R. (1992). AASHTO seismic isolation design requirements for highway bridges. *Journal of Structural Engineering, 118*(1), 284-304.

Megawati, K., Pan, T. C., & Koketsu, K. (2003). Response spectral attenuation relationships for Singapore and the Malay Peninsula due to distant Sumatran-fault earthquakes. *Earthquake Engineering & Structural Dynamics, 32*(14), 2241-2265.

Megawati, K., Pan, T. C., & Koketsu, K. (2005). Response spectral attenuation relationships for Sumatran-subduction earthquakes and the seismic hazard implications to Singapore and Kuala Lumpur. *Soil Dynamics and Earthquake Engineering, 25*(1), 11-25.

Malaysian Standard (2002). MS 1553: 2002: Code on Practice on Wind Loading for Building–1023.

Panah, E. Y., Noorzaei, J., Jaafar, M. S., & Seifi, M. (2008). Earthquake response of steel building with viscous brace damper. In *Proc. of International Conference on Construction and Building Technology, ICCBT* (pp. 59-68).

Su, L., Dong, S. L., & Kato, S. (2006). A new average response spectrum method for linear response analysis of structures to spatial earthquake ground motions, *Engineering Structures, 28*(13), 1835-1842.

Su, L., Dong, S., & Kato, S. (2007). Seismic design for steel trussed arch to multi-support excitations. *Journal of Constructional Steel Research, 63*(6), 725-734.

Yang, J., & Yan, X. R. (2009). Factors affecting site response to multi-directional earthquake loading. *Engineering Geology*, *107*(3), 77-87.

International Conference of Building Officials. (1997). Uniform building code, International Conference of Building Officials.

Pertanika J. Sci. & Technol. 24 (2): 285 - 294 (2016)

SCIENCE & TECHNOLOGY

Journal homepage: http://www.pertanika.upm.edu.my/

A Path Analysis of Mental Health among Thai Elderly with Diabetes Mellitus

Chonticha Kaewanuchit

Department of Applied Sciences, Faculty of Science and Technology, Phranakhon Si Ayutthaya Rajabhat University, Phranakhon Si Ayutthaya province, Thailand 13000

ABSTRACT

The study objectives are to verify a path analysis of mental health among Thai elderly with diabetes mellitus. The sampling method used is stratified random sampling. The sample size comprises 2,000 Thai elderly persons over 60 years old with diabetes mellitus. The variables are divided into individual (food, exercise, BMI and drugs), psychological (illness perception) and social factors (family support). Data are analysed using path analysis. The total variables described mental health change by 64.5%. It was found that exercise, illness perception, food and drugs as variables had a direct influence on mental health with standardised regression weights of 0.732, 0.347, 0.243 and 0.050, respectively (p-value<0.01). The exercise variable had a direct effect on mental health the most. The benefits of this study include providing recommendations to guide future mental health policy and to reduce the cost of health maintenance in Thailand.

Keywords: Path analysis, mental health, Thai elderly, Diabetes Mellitus

INTRODUCTION

Diabetes mellitus (DM) has become a Non-Communicable Disease (NCD) today that is also an important health issue globally. It has a severe effect worldwide, and there is a rising incidence and prevalence of diabetes mellitus. The Bureau of Policy and Strategy, Ministry of Public Health, Thailand found that diabetes mellitus killed an average of 19 patients per day in 2009. The number of Thai people with diabetes mellitus is indeed increasing (4.02 times) and the number facing the problem is also rising (6.9%) (Ministry of Public Health, 2009). The Thai diabetes database in 2012 found that patients with compliable diabetes was 17.51% (18,943.581) of the Thai population of diabetes patients over 35 years old (Ministry of Public Health, 2011). The Bureau of Epidemiology, Thailand in 2010 reported that new diabetes patients numbered 176,685 with a morbidity rate of

Article history:
Received: 21 May 2015
Accepted: 30 November 2015

E-mail address:
sim356@yahoo.com (Chonticha Kaewanuchit)

ISSN: 0128-7680

277.36 per 100,000 persons. The ratio of new cases of male to female patients was 1:1.79. Thai elderly people over 60 years old number the highest among diabetes patients in Thailand (79,023 cases). The morbidity rate was 1,060.46 per 100,000 people (Thonghong et al., 2012).

Diabetes mellitus is a cause of death among the elderly (Aekplakorn et al., 2003; Nanthamongkolchai, 2009) and leads to complications without control (Vihayanrat, 2003; Gupta et al., 2007). Diabetes can be prevented with exercise, diet and regular medicine taking (Nanthamongkolchai, 2009; Nanthamongkolchai et al., 2009; American Diabetes Association, 2010; Tripeud et al., 2010). A report found that 3% of diabetes patients who control plasma glucose level by themselves but this figure is very low. In addition, the survey data of the National Statistical Office in 2010 found that only 13% of Thai elderly persons exercised; lack of exercise is an additional factor in diabetes incidence (National Statistical Office, 2011).

The number of Thai elderly persons is increasing rapidly. The number is estimated to increase to 20% of the Thai population in 2025. The elderly face physical and mental health challenges (Chamratrithirong et al., 2010). Illness perception and family support are factors that influence mental health among the elderly (Choorat et al., 2012). Several researchers have found that factors influencing the mental health of the elderly were not linked to mental health among Thai elderly persons with diabetes mellitus by path analysis (George , 2010; Malathum et al., 2010; Tuntichaivanit et al., 2010; Choorat et al., 2012; Gray & Thongcharoenchupong, 2012; Suwanmanee et al., 2012). Some researchers studied only the relationship between patients and family and friend support, social activity and participation, and rising self-esteem among the elderly in general (Malathum et al., 2009; Nanthamongkolchai et al., 2011), and did not include causal relationship between diabetes and food, exercise, drugs, Body Mass Index (BMI), family support and illness perception. They related their findings to individual, psychological and social factors relevant to holistic health care, especially the effect on mental health among the diabetic elderly. In addition, a Thai health report on four regions in 2006 found that the Thai population were mainly depressed and anxious. Their mental health scores were the lowest when compared with other populations (National Statistical Office, Department of Mental Health Institute for Population and Social Research Mahidol University & Department of Health Promotion Foundation, 2009; Suwannoppakao & Gray, 2011).

AIM

The aim of this research was (i) to study the direct and indirect influence of path analysis among Thai elderly persons with diabetes mellitus, (ii) to examine the relationship between each variable (e.g. food, exercise, BMI, drugs, illness perception and family support) and the mental health of Thai elderly persons with diabetes mellitus.

DATA AND METHOD

Sample

This cross-sectional study was conducted among Thai elderly persons with diabetes mellitus in the central region of Thailand. The sampling method was the stratified random sampling for a quantitative study. It involved the division of the population into smaller groups. The first

stratum was region; there are five regions in Thailand. From these five areas, 2,000 Thai elderly persons with diabetes mellitus were randomly selected from the central part of Thailand. The second stratum was province. The central region of Thailand is divided into two provinces. One thousand participants were selected from each province (1,000 cases/province).

Variables and Measurement

Data consisted of individuals, causal factors (e.g. food, exercise, drugs, body mass index, illness perception, family support) and effect factors (e.g. mental health). Illness perception is the reflex result of emotions and the thinking process. It consists of consequences, timeline, personal control, treatment control, identity, coherence, emotional representation, illness concern and causal items using BIPQ (Broadbent et. al., 2006). Family support is a social factor measuring satisfaction from the five dimensions of family support (adaptation, resolve, growth, affection and partnership) using the family APGAR (Smilkstein et al., 1982). The Thai mental health indicator (THMHI-15) (Mongkol et al., 2009) was from the Department of Mental Health, Ministry of Public health, Thailand to determine a path analysis to measure the mental health variable. A questionnaire was administered. It was divided into five parts, namely:

(i) General individual data consisted of province, region, sex (coded as 1=male, 2=female), education (coded as 1=primary school, 2=secondary school, 3=bachelor's degree, 4=master's degree, 5=doctoral degree) and BMI was calculated as weigh (kg)/height (m^2). Average BMI is below 18 (thin), 18-22 (normal), 23-30 (slightly fat) and above 30 (obese)

(ii) A path analysis of mental health measurement level uses an interval scale. For this research, it was divided into three domains (e.g. food, exercise and drugs). The food scale consisted of four items (e.g. 'You eat a lot of food during every meal'; 'You usually have dessert'; 'You eat rice three times a day and have three servings per meal'; 'You like to drink Coca Cola, tea or coffee'). The exercise and medicine scales consisted of two items (e.g. 'You exercise 30 minutes/3 days/week'; 'You do yoga, walk or run 30 minutes-1 hour every day') and four items (e.g. 'You took medicine on time, regularly, frequently and periodically'), respectively. Each item was rated on a 4-point scale ranging from 1 (none) to 4 (the most)

(iii) Each item of the BIPQ assessed one dimension of illness perception: consequence, timeline, personal control, treatment control, identity, coherence scores, emotional representation and causal items. This reflects a combination of emotional and cognitive representations. In some circumstances, it may be possible to compute an overall score, which represents the degree to which the illness is perceived as threatening or benign. The internal consistency of this score will depend on the illness studied and it is recommended that this is checked. To compute the score, reverse and add the score items. A higher score reflects a more threatening view of the illness.

(iv) Family support was measured by The Family APGAR questionnaire. Its measurement is by interval scale. Its scores are low, moderate and high family support (coded as 1=0-3 scores, 2=4-6 scores, 3=7-10 scores), respectively.

(v) A major issue of THMHI-15 is to check how mental health among participants compares to the general population. In this study, the mental health scores of the participants were poor,

normal and good (below 43, 44-50, and 51-60 scores), respectively. The Cronbach's alpha for food, exercise, drugs, illness perception, family support and mental health scales were 0.75, 0.78, 0.80 and 0.82 and 0.83, respectively. The researcher created additional questions, and used a standard measurement for the reviewer's consideration. The questionnaire was sent to the Human Ethics Committee for acceptance from Mahidol University, Thailand (COA.No.2014/060.1003). After that, the suggested changes were made. The study was carried out under the Thai Clinical Trial Register code TCTR20141124001 from Thailand.

Data analysis

General data were analysed using SPSS. The total direct and indirect relationships were verified by path analysis.

RESULTS

Two thousand Thai elderly persons with diabetes mellitus (100%) were divided into female and male groups, They were located in Nonthaburi and Nakhon Pathom province (each 1,000 cases/group/province). Most (800) had education up to Bachelor's degree level (40%). The majority were aged between 71 and 75 years old (600 cases, 30%). The BMI readings classified most of them as being obese (1,026 cases, 51.3%) (Table 1).

Table 1
Number and percentage among Thai elderly persons with Diabetes Mellitus (N=2,000)

Data		Number	Percent
Province	: Nonthaburi	1,000	50.00
	: Nakhon Pathom	1,000	50.00
Age (year)	: 61-65	500	25.00
	: 66-70	500	25.00
	: 71-75	600	30.00
	: 76-80	400	20.00
Sex	: Female	1,000	50.00
	: Male	1,000	50.00
Education	: Primary school	200	10.00
	: Secondary school	300	15.00
	: Diploma	600	30.00
	: Bachelor's degree	800	40.00
	: Master's degree	100	5.00
	: Doctoral degree	0	0
Body Mass Index; BMI			
	: thin	166	8.30
	: normal	250	12.50
	: a little fat	558	27.90
	: obesity	1,026	51.30

The mean and standard deviation for the BMI, exercise, medicine, food, illness perception, family support and mental health variables among the Thai elderly with diabetes mellitus were found to be 3.222 ± 0.959, 2.050 ± 0.864, 2.075 ± 0.754, 2.587 ± 0.693, 5.029 ± 3.141, 1.987 ± 0.715 and 1.802 ± 0.784, respectively. Exercise, medicine, food, illness perception, family support and mental health variables showed a positive skewedness. Their kurtosis was -0.688, 0.341, 0.546, -1.103, -1.048 and -1.292, respectively. The BMI variable showed a negative skewedness (-1.020) and kurtosis (-0.059) (Table 2). The results of the Pearson correlation analysis confirmed the significance of all these relationships at the $p<0.01$ level of the two-tailed *t*-test.

Table 2
Statistic data among Thai elderly persons with Diabetes Mellitus (N=2,000)

Variable	Mean	Minimum	Maximum	S.D.	Skewedness	Kurtosis
BMI	3.222 (slightly fat)	1 (thin)	4 (obese)	0.959	-1.020	-0.059
Exercise	2.050 (less)	1 (none)	4 (most)	0.864	0.368	-0.688
Drugs	2.075 (less)	1 (none)	4 (most)	0.754	0.574	0.341
Illness perception	5.029 (moderate)	1 (none)	10 (most)	3.141	0.006	-1.103
Family support	1.987 (almost moderate)	1 (low)	3 (high)	0.715	0.018	-1.048
Mental health	1.802 (almost normal)	1 (poor)	3 (good)	0.784	0.362	-1.292
Food	2.587 (almost more)	1 (none)	4 (most)	0.693	0.205	0.546

This research estimated a maximum likelihood path analysis using M-plus to find the path analysis relationship. It focussed on the accuracy of fit of the index of this research. It indicated a very close fit model (Chi-square=1.987, p-value=0.3703, CFI=1.000, TLI=1.000, RMSEA=0.000, SRMR=0.003). In addition, the total variables described mental health change by 64.5% (R square=0.645, $p<0.01$).

A path analysis of mental health among Thai elderly persons with diabetes mellitus found that the variables exercise, illness perception, food and drugs had a direct influence on mental health with standardised regression weights of 0.732, 0.347, 0.243 and 0.050 at the statistically significant level of 0.01, respectively. However, the BMI variable had no direct influence on mental health (Figure 1).

DISCUSSION

The elderly constitute a group who are experiencing physical changes that can lead to many diseases (e.g. hearing, diabetes mellitus, hypertension, cancer and inactive organs). The elderly have to cope with mental health issues (e.g. depression, hopelessness and anxiety) and are faced with loss (Chamratrithirong et al., 2009). Diabetes mellitus is a major cause of mortality among the elderly in Thailand and is an important issue for global health (American Diabetes Association, 2010).

One concept of public health and determinant of mental health has identified the factors influencing mental health problems among Thai elderly persons with diabetes mellitus. Three factors were given i.e. individual factor, psychological factor and social factors (Gray & Thongcharoenchupong, 2012; Kaewanuchit, 2013). Diabetes mellitus is a major cause of mortality among the elderly in Thailand (American Diabetes Association, 2010). Its cause is the change in individual lifestyle and behaviour. Factors influencing diabetes control are related to food, drugs/medicine and lack of exercise (Tripeud et al., 2010); and change in lifestyle and symptom management (Chaves et al., 2009; Malathum et al., 2009; Nanthamongkolchai,et al., 2009; Tuntichaivanit, et al., 2010). The commonest BMI among Thai elderly persons with diabetes mellitus in this study was obesity (51.31%) (Table 1). The mental health score was almost normal (Table 2).

Additionally, the study showed that the path analysis of mental health among the Thai elderly with diabetes mellitus has goodness-of-fit indices that are most accurate for the 2,000 cases. This indicated that the important path relationships based on public health concept and determinant of mental health among the elderly with diabetes mellitus are individual, psychological and social factors; these are factors that determine the level of mental health of a person in the field of public health. Food, exercise, BMI and drugs/medicine, which are individual variables, and illness perception, which is a psychological variable, have a direct influence on mental health among the Thai elderly with diabetes mellitus. Furthermore, this finding was also in accordance with a study (Gray & Thongcharoenchupong, 2012) that found that higher age, marital status, higher education, good economic status and good health evaluation among the Thai elderly led to good mental health. It was a determinant of mental health among the Thai elderly population. However, that research found that only 30 % of Thai elderly persons exercised regularly . By contrast, other research has described factors influencing the mental health problem among the Thai elderly. It found that the elderly, who were from the central region of Thailand, risked developing mental health problems (Choorat et al., 2012; Gray & Thongcharoenchupong, 2012). In addition, one research work found that education was a factor influencing the risk of mental health problems in Thai elderly persons (Choorat et al., 2012). Moreover, the results were also in accordance with a study (Tripeud et al., 2010) that found that factors influencing diabetes control related to food, drugs/medicine and exercise. The results indicated that these factors had a positive effect on mental health. Family support, which was a social factor, had a direct influence on mental health (Figure 1). This finding was consistent with Thai research work done in Songkhla province in 2011 (Suwanmanee et al., 2012). It found that a factor influencing mental health among the elderly was family relationship. Moreover, several studies found that high family support was related to the mental health of the elderly in all aspects (Sitthisran & Naruthum, 2009; Tuntichaivanit et al., 2010; Gray & Thongcharoenchupong, 2012). The same point showed that family relationships related to life satisfaction among female elderly persons in Hong Kong (Siu & Phillips, 2002). This was also shown by Nanthamongkolchai et al., 2009 in a study. The latter found that family relationships influenced life happiness among female Thai elderly people in Thailand. The family support variable agreed with the hypothesis and matched the finding of several other research studies (Siu & Phillips, 2002; Nanthamongkolchai et al., 2009). The results indicated that the exercise variable had a direct influence on mental health the most. It

is an individual factor that determines the level of mental health in the field of public health. Moreover, exercise, illness perception and drugs showed a positive effect on mental health. This implied that good exercise, high illness perception and drug taking led to good mental health. By contrast, BMI did not have a direct effect on mental health. However, its influence should be further examined in future studies.

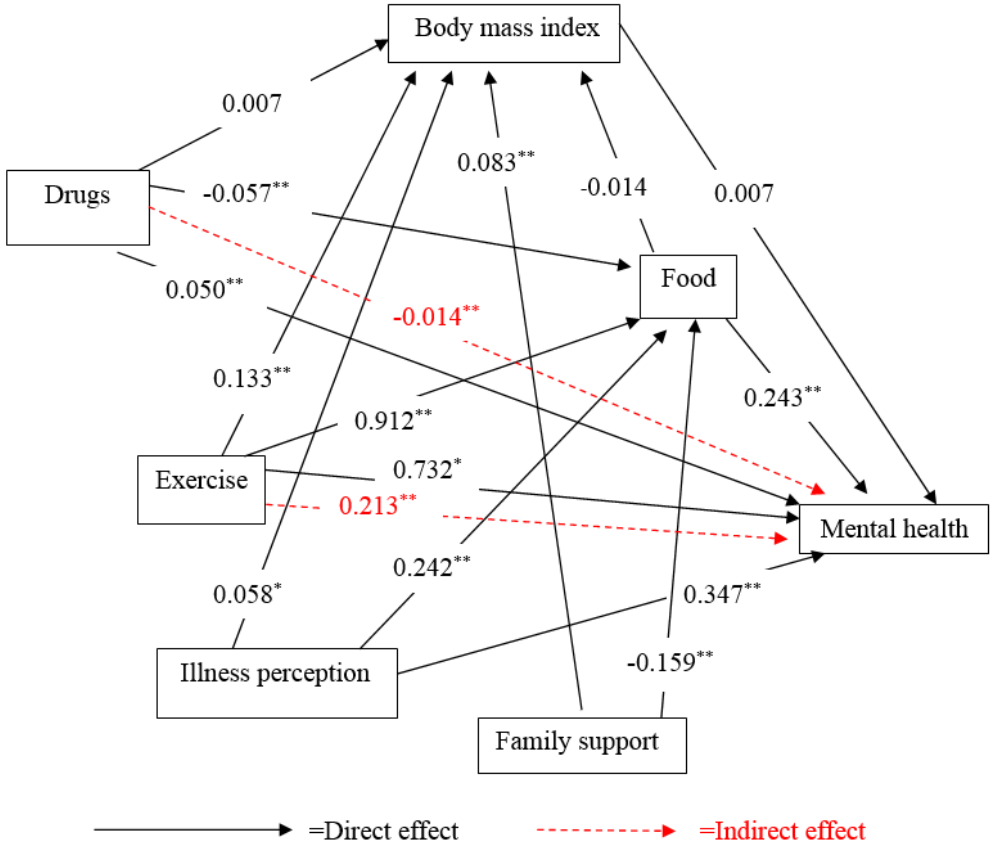

** p-value<0.01 * p-value<0.05

Figure 1. A path analysis of mental health among Thai elderly persons with diabetes mellitus (N=2,000).

The major strengths of this research were as follows; (1) This sample was representative of a large population among Thai elderly persons with diabetes. The data collected was sufficient. (2) This research focussed on factors influencing mental health among Thai elderly persons with diabetes mellitus. The results were explained by path analysis in the field of public health (Thonghong et al., 2012). Furthermore, a questionnaire was used to clarify and facilitate understanding of the participants including standard measurement (e.g. The Family APGAR questionnaire and THMHI-15 using). The results of these indicated that well-validated measures were used to drive rapid changes among the elderly in society and health policy. The benefits of this study include providing recommendations to guide future mental health

policy and to reduce the cost of health maintenance in Thailand. Several limitations influenced this research. Firstly, this research studied only Thai elderly with diabetes mellitus. It did not study other groups and other NCDs (e.g. hypertension, cardiovascular disease etc.) that are also fatal among the Thai elderly population as well as world population. Some suggestions for further research are that researchers should increase important research among the Thai elderly population suffering from other NCDs, especially bio-psychosocial research. Secondly, this research studied only quantitative methods. Qualitative methods to help data support should be added. Thirdly, important statistical data used only path analysis. Further research could also use SEM analysis to analyse data more deeply.

Table 3
Direct Effect (DE), Indirect Effect (IE) and Total Effect (TE) Among Thai Elderly Persons with Diabetes Mellitus (N=2,000)

Endogenous / Exogenous variables	Endogenous variables								
	Food			BMI			Mental health		
	DE	IE	TE	DE	IE	TE	DE	IE	TE
Drugs	-0.057**	-	-0.057**	0.007	-	0.007	0.050*	-0.014**	0.036**
Exercise	0.912**	-	0.912**	0.133**	-	0.133**	0.732**	0.213**	0.945**
Illness perception	0.242**	-	0.242**	0.058*	-	0.058*	0.347**	-	0.347**
Food	-	-	-	-0.014	-	-0.014	0.243**	-	0.243**
BMI	-	-	-	-	-	-	0.007	-	0.007
Family support	-0.159**	-	-	0.083**	-	0.083**	-	-	-

*p-value <0.05
**p-value <0.01

CONCLUSION

Exogenous variables or causal variables of this research influenced mental health. They were divided into three variables (exercise, illness perception and drugs). The exercise variable (individual factor) had a direct effect on mental health the most at a statistically significant level. Every exogenous variable had a positive influence on the mental health variable. Family support, which was an exogenous variable, had a direct effect on the food and BMI variables. It had no direct effect on mental health. The food variable became a mediated variable like the BMI variable. However, the BMI variable had no direct or indirect effect on mental health, which should be studied in future. The benefits of this study include providing recommendations to guide future mental health policy and to reduce the cost of health maintenance in Thailand.

DECLARATION OF CONFLICTING INTERESTS

The author declares no conflict of interest with respect to the research, authorship and publication of this research.

ACKNOWLEDGEMENTS

The author is grateful for support from Phranakhon Si Ayutthaya Rajabhat University, Phranakhon Si Ayutthaya province, Thailand.

REFERENCES

Aekplakorn, W., Stolk, R. P., Neal, B., Suriyawongpaisal, P., Chongsuvivatwong, V., Cheepudomwit, S., Woodward, M., & Interasia Collaborative Group. (2003). The prevalence and management of diabetes in Thai adults. *Diabetes Care, 26*(10), 2758-2763.

American Diabetes Association. (2010). Standards of medical care in diabetes-2010. *Diabetes care*, *33*(Suppl 1), S11-S61.

Broadbent, E., Petrie, K. J., Main, J., & Weinman, J. (2006). The brief illness perception questionnaire (BIPQ). *Journal of Psychosomatic Research, 60*(6), 631-637.

Chamratrithirong, A., Prasartkul, P., & Choolert, P. (2010). *Thai mental health satiation.* Nakhon Pathom: Institute of Population and Social Research, Mahidol University.

Chaves, M. L., Camozzato, A. L., Eizirik, C. L., & Kaye, J. (2009). Predictors of normal and successful ageing among urban-dwelling elderly Brazilians. *Journal of Gerontology: Psychological Sciences, 64B*(5), 597-602.

Choorat, W., Sawangdee, Y., & Arunraksombat, S. (2012). Factors influencing the risk of having mental health problems of Thai elderly. *Thai Population Journal, 3*(2), 87-109.

George , L. K. (2010). Still happy after all these years: Research frontiers on subjective well-being in later life. *Journal of Gerontology: Social Sciences, 65B*(3), 331-339.

Gray, R., & Thongcharoenchupong, N. (2012). Determinants of mental health among older persons. *Thai Population Journal, 3*(2), 45-63.

Gupta, S., Koirala, J., Khardori, R., & Khardori, N. (2007). Infections in diabetes mellitus and hyperglycemia. *Infectious Disease Clinics of North America, 21*(3), 617-638.

Kaewanuchit, C. (2013). Health determinants and social determinants of health under global and Thai health system. *Journal of Nursing Science and Health, 36*, 123- 131.

Malathum, P., Kongiem, J., & Intarasombat, P. (2009). Relationships of family support and friend support to life satisfaction of older adults in rural areas. *Ramathibodi Nursing Journal, 15*(3), 431-448.

Malathum, P., Promkong, P., & Intarasombat, P. (2010). Factors predicting the plasma glucose level in older persons with type 2 diabetes mellitus. *Ramathibodi Nursing Journal, 16*(2): 218-237.

Ministry of Public Health. (2009). *The Statistic of Public Health in 2008.* Bangkok: The War Veterans Organization of Thailand Printing.

Ministry of Public Health. (2011). *NCD 1 Report in 2011 under the responsible Majesty King who is concerned about health of the Thai people*. Nonthaburi: Ministry of Public Health.

Mongkol, A., Vongpiromsan, Y., Tangseree, T., Huttapanom, W., Romsai, P., & Chutha, W. (2009). The development and testing of Thai mental health indicator version 2007. *Journal of the Psychiatric Association of Thailand, 54*(3), 299-316.

Nanthamongkolchai, S. (2009). Elderly people: In Thai people's view. *Journal of Public Health, 39*(3), 231-232.

Nanthamongkolchai, S., Tuntichaivanit, C., Munsawaengsub, C., & Charupoonphol, P. (2009). Factors influencing life happiness among elderly females in Rayong province. *Journal of the Medical Association of Thailand, 92*(Suppl 7), S8-S12.

Nanthamongkolchai, S., Tuntichaivanit, C., Munsawaengsub, C., & Charupoonphol, P. (2011). Successful ageing: A case study of Rayong Province, Thailand. *Asia Journal of Public Health, 2*(1), 35-39.

National Statistical Office, Department of Mental Health Institute for Population and Social Research Mahidol University, & Department of Health Promotion Foundation. (2009). *Executive summary: The Thai mental health survey.* Bangkok: National Statistical Office.

National Statistical Office. (2011). *Male and female dimensions: Trend to develop equity*. Bangkok: Charansanitwong Printing.

Sitthisran, T., & Naruthum, C. (2009). Factors influence on the mental health of the elderly in the Kamphaeng Saen hospital elderly club, Nakhon Pathom Province. *Journal of Social Sciences and Humanities, 35*(1), 160-172.

Smilkstein, G., Ashworth, C. T., & Montano, D. (1982). Validity and reliability of the family APGAR: A test of family function. *Journal of Family Practice, 15*(2), 303-311.

Siu, O., & Phillips, D. R. (2002). A study of family support, friendship, and psychological well-being among older women in Hong Kong. *International Journal of Aging and Human Development, 55*, 299-319.

Suwanmanee, S., Nanthamongkolchai, S., Munsawaengsub, C., & Taechaboonsermsak, P. (2012). Factors influencing the mental health of the elderly in Songkhla, Thailand. *Journal of the Medical Association of Thailand, 95*(Suppl. 6), S8-S15.

Suwannoppakao, R., & Gray, R. (2011). Quality of life of older persons. In Kanchanaburi demographic surveillance system. *Thai Population Journal, 2,* 31-54.

Thonghong, A., Thepsitta, K., Chongpiriyaanun, P., & Kabpirom, T. (2012). Report of epidemiological surveillance in week: The surveillance of communicable disease in 2009. *Epidemiological Journal*, *43*(17), 257-264.

Tripeud, K., Malathum, P., Hanpraitkam, K., & Kantaratanakul, V. (2010). A synthesis of research of exercise influencing glycemic control in persons with type 2 diabetes. *Ramathibodi Nursing Journal, 16*(2), 259-278.

Tuntichaivanit, C., Nanthamongkolchai, S., Munsawaengsub, C., & Charupoonplo, P. (2009). Life happiness of the elderly in Rayong Province. *Journal of Public Health, 39*, 34-47.

Vihayanrat, A. (2003). *Textbook of diabetes mellitus endocrine society of Thailand*. Bangkok: Reingkaew printing.

Pertanika J. Sci. & Technol. 24 (2): 295 - 306 (2016)

SCIENCE & TECHNOLOGY

Journal homepage: http://www.pertanika.upm.edu.my/

Data Clustering using Differential Search Algorithm

Vijay Kumar[1]*, Jitender Kumar Chhabra[2] and Dinesh Kumar[3]

[1]*Department of Computer Science and Engineering, Thapar University, Patiala, Punjab, India-147001*

[2]*Department of Computer Engineering, National Institute of Technology, Kurukshetra, Haryana, India-136119*

[3]*Department of Computer Science and Engineering, Guru Jambheshwar University of Science and Technology, Haryana, India-125001*

ABSTRACT

The main challenges of clustering techniques are to tune the initial cluster centres and to avoid the solution being trapped in the local optima. In this paper, a new metaheuristic algorithm, Differential Search (DS), is used to solve these problems. The DS explores the search space of the given dataset to find the near-optimal cluster centres. The cluster centre-based encoding scheme is used to evolve the cluster centres. The proposed DS-based clustering technique is tested over four real-life datasets. The performance of DS-based clustering is compared with four recently developed metaheuristic techniques. The computational results are encouraging and demonstrate that the DS-based clustering provides better values in terms of precision, recall and G-Measure.

Keywords: Data clustering, differential search algorithm, metaheuristic

INTRODUCTION

Data clustering is an unsupervised technique that partitions a set of data points into a number of clusters such that data points in the same cluster are similar to each other according to some criteria. It has been found applicable in various applications such as engineering (artificial intelligence, pattern recognition, mechanical engineering), computer sciences (image segmentation, web mining), medical sciences (biology, microbiology), earth sciences (geology, remote sensing), social sciences (sociology, psychology) and economics (Everitt, 1993; Abraham et al., 2008). Data clustering algorithms are broadly classified into two main categories: hierarchical and partitional (Leung et al., 2000). The hierarchical clustering algorithms provide a tree structure output that represents the nested grouping of the elements of a dataset (Frigui & Krishnapuram, 1999).

Article history:
Received: 8 July 2015
Accepted: 5 October 2015

E-mail addresses:
vijaykumarchahar@gmail.com (Vijay Kumar),
jitenderchhabra@gmail.com (Jitender Kumar Chhabra),
dinesh_chutani@yahoo.com (Dinesh Kumar)
*Corresponding Author

ISSN: 0128-7680

These do not require *a priori* knowledge about the number of clusters present in the dataset. The main drawback of hierarchical clustering algorithms is that these may fail to separate overlapping clusters (Jain et al., 1999).

On the other hand, partitional clustering algorithms divide the dataset into a number of groups based upon certain clustering criteria. The clustering criterion directly affects the nature of clusters formed. The advantages of partitional clustering algorithms are the disadvantages of the hierarchical algorithms and vice versa. A large number of partitional clustering algorithms have been reported in the literature (Jain et al., 1999; Xu & Wunsch, 2009). The focus of this paper is on the partitional clustering algorithm. It is also worth mentioning that the hierarchical clustering algorithms are unable to differentiate the overlapping clusters and are computationally expensive. The well-known partitional clustering technique is K-Means. The performance of the K-Means clustering algorithm is heavily influenced by the number of clusters specified and the random choice of initial cluster centers. To solve these problems, a lot of metaheuristic techniques are available for use, such as genetic algorithm (GA), ant colony optimisation (ACO), particle swarm optimisation (PSO), gravitational search algorithm (GSA).

Recently, Civicioglu (2012) developed a novel metaheuristic algorithm, namely, the differential search algorithm (DS), which mimics the Brownian-like random-walk movement used for migration of organisms. DS is preferred over other metaheuristic techniques as it is easy to implement and has fewer control parameters. Due to these advantages of the DS, it is employed on data clustering. The novel approach is proposed, in which DS is used to generate the optimal cluster centres.

This paper aimed to explore the applicability of differential search approach to the development of clustering technique. It includes a general overview of data clustering with emphasis on recently developed metaheuristic-based clustering techniques followed by the proposed Differential Search-based clustering technique. The performance evaluation has been done on real-life datasets.

BACKGROUND

This section describes the related concept of clustering and related works.

Basic Concepts of Clustering

The mathematical formulation of partitional clustering technique is described (Abraham et al., 2008). Consider a dataset that consists of n data points, $X = \{x_1, x_2, ..., x_n\}$. Each data point is described by d features, where $x_j = (x_{j1}, x_{j2}, ..., x_{jd})$ is a vector representing the j^{th} data point and x_{ji} represents the i^{th} feature of x_j. As we know, the main objective of any clustering technique is to partition the dataset into a number of clusters (say K) $\{C_1, C_2, ..., C_K\}$ based on some similarity measure. The value of K may or may not be known beforehand. The partition matrix is represented as $U = [u_{kl}]$, $k = 1, 2, ..., K$ and u_{kl}, where u_{kl} is the membership of data point x_j to cluster C_k. For the hard and fuzzy partitioning of the dataset, the conditions that must be satisfied are as follows (Xu & Wunsch, 2009):

$$u_{kl} = \begin{cases} 1 & if\ x_l \in C_k \\ 0 & if\ x_l \notin C_k \end{cases} \quad (1)$$

$$0 < \sum_{l=1}^{n} u_{kl} < n, \quad \forall k \in \{1, 2, ..., K\} \quad (2)$$

Related Works

Though classical clustering algorithms are computationally simple, they have certain shortcomings such as sensitivity towards initialisation of cluster centres and trapping in local optima. There are many algorithms available in the literature to solve these problems such as the evolutional or population-based algorithms. Selim and Al-Sultan (1991) proposed a simulated annealing algorithm for the clustering algorithm. They proved theoretically that a clustering problem's global solution can be reached. Sung and Jin (2000) proposed a tabu search-based heuristic for clustering. They combined the packing and releasing procedures with a tabu search. Krishna and Murty (1999) developed a novel approach called genetic K-Means algorithm for clustering analysis that defines a mutation operator specific to clustering. Maulik and Bandyopadhyay (2000) proposed a genetic algorithm-based method for data clustering problems. The clustering solutions move towards better solutions via selection, crossover and mutation. An ant colony algorithm for clustering was presented by Shelokar et al. (2004). This algorithm mimics the behaviour of ants to find the shortest path from their nest to a food source and back. Its performance was compared with the genetic algorithm, simulated annealing and tabu search and was found to show better performance in comparison to others. Fathian et al. (2007) developed an application of the honey-bee mating optimisation algorithm for data clustering. Particle swarm optimisation (PSO), which simulates the social behaviour of bird flocking, was used for clustering by Kao et al. (2008). Its performance was further enhanced by hybridisation of K-Means with PSO and compared with GA (Murthy & Chowdhury, 1996) and KGA (Bandyopadhyay & Maulik, 2002).

Karaboga and Basturk (2008) described an artificial bee colony (ABC) algorithm for the data clustering problem. Zhang et al. (2010) extended the ABC for data clustering. Its performance was compared with other heuristic-based clustering techniques. Satapathy and Naik (2011) used the teaching learning-based optimisation technique for data clustering. They optimised the cluster centres for a user-specified number of clusters. Hatamlou et al. (2011a) presented the Big Bang-Big Crunch algorithm (BB-BC) for the data clustering problem. In the Big Bang phase, some candidate solutions are randomly generated, which are uniformly spread over the search space. In the Big Crunch phase, some randomly distributed solutions are treated as a single delegate point using a centre of population. Hatamlou et al. (2011b) also presented a gravitational search algorithm-based data clustering technique. Hassanzadeh et al. (2012) presented a firefly algorithm for data clustering. They optimised the cluster centres and extended it to use K-Means clustering to further refine cluster centres. Hatamlou (2013) introduced a new algorithm named Black Hole (BH) algorithm and applied it to solve the clustering problem. Hatamlou and Hatamlou (2013) investigated the combination of GSA and

BB-BC algorithms for clustering problems. They used GSA for exploring the search space for finding the optimal locations of cluster centres and BB-BC was used to diversify the problem. Kumar et al. (2014a) used the gravitational search-based clustering technique for MRI brain image segmentation. Kumar et al. (2014b) also proposed four new variants of harmony search clustering algorithms. They used these variants for solving the clustering problem. They used the search capability of harmony search for optimisation of the within-cluster variation. Saida et al. (2014) presented a cuckoo search for solving data clustering problems. Kumar et al. (2014c) developed a variance-based harmony search algorithm, which is used to solve cluster centre computation problems.

In this paper, differential search-based clustering technique were developed. There are two main reasons for adopting the differential search as a metaheuristic technique for clustering. First is its simplicity, robustness and ease of implementation. Second, it has few control parameters to fine-tune. The proposed approach is applied on real-life datasets.

PROBLEMS AND SOLUTION OF DATA CLUSTERING

Problems and challenges of data clustering

A large number of partitional clustering techniques already exist and are reported in the literature. Some of the well-known clustering techniques are K-Means, Fuzzy C-Means, K-Medoid etc. Among these techniques, the K-Means algorithm is the most widely used clustering technique. It is used for high dimensional datasets due to its simplicity of understanding, ease of implementation and speed of convergence (Duda et al., 2001). Most of the clustering algorithms are sensitive towards the initialisation of cluster centres. Another problem is convergence of the final cluster towards the nearest local optimum solution (Jain, 2010). The K-Means algorithm also suffers from these problems.

Solution to the Problems

Recently, researchers used metaheuristic techniques to overcome problems mentioned in the preceding section. Metaheuristic algorithms are believed to be able to solve NP-hard problems with satisfactory near-optimal solutions with less computational time compared to other classical methods. Although many meta-heuristic algorithms for solving clustering problems have been proposed, the results obtained in terms of accuracy are not up to the mark as reported by Omran et al. (2006), thereby giving rise to the proposal of a DS-based clustering approach.

The proposed approach uses the basic steps of DS. It utilises the concept of population to explore the search space of the given dataset and ensures a greater probability in achieve the near-optimal cluster centres. The cluster centres obtained from the DS algorithm are computed using the inter-cluster distance measure.

Clustering using Differential Search Algorithm

The DS algorithm is used for evolving a set of candidate cluster centres for a fixed number of clusters and determining a near optimal partitioning of the dataset. It is also able to cope

with local optima by comparing several solutions simultaneously. The well-known clustering criterion is the sum of squared Euclidean distances between data points, taken individuallys, and the centre of the cluster belonging to every such allocated data point. It is described mathematically as (Xu & Wunsch, 2009):

$$\sum_{i=1}^{n}\sum_{j=1}^{K}\left\|x_i - m_{ij}\right\|^2 \tag{3}$$

where m_{ij} refers to the cluster centre vector of the i^{th} member in j^{th} cluster (say C_{ij}).

The main goal of the proposed DSA-based clustering technique is to search for the appropriate cluster centres such that the above-mentioned clustering criterion is minimised.

Differential Search Algorithm

Civicioglu (2012) developed a novel metaheuristic technique, namely, the differential search algorithm (DS). It is inspired from the migration of living beings, which comprise super-organisms during the climate change of the year. In the DS algorithm, the search space is simulated as the food areas and each point in the search space corresponds to an artificial-super-organism migration (Liu, 2014). The goal of the migration process is to find a global optimal solution to the problem. During this process, the artificial-super-organism chooses the randomly selected positions to be retained temporarily. The members of artificial-super-organisms continue to settle at a position so long as the randomly selected position is suitable for them. As soon as the position becomes unsuitable, members start migrating from that position to another suitable position. The main steps of DS are shown in Figure 1 and described below (Liu, 2014):

In DS algorithm, artificial-super-organisms are made up of artificial-organisms $\left(i.e.,\ X_i,\ i=\{1,2,....,N\}\right)$.

A member of an artificial-organism $\left(i.e.,\ x_{i,j},\ j=\{1,2,....,D\}\right)$ is randomly initialised using the following equation:

$$x_{i,j} = x_j^{min} + rand \times \left(x_j^{max} - x_j^{min}\right) \tag{4}$$

Here, N indicates the number of artificial organisms in a super-organism and D indicates the size of the respective problem. x_j^{min} and x_j^{max} are the minimum and maximum value of the j^{th} component, respectively.

After initialisation, the mechanism of finding a stopover site $\left(S_i\right)$ at the areas between the artificial-organisms may be described by a Brownian-like random walk model. The algorithm creates a stopover site corresponding to each population individual vector in the current population. The method for producing the stopover site can be described as:

Differential Search Algorithm

begin

Generate initial population of n *superorganism,* $X_i \ (i = 1, 2, ..., n)$

Initialize the parameter P_1 *and* P_2

Evaluate the fitness of each individual in population

while $(t < MaxGeneration)$ or $(stop\,criterion)$

$Scale = randg(2 \times rand) \times (rand - rand)$

for *i = 1 to n* ***do***

Select randomly select an individual (x_a)

end for $S_i = x_i + Scale \times (x_a - x_i)$

$r = rand(N, D)$

if $rand < rand$ ***then***

if $rand < P1$ ***then***

for *i = 1 to n* ***do***

$r(i,:) = r(i,:) < rand$

end for

else

for *i = 1 to n* ***do***

$r(i, \text{randi(D)}) = 0$

end for

end if

else

for *i = 1 to n* ***do***

$d = randi(D, 1, \lceil P2.rand \rceil)$

for *j = 1 to size (d, 2)* ***do***

$r(i, d(j)) = 0$

end for

end for

end if

$r = r > 0$

$S(r) = X(r)$

for *j = 1 to n* ***do***

Evaluate the offspring S_i

if S_i *is better than* X_i ***then***

$X_i = S_i$

end if

end for

Store the best solution achieved so far

end while

end

Figure 1. Pseudo code of differential search algorithm (DS)

$$S_i = x_i + Scale \times \left(x_a - x_i \right) \tag{5}$$

where $a \in [1,....,N]$ is a randomly chosen integer and $a \neq i$. The variable, *scale*, is used to control the size of change in the positions of the individuals of the artificial-organisms. The search process of the stopover site is computed as:

$$S'_{i,j} = \begin{cases} S_{i,j} & if\ r_{i,j} = 0 \\ x_{i,j} & if\ r_{i,j} = 1 \end{cases} \tag{6}$$

where $r_{i,j}$ is an integer number. $S'_{i,j}$ indicates the trail vector. The selection operation helps in selecting the better of the two populations, the stopover site and the artificial-organism as the next population.

DS-Based Clustering Technique

The basic steps of DS, as shown in Figure 1, are used in the proposed clustering technique. In the context of clustering, a member of the artificial super-organism represents the K cluster centres. That is, each member is represented as:

$$x_i = \left[m_{i1}, m_{i2}, ..., m_{ij}, ..., m_{iK} \right] \tag{7}$$

Therefore, a member of the super-organism represents a number of candidate cluster centres for the given dataset. The fitness of each member is computed using Equation 3. The pseudo code of DS-based clustering algorithm is shown in Figure 2.

DS-based Clustering Algorithm

begin

Initial each individual with K *random cluster centres*.
for *iter = 1 to maximum_iteration* ***do***
for *all individual i* ***do***

for *all data point* X_P *in dataset* ***do***

Compute Euclidean distance of X_P *with all cluster centres*

Assign X_P *to the cluster that have nearest cluster centre to* X_P
end for
Compute the fitness function mentioned in Eq.3
end for
Update the cluster centres using DS.
end for
end

Figure 2. Pseudo code of DS-based clustering algorithm

VALIDATION AND DISCUSSIONS

Datasets used

The proposed clustering approach was applied to five benchmark datasets to evaluate its performance (Blake & Merz, 1998). The datasets are *Iris*, *Wine*, *Haberman* and *Contraceptive Method Choice* (*CMC*). Table 1 describes the main characteristics of the used datasets.

Table 1
Description of Datasets Used

Dataset	Number of Instances	Number of Features	Number of Classes	Type
Iris	150	4	3	Real
Wine	178	13	3	Real
Glass	214	9	6	Real
Haberman	306	3	2	Real
CMC	1473	9	3	Real

Performance Metrics

Three well-known cluster quality measures such as precision, recall and G-Measure were used to evaluate the performance of the clustering algorithms. These were defined mathematically for cluster j with respect to class i as follows (Kowalski, 1997):

$$\text{Precision}(i,j)=\frac{N_{ij}}{N_j} \tag{8}$$

$$\text{Recall}(i,j)=\frac{N_{ij}}{N_i} \tag{9}$$

$$\text{GM}(i,j)=\sqrt{\text{Precision}(i,j)\times\text{Recall}(i,j)} \tag{10}$$

where N_{ij} is the number of data points of class i in the cluster j. N_j is the number of data points of cluster . N_i is the number of data points of class i. N_T is the total number of cases. A large value of these measures were required for better clustering. The values reported in the tables are average and standard deviation (mentioned in parenthesis) of solutions over 20 independent runs of algorithms.

Algorithms for Comparison

The performance of the DSA-based clustering (DSC) technique was compared with six well-known clustering algorithms such as K-Means (Jain et al., 2010), genetic algorithm-based clustering (GAC) (Maulik & Bandyopadhyay, 2000), modified harmony search-based clustering (MHSC) (Kumar et al., 2014b), particle swarm-based clustering (PSOC) (Omran et al., 2006), flower pollination algorithm-based clustering (FPAC) (Yang, 2012), and bat algorithm-based clustering (BATC) (Yang, 2010).

The population size and maximum number of iterations for all algorithms were set as 30 and 500, respectively. The parameter settings of the above-mentioned algorithms were the same as reported in their original papers.

EVALUATION AND DISCUSSION

Tables 2 to 5 show the comparison between the proposed DS-based clustering approach and above-mentioned techniques for *Iris*, *Wine*, *Haberman* and *CMC* datasets, respectively. For the *Iris* dataset, DSC performed better than the other techniques. The performance of other metaheuristic-based clustering algorithms were almost similar. For the *Wine* dataset, DSC outperformed other clustering techniques. The MHSC was the second best clustering technique among the compared techniques. For *Haberman* and *CMC* datasets, DSC provided better cluster quality measures than the other competitive techniques.

Table 2
Cluster Quality Matrices for Iris Dataset

	KM	GAC	MHSC	PSOC	FPAC	BATC	DSC
Precision	0.3018	0.3534	0.4586	0.4299	0.4266	0.4396	0.6591
	(0.2584)	(0.3193)	(0.3178)	(0.3482)	(0.1936)	(0.4159)	(0.2859)
Recall	0.3020	0.3733	0.4427	0.4460	0.4385	0.4360	0.6466
	(0.2569)	(0.3011)	(0.3126)	(0.3316)	(0.1870)	(0.4090)	(0.2887)
G Measure	0.1144	0.2046	0.4082	0.4364	0.4319	0.4359	0.6502
	(0.2828)	(0.3735)	(0.3454)	(0.3385)	(0.1893)	(0.4107)	(0.2853)

Table 3
Cluster Quality Matrices for Wine Dataset

	KM	GAC	MHSC	PSOC	FPAC	BATC	DSC
Precision	0.2718	0.2925	0.4343	0.3851	0.4074	0.3872	0.4366
	(0.1365)	(0.2191)	(0.2108)	(0.2002)	(0.1290)	(0.2381)	(0.2573)
Recall	0.2742	0.3105	0.4087	0.3757	0.3900	0.3773	0.4302
	(0.1409)	(0.2323)	(0.1897)	(0.1805)	(0.1045)	(0.2233)	(0.2329)
G Measure	0.0777	0.1082	0.2519	0.3795	0.3629	0.3807	0.4263
	(0.2457)	(0.2445)	(0.2940)	(0.1913)	(0.1286)	(0.2296)	(0.2419)

Table 4
Cluster Quality Matrices for Haberman Dataset

	KM	GAC	MHSC	PSOC	FPAC	BATC	DSC
Precision	0.4972	0.4995	0.4996	0.4981	0.4983	0.4941	0.5149
	(0.0141)	(0.0181)	(0.0157)	(0.0144)	(0.0158)	(0.0106)	(0.0195)
Recall	0.4964	0.4994	0.4994	0.4977	0.4978	0.4925	0.5185
	(0.0179)	(0.0229)	(0.0189)	(0.0184)	(0.0206)	(0.0134)	(0.0247)
G Measure	0.4556	0.4647	0.4602	0.4756	0.4764	0.4703	0.4919
	(0.0161)	(0.0226)	(0.0209)	(0.0105)	(0.0241)	(0.0090)	(0.0209)

Table 5
Cluster Quality Matrices for CMC Dataset

	KM	GAC	MHSC	PSOC	FPAC	BATC	DSC
Precision	0.3432 (0.0417)	0.3378 (0.0599)	0.3615 (0.0185)	0.3502 (0.0589)	0.3090 (0.0806)	0.3166 (0.0863)	0.3651 (0.0247)
Recall	0.3320 (0.0444)	0.3372 (0.0570)	0.3569 (0.0184)	0.3472 (0.0514)	0.3124 (0.0748)	0.3186 (0.0827)	0.3551 (0.0290)
G Measure	0.3139 (0.0569)	0.3196 (0.0588)	0.3459 (0.0223)	0.3440 (0.0535)	0.3061 (0.0759)	0.3134 (0.0842)	0.3549 (0.0256)

FUTURE RESEARCH DIRECTIONS

The field of metaheuristic-based partitional clustering is relatively novel and promising with new ideas and applications. Future research directions are as follows.

- The performance of metaheuristic-based clustering algorithms greatly depends upon the setting of algorithm parameters and an encoding scheme. Hence, theoretical analysis is required before the simulation and its implementation.
- The performance consistency of these metaheuristic algorithms need to be ensured.
- Most of the real-life datasets contain data points that are overlapping in nature. There is a need to further explore the possibility of clustering algorithms that take care of overlapped data points and to group them in the appropriate cluster.

CONCLUSION

A novel differential search algorithm-based clustering technique was developed to solve clustering problems. The DSC was applied for data clustering as the number of clusters was known *a priori*. It was compared with four well-known metaheuristic techniques and tested on four datasets. The results revealed that DSC outperformed the four well-known metaheuristic-based clustering techniques.

REFERENCES

Abraham, A., Das, S., & Roy, S. (2008). Swarm intelligence algorithms for data clustering. In O. Maimon, & L. Rokach (Eds.), *Soft Computing for Knowledge Discovery and Data Mining,* pp. 279-313. Berlin: Springer.

Bandyopadhyay, S., & Maulik, U. (2002). An evolutionary technique based on K-means algorithm for optimal clustering. *Information Science*, *146*(1), 221-237.

Blake, C. L., & Merz, C. J. (1998). UCI repository of machine learning. Retrieved from http:/www.ics.uci.edu/_mlearn/databases/.

Civicioglu, P. (2012). Transforming geocentric Cartesian coordinates to geodetic coordinates by using differential search algorithm. *Computer & Geosciences, 46,* 229-247.

Everitt, B. S. (1993). *Cluster analysis*. New York: Edward Arnold and Halsted Press.

Fathian, M., Amiri, B., & Maroosi, A. (2007). Application of honey bee mating optimization algorithm on clustering. *Applied Mathematics and Computation*, *190*(2), 1502-1513.

Frigui, H., & Krishnapuram, R. (1999). A robust competitive clustering algorithm with applications in computer vision. *IEEE Transactions on Pattern Analysis and Machine Intelligence*, *21*(5), 450-465.

Hassanzadeh, T., & Meybodi, M. R. (2012). A new hybrid approach for data clustering using firefly algorithm and K-means, In CSI *International Symposium on Artificial Intelligence and Signal Processing*, 7-11, Shiraz, Fars, Iran.

Hatamlou A., Abdullah, S., & Hatamlou, M. (2011a). Data clustering using big bang-big crunch algorithm. In P. Pichappan, H. Ahmadi, & E. Ariwa (Eds.), *Innovative Computing Technology*. *Lecture notes in communications in computer and information science* (pp. 383-388). US: Springer.

Hatamlou, A., Abdullah, S., & Nezamabadi-pour, H. (2011b). Application of gravitational search algorithm on data clustering, In J. Yao, S. Ramanna, G. Wang, & Z. Suraj (Eds.), *Rough Set and Knowledge Technology*, Lecture notes in computer science (Vol. 6954, pp. 337-346). US: Springer.

Hatamlou, A., & Hatamlou, M. (2013). Hybridization of the gravitational search algorithm and big bang-big crunch algorithm for data clustering. *Fundamental Informaticae*, *126*(4), 319-333.

Hatamlou, A. (2013). Black hole: A new heuristic optimization approach for data clustering. *Information Sciences*, *222*(1), 175-184.

Jain, A. K. (2010). Data clustering: 50 years beyond *K*-means. *Pattern Recognition Letters*. *31*(8), 651-666.

Jain, A. K., Murty, M. N., & Flynn, P. J. (1999). Data clustering a review. *ACM Computing Surveys, 31*(3), 264-323.

Kao, Y. -T., Zahara, E., & Kao, I. W. (2008). A hybridized approach to data clustering. *Expert Systems with Applications, 34*(3), 1754-1762.

Krishna, K., & Murty, M. N. (1999). Genetic k-means algorithm. *IEEE Transactions on System, Man, and Cybernetics, Part B: Cybernetics, 29*(3), 433-439.

Karaboga, D., & Basturk, B. (2008). On the performance of artificial bee colony algorithm. *Applied Soft Computing, 8*(1), 687-697.

Kumar, V., Chhabra, J. K., & Kumar, D. (2014a). Automatic MRI brain image segmentation using gravitational search based clustering technique. In Dr. R. Srivastava, Dr. S. K. Singh, and Dr. K. K. Shukla (Eds.), *Recent Advances in Computer Vision and Image Processing: Methodologies and Applications* (pp. 313-326). IGI Global, USA.

Kumar, V., Chhabra, J. K., & Kumar, D. (2014b). Parameter adaptive harmony search algorithm for unimodal and multimodal optimization problems. *Journal of Computational Science, 5*(2), 144-155.

Kumar, V., Chhabra, J. K., & Kumar, D. (2014c). Variance-based harmony search algorithm for unimodal and multimodal optimisation problems with application to clustering. *Cybernetics and Systems: An International Journal*, *45*(6), 486-511.

Leung, Y., Zhang, J., & Xu, Z. (2000). Clustering by space-space filtering. *IEEE Transactions on Pattern Analysis and Machine Intelligence, 22*(12), 1396-1410.

Liu, B. (2014). Composite differential search algorithm. *Journal of Applied Mathematics*. Retrieved from http://www.hindawi.com/journals/jam/2014/294703/

Maulik, U., & Bandyopadhyay, S. (2000). Genetic algorithm based clustering technique. *Pattern Recognition, 33*(9), 1455-1465.

Murthy, C. A., & Chowdhury, N. (1996). In search of optimal clusters using genetic algorithms. *Pattern Recognition Letters, 17*(8)*,* 825-832.

Nanda, S. J., & Panda, G. (2014). A survey on inspired metaheuristic algorithms for partitional clustering. *Swarm and Evolutionary Computation, 16*(2)*,* 1-18.

Omran, M. G. H., Engelbrecht, A. P., & Salman, A. (2006). Dynamic clustering using particle swarm optimization with application in image segmentation. *Pattern Analysis and Applications, 8*(4)*,* 332-344.

Saida, I. B., Nadjet, K., & Omar B. (2014). A new algorithm for data clustering based on cuckoo search optimization. In J. -S. Pan, P. Kromer, & V. Snasel (Eds.), *Genetic and Evolutionary Computing*. Lecture notes in advances in intelligent systems and computing, Vol. 238, pp. 55-64. Berlin: Springer.

Satapathy, S. C., & Naik, A. (2011). Data clustering based on teaching learning-based optimization. In B. K. Panigrahi, P. N. Suganthan, S. Das, & S. C. Satapathy (Eds.), *Swarm, Evolutionary, and Memetic Computing*. Lecture notes in Computer Science, Vol. 7077, pp. 148-156. Berlin: Springer.

Selim, S. Z., & Al-Sultan, K. (1991). A simulated annealing algorithm for the clustering problem. *Pattern Recognition, 24*(10), 1003-1008.

Shelokar, P. S., Jayaraman, V. K., & Kulkarni, B. D. (2004). An ant colony approach for clustering. *Analytica Chimica Acta, 509*(2)*,* 187-195.

Sung, C. S., & Jin, H. W. (2000). A tabu search-based heuristic for clustering. *Pattern Recognition, 33*(5)*,* 849-858.

Xu, R., & Wunsch II, D. C. (2009). *Clustering*. USA: John Wiley and Sons.

Yang, X. S. (2012). Flower pollination algorithm for global optimization. In *Unconventional computation and natural computation* (pp. 240-249). Springer Berlin Heidelberg.

Yang, X. S. (2010). A new metaheuristic bat-inspired algorithm. In J. R. Gonzalez et al. (Eds.), *Proceedings of Nature Inspired Cooperative Strategies for Optimization,* Studies in Computational Intelligence, Vol. 284, pp. 65-74. Springer: Berlin.

Zhang, C., Ouyang, D., & Ning, J. (2010). An artificial bee colony approach for clustering. *Expert Systems and Applications, 37*(7)*,* 4761-4767.

Pertanika J. Sci. & Technol. 24 (2): 307 - 317 (2016)

SCIENCE & TECHNOLOGY

Journal homepage: http://www.pertanika.upm.edu.my/

Effect of Silica Filler on Viscosity, Peel Strength, Shear Strength and Tack of Styrene-Butadiene Rubber-Based Adhesive

Poh, B. T.* and Loh, W. S.

School of Industrial Technology, Universiti Sains Malaysia, 11800 Penang, Malaysia

ABSTRACT

Viscosity, peel strength, shear strength and tack of styrene-butadiene rubber (SBR)-based pressure-sensitive adhesive were studied using silica as the filler. The silica content was varied from 10-50 parts per hundred parts of rubber (phr). The tackifying resin, solvent and coating substrate used were gum rosin, toluene and poly(ethylene terephthalate) (PET) respectively. Viscosity of the adhesive was determined by a Brookfield Viscometer. Both peel strength, shear strength and tack were measured by a Lloyd Adhesion Tester operating at 10-60 cm/min. Results show that viscosity increases with silica loading due to the concentration effect. Peel strength, shear strength and tack passes through a maximum value at 20 phr silica loading, an observation which is attributed to the culmination of wettability at the optimum silica content. Peel strength decreases with the angle of testing at a fixed silica loading and coating thickness. Both peel strength, shear strength and tack increases with coating thickness and testing rates.

Keywords: Adhesion, adhesive, peel, shear, tack, rate of testing

INTRODUCTION

Several investigations have been carried out to study the effect of fillers on adhesion properties of adhesives. These include the study of the cohesive strength of silicone rubber adhesive containing an organic montmorillonite (Wang et al., 2006), surface modifications and adhesion of SBS rubber containing calcium carbonate filler by treatment with UV radiation (Romero-Sanchez et al., 2007). The effect of nanosilica and precipitated calcium carbonate on the adhesion properties of thermoplastic polyurethane adhesives were reported (Bahattab et al., 2011; Donate-Robles & Martin-Martinez, 2011). The addition of nanosilica increased the surface energy of the polyurethane as indicated by the moderate increase in the single lap shear strength of stainless steel/ polyurethane adhesive joints. It was also observed that 10 wt % of precipitated calcium

Article history:
Received: 22 July 2015
Accepted: 30 November 2015

E-mail addresses:
btpoh@usm.my (Poh, B. T.),
wwwaisan@hotmail.com (Loh, W. S.)
*Corresponding Author

ISSN: 0128-7680

carbonate filler produced the highest final adhesive strength. The adhesion properties of filled epoxy resin adhesives have also been studied by other researchers. Wolf et al. (2012) found that with the addition of less than 1% wt of carbon nanotube/protein moiety filler to epoxy adhesive, peel strength and shear strength were improved by 50% and 24%, respectively. Ghosh et al. (2013) reported that thermal stability and single lap shear joint strength of filled epoxy adhesive showed significant improvement with 10 wt % loading of Al_2O_3, Al and Cu particles compared to neat epoxy adhesive. On the other hand, Ho et al. (2013) observed that silane coupling agent-treated Ag flakes have a significant effect on the electrical resistivity and shear strength in phenolic-based Ag-filled conductive adhesive. Recently, we have investigated the effect of zinc oxide and kaolin on the shear property of natural rubber adhesives (Poh & Ng, 2013; Poh & Sulaiman, 2015). For both fillers used, viscosity increases with filler loading. However, shear strength of adhesive increases up to 20 phr of filler loading after which it decreases with further addition of filler. This observation is attributed to the culmination of cohesive strength at the optimum filler loading for both filler systems. For a fixed filler loading, shear strength increases with coating thickness and testing rate. In view of the scarcity of research carried out on filled rubber adhesives, it is thus the aim of this article to report our findings on the adhesion properties of styrene-butadiene rubber (SBR)-based adhesive using silica as the filler.

MATERIALS AND METHODS

Styrene-butadiene rubber (SBR) with a 33.5% by weight of target-bound styrene and Mooney viscosity of 50 was used as the elastomer. It was supplied by Bayer Company (Penang, Malaysia). Silica with a surface area of 50 m^2/g and specific gravity of 2.0 was selected as the filler. Gum rosin, toluene and poly(ethylene terephthalate) (PET) were used as the tackifier, solvent and coating substrate respectively in this study. All the materials were freshly supplied commercial grades and purification was not carried out prior to use.

Preparation of Adhesive

SBR was masticated on a two roll-mill for 10 minutes. An amount of 5 g of the masticated rubber was cut into small pieces to facilitate easy dissolution in 30 mL of toluene. The rubber solution was tightly closed and kept overnight at 30° C until complete dissolution of SBR occurred. This was followed by the addition of 2 g, corresponding to 40 phr of tackifier, of pulverised gum rosin into the rubber solution with constant stirring. The rubber adhesive thus produced was kept for 2 hours before the addition of silica. In this study, five different loadings of silica i.e. 0.5, 1.0, 1.5, 2.0 and 2.5 g corresponding to 10, 20, 30, 40 and 50 phr of filler were used. One control sample without silica loading was also prepared for comparison purposes.

Measurements

Viscosity. A Brookfield viscometer (model DV-II + Pro) (Middleboro, MA, USA) fitted with spindle (CPE-51) and metal cup (CPE-44Y) was used to determine the viscosity of the silica-filled SBR adhesive. The testing speed was set at 1 rpm. Both the platform and spindle head were cleaned with isopropyl alcohol to eliminate any trace of contamination. A drop of adhesive

was then put in the middle of the platform and measurement was carried out for one minute. The average viscosity was computed from at least five readings displayed.

Peel strength. Three peel modes i.e. T-, 90º and 180º peel were used in the determination of peel strength using PET film as the coating substrate. Table 1 shows the respective dimensions of the peel testing samples. The effect of angle on the peel strength was also investigated using PET substrate having the same dimension as that of a 90º sample. For all the modes of peel testing, the end of a base stock was coated using a SHEEN hand coater (Teddington, Middlesex, UK) at a coating area of 10 cm × 4 cm at 60 µm and 120 µm coating thicknesses. The face stock was then gently laid on the coated base stock to form the test specimen, which was then conditioned at 30° C for 24 hours. A Lloyd Adhesion Tester (Hampshire, UK) operating at 10-60 cm min^{-1} was used to determine the peel strength of the samples. The average peel force was calculated from the three highest peaks recorded from the load-propagation plot. Peel strength is expressed as the average load per width of the bond line required to separate progressively a flexible member from a rigid member or another flexible member (ASTM D 907).

Table 1
Dimensions of peel test sample

Mode of Peel Test	Base Stock	Face Stock
T- Peel	20 cm x 4 cm	20 cm x 4 cm
90° Peel	20 cm x 4 cm	15 cm x 7 cm
180° Peel	25 cm x 4 cm	10 cm x 10 cm

Shear strength. PET film with dimension of 20 cm x 4 cm was used as the substrate. A SHEEN hand coater was used to coat the base stock from the end of the film at a coated area of 10 cm x 4 cm at 60 µm and 120 µm coating thicknesses. One end of the uncoated PET film (face stock) was then carefully placed on the coated area of the base stock so that the testing distance was 10 cm corresponding to the coated length. The test sample was conditioned at 30° C for 24 hours before testing on a Lloyd Adhesion Tester operating at 10-60 cm min^{-1}. Shear strength was defined as the shear force per unit area of testing (N m^{-2}).

Loop tack. A PET film with dimensions of 4 cm × 25 cm was used as the substrate. It was coated at the centre with a coated area of 4 cm × 4 cm using a SHEEN hand coater at 60 µm and 120 µm coating thicknesses. The coated sample was then conditioned at 30° C for 24 hours. This was followed by the formation of a loop and the outer coated surface was gently brought into contact with a glass plate. A Lloyd Adhesion Tester operating at 10-60 cm min^{-1} was used to determine the debonding force to detach the loop from the glass plate. The loop tack was expressed as the average debonding force per area of contact (N m^{-2}).

RESULTS AND DISCUSSION

The effects of silica loading, testing rate and angle of testing on the adhesion properties are systematically discussed below.

Viscosity

The dependence of viscosity of SBR-based adhesive on silica loading is shown in Figure 1. The graph shows that viscosity of adhesive increased steadily with silica loading; the increase was greater as the filler concentration was increased. This observation is attributed to the concentration effect of the silica whereby interaction between silica and SBR occurred, resulting in the increase in viscosity of adhesive. The nonlinear dependence of viscosity on silica concentration indicates that the molecular interaction between SBR and silica did not increase linearly with silica loading, suggesting that the adhesive system was a non-ideal mixture. This observation is consistent with our previous results reported on zinc oxide and kaolin-filled natural rubber adhesives (Poh & Ng, 2013; Poh & Sulaiman, 2015).

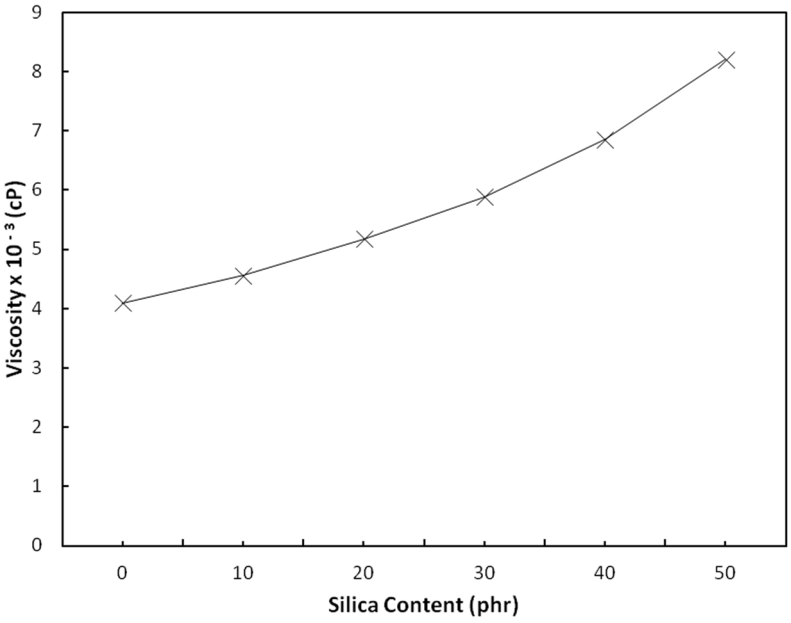

Figure 1. Variation of viscosity of SBR-based adhesive with silica content.

Peel Strength

Figures 2-4 show the dependence of peel strength on silica loading for the T-, 90º and 180º peel tests at 60 μm and 120 μm coating thicknesses. For the three modes of peel tests, peel strength increased with filler loading up to 20 phr silica content before it decreased with further addition of silica for both coating thicknesses. The initial increase in peel strength is attributed to the increase in wettability, which enhanced mechanical interlocking and anchorage of the adhesive in pores and irregularities in the adherent (Lee, 1991; Gierenz & Karmann, 2001). At the optimum silica content of 20 phr, culmination of wettability occurred whereby the lowering of surface tension provided proper flow and wetting characteristics (Poh & Chow, 2007). However, at higher filler content, the wettability of adhesive decreased as viscosity increased

with further addition of silica filler. The viscous component of adhesive was decreased by the increase in viscosity, which hindered the rubber chain mobility, hence decreasing the wettability of adhesive as shown by the drop in peel strength at the higher loading of silica. Figures 2-4 also show that for a fixed silica loading, the 120 μm coated sample consistently indicated higher peel strength compared to that of 60 μm coating thickness. This phenomenon is associated with the higher amount of adhesive in 120 μm coated substrate, which enhances the viscoelastic response of the adhesive (Leong et al., 2003) and is consistent with the general belief that peel force increases with increasing adhesive thickness up to a certain limit (Satas, 1982). The effect of testing rate on the peel strength (90º peel) at the optimum silica loading of 20 phr for 60 μm and 120 μm coating thicknesses is shown in Figure 5. Peel strength increased steadily with testing rate for both coating thicknesses, an observation that is attributed to the different viscoelastic responses as the testing rate was increased. At low testing rate, the viscoelastic response was predominantly viscous in nature and cohesive failure occurred. However, at high testing rate, the viscoelastic response was predominantly elastic, resulting in adhesive failure mode (Satas, 1982). The dependence of peel strength on peel angle is shown in Figure 6 at the optimum silica loading of 20 phr for 120 μm coating thicknesses. The plot indicates that the peel strength decreased steadily as the angle of peel test was increased. This observation is attributed to the increase of dissipation of energy in bending the tape away from the substrate at the line of detachment as the angle of detachment increased (Gent, 1987).

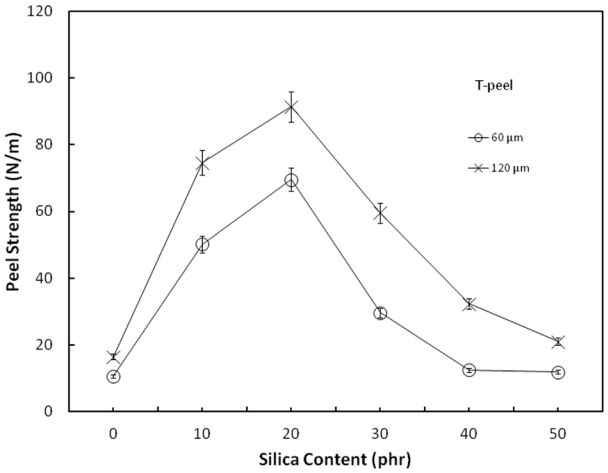

Figure 2. Variation of peel strength (T-peel) with silica content at 30 cm/min for 60 micron and 120 micron coating thicknesses.

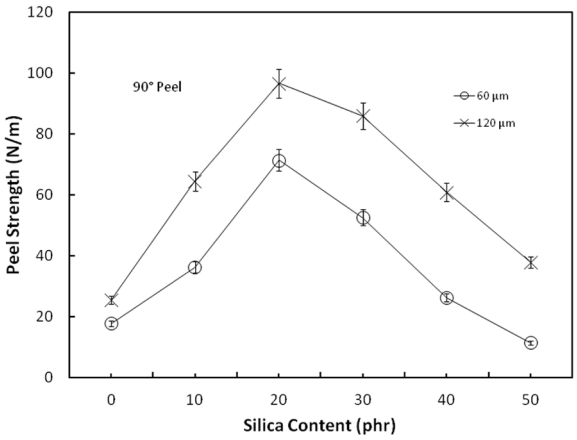

Figure 3. Variation of peel strength (90° peel) with silica content at 30 cm/min for 60 micron and 120 micron coating thicknesses.

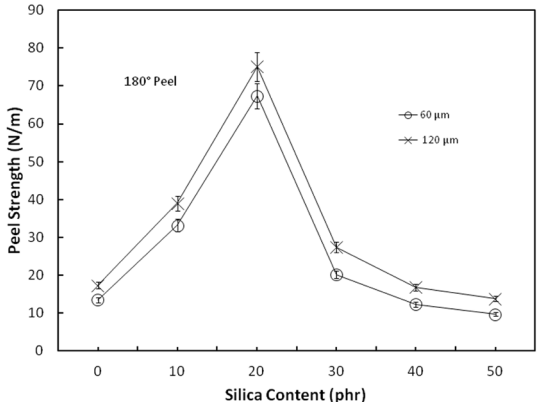

Figure 4. Variation of peel strength (180° peel) with silica content at 30 cm/min for 60 micron and 120 micron coating thicknesses.

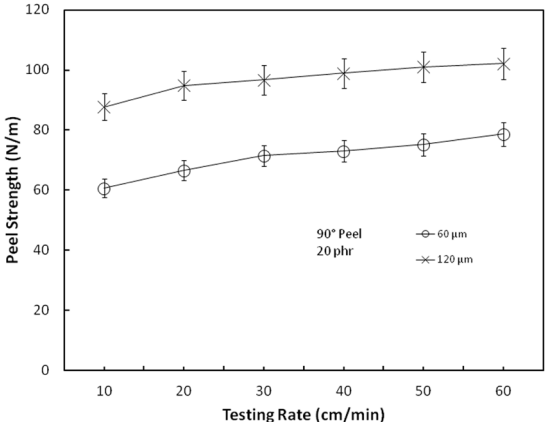

Figure 5. Dependence of peel strength (90° peel) on testing rate at 20 phr silica content for 60 micron and 120 micron coating thicknesses.

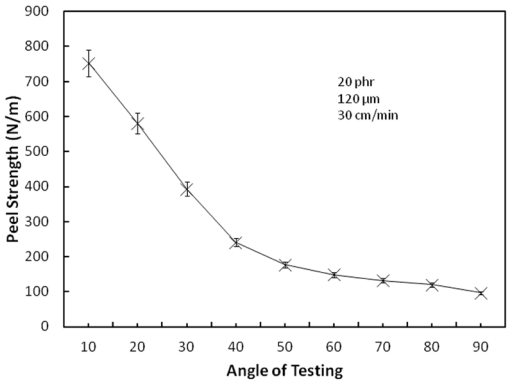

Figure 6. Dependence of peel strength on angle of testing at 30 cm/min and 20 phr silica content for 120 micron coating thicknesses.

Shear Strength

Figure 7 shows the effect of silica loading on the shear strength of SBR-based adhesive at 60 µm and 120 µm coating thicknesses. As in the case of peel strength, the shear strength also increased with silica content up to an optimum loading of 20 phr filler. This observation is attributed to the steady increase in the cohesive and adhesive strength up to the optimum filler loading where maximum cohesive strength occurred as reflected by the peak value of shear strength in Figure 7. However, after the optimum filler loading, cohesive strength decreased due to the increasing dilution effect of silica with further filler loading. For a fixed silica loading, the shear strength increased with coating thickness. The observation is attributed to the increase in the amount of adhesive in thicker coated samples, which enhanced the shearing resistance; hence, this increased the cohesive strength of the adhesive. Figure 8 shows the effect of testing rate on shear strength of silica-filled SBR adhesive at 20 phr filler for 60 µm and 120 µm coating thicknesses. As in the case of peel strength, shear strength also increased steadily with testing rate for both coating thicknesses. This finding is attributed to the difference in viscoelastic response of the rubber adhesive as testing rate was increased. At low testing rate, the viscoelastic response was predominantly viscous in nature, resulting in lower shear strength. On the other hand, at higher testing rate, the viscoelastic response was predominantly elastic, contributing to higher shear strength where adhesive failure mode occurred.

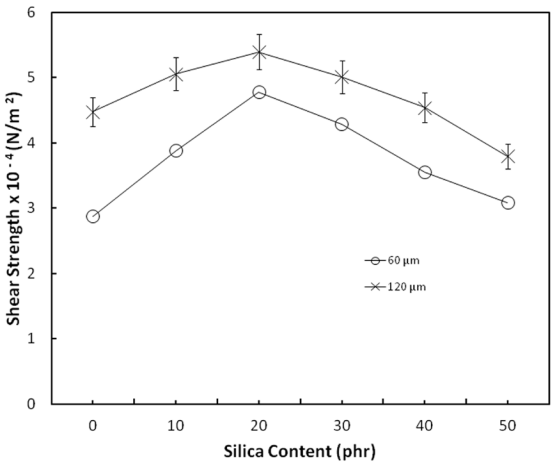

Figure 7. Variation of shear strength with silica content at 30 cm/min for 60 micron and 120 micron coating thicknesses.

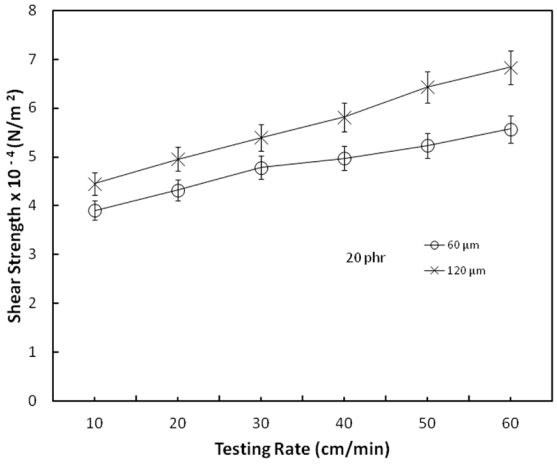

Figure 8. Dependence of shear strength on testing rate at 20 phr silica content for 60 micron and 120 micron coating thicknesses.

Tack

The dependence of tack on silica loading at 60 µm and 120 µm coating thicknesses is shown in Figure 9. As in the case of peel and shear strength, tack also increased with silica loading up to the optimum value of 20 phr content for both coating thicknesses. This observation is again attributed to the increase in wettability, which culminated at 20 phr silica loading as shown by the maximum tack value. At the optimum silica loading, the adhesive was able to conform to the irregularities of the adherend i.e. low surface energy condition was observed (Satas, 1982). However, as the filler loading was further increased beyond 20 phr, wettability decreased due to the increase in viscosity, which reduced the ability of the adhesive to flow and wet the substrate. For a fixed silica content, the 120 µm coated substrate consistently showed higher tack value compared to the 60 µm coated sample. This observation is ascribed to the higher

amount of adhesive, which increased the mechanical interlocking of adhesive molecules in the porous or rough substrates (Rezaeian et al., 2012) as coating thickness was increased and consequently, increased the wettability as shown by the higher tack value in thicker-coated samples as shown in Figure 9. The effect of testing rate on the tack property is illustrated in Figure 10. The graph indicates that tack increased steadily with testing rate for both coating thicknesses. This phenomenon is associated to the change in viscoelastic responses as testing rate was increased. At low testing rate, the response was predominantly viscous and cohesive failure occurred whereas at high testing rate, the response was predominantly elastic, resulting in the adhesion failure (Satas, 1982). The increase in tack value at high testing rate is thus attributed to the increase in elastic component of the viscoelastic response of the silica-filled adhesive.

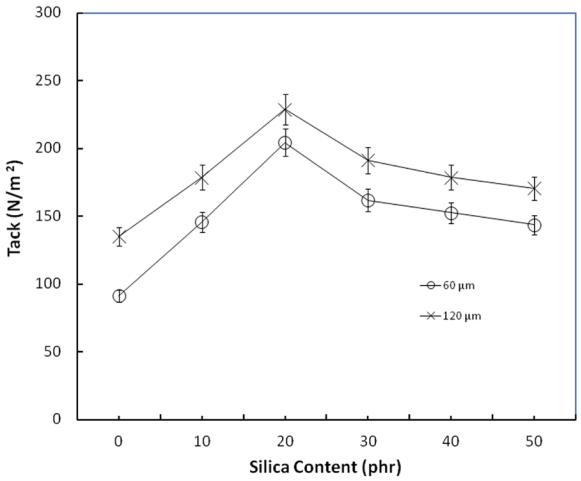

Figure 9. Variation of tack with silica content at 30 cm/min for 60 µm and 120 µm coating thicknesses.

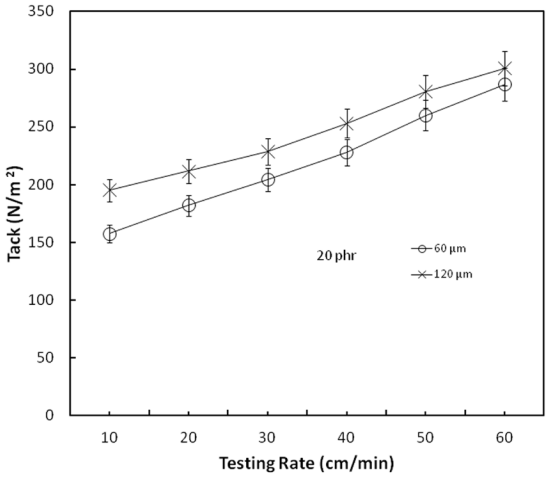

Figure 10. Dependence of tack on testing rate at 20 phr silica content for 60 µm and 120 µm coating thicknesses.

CONCLUSION

The viscosity of SBR-based adhesive increased with increases in silica loading, an observation which is attributed to the molecular interaction between silica and SBR. This concentration effect increased as silica content was increased. Peel strength, shear strength and tack increase with silica loading up to 20 phr of the filler before decreasing with further addition of silica filler. This observation is attributed to the increase in wettability and cohesive strength, which culminates at 20 phr of silica loading. Peel strength decreased with angle of peel test. In all cases, peel strength, shear strength and tack increased with coating thicknesses, an observation that is attributed to the higher amount of adhesive in thicker-coated samples. All the adhesion properties increased with increase in testing rate due to the difference in viscoelastic response as testing rate was increased, whereby viscous and elastic response occurred at low and high testing rates, respectively.

ACKNOWLEDGEMENTS

The authors acknowledge the Fundamental Research Grant Scheme (FRGS) and help from Universiti Sains Malaysia that enabled this work to be completed.

REFERENCES

Bahattab, M. A., Donate-Robles, J., Garcia-Pacios, V., & Martin-Martinez, J. M. (2011). Characterization of polyurethane adhesives containing nanosilicas of different particle size. *International Journal of Adhesion and Adhesives, 31*(2), 97-103.

Donate-Robles, J., & Martin-Martinez, J. M. (2011). Addition of precipitated calcium carbonate filler to thermoplastic polyurethane adhesives. *International Journal of Adhesion and Adhesives, 31*(8), 795-804.

Gent, A. N., & Kaang, S. Y. (1987). Effect of peel angle upon peel force. *The Journal of Adhesion, 24*(2-4), 173-181.

Ghosh, P. K., Halder, S., Goyat, M. S., & Karthik, G. (2013). Study on thermal and lap shear characteristics of epoxy adhesive loadied with metallic and non-metallic particles. *The Journal of Adhesion, 89*(1), 55-75.

Gierenz, G., & Karmann, W. (Eds.). (2001). *Adhesives and adhesive tapes* (p.4). New York: Wiley-VCH.

Ho, L. N., Wu, T. F., & Nishikawa, H. (2013). Properties of phenolic-based Ag-filled conductive adhesive affected by different coupling agents. *The Journal of Adhesion, 89*(11)*,* 847-858.

Lee, L. H. (1991). *Adhesive bonding* (p. 19). New York: Plenum Press.

Leong, Y. C., Lee, L. M. S., & Gan, S. N. (2003). The viscoelastic properties of natural rubber pressure-sensitive adhesive using acrylic resin as a tackifier. *Journal of Applied Polymer Science, 88*(8), 2118-2123.

Poh, B. T., & Chow, S. K. (2007). Effect of zinc oxide on the viscosity, tack and peel strength of ENR 25-based pressure-sensitive adhesives. *Journal of Applied Polymer Science, 106*(1)*,* 333-337.

Poh, B. T., & Ng, W. C. (2013). Effect of zinc oxide concentration and testing rate on shear properties of standard Malaysian rubber (SMR) L-based pressure-sensitive adhesives. *Journal of Elastomers and Plastics, 45*(1), 95-103.

Poh, B. T., & Sulaiman, N. S. (2015). Shear property of kaolin-filled standard Malaysian rubber (SMR L) pressure-sensitive adhesive. *The Journal of Adhesion, 91*(4), 309-319.

Rezaeian, I., Zahedi, P., & Rezaein, A. J. (2012). Rubber adhesion to different substrates and its importance in industrial applications: A review. *Journal of Adhesion. Science and Technology*, *26*(6), 721-744.

Romero-Sanchez, M. D., Walzak, M. J., Torregrosa-Macia, R., & Martin-Martinez, J. M. (2007). Surface modifications and adhesion of SBS rubber containing calcium carbonate filler by treatment with UV radiation. *International Journal of Adhesion and Adhesives, 27*(6), 434-445.

Satas, D. (Ed.). (1982). *Handbook of pressure-sensitive adhesive technology* (pp. 63, 54, 40-41). New York: Van Nostrand Reinhold.

Wang, J. C., Chen, Y., & Jin, Q. J. (2006). New organic montmorillonite: Application to room-temperature vulcanized silicone rubber adhesive system. *The Journal of Adhesion. 82*(4)*,* 389-405.

Wolf, A., Buchman, A., Eitan, A., Fine, T., Nevo, Y., Heyman, A., & Shoseyov, O. J. (2012). Improved adhesives containing CNT/SP1 nano fillers. *The Journal of Adhesion, 88*(4-6)*,* 435-451.

Pertanika J. Sci. & Technol. 24 (2): 319 - 330 (2016)

SCIENCE & TECHNOLOGY

Journal homepage: http://www.pertanika.upm.edu.my/

Artificial Neural Network for Modelling Rainfall-Runoff

Aida Tayebiyan[1]*#, Thamer Ahmad Mohammad[1], Abdul Halim Ghazali[1] and Syamsiah Mashohor[2]

[1]Department of Civil Engineering, Faculty of Engineering, Universiti Putra Malaysia, 43400 Serdang, Selangor, Malaysia

[2]Department of Computer and Communication Systems Engineering, Faculty of Engineering, Universiti Putra Malaysia, 43400 Serdang, Selangor, Malaysia

ABSTRACT

The use of an artificial neural network (ANN) is becoming common due to its ability to analyse complex nonlinear events. An ANN has a flexible, convenient and easy mathematical structure to identify the nonlinear relationships between input and output data sets. This capability could efficiently be employed for the different hydrological models such as rainfall-runoff models, which are inherently nonlinear in nature and therefore, representing their physical characteristics is challenging. In this research, ANN modelling is developed with the use of the MATLAB toolbox for predicting river stream flow coming into the Ringlet reservoir in Cameron Highland, Malaysia. A back propagation algorithm is used to train the ANN. The results indicate that the artificial neural network is a powerful tool in modelling rainfall-runoff. The obtained results could help the water resource managers to operate the reservoir properly in the case of extreme events such as flooding and drought.

Keywords: Artificial neural networks, back propagation algorithm, rainfall-runoff modelling

INTRODUCTION

Rainfall-Runoff modelling is significantly useful for the design and operation of various components of water resource projects like dams, barrages, water supply schemes etc. (Ghumman et al., 2011). Furthermore, the results of modelling could support hydrologists in decision-making in the face of bad predictions. It could, therefore, help water resource managers to prevent damage to private and public property as well as to avoid health and ecological dangers that can

Article history:
Received: 18 August 2015
Accepted: 4 February 2016

E-mail addresses:
ida_tayebiyan@yahoo.com (Aida Tayebiyan),
thamer@upm.edu.my (Thamer Ahmad Mohammad),
abdhalim@upm.edu.my (Abdul Halim Ghazali)
syamsiah@upm.edu.my (Syamsiah Mashohor)
*Corresponding Author
Author's Current Affiliation
Environmental Health Engineering Research Centre,
Kerman University of Medical Sciences, Kerman, Iran

ISSN: 0128-7680

result from flooding. Due to the great temporal and spatial variability of precipitation patterns, watershed characteristics and the number of parameters involved in the process of modelling and due to the presence of complex nonlinear relationships in the transformation of rainfall into runoff, the rainfall-runoff relationship is one of the most difficult hydrologic problems facing water resource managers (Wu & Chau, 2011; Young & Liu, 2014). Many approaches have been applied to estimate runoff, such as distributed physical-based models, stochastic models, conceptual models and black box models (Tingsanchali & Gautam, 2000; Bahremand & De Smedt, 2008; Bahremand & De Smedt, 2010). Conceptual modelling uses an approximation to forecast daily, monthly or seasonal stream flows in the long term. The Stanford Watershed Model (SWM) is an instance of conceptual modelling, which uses 20-30 variables for runoff forecasting (El-Shafie et al., 2011). Due to the numerous parameters and the high complexity of parameter interaction, the optimisation of model parameters is mostly applied by method of trial-and-error.

In order to overcome these difficulties, Artificial Neural Networks (ANNs) have been proposed. Indeed, they have recently received considerable attention as powerful computing systems in approaching hydrology problems due to their practical applications and ability to map the extremely complex and nonlinear systems among hydrological variables such as rainfall-runoff (Govindaraju, 2000; Wu & Chau, 2011). Since ANNs do not consider the physics of the problem, they are treated as black-box models; however, some researchers have recently reported that it is possible to detect physical processes in training ANN hydrologic models (Jain & Srinivasulu, 2004; Sudheer & Jain, 2004). Although there are extensive sorts of ANN algorithms, the main duty of all ANNs is to map a set of inputs into a set of outputs. ANNs are an information-processing system, which comprises many nonlinear interconnected elements called neurons (Srinivasulu & Jain, 2006). Researchers have investigated and concluded that ANNs gave better results when applied to problems that encountered noise or involved pattern generalisation, abstraction, diagnosis and recognition, and also in complex systems that do not have enough information or poor descriptions (Zhang & Govindaraju, 2000; Jain & Srinivasulu, 2004). In addition, ANNs can be used in situations when input data are insufficient or obscured by nature. It can be summarised that ANN approaches have the capability to map the patterns of the highly unknown input and output relationship and overcome the aforementioned difficulties. So, many researchers have used the ANN algorithm to discover the rainfall-runoff relationship due to its ability to generalise patterns in cases of ambiguous and insufficient data and to incorporate a complex model without enough knowledge or probability distributions. However, the conceptual models need numerous parameters for modelling, but all the required data are not available in many watersheds.

Another drawback of the conceptual method is using an approximation for prediction, which affects the accuracy of the results. In addition, the performance of the model is highly subjective and dependent on the user's knowledge, ability, understanding of watershed characteristics and skill in running the model. Although this type of modelling provides reasonable accuracy, its application is limited due to the aforementioned difficulties (Gökbulak et al., 2015). All these gaps can be covered by ANNs.

The purpose of this study was to develop an artificial neural network (ANN) model for simulation of daily runoff. So, the application of ANN methodology for modelling daily

runoff discharge of the Bertam River was investigated in this research. The Bertam River is the main river feeding the Ringlet reservoir in Cameron Highland, Malaysia. Since the Ringlet reservoir is a hydropower reservoir system, the results of the present study could help the managers to predict the future discharge to predict the future hydropower as well as to control the danger of flooding in times of extreme phenomena. In order to develop a rainfall-runoff model, three parameters, such as daily observed rainfall, daily observed stream flow and daily evapotranspiration data (estimated by Hargreaves-Samani equation) from 2003-2012 were used to train the network based on the back propagation learning rule. Afterwards, the performance of the developed ANN model in simulating the rainfall-runoff was assessed by four quantitative statistical indicators, such as the Nash-Sutcliffe Coefficient (E), Pearson Correlation of Coefficient (r), Root Mean Square Error (RMSE) and Mean Bias Error (MBE). The description of methods and the given resluts are described in detail in the following sections.

STUDY AREA AND DATA COLLECTION

The present research focused on the Cameron Highlands, Pahang, Malaysia. The Sultan Abu Bakar dam was constructed on the Bertam River in the district of Cameron Highland. The lake that was created from the construction of the dam is known as the Ringlet Reservoir (Figure 1).

The Ringlet Reservoir is nearly 3.2 km long and 0.4 km wide. It impounds the combined stream flow from Telom Tunnel and the Bertam River and other minor tributaries. The total Bertam catchment area is 159km^2. The principal aim of this research was to build a model for simulating the Bertam River stream flow coming into the Ringlet Reservoir. An average monthly inflow of the Bertam River is shown in Figure 2.

The data of rainfall, evapotranspiration and stream flow were collected to map the rainfall-runoff relationship. Daily rainfall and stream flow data were gathered from Tenaga Nasional Berhad Company. Evapotranspiration data were estimated by the Hargreaves-Samani equation, which needs the observed temperature data for estimation. The temperature data were collected from the nearest station into the reservoir (Table 1).

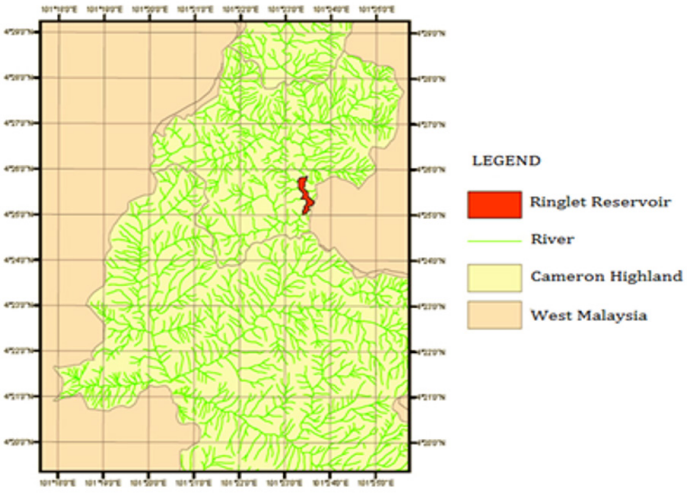

Figure 1. Location of Ringlet Reservoir in Cameron Highland, Malaysia.

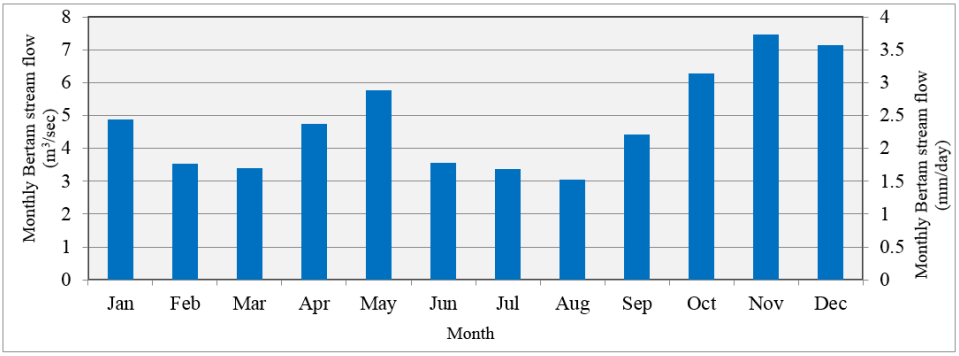

Figure 2. Average monthly inflow of Bertam River coming into Ringlet Reservoir.

Table 1
Weather Data Used as LARS-WG Input

Station	Climate parameters	Longitude	Latitude	Altitude (m)	Source
Kajiklim Habu	Daily precipitation	101° 23' E	4° 25' N	1101.46	Tenaga Nasional Berhad
Cameron Highland	Daily min and max temperatures	101° 22' E	4° 28' N	1545	Meteorological Department

Evapotranspiration Estimation Method

In this research, the Hargreaves-Samani (HS) equation was employed to estimate the amount of evapotranspiration (ET_0) at the reservoir (Lima et al., 2013; Raziei & Pereira, 2013). The required data for the HS method are only the observed minimum temperature (T_{min}) and maximum temperature (T_{max}) for the estimation of daily evapotranspiration (mm/day), which is expressed as:

$$ET_0 = 0.0135\ K_{Rs}\ R_a\ (T_{max} - T_{min})^{0.5}\ (T_a + 17.8) \quad [1]$$

In this equation, 0.0135 is a constant, which converts American units to the international system of units. K_{Rs} is the adjustment coefficient of radiation. In the typical version of HS, the value of K_{Rs} is equal to 0.17. R_a is called extraterrestrial radiation, which will be explained in detail in the next section. T_{min}, T_{max}, T_a are minimum, maximum and average daily air temperature (°C), respectively (Hargreaves & Allen, 2004).

Extraterrestrial radiation (Ra). The extraterrestrial radiation (R_a) for each day of the year and for various latitudes is estimated from the solar declination, solar constant and the time of the year (Raes & MUNOZ, 2008). So, for a certain latitude, the R_a is constant for each day of every year. The R_a formula is expressed as follows:

$$R_a = (24*60/\prod)\ G_{sc}\ d_r\ [w_s \sin(\alpha) \sin(\varphi) + \cos(\alpha) \cos(\varphi) \sin(w_s)] \quad [2]$$

In this equation, R_a = extraterrestrial radiation (MJ m^{-2}. Day^{-1}); G_{sc} = solar constant (0.0820 MJ m^{-2} min^{-1}); d_r = inverse relative distance Earth-Sun; w_s = sunset hour angle (rad); α = latitude (rad); φ = solar declination (rad). The unit of latitude (α) is in radians, which has a positive sign for the northern hemisphere and negative sign for the southern hemisphere. The conversion equation from decimal degrees to radians is given by:

$$[Radians] = (\prod/180)[decimal\ degrees] \quad [3]$$

The inverse relative distance Earth-Sun and solar declination is expressed by:

$$d_r = 1+0.003\cos[(2\prod/365)J] \quad [4]$$

$$\varphi = 0.409\sin[(2\prod J/365)-1.39] \quad [5]$$

In these equations, J is the number of days in any year (from 1 January to 31 December).

In order to compute the evapotranspiration based on the Hargreaves-Samani equation, minimum and maximum temperature data were collected from Cameron Highland station, and extraterrestrial radiation was calculated as a function of day and latitude. The latitude of the reservoir is 4.42.

Artificial Neural Networks Procedure

Artificial Neural Networks (ANNs) are information-processing systems that imitate the functions of the human brain. The ANN structure comprises a number of processing elements, which are called neurons, and the interconnections between the neurons are called weights (Kisi et al., 2013). In the architecture of ANN, neurons are classified in groups, and are called layers. The neurons in one layer have connections to those neurons in adjacent layers, but not to those in the same layer. The strength of the connection between two neurons in adjacent layers is known as their weight (Lake et al., 2009). Most of the developed ANN models use three layers: input, hidden and output layers. The input layer is the layer where the data import to the network, data processing is done in the hidden layer, and the output layer is where the results of imported data are generated. Overall, ANN models can be either 'feed forward' or feedback networks. The feed forward network is selected for use in this study. Based on this network, the information from the input layer passes into the output layer in the forward direction only. An important stage in developing an ANN model is its training to determine the weight matrix in order to learn the relationship between the data introduced. There are two principal types of training mechanisms: supervised and unsupervised. A supervised training method needs an external teacher or a guide to be involved throughout the training process. The main objective of this training is to minimise the error at the output layer by searching for a strong connection from generated outputs that are equal or close to the targets. The most popular supervised training method employed in the sciences and engineering for the training of the feed forward ANN is called the back propagation method (Srinivasulu & Jain, 2006). Back propagation is part of a gradient descent method used to train the ANN model. ANN has a parallel processing system that interconnects the neural computing elements. The system architecture is illustrated in Figure 3 (Shirke et al., 2012).

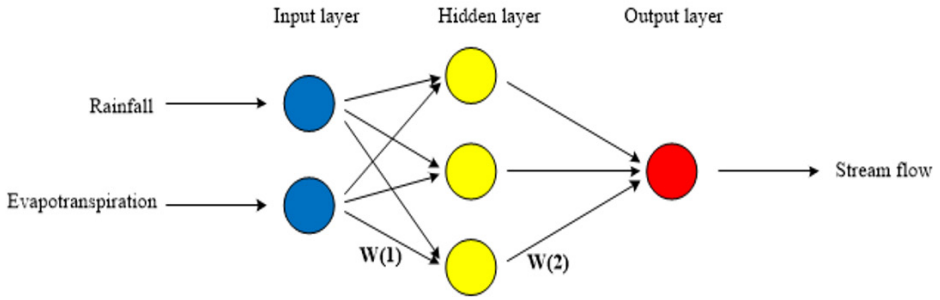

Figure 3. Architecture of back propagation ANN model.

The many neurons (also known as 'nodes') of the ANN process the information. The signals are transferred by employing the connecting links. These links have associated weights, which will be multiplied by the incoming signal (input). Furthermore, the output signal is determined using activation functions to the net input. There are different learning mechanisms, which help the ANN to discover knowledge (Kohonen, 2012).

In the ANN structure, each layer comprises several nodes. The layers are interconnected by associated weights. Each node in the input layer (k=1,2,..,m) disseminates the input signal to the hidden layer. Any hidden node (i=1,2,…,n) calculates its weighted input signals according to:

$$U_{ink}=b_i+X_kW_{ki} \quad [6]$$

In this equation, W_{ki} is an associated weight between input layer node (k) and output layer node (i), X_k is an input signal and b_i is the weight for any bias. Later, the current formulation will be used to apply the activation function in order to calculate the output signal from any input signal according to:

$$U_i=f(U_{ink}) \quad [7]$$

The neurons go through an activation function to generate the result. The system, therefore, needs continuous-transfer functions in order to determine the output of neurons based on its input. The most common transfer functions are identity functions, binary functions, binary sigmoid (Logistic) functions and binary sigmoid (Hyperbolic Tangent) functions. In the present research, the sigmoid function is used (Ehret, 2014). This transfer function is a continuous, differential and monotonically increasing function, which is typically employed in back propagation network. Later, the signal transmits from the second to third layer and the error is transmitted from the output layer back to the earlier layers. This process is called back propagation because the output error goes back to the input nodes in order to revise the weights.

ANN learning process. The learning process is a procedure that modifies the network weights and biases. The duty of the learning process is to train the network system to do some tasks. There are three different learning rules: supervised learning, unsupervised learning and reinforcement learning. In the current research, supervised learning is used.

The system will be trained based on the training data to map the relationship between input-output. When the inputs are imported to the network, the outputs will be compared with

the targets. In this step, the learning rule is employed to modify the weights and biases of the system in order to decrease the difference between the outputs and targets.

ANN training procedure. An ANN is used to discover the relationship between the input and output data. Several techniques can be employed to assign a strength connection among data sets. One method is to set the weights based on prior knowledge. This method cannot be applied for some models due to lack of information and knowledge. A neural network is an efficient way to overcome these difficulties. In this technique, the network will be trained by teaching patterns and letting it adjust its weights and biases based on the learning rules. The problem still exists of how to adjust the associated weights from the input layer to the hidden layer. In order to solve this problem, the back propagation learning rule is used. Based on the back propagation, the errors for the elements of the hidden layer are specified by back-propagating the errors from the elements of output layer. The weights of the network are adjusted by minimising the error between the target and computed outputs. The network weights are continuously revised until the minimum error is obtained (Nayak et al., 2013; Kisi et al., 2013). As a result, training pairs are chosen from the training set, and the network computes the outputs according to the inputs used for the training pair. The obtained result from the network is then compared with the outputs by the training pair. According to this result, the weights add biases to all neurons, modified by a coefficient is based on the discrepancy between actual output and calculated output (errors), the derivation of the sigmoid function and actual output. The amount of neuron weight adjustment depends largely on the learning rate (α), which is a single coefficient that is multiplied by all adjustments. A small learning rate does not allow the network to learn and therefore, it will capture a local minimum, meaning it will not discover more precise weights. However, large learning rates produce extremely poor network results. Therefore, selecting the proper learning rate is very important before starting ANN training (Shirke et al., 2012).

Model development. In the present research, an ANN was developed to map the rainfall-runoff relationship. The more factors used, the more accurate results were obtained. Three types of data were therefore gathered: rainfall, evapotransipration and stream flow. The input layer comprised two layers (rainfall and evapotranspiration) and the stream flow constituted the output layer.

The whole data set was divided into two subsets, including the training set and testing set. Seventy per cent of the data was used for training and the remaining 30 per cent comprised the testing set. In the training sets, the adjusted weights and biases of the network were determined, and the test set was employed to prevent the networks from being over-trained. The overall idea in selecting a good training set from the available data series was to have extreme events (including all minimum and maximum values in the training sets).

Another factor, which is one of the most significant characteristics of ANNs, is the number of neurons in the hidden layers. If the number of neurons is insufficient, the network cannot configure the complex data set and the obtained results will be a poor fit. Conversely, if the number of neurons is too high, the time required for network training will be long, and the network might over-fit the data (Rodríguez-González et al., 2011). In the present research, the number of neurons was determined by trial and error. The best result was obtained using 10 neurons. The proposed architecture was developed in order to predict the Bertam River runoff coming into the Ringlet Reservoir. The obtained results give valuable information to water

resource managers to operate the reservoir efficiently and protect the system from extreme events such as flooding.

Model evaluation. The performance of the developed ANN model in simulating the rainfall-runoff was assessed by four statistical evaluation measurements: the Nash-Sutcliffe Coefficient (Riad et al., 2004), Pearson Correlation of Coefficient (*r*), Root Mean Square Error (*RMSE*) and Mean Bias Error (*MBE*) (Riad et al., 2004). *RMSE* and *MBE* statistics evaluate the efficiency of the model in terms of its ability to predict data from a calibrated model. The other statistics *E* and *r* quantify the effect of the ANN model in capturing the dynamic, complex and nonlinear rainfall-runoff processing. These statistical criteria are calculated according to the following equations

Nash-Sutcliffe Coefficient (*E*)

$$E=1-\frac{\sum_{i=1}^{n}(X_{obs,i}-X_{model,i})^2}{\sum_{i=1}^{n}(X_{obs,i}-\overline{X_{obs,i}})^2} \quad [8]$$

(Correlation Coefficient (*r*)

$$r=\frac{\sum_{i=1}^{n}(X_i-\overline{X_i}).(Y_i-\overline{Y_i})}{\sqrt{\sum_{i=1}^{n}(X_i-\overline{X_i})^2.(Y_i-\overline{Y_i})^2}} \quad [9]$$

Root Mean Square Error (*RMSE*)

$$RMSE=\sqrt{\frac{\sum_{i=1}^{n}(X_{obs,i}-X_{model,i})^2}{n}} \quad [10]$$

Mean Bias Error (*MBE*)

$$MAE=\frac{\sum_{i=1}^{n}(X_{model,i}-X_{obs,i})}{n} \quad [11]$$

In these equations, the parameters $X_{model,i}$ and $X_{obs,i}$ are simulated and observed values, respectively and $\overline{X_{obs,i}}$ is the mean value of observed data and n is the number of samples. Furthermore, X_i and Y_i are the input and output values of the ANN model respectively and $\overline{X_i}$ and $\overline{Y_i}$ are the mean values of input and output data, respectively.

RESULTS AND DISCUSSION

An ANN was developed using three types of data: rainfall, evapotranspiration and stream flow. The available data covering the duration of 10 years (2003-2012) were employed in this research. The imported data used to build the ANN model were taken from the Bertam River catchment, Malaysia. The daily rainfall data were collected from the nearest station (Kajiklm Habu station) to the Ringlet reservoir, and daily evapotransipation data were estimated by the Hargreaves-Samani equation. Another required data set was stream flow, which was taken

from the Bertam River catchment and constituted the output layer. The units of stream flow were converted from m^3/sec into mm/day and then used in the model. This conversion was made due to improve the network performance. The number of neurons and hidden layers was determined by trial and error. The results indicated that ANN could give the best output by using 10 neurons and three hidden layers.

A number of statistical measurements were calculated to evaluate the network performance in both training and test sets (Table 2). The Nash-Sutcliffe coefficient was used to specify the predictive power of the hydrological models, which obtained 0.77 in training sets and 0.74 in testing sets. These results show that the constructed network had an acceptable predictive power. The correlation coefficient is a measure of the strength and direction of the linear relationship between two or more variables. The results indicate that the ANN model had good ability to capture the relationship between input/output in both training and test sets. RMSE and MBE are frequently-used measures of the differences between values (sample values) predicted by a model and the values actually observed, and in this model the differences were found to be negligible. Overall, the evolution measurements illustrate the ability of the ANN as a predictor to simulate the observed data. The results indicate that the ANN model has good ability to capture the nonlinearity of input/output in both training and test sets. It could, therefore, be used as a predictor to simulate the rainfall-runoff model.

Table 2
Statistical Evaluation Measurements of the Ringlet Reservoir

Model Evaluation	Training Set	Test Set
Nash-Sutcliffe Coefficient (*E*)	0.77	0.74
Correlation Coefficient (*r*)	0.88	0.86
Root Mean Square Error (*RMSE*)	0.17	0.17
Mean Bias Error (*MBE*)	0.001	0.004

The comparison between daily observed (actual) and simulated (predicted) Bertam river stream flow data from 2003-2012 was calculated and sis hown in Figure 4. The coefficient of determination (R^2) is the measurement that indicates the goodness fit of a model or represents how well data fit a statistical model. This measurement can vary from 0 to 1. The closest value to 1 shows the strongest fit between observed and simulated data. The R^2 result was found to be 0.76 in this model, which is an acceptably good result.

Furthermore, the linear regression between observed stream flow (Y) and the simulated stream flow (X) was found, and the best line fit for simulation period (2003-2012) was determined (Eq. 12). This equation shows the general relationship between observed and predicted values. This equation can be used to validate the predicted value. For example, for predicting stream flow, observed rainfall and evapotranspiration data should be imported to the constructed model and the model should then be run to give the predicted (modelled) stream flow. After determination of the modelled stream flow value (X), Eq (11) can be used to modify this value for a more accurate stream flow (Y) reading.

$$Y=0.9921X \quad [11]$$

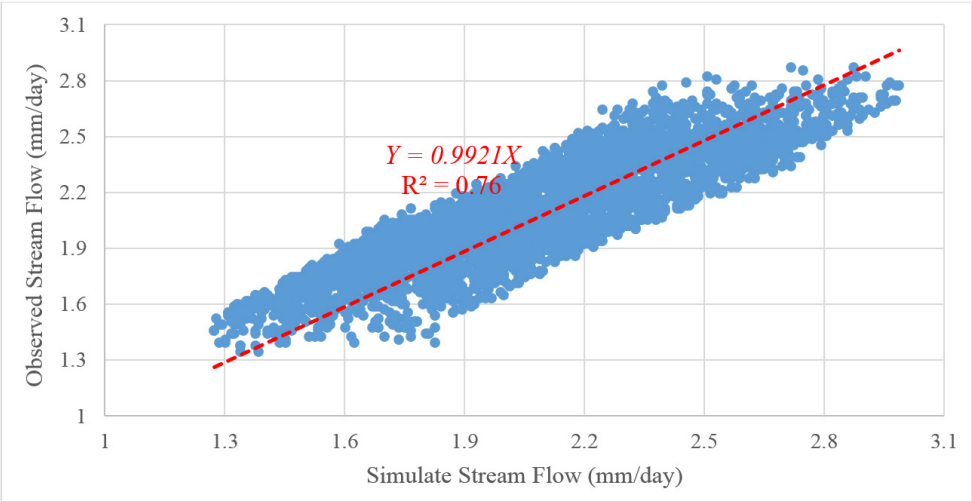

Figure 4. Comparison between daily observed (actual) and simulated (predicted) Bertam River runoff from 2003-2012.

CONCLUSION

In the present research, an Artificial Neural Network (ANN) was used to predict daily river runoff as a function of daily evapotranspiration and rainfall for the Bertam river stream flow coming into the Ringlet Reservoir in Cameron Highland, Malaysia. The back propagating learning rule was employed to train the network. The performance of the developed model was then evaluated by statistical evaluation measurements, such as the Nash-Sutcliffe Coefficient (E), Pearson Correlation of Coefficient (r), Root Mean Square Error (RMSE) and Mean Bias Error (MBE). The results indicated that ANN could capture the nonlinearity of rainfall-runoff modelling very well with 76% predictive power for simulation in hydrological models. The given results provide valuable information, which could help water resource managers to predict future stream flow into the reservoir, especially in extreme phenomena in order to mitigate the danger of damage. To improve the predictive power of the ANN model, it is recommended to include in the future other environmental factors as assessed parameters, such as deforestation, agricultural activities and land use.

REFERENCES

Bahremand, A., & De Smedt, F. (2008). Distributed hydrological modeling and sensitivity analysis in Torysa Watershed, Slovakia. *Water Resources Management, 22*(3), 393-408.

Bahremand, A., & De Smedt, F. (2010). Predictive analysis and simulation uncertainty of a distributed hydrological model. *Water resources management, 24*(12), 2869-2880.

Ehret, A. (2014). *Artificial Neural Networks for Genome-enabled Prediction in Cattle: Potential and Limitations* (Doctoral dissertation, Selbstverl. des Inst. für Tierzucht und Tierhaltung der Christian-Albrechts-Univ. zu Kiel).

El-Shafie, A., Mukhlisin, M., Najah, A. A., & Taha, M. (2011). Performance of artificial neural network and regression techniques for rainfall-runoff prediction. *International Journal of the Physical Sciences, 6*(8)*,* 1997-2003.

Ghumman, A., Ghazaw, Y. M., Sohail, A., & Watanabe, K. (2011). Runoff forecasting by artificial neural network and conventional model. *Alexandria Engineering Journal, 50*(4)*,* 345-350.

Gökbulak, F., Şengönül, K., Serengil, Y., Yurtseven, İ., Özhan, S., Cigizoglu, H. K., & Uygur, B. (2015). Comparison of rainfall-runoff relationship modeling using different methods in a forested watershed. *Water resources management*, *29*(12), 4229-4239.

Govindaraju, R. S. (2000). Artificial neural networks in hydrology, II: hydrologic applications. *Journal of Hydrologic Engineering, 5,* 124-137.

Hargreaves, G. H., & Allen, R. G. (2004). Closure to 'history and evaluation of Hargreaves evapotranspiration equation' by George H. Hargreaves and Richard G. Allen. *Journal of Irrigation and Drainage Engineering, 130*(5), 448-449.

Jain, A., & Srinivasulu, S. (2004). Development of effective and efficient rainfall-runoff models using integration of deterministic, real-coded genetic algorithms and artificial neural network techniques. *Water Resources Research, 40*(4).

Kisi, O., Shiri, J., & Tombul, M. (2013). Modeling rainfall-runoff process using soft computing techniques. *Computers and Geosciences, 51,* 108-117.

Kohonen, T. (2012). *Self-organization and associative memory.* New York: Springer .

Lake, H. R., Akbarzadeh, A., & Mehrjardi, R. T. (2009). Development of pedotransfer functions (PTFs) to predict soil physico-chemical and hydrological characteristics in southern coastal zones of the Caspian Sea. *Journal of Ecology and the Natural Environment, 1*(7)*,* 160-172.

Lima, J. R. D. S., Antonino, A. C. D., Souza, E. S. D., Hammecker, C., Montenegro, S. M. G. L., & Lira, C. A. B. D. O. (2013). Calibration of Hargreaves-Samani Equation for estimating reference evapotranspiration in sub-humid region of Brazil. *Journal of Water Resource and Protection, 5,* 1-5.

Nayak, P., Venkatesh, B., Krishna, B., & Jain, S. K. (2013). Rainfall-runoff modeling using conceptual, data driven, and wavelet based computing approach. *Journal of Hydrology, 493*, 57-67.

Raes, D,. & Munoz, G. (2008). *The ETo calculator*. *Land and water digital media series*. FAO, Water Development and Management Unit.

Raziei, T., & Pereira, L. S. (2013). Estimation of ETo with Hargreaves-Samani and FAO-PM temperature methods for a wide range of climates in Iran. *Agricultural water management, 121,* 1-18.

Riad, S., Mania, J., Bouchaou, L., & Najjar, Y. (2004). Rainfall-runoff model usingan artificial neural network approach. *Mathematical and Computer Modelling, 40*(7)*,* 839-846.

Rodríguez-González, A., García-Crespo, Á., Colomo-Palacios, R., Iglesias, F. G., & Gómez-Berbís, J. M. (2011). CAST: Using neural networks to improve trading systems based on technical analysis by means of the RSI financial indicator. *Expert systems with Applications, 38*(9)*,* 11489-11500.

Shirke, Y., Kawitkar, R., & Balan, M. S. (2012). Artificial neural network based runoff prediction model for a reservoir. *International Journal of Engineering Research and Technology, 1*(3), May 2012. ESRSA Publications.

Srinivasulu, S., & Jain, A. (2006). A comparative analysis of training methods for artificial neural network rainfall–runoff models. *Applied Soft Computing, 6*(3), 295-306.

Sudheer, K., & Jain, A. (2004). Explaining the internal behaviour of artificial neural network river flow models. *Hydrological Processes, 18*(4)*,* 833-844.

Tingsanchali, T., & Gautam, M. R. (2000). Application of tank, NAM, ARMA and neural network models to flood forecasting. *Hydrological Processes, 14*(14)*,* 2473-2487.

Wu, C., & Chau, K. (2011). Rainfall–runoff modeling using artificial neural network coupled with singular spectrum analysis. *Journal of Hydrology, 399*(3)*,* 394-409.

Young, C.-C., & Liu, W.-C. (2014). Prediction and modelling of rainfall-runoff during typhoon events using a physically-based and artificial neural network hybrid model. *Hydrological Sciences Journal, 60*(12), 2102-2116.

Zhang, B., & Govindaraju, R. S. (2000). Prediction of watershed runoff using Bayesian concepts and modular neural networks. *Water Resources Research, 36*(3)*,* 753-762.

Pertanika J. Sci. & Technol. 24 (2): 331 - 350 (2016)

SCIENCE & TECHNOLOGY

Journal homepage: http://www.pertanika.upm.edu.my/

Modified Levels of Parallel Odd-Even Transposition Sorting Network (OETSN) with GPU Computing using CUDA

Neetu Faujdar* and SP Ghrera

Jaypee University of Information Technology Waknaghat, P.O. Waknaghat, The Kandaghat, Distt. Solan, India

ABSTRACT

Sorting huge data requires an enormous amount of time. The time needed for this task can be minimised using parallel processing devices like GPU. The odd-even transposition sorting network algorithm is based on the idea that each level uses an equal number of comparators to arrange data. The existing parallel OETSN algorithm compares the elements in each phase for any type of test case. If the elements are not in the increasing order, then they are swapped. In this way, the algorithm takes the same time for sorting and for unique test cases. In this paper, we propose an algorithm that is the modified version of the existing OETSN algorithm. Our approach reduces the number of levels in the OETSN based on the nature of the data. Time complexity is also reduced from $O(n)$ to $O(1)$ for sorted and zero test cases. The proposed algorithm is tested for six types of test case, which are uniform, Gaussian, zero, bucket, staggered and sorted. The comparison with existing techniques is also presented in this paper. After evaluation, the proposed modified version of OETSN is found to be more efficient in two types of test case i.e. sorted and zero test cases. GPU computing using CUDA hardware is used to test the algorithms. The speedup achieved by the parallel OETSN algorithm over sequential OETSN is also computed. The proposed approach achieves an improvement in execution time that is 981661.6 times faster in the sorted test case and 904620.7 times faster in the zero test case using 2500000 elements and 1024 threads in comparison to the existing parallel OETSN.

Keywords: Sorting, GPU computing, CUDA, comparators, OETSN

INTRODUCTION

Nowadays, sorting is in big demand. There are many sorting algorithms available to arrange data (Ye et al., 2014). In computer science, sorting network algorithms also exist to arrange data over the network. In sorting networks, comparators (Amin et al., 2013) are

Article history:
Received: 8 September 2015
Accepted: 17 February 2016

E-mail addresses:
neetu.faujdar@mail.juit.ac.in, neetu.faujdar@gmail.com (Neetu Faujdar),
sp.ghrera@juit.ac.in, spghrera@rediffmail.com (SP Ghrera)
*Corresponding Author

ISSN: 0128-7680

used to compare and exchange data. Compare-exchange operation is used in sorting networks (Martinet et al., 1989). There are two types of comparators: 1) Increasing (low to high) and 2) Decreasing (high to low) comparator. These comparators (Amin et al., 2013) are shown in Figure 1.

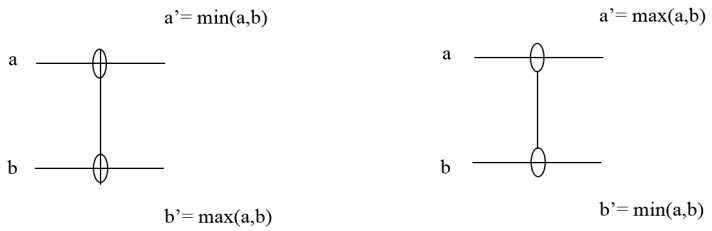

Figure 1. (a) Increasing comparator (b) Decreasing comparator.

The odd-even transposition sorting network (OETSN) (Perrie et al., 1999; Behzad et al., 2010) algorithm is designed for network models. The comparators are used to rearrange the numbers in network models. In the odd-even transposition sorting network, an increasing comparator is used to compare and exchange data. The OETSN algorithm performs $n/2$ iteration. Each iteration has two phases: 1) Odd-even exchange and 2) Even-odd exchange. The concept of OETSN is explained with the help of an example shown in Figure 2 (Ushijima & Fugiwara, 2005).

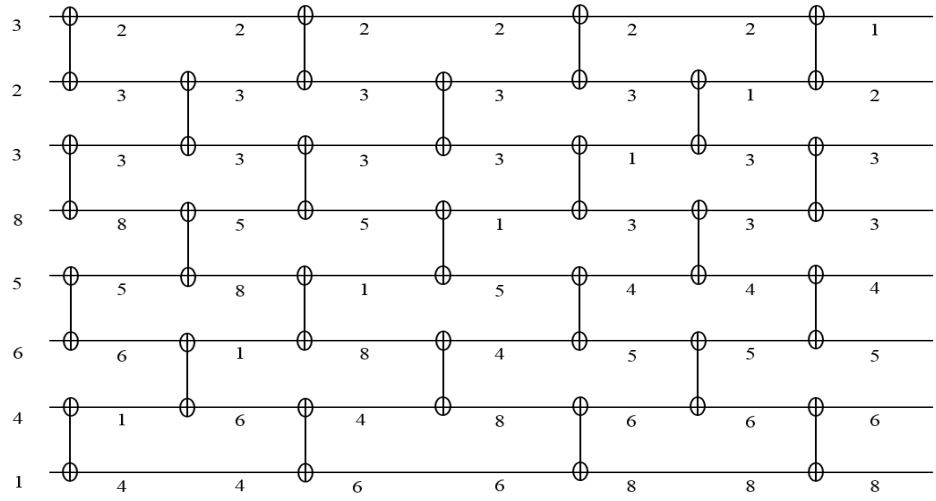

Figure 2. Example of OETS network.

The OETSN algorithm operates alternatively for odd and even phases. In the odd phase, the odd position number of items is compared with the adjacent element. Similarly in the even phase, the even position number of items is compared with the adjacent element. If the items are not in increasing order, swapping is performed as shown in Figure 2. After '*n*' phases of odd-even exchange, the sequence is sorted. Each phase of the algorithm, either odd or even,

requires $O(n)$ comparisons. There are a total of 'n' phases; thus, the sequential complexity of OETSN is $O(n^2)$. In this paper, we parallelised the OETSN algorithm using CUDA with C language. We tested the OETSN using a benchmark of sorting. We used the following distributions for benchmark to compare the performance of the OETSN algorithm. We tested the OETSN algorithm in six types of test case, which are uniform, sorted, zero, bucket, Gaussian and staggered. The parallel time complexity of OETSN is $O(n)$. In this work, we introduced a modified parallel odd-even transposition sorting algorithm, which is more efficient in comparison to parallel OETSN on the zero and sorted test cases.

The literature review on GPU is presented in Section 2. The problem statement is given in Section 3. A review of the literature on parallel OETSN is provided in Section 4. The proposed algorithm is described in Section 5. The benchmark of sorting is described in Section 6. Section 7 describes the hardware configuration. Experimental evaluation of parallel OETSN and modified parallel OETSN are given in Sections 8 and 9. In Section 10, we make our conclusions and suggest future work in this area.

RELATED WORK

Sorting is a common problem in computer science. A huge number of algorithms have been suggested to find an efficient solution to solve the problem. In this work, we focused on GPU technology using the CUDA paradigm. In this section, we briefly review the related work by other researchers on GPU sorting algorithms using CUDA.

A version of the parallel odd-even sorting algorithm implemented using CUDA was presented by Ajdari et al. in 2015. The design of parallel radix sort and merge sort using CUDA was given by Nadathur et al. (2009). They achieved higher performance in their experiments.

Shifu et al. (2009) proposed a sorting algorithm that is a combination of the bucket sort and internal bitonic sort types. This algorithm achieved acceleration of many times over the STL Quicksort implementation. They also showed that their implementation had higher performance than the GPU quick and GPU radix sort.

Daniel and Philippas in (Daniel et al., 2009) proposed a parallel Quicksort algorithm designed to take advantage of the high bandwidth of GPUs by minimising the amount of bookkeeping and inter-thread synchronisation needed. They showed that their GPU-Quicksort implementation performed better than the fastest known sorting implementations for GPU, such as radix and bitonic sort.

Performance Evaluation of Merge and QuickSort using GPU Computing with CUDA was presented by Neetu et al. (2015). In this paper the authors achieved better experimental results using GPU technology.

Greb et al. presented parallel sorting based on stream processing architecture. The proposed sorting was based on adaptive bitonic sorting. The input of 'n' requires 'p' stream processor to sort. The optimal time complexity of the proposed approach achieved $O(n\log n)/p)$. The proposed approach was more competitive than sequential sorting from the theoretical as well as a practical perspective viewpoint. The proposed algorithm was faster than sequential sorting as well as previous non-optimal sorting approaches on the GPU. The proposed algorithm was specially designed for practicability on modern GPU, so the name GPU-ABiSort was used for it (Grab et al., 2006).

Peters et al. presented Batcher's bitonic sorting network using CUDA hardware with GPUs. The arbitrary numbers were taken as input and assigned compare-exchange operation to threads using the adapted bitonic sort. The proposed algorithm greatly increased the performance of implementation (Peters et al., 2010). Jan et al. presented the analysis of three widely used parallel-sorting algorithms. The algorithms were odd-even sort, rank sort and bitonic sort. The comparative analysis was performed in terms of sorting rate, sorting time and speedup on CPU and different GPU architecture. The author also implemented the parallel algorithm: min-max butterfly network. The min-max butterfly network sorting was used to find minimum and maximum numbers in huge data sets. The purpose of all algorithm implementation was used to exploit the data parallelism model in order to achieve high performance on available GPU using the OpenCL specification. The results showed minimum speedup 19x of bitonic sort against the odd-even sort. The implementation results of the full-butterfly network were relatively better than the three sorting techniques: bitonic, odd-even and rank sort. The author achieved the high speedup of NVIDIA quadro 6000 GPU for min-max butterfly network, reaching much lower sorting for high data (Jan et al., 2012).

Ajdari et al. described the modification of the odd-even sort. The modification of the algorithm consisted of the ability to work with the blocks of elements instead of working with individual elements. The modification was done using CUDA technology. The experimental analysis of odd-even sort was done in both theoretical and experimental with its parallel implementation. The results showed that sorting of integers in a CUDA environment was much faster (Ajdari et al., 2015).

PROBLEM STATEMENT

Odd-even transposition sorting is designed for networks. In networks, the compare-exchange operation is used to compare the elements. We found that the time taken for sorting by OETSN was the same for all test cases such as uniform, sorted, zero, Gaussian, staggered and bucket. The sequential and parallel time complexity was $O(n^2)$ and $O(n)$, respectively for OETSN using any kind of test case.

In our approach, we reduced the time complexity $O(n)$ to $O(1)$ over two types of test case, which are sorted and zero. We have used the the bubble sort technique. If the data are sorted and unique, bubble sorting requires only one pass and then terminates the programme. In our approach we used this technique, and are able to reduce the number of levels in the network and the time complexity for sorted and zero test cases.

PARALLEL OETSN ALGORITHM

It is easy to parallelise OETSN algorithm (Grama et al., 1994). Compare-exchange operation was performed simultaneously on each pair of elements. There are two cases: 1) when $n=p$ where 'p' is the number of processing elements and 'n' is the number of elements to be sorted. In both the phases compare-exchange operation is performed on the right adjacent element. This required time $O(1)$. A total of 'n' phases is performed. So the parallel run time of this formulation is $O(n)$. 2) When $p<n$ or $p>n$ initially, each process is assigned a block of n/p

elements, which it sorted internally in $O((n/p)(n/p))$ time. After these processes, 'p' phases ($p/2$ odd and $p/2$ even) are executed. During each phase $O(n)$ comparisons are performed and time $O(n)$ is spent in communication. We did not use any local sort before the odd-even phase. The parallel run time of this formulation is shown in equation (1).

$$T_p = O\left(\frac{n^2}{p^2}\right) + O(n) + O(n) \quad [1]$$

Since the sequential complexity of OETSN is $O(n^2)$, the speedup (S) of this formulation is shown in equation (2).

$$S = \frac{O\left(n^2\right)}{O\left(\frac{n^2}{p^2}\right) + O\left(n\right)} \quad [2]$$

PROPOSED MODIFIED PARALLEL OETSN ALGORITHM

ALGORITHM 1: Proposed Modified OETSN Algorithm
Input: Unsorted List *A*, Number of threads
Output: Sorted List *A*
for*i*= 1 to *N*/2 **do**
Initialise the P array to zero for GPU *; /* N/2 number of passes */*
Odd Phase(*A*, *P*, *N*) ; */* comparison of odd positions of array */*
Even Phase(*A*, *P*, *N*) ; */* comparison of even positions of array */*
if (*i*==0 OR *i*== *N*/4 OR *i*==*N*/8 OR *i*==*N*/16)*;/* check whether list has been sorted, then not performing any swaps at 0,1/8,1/4,1/2 passes */*
then
Evalute (*P*) ; */* sum the number of swap of various threads */*
Read sum from GPU ;
if sum == 0 **then** */* number of swap has been done */*
break: */* terminate if no swap performed */*
end
end
end

The proposed sorting algorithm is inspired by the traditional bubble sorting algorithm. In the traditional bubble sorting algorithm, we compared the adjacent elements. If the elements are sorted, no swapping is done. Traditional bubble sorting takes 'n' passes to complete the sorting in the best case. In the modified version of bubble sorting, we used the flag variable to keep the track of swapping. If the variable highlighted swapping, the next pass is executed. The same concept is applied to the odd-even transposition sorting algorithm using GPU. Let the number of elements to be sorted be 'N' and 'T' is the number of threads. The number of threads

is restricted to a maximum limit of the hardware. According to the hardware configuration, our hardware support is T=1024 threads in one block. In our algorithm, we have used three functions.

1. Odd ()
2. Even ()
3. Evaluate ()

The odd () function can generate a maximum number of threads of T=1024 while the blocks are N/1024, where N is the data element. Similarly, the even () function has the same configuration as the odd () function. The evaluate () function does not execute with every iteration. Its data element is based on the number of threads and varies according to T. This evaluate () function is evaluated in sequential manner in a single block and uses single data. The reason for keeping it sequential is that the thread value is limited to T=1024.

In GPU instead of using a single variable array we used two variable arrays i.e. 'P' and 'T'. 'T' is equal to the number of threads and 'P' is the sum of total swapping performed in the proposed algorithm. The odd-even pass is executed. If there is no swapping then the sum of 'P' was zero and we got the sorted array. This gave an added advantage as the sorted and unique test cases did not need to be executed in the code on the GPU unnecessarily as is the case when the data are sorted or unique. On the other hand, a slight increase in the execution time for the uniform, staggered, bucket and Gaussian test cases was noted. This made them unable to take advantage of the above proposed approach. We observed the same with N/2, N/4 and N/8 of the data.

We used the GPU NVDIA GeForce GTX 460 with compute capability 2.1 but the new version of GPU cards come with the compute capability 3.0, which has unified memory for GPU and CPU, and can therefore, further enhance the performance of the suggested algorithm. Future enhancements may be possible to get a further speedup. For instance, we may use the scan function to speed up the sum up. The functionality of the proposed algorithm is described through the flowchart shown in Figure 3. The green-coloured box shows the modules running on GPU. The proposed algorithm is more efficient in comparison with the existing techniques using two types of test case i.e. zero and sorted test cases.

Sorting Benchmark

We have tested the sequential, parallel and proposed modified parallel OETSN algorithms on six types of test case (uniform, sorted, zero, bucket, Gaussian and staggered) (Matsumoto & Nishimura, 1998; Daniel et al, 2009; Leischner, Sanders , 2010). We varied the data from 1000 to 2500000 and the thread in multiples of two from 1 to 1024.

1. Uniform test case: In this test case values are picked randomly from 0 to 2^{31}.
2. Gaussian test case: In this test case the distribution of data is created by taking the average of four randomly picked values from the uniform distribution.
3. Zero test case: In this test case a constant value is used.

4. Bucket test case: For $p \in N$, the input of size 'N' is split into 'p' blocks, such that the first n/p^2 elements in each are random numbers in $[0, 2^{31}/p-1]$, the second n/p^2 elements in $[2^{31}/p, 2^{32}/p- 1]$, and so forth.
5. Staggered test case: For $p \in N$, the input of size 'N' is split into 'p' blocks such that if the block index is $i \leq p/2$, all its n/p elements are set to a random number in $[(2i- 1)2^{31}/p, (2i)(2^{31}/p- 1)]$.
6. Sorted test case: In this test case sorted uniformly distributed values are taken.

Hardware Configuration

We ran the algorithms on a Windows 7 32-bit operating system Intel® core™ I3 processor 530@ 2.93 GHz machine. The system has a GeForce GTX 460 graphic processor with (7 multiprocessors X (48) CUDA cores\MP) = 336 CUDA cores. There are a maximum of 1536 threads per multiprocessor and 1024 threads per block. A system having the CUDA runtime version is 6.0. The total amount of global memory of the system is 768 Mbytes and the total amount of constant memory is 65536 bytes. The total amount of shared memory per block is 49152 bytes. The system has a total number of registers available per block of 32768 and its warp size is 32. The maximum size of each dimension of a block is 1024 x 1024 x 64 and the maximum size of each dimension of a grid is 65535 x 65535 x 65535.

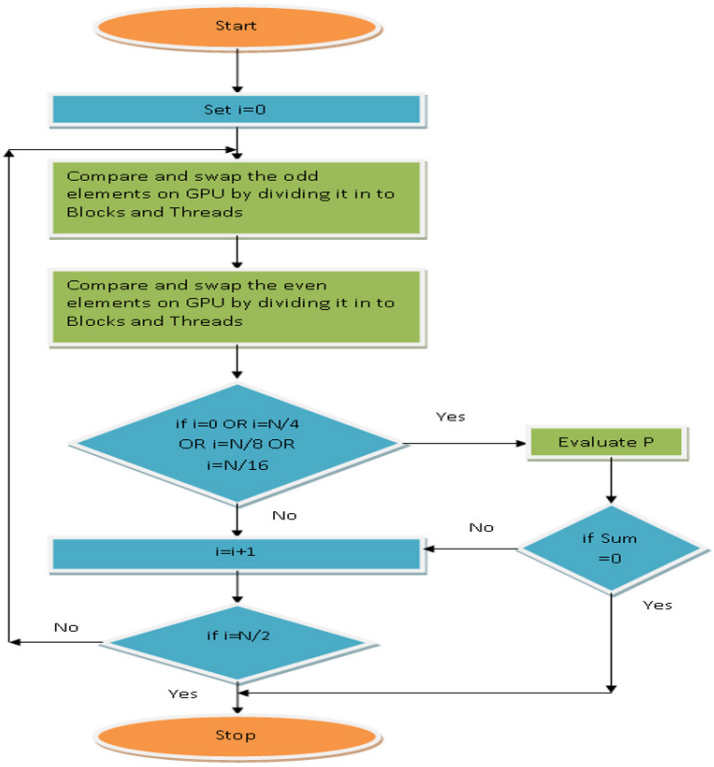

Figure 3. Flowchart for the proposed modified parallel OETSN.

Experimental Evaluation of Sequential and Parallel OETSN Algorithm

Sorting benchmark is used for testing the algorithms. We have tested the sequential and parallel OETSN algorithms on six types of test case using GPU computing that used CUDA hardware. Table 1 shows the execution time in seconds of the sequential OETSN algorithm. '*N*' is the size of the data used for the particular cases here for the performance analysis of the algorithm. The value of '*N*' varied from 1000 to 2500000. Table 2 shows the execution time in seconds of the parallel OETSN algorithm using different types of test cases. The size of the data is denoted by '*N*'. The number of threads is denoted by '*T*'. The values of '*T*' varied from 1 to the maximum of 1024. The threads increased in the power of 2. The CUDA hardware version 2.1 has a total of 1024 threads per block so the maximum value of thread is selected as 1024. In Table 1, the sequential execution time is shown for the six types of test case. Table 1 shows, that the zero test case has less execution time in comparison to the others. It has less execution time for all the values of '*N*'. The sorted test case has less execution time in comparison to the bucket, staggered, uniform and Gaussian tests for all the values of '*N*'. The remaining test cases has nearly equal execution time as shown in Table 1. This is because in the zero and sorted test cases, the comparison is performed to the adjacent element and swapping is not required for both. Comparison and swapping are performed in the remaining test cases.

Table 1
Execution Time in Seconds of Sequential OETSN Using Different Types of Test Case

N	Uniform	Gaussian	Zero	Staggered	Bucket	Sorted
1000	0.016	0.016	0.001	0.015	0.016	0.015
5000	0.062	0.062	0.015	0.078	0.063	0.031
10000	0.203	0.187	0.078	0.187	0.234	0.062
50000	4.602	4.681	0.905	4.145	5.704	0.842
100000	18.86	19.282	3.26	16.645	22.687	3.292
500000	496.988	501.091	82.681	425.274	584.469	101.713
1000000	2067.263	2050.446	400.33	1861.966	2734.954	577.812
1500000	4671.309	5135.357	912.34	4843.285	6035.218	1342.607
2000000	8095.204	7666.997	2072.224	7958.578	11156.45	4119.251
2500000	17099.89	17128.84	3719.095	16171.63	15732.54	6368.703

Next, we have evaluated the speedup achieved by the parallel OETSN over the sequential OETSN. Speedup measures the performance gain achieved by parallelising a given application over sequential application. In Tables 1 and 2, we have evaluated the execution time in seconds of sequential and parallel OETSN. Using equation (2) and the results from Table 1 and 2, the speedup is calculated. The speedup results are described in Table 3. From Table 2 and 3, it can be observed that the execution time is minimum when the number of threads is 512. The speedup is increased by eight times more than the sequential code when T=512. The performance of the algorithm got degraded at T=1024. The reason behind this is that the data we took is not evenly divided over the threads. So, some of the threads are executed ideally and degraded the overall performance of the algorithm. The speedup for all the six mentioned test cases is

shown in Figures 4 to 9. The *X*-axis represent the number of threads, the *Y*-axis represent the speedup achieved by the parallel OETSN and the *Z*-axis represent the size of the dataset.

Table 2
Execution Time in Seconds of Parallel OETSN Using Different Types of Test Case

N/T	Test case	1	2	4	8	16	32	64	128	256	512	1024
1000	Uniform	0.019	0.014	0.009	0.006	0.005	0.005	0.004	0.004	0.004	0.004	0.005
	Gaussian	0.019	0.014	0.009	0.006	0.005	0.005	0.005	0.004	0.004	0.004	0.006
	Zero	0.019	0.014	0.009	0.006	0.005	0.005	0.004	0.004	0.004	0.004	0.005
	Staggered	0.019	0.014	0.009	0.007	0.005	0.004	0.004	0.004	0.003	0.003	0.005
	Bucket	0.019	0.014	0.009	0.006	0.005	0.004	0.004	0.004	0.004	0.004	0.007
	Sorted	0.019	0.014	0.009	0.006	0.006	0.005	0.005	0.005	0.004	0.004	0.005
5000	Uniform	0.441	0.322	0.173	0.096	0.056	0.035	0.026	0.023	0.023	0.023	0.025
	Gaussian	0.442	0.321	0.173	0.096	0.055	0.034	0.026	0.025	0.024	0.024	0.026
	Zero	0.441	0.321	0.167	0.091	0.051	0.031	0.021	0.021	0.021	0.021	0.022
	Staggered	0.441	0.322	0.171	0.093	0.052	0.033	0.029	0.023	0.022	0.021	0.025
	Bucket	0.442	0.322	0.169	0.092	0.052	0.033	0.025	0.023	0.023	0.023	0.025
	Sorted	0.439	0.319	0.168	0.168	0.091	0.054	0.024	0.024	0.023	0.023	0.032
10000	Uniform	1.742	1.265	0.667	0.358	0.197	0.114	0.071	0.066	0.062	0.061	0.079
	Gaussian	1.744	1.263	0.667	0.359	0.197	0.115	0.072	0.064	0.061	0.061	0.079
	Zero	1.733	1.257	0.643	0.336	0.182	0.104	0.065	0.056	0.053	0.052	0.071
	Staggered	1.744	1.271	0.657	0.345	0.188	0.108	0.067	0.06	0.058	0.058	0.074
	Bucket	1.744	1.265	0.649	0.339	0.185	0.108	0.07	0.065	0.062	0.062	0.079
	Sorted	1.733	1.256	0.643	0.335	0.182	0.104	0.065	0.057	0.054	0.054	0.072
50000	Uniform	43.438	31.472	16.462	8.602	4.499	2.41	1.353	1.094	1.09	1.08	1.235
	Gaussian	43.452	31.433	16.43	8.588	4.492	2.406	1.351	1.093	1.091	1.083	1.235
	Zero	43.328	31.338	15.931	8.02	4.089	2.16	1.204	0.943	0.925	0.919	1.078
	Staggered	43.574	31.69	16.276	8.273	4.249	2.247	1.255	0.999	0.988	0.984	1.134
	Bucket	43.573	31.535	16.081	8.092	4.127	2.228	1.24	1.11	1.09	1.08	1.231
	Sorted	43.248	31.282	15.884	7.996	4.073	2.153	1.195	0.939	0.919	0.916	1.069
100000	Uniform	213.99	130.446	70.589	36.806	19.111	9.994	5.457	4.151	4.129	4.125	4.948
	Gaussian	213.996	130.335	70.571	36.805	19.119	9.995	5.459	4.151	4.131	4.131	4.951
	Zero	213.105	129.583	69.112	34.693	17.491	9.063	4.882	3.579	3.547	3.539	4.378
	Staggered	213.938	130.885	70.171	35.605	18.077	9.373	5.069	3.786	3.757	3.751	4.564
	Bucket	213.831	130.282	69.621	34.961	17.626	9.991	4.975	3.735	3.811	3.133	4.947
	Sorted	213.189	129.58	69.117	34.681	17.491	9.053	4.877	3.578	3.543	3.535	4.366
500000	Uniform	4770.3	3349.3	1749.8	914.91	472.11	244.11	130.31	98.141	97.991	96.471	119.91
	Gaussian	4755.1	3340.3	1749.6	914.91	472.11	243.81	130.21	98.071	98.112	96.431	119.91
	Zero	4686.2	3264.3	1683.6	862.11	432.12	220.21	116.11	83.841	83.651	82.021	105.81
	Staggered	4705.3	3295.6	1705.1	878.7	438.91	228.21	120.51	88.861	88.781	87.211	110.21
	Bucket	4694.9	3287.8	1694.3	869.1	435.11	226.31	117.41	92.651	91.151	90.201	119.91
	Sorted	4686.2	3264.4	1683.6	861.9	431.81	220.12	115.91	83.781	83.591	83.096	105.81
1000000	Uniform	18833.7	13246.5	6886.4	3698	1799.5	921.41	488.11	359.71	359.61	358.11	476.81
	Gaussian	18805.3	13215.4	6855.2	3578.4	1799.5	922.31	488.11	359.61	359.41	358.71	476.41
	Zero	18716.1	13055.2	6755.8	3505.9	1719.1	873.71	459.21	331.31	330.91	330.92	420.71
	Staggered	18759.6	13170.4	6844.5	3556.4	1746.9	890.11	468.61	341.41	341.21	340.71	438.31
	Bucket	18746.3	13105.1	6821.3	3544.3	1724.8	884.5	461.91	334.81	332.31	331.61	476.71
	Sorted	18736.3	13095.8	6798.5	3526.7	1718.9	872.8	459.41	333.61	332.91	332.11	420.51
1500000	Uniform	60324.2	31243.2	15348.8	8155.1	4299.8	2078.1	1096.3	808.1	807.81	806.61	1071.5
	Gaussian	60297.8	31199.2	15329.7	8134.3	4255.2	2072.6	1096.3	807.91	807.81	806.31	1071.8
	Zero	60155.4	31056.2	15255.4	8005.8	4150.9	1964.2	1031.3	744.71	743.61	743.11	946.21
	Staggered	60266.4	31178.3	15299.8	8099.2	4239.3	1999.3	1052.4	766.81	766.61	765.17	985.81
	Bucket	60243.8	31141.2	15279.4	8055.3	4199.7	2070.6	1039.1	752.31	751.91	750.31	995.31
	Sorted	60196.4	31098.3	15299.4	8023.3	4162.9	1964.1	1030.9	744.21	743.51	743.31	946.21

Table 2 (*continue*)

2000000	Uniform	90655.3	46143.2	24199.3	12693.9	6678.4	3688.1	1948.4	1435.5	1435.1	1434.5	1903.5
	Gaussian	90605.4	46099.4	24210.3	12649.9	6648.9	3689.8	1948.5	1435.4	1434.7	1433.9	1902.7
	Zero	90395.3	45905.3	24065.4	12544.4	6533.5	3494.9	1833.7	1322.1	1321.2	1321.1	1681.6
	Staggered	90555.4	46055.3	24188.5	12627.9	6633.4	3556.4	1869.1	1361.7	1361.7	1360.4	1855.9
	Bucket	90498.9	45999.4	24148.8	12599.5	6598.9	3520.1	1842.6	1342.2	1340.2	1340.1	1806.9
	Sorted	90445.4	45972.8	24105.4	12555.2	6555.3	3494.1	1832.9	1321.8	1320.2	1318.7	1742.9
2500000	Uniform	165205.3	82815.4	42674.4	23139.4	12349.2	7299.8	3041.9	2241.6	2241.6	2221.1	2797.2
	Gaussian	165193.3	82793.5	42648.8	23099.8	12344.7	7291.4	3043.1	2241.4	2241.1	2241.1	2796.7
	Zero	164560.8	82555.3	42556.4	23005.3	12259.8	7233.3	2866.2	2063.6	2063.1	2060.7	2623.4
	Staggered	165149.3	82740.1	42631.9	23089.1	12316.4	7266.3	2917.1	2126.7	2126.5	2022.9	2677.5
	Bucket	165105.9	82693.3	42599.3	23049.8	12299.2	7249.4	2881.5	2084.3	2027.1	2021.6	2680.1
	Sorted	165060.8	82649.8	42574.7	23019.4	12268.5	7238.7	2862.1	2064.2	2072.1	2077.5	2622.1

Table 3

Speedup Achieved by Parallel OETSN Using Different Types of Test Case

N/T	Test case	1	2	4	8	16	32	64	128	256	512	1024
1000	Uniform	0.84	1.14	1.78	2.67	3.2	3.2	4	4	4	4	3.2
	Gaussian	0.84	1.14	1.78	2.67	3.2	3.2	3.2	4	4	4	2.67
	Zero	0.05	0.07	0.11	0.17	0.2	0.2	0.25	0.25	0.25	0.25	0.2
	Staggered	0.79	1.07	1.67	2.14	3	3.75	3.75	3.75	5	5	3
	Bucket	0.84	1.14	1.78	2.67	3.2	4	4	4	4	4	2.29
	Sorted	0.79	1.07	1.67	2.5	2.5	3	3	3	3.75	3.75	3
5000	Uniform	0.14	0.19	0.36	0.65	1.11	1.77	2.38	2.7	2.7	2.7	2.48
	Gaussian	0.14	0.19	0.36	0.65	1.13	1.82	2.38	2.48	2.58	2.58	2.38
	Zero	0.03	0.05	0.09	0.16	0.29	0.48	0.71	0.71	0.71	0.71	0.68
	Staggered	0.18	0.24	0.46	0.84	1.5	2.36	2.69	3.39	3.55	3.71	3.12
	Bucket	0.14	0.2	0.37	0.68	1.21	1.93	2.52	2.74	2.74	2.74	2.52
	Sorted	0.07	0.1	0.18	0.18	0.34	0.57	1.29	1.29	1.35	1.35	0.97
10000	Uniform	0.12	0.16	0.3	0.57	1.03	1.78	2.86	3.08	3.27	3.33	2.57
	Gaussian	0.11	0.15	0.28	0.52	0.95	1.63	2.6	2.92	3.07	3.07	2.37
	Zero	0.05	0.06	0.12	0.23	0.43	0.75	1.2	1.39	1.47	1.5	1.1
	Staggered	0.11	0.15	0.28	0.54	0.99	1.73	2.79	3.12	3.22	3.22	2.53
	Bucket	0.13	0.18	0.36	0.69	1.26	2.17	3.34	3.6	3.77	3.77	2.96
	Sorted	0.04	0.05	0.1	0.19	0.34	0.6	0.95	1.09	1.15	1.15	0.86
50000	Uniform	0.11	0.15	0.28	0.53	1.02	1.91	3.4	4.21	4.22	4.26	3.73
	Gaussian	0.11	0.15	0.28	0.55	1.04	1.95	3.46	4.28	4.29	4.32	3.79
	Zero	0.02	0.03	0.06	0.11	0.22	0.42	0.75	0.96	0.98	0.98	0.84
	Staggered	0.1	0.13	0.25	0.5	0.98	1.84	3.3	4.15	4.2	4.21	3.66
	Bucket	0.13	0.18	0.35	0.7	1.38	2.56	4.6	5.14	5.23	5.28	4.63
	Sorted	0.02	0.03	0.05	0.11	0.21	0.39	0.7	0.9	0.92	0.92	0.79
100000	Uniform	0.09	0.14	0.27	0.51	0.99	1.89	3.46	4.54	4.57	4.57	3.81
	Gaussian	0.09	0.15	0.27	0.52	1.01	1.93	3.53	4.65	4.67	4.67	3.9
	Zero	0.02	0.03	0.05	0.09	0.19	0.36	0.67	0.91	0.92	0.92	0.74
	Staggered	0.08	0.13	0.24	0.47	0.92	1.78	3.28	4.4	4.43	4.44	3.65
	Bucket	0.11	0.17	0.33	0.65	1.29	2.27	4.56	6.07	5.95	7.24	4.59
	Sorted	0.02	0.03	0.05	0.09	0.19	0.36	0.68	0.92	0.93	0.93	0.75
500000	Uniform	0.1	0.15	0.28	0.54	1.05	2.04	3.81	5.07	5.07	5.15	4.15
	Gaussian	0.11	0.15	0.29	0.55	1.06	2.06	3.85	5.11	5.11	5.2	4.18
	Zero	0.02	0.03	0.05	0.1	0.19	0.38	0.71	0.99	0.99	1.01	0.78
	Staggered	0.09	0.13	0.25	0.48	0.97	1.86	3.53	4.79	4.79	4.88	3.86
	Bucket	0.12	0.18	0.34	0.67	1.34	2.58	4.98	6.31	6.41	6.48	4.88
	Sorted	0.02	0.03	0.06	0.12	0.24	0.46	0.88	1.21	1.22	1.21	0.96

Table 3 (*continue*)

1000000	Uniform	0.11	0.16	0.3	0.56	1.15	2.24	4.24	5.75	5.75	5.77	4.34
	Gaussian	0.11	0.16	0.3	0.57	1.14	2.22	4.2	5.7	5.71	5.72	4.3
	Zero	0.02	0.03	0.06	0.11	0.23	0.46	0.87	1.21	1.21	1.21	0.95
	Staggered	0.1	0.14	0.27	0.52	1.07	2.09	3.97	5.45	5.46	5.46	4.25
	Bucket	0.15	0.21	0.4	0.77	1.59	3.09	5.92	8.17	8.23	8.25	5.74
	Sorted	0.03	0.04	0.08	0.16	0.34	0.66	1.26	1.74	1.74	1.74	1.37
1500000	Uniform	0.08	0.15	0.3	0.57	1.09	2.25	4.26	5.78	5.78	5.79	4.36
	Gaussian	0.09	0.16	0.33	0.63	1.21	2.48	4.68	6.36	6.36	6.37	4.79
	Zero	0.02	0.03	0.06	0.11	0.22	0.46	0.88	1.23	1.23	1.23	0.96
	Staggered	0.08	0.16	0.32	0.6	1.14	2.42	4.6	6.32	6.32	6.33	4.91
	Bucket	0.1	0.19	0.39	0.75	1.44	2.91	5.81	8.02	8.03	8.04	6.06
	Sorted	0.02	0.04	0.09	0.17	0.32	0.68	1.3	1.8	1.81	1.81	1.42
2000000	Uniform	0.09	0.18	0.33	0.64	1.21	2.19	4.15	5.64	5.64	5.64	4.25
	Gaussian	0.08	0.17	0.32	0.61	1.15	2.08	3.93	5.34	5.34	5.35	4.03
	Zero	0.02	0.05	0.09	0.17	0.32	0.59	1.13	1.57	1.57	1.57	1.23
	Staggered	0.09	0.17	0.33	0.63	1.2	2.24	4.26	5.84	5.84	5.85	4.29
	Bucket	0.12	0.24	0.46	0.89	1.69	3.17	6.05	8.31	8.32	8.32	6.17
	Sorted	0.05	0.09	0.17	0.33	0.63	1.18	2.25	3.12	3.12	3.12	2.36
2500000	Uniform	0.1	0.21	0.4	0.74	1.38	2.34	5.62	7.63	7.63	7.7	6.11
	Gaussian	0.1	0.21	0.4	0.74	1.39	2.35	5.63	7.64	7.64	7.64	6.12
	Zero	0.02	0.05	0.09	0.16	0.3	0.51	1.3	1.8	1.8	1.8	1.42
	Staggered	0.1	0.2	0.38	0.7	1.31	2.23	5.54	7.6	7.6	7.99	6.04
	Bucket	0.1	0.19	0.37	0.68	1.28	2.17	5.46	7.55	7.76	7.78	5.87
	Sorted	0.04	0.08	0.15	0.28	0.52	0.88	2.23	3.09	3.07	3.07	2.43

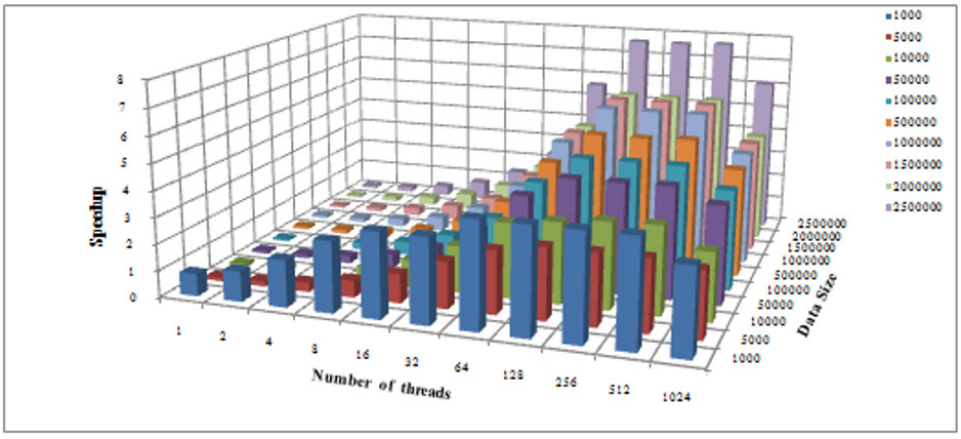

Figure 4. Speedup achieved by parallel OETSN using the uniform test case.

From Figure 4, the speedup for the uniform test case is observed. The 7 times more speedup is achieved when thread (T) =512 and data size (N) =2500000 in comparison to the sequential OETSN. We have also found that for *T*=1024, the speedup got decreased. This is because the data is not evenly distributed over the threads and some threads are ideal, hence the performance of the algorithm is degraded.

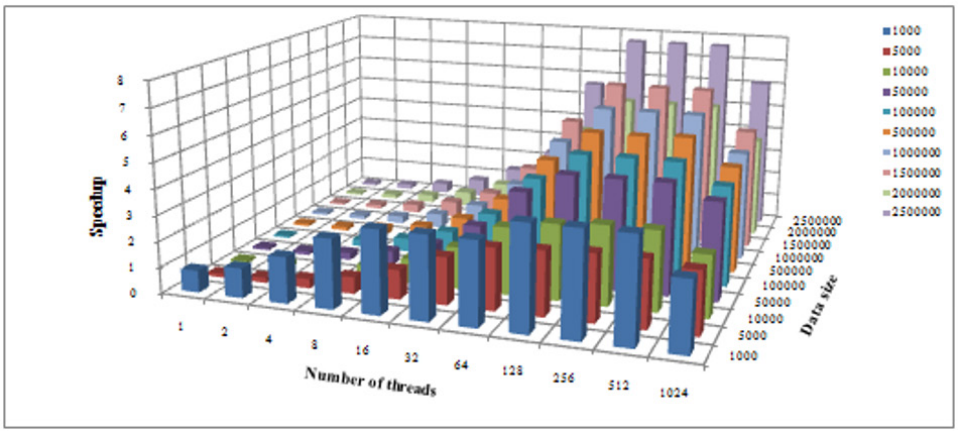

Figure 5. Speedup achieved by parallel OETSN using the Gaussian test case.

Figure 5 shows, the speedup for the Gaussian test case. Here we have achieved speedup seven times greater for the thread (T)=512 and data size (N)=2500000 in comparison to the sequential OETSN. The speedup difference can be seen at larger inputs, or we may say that speedup is directly proportional to the number of threads and size of the input.

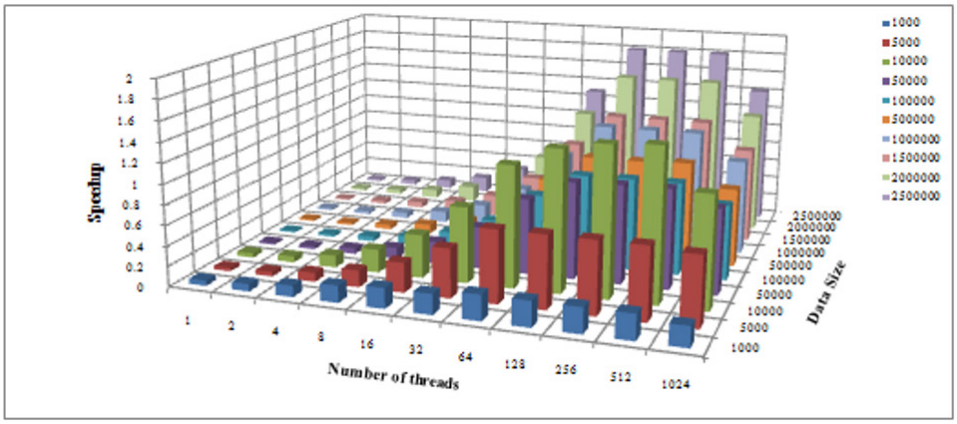

Figure 6. Speedup achieved by parallel OETSN using the zero test case.

Figure 6 shows, the speedup for a zero test case, highlighting that speedup is at least two times greater at T=512 and N=2500000 in comparison to the sequential OETSN. This is achieved in the zero test case.

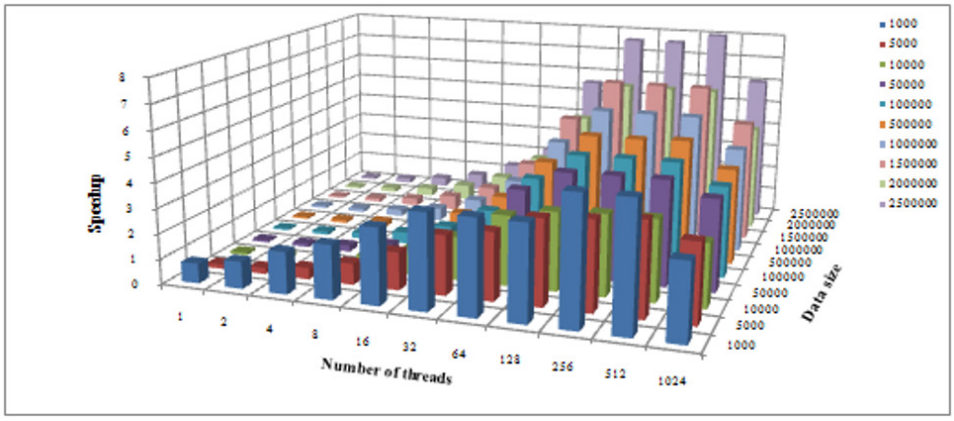

Figure 7. Speedup achieved by parallel OETSN using the staggered test case.

Figure 7 shows, the speedup for the staggered test case. In this test case, speedup is eight times greater at T=512 and N=2500000 in comparison to the sequential OETSN.

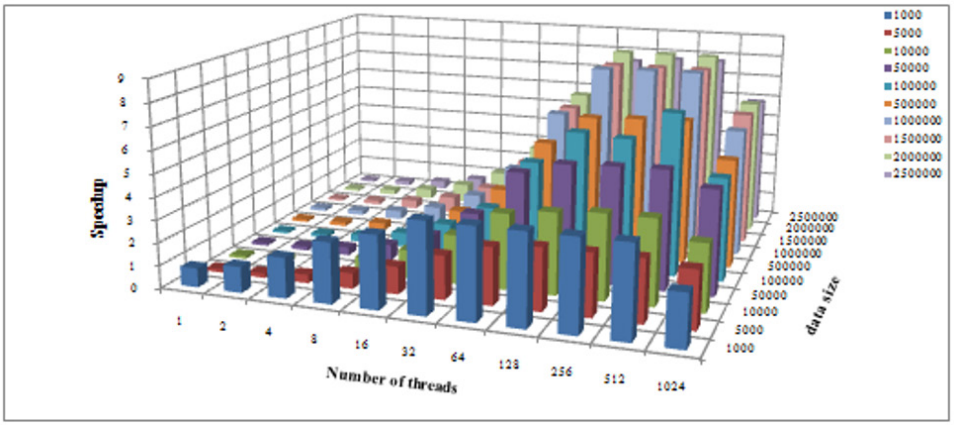

Figure 8. Speedup achieved by parallel OETSN using the bucket test case.

Figure 8 shows, the speedup for the bucket test case. The speedup increased by eight times at T=512 & N=2000000 in comparison to the sequential OETSN. Speedup is less at N=500 due to the smaller amount of data.

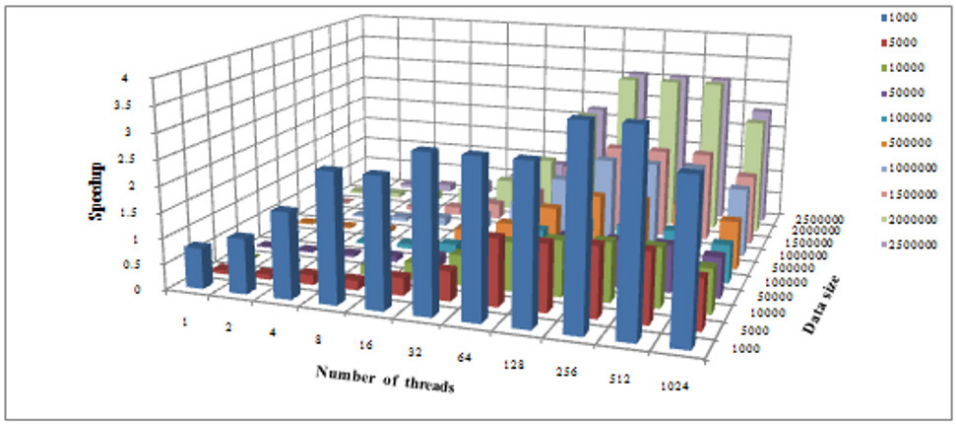

Figure 9. Speedup achieved by parallel OETSN using the sorted test case.

Figure 9 shows, the speedup for the sorted test case. The speedup is achieved three times greater at T=512 and N=1000 in comparison to the sequential OETSN. But in other test cases more speedup is achieved at N=2500000 or 2000000. This is because comparison is performed to the adjacent element only. There is no swapping performed as the data is already sorted.

In conclusion, we found that speedup is directly proportional to the number of threads and size of data in most of the tests. Maximum speedup is achieved by the bucket and staggered test case i.e. eight times greater in comparison to the sequential OETSN. Minimum speedup is achieved by the zero test case i.e. two times. We also found that in some cases good speedup is also achieved at N=1000 and 5000 at nearly seven and eight times greater.

EXPERIMENTAL EVALUATION OF PROPOSED MODIFIED PARALLEL OETSN ALGORITHM

Testing of proposed modified parallel OETSN algorithm is done on the sorting benchmark using GPU computing on CUDA hardware. Table 4 shows the execution time in seconds of proposed modified parallel OETSN algorithm using different types of test case. By examining Table 4, we found that the proposed approach is very efficient in comparison to the parallel OETSN only for the zero and sorted test cases. The execution time comparison for the sorted and zero test cases of parallel and proposed modified parallel OETSN are shown in Figures 10 and 11.

The results obtained in Table 4 are justified with the proposed algorithm discussed above. In the zero and sorted test cases, data did not require any swapping. In the odd-even module an evaluation function is called after one pass. It is a serial function, which added the number of swaps after every function was performed. The number of swaps is zero for the sorted and zero test case, so the algorithm is terminated. Now in the case of other test cases, we do not know how the data are placed, but we still tried to take advantage of the proposed approach. However, it added an extra overhead on the execution time of the programme of the remaining test cases.

Figures 10 and 11 are shown with the sub-figures from (a) to (j). In all the sub-figures the *X*-axis represent the number of threads and the *Y*-axis represent the execution time in seconds. The execution time comparison of the zero and sorted test case of parallel OETSN and the proposed modified parallel OETSN is shown in Figure 10 and 11. The analysis of Figures 10 and 11 show that the execution time of the proposed modified parallel OETSN algorithm is much less compared to that of the existing parallel OETSN algorithm. The scale of the *Y*-axis was taken in logarithmic, using base to the power 2 because the execution time of the proposed approach is much less in comparison to the existing one.

Figure 10 describes the execution time comparison of the existing parallel OETSN and proposed modified parallel OETSN over the zero test case. As the modified parallel OETSN is exploiting the nature of the data, we got better results in all the cases of data size from *N*=1000 to 2500000. For the small data set we could see that the execution time of modified parallel OETSN was trending towards the existing parallel OETSN. This is due to the fact that each tread had very little data elements to sort.

Figure 11 compares the execution time comparison of the parallel OETSN and modified parallel OETSN over the sorted test case. The zero test case was the special case of the sorted data. There is no swapping in both cases, and so, the trends of the modified OETSN are almost similar to those of the zero test case.

Table 4
Execution Time in Seconds of Modified Parallel OETSN Using Different Types of Test Case

N/T	Test case	1	2	4	8	16	32	64	128	256	512	1024
1000	Uniform	0.039	0.03	0.012	0.008	0.007	0.006	0.006	0.006	0.005	0.005	0.005
	Gaussian	0.029	0.019	0.012	0.008	0.006	0.004	0.004	0.004	0.004	0.004	0.006
	Zero	0.0004	0.0003	0.0003	0.0002	0.0002	0.0002	0.0002	0.0001	0.0001	0.0001	0.0005
	Staggered	0.029	0.02	0.012	0.008	0.007	0.006	0.006	0.005	0.004	0.004	0.006
	Bucket	0.029	0.019	0.011	0.008	0.006	0.004	0.004	0.003	0.003	0.003	0.005
	Sorted	0.00017	0.00016	0.00009	0.00008	0.00007	0.00006	0.00005	0.00005	0.00004	0.00004	0.00009
5000	Uniform	0.656	0.435	0.234	0.128	0.072	0.042	0.031	0.027	0.026	0.025	0.028
	Gaussian	0.657	0.437	0.235	0.129	0.072	0.042	0.033	0.026	0.025	0.024	0.029
	Zero	0.0003	0.0003	0.0001	0.0001	0.0001	0.0001	0.0001	0.0001	0.0001	0.0001	0.0006
	Staggered	0.657	0.462	0.24	0.129	0.07	0.042	0.032	0.032	0.028	0.029	0.029
	Bucket	0.656	0.43	0.227	0.122	0.069	0.041	0.033	0.026	0.025	0.025	0.029
	Sorted	0.00032	0.00025	0.00021	0.00013	0.00011	0.00008	0.00007	0.00007	0.00006	0.00006	0.00014
10000	Uniform	2.598	1.72	0.909	0.483	0.263	0.146	0.091	0.081	0.074	0.073	0.095
	Gaussian	2.597	1.718	0.909	0.484	0.263	0.147	0.091	0.082	0.075	0.074	0.096
	Zero	0.0005	0.0004	0.0002	0.0001	0.0001	0.0001	0.0001	0.0001	0.0001	0.0001	0.0007
	Staggered	2.6	1.825	0.932	0.483	0.259	0.142	0.088	0.078	0.072	0.072	0.094
	Bucket	2.6	1.695	0.879	0.457	0.245	0.139	0.09	0.082	0.075	0.074	0.095
	Sorted	0.00062	0.00037	0.00024	0.00013	0.00018	0.00009	0.00006	0.00007	0.00006	0.00006	0.00006
50000	Uniform	64.64	42.9	22.52	11.67	6.03	3.15	1.76	1.4	1.4	1.39	1.5
	Gaussian	64.66	42.91	22.52	11.66	6.03	3.15	1.76	1.41	1.4	1.4	1.5
	Zero	0.0025	0.0016	0.0009	0.0005	0.0003	0.0002	0.0001	0.0002	0.0002	0.0004	0.0007
	Staggered	64.64	45.54	23.11	11.61	5.88	3.04	1.69	1.34	1.33	1.33	1.44
	Bucket	64.64	42.25	21.81	11	5.58	2.89	1.62	1.4	1.4	1.4	1.5
	Sorted	0.00255	0.00167	0.00087	0.00047	0.00026	0.00015	0.00013	0.00013	0.00011	0.00011	0.00013
100000	Uniform	225.65	174.34	94.25	48.95	25.27	13.12	7.1	5.33	5.31	5.31	6.04
	Gaussian	223.12	174.21	94.24	48.96	13.12	7.11	5.34	5.34	5.32	5.31	6.04
	Zero	0.006	0.0032	0.0018	0.0009	0.0005	0.0003	0.0002	0.0002	0.0003	0.0004	0.0007
	Staggered	225.87	184.77	97.43	49.1	24.79	12.69	6.82	5.09	5.07	5.06	5.8
	Bucket	224.53	171.3	92.32	46.7	23.57	12.04	6.51	4.98	4.18	4.02	6.04
	Sorted	0.00584	0.00321	0.00178	0.00091	0.00054	0.00028	0.00017	0.00016	0.00015	0.00015	0.00024

Table 4 (*continue*)

500000	Uniform	4870.8	3550.6	1921.6	1217.1	625.3	321.5	170.3	126.2	126.1	126	146.3
	Gaussian	4870.2	3521.9	1911.7	1216.8	624.5	320.4	170.2	126.4	126.3	126.2	146.3
	Zero	0.0258	0.0162	0.0083	0.0044	0.0022	0.0012	0.0007	0.0006	0.0006	0.0008	0.0011
	Staggered	4770.2	3421.9	1811.7	1116.8	613	310.8	163.2	120.4	120.3	120.3	140.3
	Bucket	4690.2	3391.9	1791.7	1196.8	583.5	295	155.4	124.3	123.6	123.2	146.4
	Sorted	0.02576	0.01631	0.0084	0.00435	0.00226	0.00116	0.00072	0.00052	0.00052	0.00049	0.00057
1000000	Uniform	18999.6	13446.8	6986.6	3749.7	1999.8	1288.9	688.4	504.7	506.4	505.6	593.4
	Gaussian	18931.6	13412.7	6931.6	3721.6	1958.7	1231.6	612.6	484.3	481.6	478.6	521.3
	Zero	0.0519	0.0327	0.0169	0.0088	0.0043	0.0023	0.0013	0.001	0.0011	0.0013	0.0016
	Staggered	18998.6	13487.8	6998.5	3798.4	1998.9	1287.6	698.9	584.3	581.6	578.6	621.3
	Bucket	18811.6	13337.8	6838.5	3658.4	1985.8	1197.6	658.8	524.4	511.4	508.6	611.3
	Sorted	0.05187	0.03265	0.01701	0.0088	0.00432	0.00222	0.00132	0.00106	0.00101	0.00096	0.00113
1500000	Uniform	60576.7	31467.7	15587.6	8368	4599.6	2251.7	1264.8	1156.6	1145.9	1142	1333.6
	Gaussian	60521.7	31421.7	15531.9	8315.7	4523.6	2121.7	1212.6	1115.7	1106.7	1101.7	1312.7
	Zero	0.0761	0.049	0.0252	0.0132	0.0075	0.0033	0.0018	0.0015	0.0015	0.0016	0.0022
	Staggered	60621.7	31496.6	15588	8393.9	4589.9	2179.7	1289.8	1198.8	1188.7	1179.7	1389.7
	Bucket	60511.7	31336.6	15428	8283.9	4679.6	2119.7	1199.9	1088.8	1078.7	1069.7	1319.7
	Sorted	0.07624	0.049	0.02521	0.01322	0.00751	0.00338	0.00175	0.00138	0.00137	0.0013	0.00162
2000000	Uniform	90841.8	46324.8	24343.8	12843.7	6834.9	3873.7	2052.7	1665.9	1645.9	1611.7	2012.6
	Gaussian	90759.3	46289.6	24289.6	12789.5	6779.6	3812.6	2012.6	1612.7	1601.7	1589.6	1989.6
	Zero	0.1021	0.0652	0.0336	0.0176	0.009	0.0044	0.0023	0.0019	0.002	0.0021	0.0026
	Staggered	90859.3	46389.9	24389.5	12889.2	6879.6	3899.9	2079.9	1612.7	1609.7	1604.6	1999.6
	Bucket	90710.3	46124.9	24249.5	12779.2	6789.6	3789.9	2010.8	1582.7	1579.7	1564.6	1919.6
	Sorted	0.10196	0.06515	0.03359	0.01761	0.00896	0.00436	0.00242	0.00181	0.00179	0.0017	0.0021
2500000	Uniform	167205.5	83211.7	42817.7	23834.8	12887.7	7934.9	3476.5	2483.7	2454.9	2444.7	2984.9
	Gaussian	165803.7	83204.8	42253.6	23765.6	12754.6	7911.6	3432.7	2426.5	2423.5	2422.5	2932.3
	Zero	0.1281	0.0813	0.042	0.0221	0.0119	0.0069	0.0025	0.0019	0.0018	0.0017	0.0029
	Staggered	165898.7	83298.8	42353.9	23865.2	12854.6	7997.6	3489.9	2432.5	2424.5	2422.5	2989.3
	Bucket	165721.7	83198.8	42213.9	23745.2	12744.6	7867.7	3399.7	2329.5	2324.5	2322.5	2929.3
	Sorted	0.12802	0.0816	0.04196	0.0221	0.01186	0.00687	0.00286	0.00233	0.00228	0.0022	0.00267

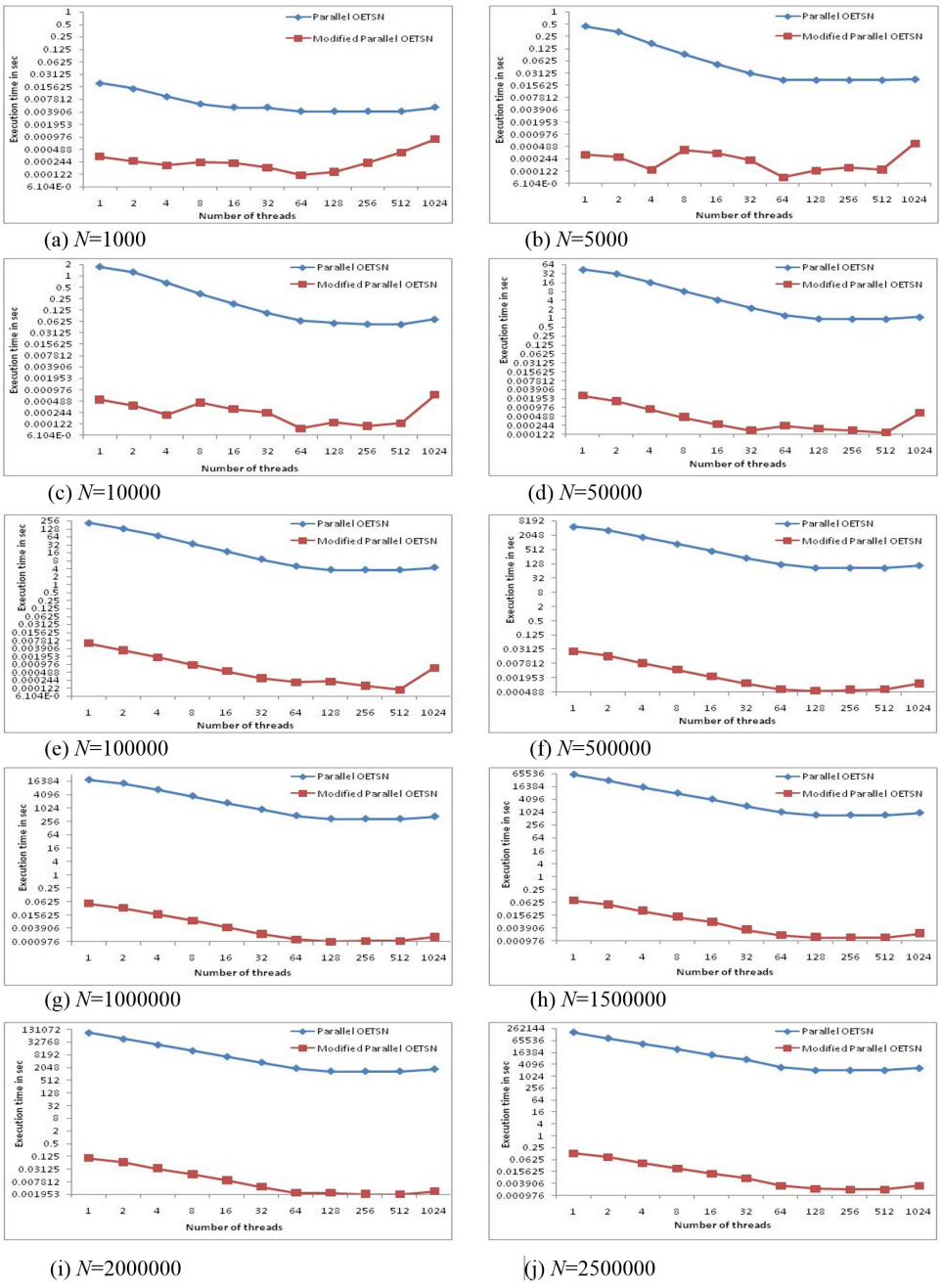

(a) N=1000 (b) N=5000

(c) N=10000 (d) N=50000

(e) N=100000 (f) N=500000

(g) N=1000000 (h) N=1500000

(i) N=2000000 (j) N=2500000

Figure 10. Execution time comparison of parallel and modified parallel OETSN using the zero test case.

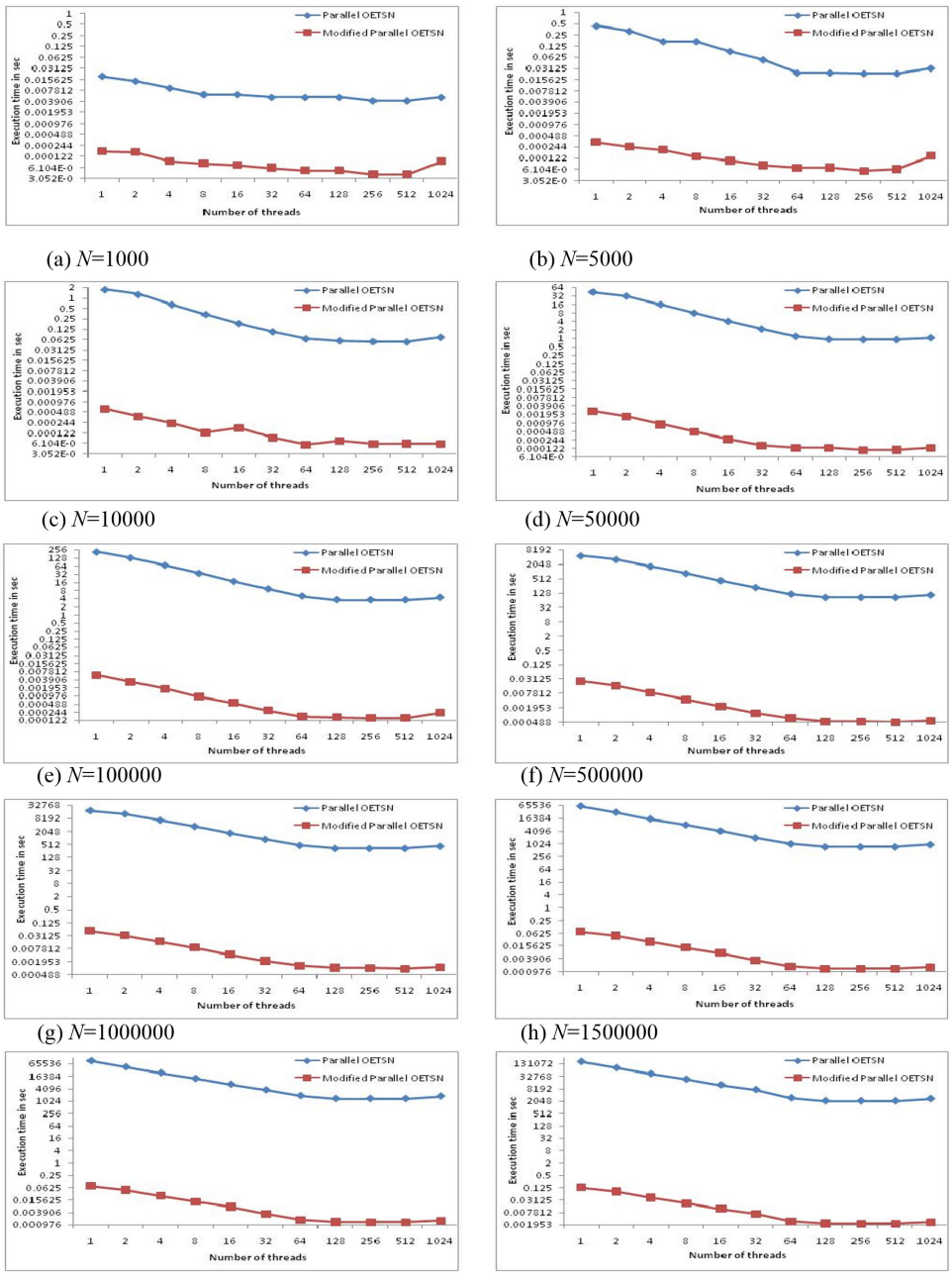

(a) N=1000 (b) N=5000

(c) N=10000 (d) N=50000

(e) N=100000 (f) N=500000

(g) N=1000000 (h) N=1500000

(i) N=2000000 (j) N=2500000

Figure 11. Execution time comparison of parallel and modified parallel OETSN using the sorted test case.

The overall conclusion of the paper is that odd-even transposition sorting has the sequential time complexity, $O(n^2)$. So, we parallelised the OETSN using GPU computing on CUDA hardware and then proposed the modified parallel OETSN using GPU computing. In the

proposed modified parallel OETSN, we reduced the number of levels of the network. After testing, we found that the number of levels of the OETSN are reduced for two types of test case i.e. zero and sorted test cases.

CONCLUSION AND FUTURE WORK

The suggested approach provided the best results when the data did not require swapping i.e. the data are sorted or unique. This significantly reduced the execution time in comparison to the existing one. The proposed approach achieved an improvement in execution time of 981661.6 times faster in the sorted test case and 904620.7 times in the zero test case using 2500000 elements and 1024 threads in comparison to the existing parallel OETSN. The time complexity is reduced from $O(n)$ to $O(1)$ because the proposed approach is executed using GPU. Some tasks are done sequentially on parallel machines so the time required in other types of test cases is slightly increased. We tested six types of test case. We varied the data from 1000 to 2500000 and the thread in multiples of two from 1 to 1024. The suggested approach can be further improved by using parallel reduction as we used linear addition. We used GPU computing using CUDA hardware with the computing capability 2.1 to test the algorithms. However, if the same algorithms will be used on hardware with the computing capability 3.0, then they will give an added advantage of unified memory architecture.

ACKNOWLEDGEMENTS

This work is performed in the frame of research-concerted action. All experiments are done in the research lab of Jaypee University of Information Technology, Waknaghat Solan, India. My co-author supervised me in using GPU computing with CUDA hardware.

REFERENCES

Ajdari, J., Raufi, B., Zenuni, X., & Ismaili, F. (2015). A Version of Parallel Odd-Even Sorting Algorithm Implemented in CUDA Paradigm. *International Journal of Computer Science Issues, 12*(3), 68-75.

Cederman, D., & Tsigas , P. (2009). GPU-quicksort: A practical quicksort algorithm for graphics processors. *Journal of Experimental Algorithmics (JEA), 14*(4), 1-22.

Dowd, M., Perl, Y., Rudolph, L., & Saks, M. (1989). The Periodic Balanced Sorting Network. *Journal of the ACM, 36*(4): 738-757..

Farmahini-Farahani, A., Duwe, H. J., Schulte, M. J., & Compton, K. (2013). Modular design of high throughput, low-latency sorting units. *IEEE Transactions on Computers 62*(7), 1389-1402.

Grama, A., Gupta, A. & Karypis, G. (1994). I*ntroduction to parallel computing: Design and analysis of algorithms*. Redwood City, CA: Benjamin/Cummings Publishing Company.

Greb, A., & Zachmann, G. (2006). GPU-ABiSort: Optimal parallel sorting on stream architectures. *Parallel and Distributed Processing Symposium, IPDPS. 20th International*. IEEE, 1-10.

Jan, B., Montrucchio, B., Ragusa, C., Khan, F. G., & Khan, O. (2012). Fast parallel sorting algorithms on GPUs. *International Journal of Distributed and Parallel Systems*, *3*(6), 107-118.

Leischner, N., Osipov, V., & Sanders, P. (2010). GPU sample sort. *Parallel and distributed processing (IPDPS), IEEE International Symposium on IEEE*, 1-55.

Matsumoto, M., & Nishimura, T. (1998). Mersenne twister: A 623-dimensionally equidistributed uniform pseudo-random number generator. *ACM Transactions on Modeling and Computer Simulation (TOMACS), 1*(8), 3-30.

Mozaffari, B. (2010). Optimization of odd-even transposition network. *2nd International Conference on Education Technology and Computer, 3,* 364-366.

Nadathur, S., Mark, H., & Michael, G . (2009). Designing efficient sorting algorithms for manycore GPU. *IEEE International Parallel and Distributed Processing Symposium*, 1-10.

Faujdar, N., & Ghrera, S. P. (2015). Performance evaluation of merge and quick sort using GPU Computing with CUDA. *International Journal of Applied Engineering Research*, *10*(18), 39315-393192 .

Peters, H., Schulz-Hildebrandt, O., & Luttenberger, N. Fast in-place sorting with CUDA based on bitonic sort. *Parallel Processing and Applied Mathematics* (pp. 403-410). Springer: Berlin Heidelberg.

Quinn, M. J. (1994). *Parallel computing: Theory and practice*. McGraw-Hill, Inc.

Salloum, S. N., & Perrie, A. L. (1999). Fault tolerance analysis of odd-even transposition sorting networks. *Communications, Computers and Signal Processing, IEEE Pacific Rim Conference on. IEEE*, *1,* 193-196.

Shifu, C., Qin, J., Xie, Y., Zhao, J., & Heng, P. A. (2009). A fast and flexible sorting algorithm with CUDA (pp. 281-290). In S.-L. C. Arrems Hua (Ed.). *Algorithms and Architectures for Parallel Processing* .

Ushijima, M., & Fujiwara, A. (2005). Sorting algorithms based on the odd-even transposition sort and the shearsort with DNA strands. *FCS*, 52-58.

Ye, Y., Du, Z., Bader, D. A., Yang, Q., & Huo, W. (2014). GPUMemSort: A high performance graphics co-processors sorting algorithm for large scale in-memory data. *Journal on Computing, 1*(2), 23-28.

Pertanika J. Sci. & Technol. 24 (2): 351 - 370 (2016)

SCIENCE & TECHNOLOGY

Journal homepage: http://www.pertanika.upm.edu.my/

Identification, Characterisation and Phylogenetic Analysis of Commensal Bacteria Isolated from Human Breast Milk in Malaysia

Zubaida Hassan[1], Shuhaimi Mustafa[2,3], Raha Abdul Rahim[1] and Nurulfiza Mat Isa[1,3]*

[1]*Department of Cell and Molecular Biology, Faculty of Biotechnology and Biomolecular Sciences, Universiti Putra Malaysia, 43400 Serdang, Selangor, Malaysia*

[2]*Department of Microbiology, Faculty of Biotechnology and Biomolecular Sciences, Universiti Putra Malaysia, 43400 Serdang, Selangor, Malaysia*

[3]*Halal Products Research institutes, Universiti Putra Malaysia, 43400 Serdang, Selangor, Malaysia*

ABSTRACT

Human breast milk microbiota is essential for infant immune system development, maturation and protection against infection. However, there is scarce information on the fluid's microbiological composition from Malaysia. The objective of the study was to isolate, identify and characterise commensal bacterial population present in human breast milk from Malaysia. One hundred bacteria were isolated from the human breast milk of healthy lactating women (n=30). After preliminary screening, 20 isolates were characterised using both phenotypic and molecular techniques. The results indicated that most frequently identified bacteria in this study were *E. faecalis* and *S. hominis.* These organisms alongside *E. cloacae* were all metabolised D-Maltose, Sucrose, D-Turanose, α-D-Glucose, D-Fructose, D-Mannose, D-Galactose, D-sorbitol and D-Mannitol and were able to grow at pH 5 and 6, 1% sodium lactate, 1%, 2% and 8% NaCl. BLAST showed over 99% similarity to those deposited in Genbank. Phylogenetic-relatedness was depicted using neighbour-joining method and had two clades with 100% bootstrap. These findings provided insight into the nature, characteristics and also phylogenetic-relatedness of bacteria present in human milk from Malaysia. Isolation and identification of commensal bacteria from human milk are considered the first step for future studies on the benefit of these organisms towards human health.

Keywords: Commensal bacteria, human breast milk, Malaysia, phenotype, phylogeny

Article history:
Received: 25 July 2015
Accepted: 28 January 2016

E-mail addresses:
zubaidatuhassan@yahoo.com (Zubaida Hassan),
shuhaimi@upm.edu.my (Shuhaimi Mustafa),
raha@upm.edu.my (Raha Abdul Rahim)
nurulfiza@upm.edu.my (Nurulfiza Mat Isa)
*Corresponding Author

ISSN: 0128-7680

INTRODUCTION

Human breast milk is a vital postpartum fluid and is considered the most important element in metabolic and immunologic programming of the health of neonates (Wagner, 2012). The presence of live cells in the fluid has been established across the world but such information from Malaysia is missing. Microbial populations in human milk vary with geographical location (Dubos et al., 2011; Nasiraii et al., 2011; Nuraida et al., 2012). Thus, the aim of this study was to isolate, identify and characterise bacteria present in human milk from Malaysia.

Human milk is an important factor in the initiation, development and of course, the composition of the neonatal gut microflora as it is a source of microorganisms to the infant gut for several weeks after birth (Martin et al., 2005). Wagner (2012) defined breast milk as a bioactive fluid that evolved from colostrum to mature milk. Heikkilä and Saris (2003) and Martín et al. (2002) estimated the ingestion of about 1×10^5 to 1×10^7commensal bacteria by infants consuming approximately 800 mL per day while suckling.

The human body is inhabited by 10 times more bacteria than body cells. Reports evaluating the beneficial effects of these bacteria have been shared in past decades (Gregoret et al., 2013). Human breast milk is not an exception as it contains numerous live cells. It is considered a symbiotic fluid. It is not sterile, as traditionally believed. Human breast milk is a complex fluid rich in nutritional and non-nutritional bioactive components (Prentice, 1996). These include prebiotic oligosaccharides (Kralj et al., 2002; Pridmore et al., 2004; Nasiraii et al., 2011) in addition to the potential probiotic and the biotherapeutic commensal (Holzapfel et al., 1998; Martin et al., 2005; Nasiraii et al., 2011).

Research on commensal bacteria from human milk has just resumed as previously breast milk studies focused on pathogens (Heikkila & Saris, 2003). Commensal bacterial strains reported from human milk are widely used in the health and industrial sectors as they have the ability to inhibit the growth of a wide spectrum of pathogenic bacteria by competitive exclusion and/or through the production of antimicrobial compounds, such as bacteriocins, organic acids and hydrogen peroxide (Fooks et al., 1999; Reid, 2001; Beasley, 2004; Martín et al., 2007). Martin et al. (2005) and Olivares et. al. (2006) suggested that the milk of healthy woman may be a source of potentially probiotic or biotherapeutic bacteria and can play a role in protecting mothers and/or infants against infectious and clinical diseases. In the present study, we characterised the commensal bacterial composition of expressed breast milk in Malaysia and determined their evolutionary relationship by sequence and phylogenetic analyses.

MATERIALS AND METHODS

Sample Collection

Expressed breast milk was collected from 30 healthy women aged between 23 and 38 years who were breastfeeding children from birth to two years old. They were randomly selected from four states and two federal territories in Peninsular Malaysia, namely Selangor, Johor, Perak, Negeri Sembilan, Kuala Lumpur and Putrajaya. Consent forms were obtained from the respondents. The samples were received as freshly expressed, chilled or iced. All samples collected were immediately stored at -20 ºC until further analyses.

Bacterial Culture and Isolation

A total of 100 isolates were obtained by plating 100 µL of the milk sample on non-selective MRS agar plates after thawing at 4 ºC overnight. The plates were incubated aerobically at 37 ºC for 48 to 72 h. An MRS medium was used to support growth of nutritionally fastidious microbes as previously reported (Heikkila & Saris, 2003). Based on colony morphology, colonies were randomly picked from culture plates and purified twice in the same conditions for 18 to 24 h. The purified strains were stored at -80ºC in growth media containing 20% (v/v) glycerol.

Bacterial Identification and Phenotyping

Isolates were identified and metabolically profiled using Biolog GenIII MicroPlate™ microbial identification system (Biolog; Haywood, CA, USA). Pure bacterial isolates were suspended in minimal media (Inoculating Fluid A (IF-A); Biolog; Haywood, CA, USA) using a sterile cotton swab and adjusted to approximately 90 to 98% transmission using a Biolog turbidimeter. From the bacterial suspension, 100µL was inoculated into each well of GenIII micro titre plates. The plates were incubated at 33 ºC for 16 to 22 h. Bacteria were speciated using algorithms provided by ML5 on the Biolog microstation 2 reader (Microlog 3/5.2.01 35, Biolog, USA). For all isolates, end-point raw absorbance data from the 96-well GenIII identification plates were normalised by subtracting absorbance in the negative control well and then exported automatically into a separate programme (Statistica†; Statsoft, Tulsa, OK, USA) for data analysis. Isolate metabolic profile was compared to the Biolog identification database (Biolog GEN III 2_6_1_08.15G). All isolates identified as microaerophilic based on the results obtained using IF-A were double confirmed with group specific fluid - IF-C (Biolog; Haywood, CA, USA).

Molecular Identification and Typing of the Isolates

Bacterial genomic DNA was extracted using the Qiagen DNA extraction kit (QIAamp®, Hilden, Germany) according to the protocols of Gram positive bacteria from DNeasy Blood and tissue culture handbook (2006) with modifications. Prior to the addition of buffer AL, 10µL of RNase A/T1 (2mg/mL, Fermentas) was added to the mixture after Proteinase K, vortexed and incubated at room temperature for 2 min. The genomic DNA was eluted with 50µL of sterile deionised distilled water instead of 200 µL of elution buffer and then stored at -20°C.

The extracted bacterial genomic DNA was visualised using 1% Agarose (TopVision™, Thermo scientific, Fermentas) stained with 1µL of Redsafe™ (iNtRoN Biotechnology, Korea) at 99V for 30 min. UV illuminator (G-Box, Syngene) with Gene system software (version 1.4.0.0) was used to view and capture the gel image.

Amplification was carried out using a Bio-Rad Thermocycler (Berkeley, California). The reaction mixture (25µL) contained 12.5µL of PCR master mix (DreamTaq Green, Thermo scientific, USA), 10.5µL of nuclease free water, 1µL of genomic DNA template and 0.5µL of 10mM of forward and reverse primers; 27F (5´-AGAGTTTGATCCTGGCTCAG-3´) and WLAB2R (5´-TCGAATTAAACCACATGCTCCA-3´) (Integrated DNA Technologies) as previously described by Emerenini et al. (2013) and Lopez et al. (2003). The amplification

programme was initial denaturation at 95 ºC for 2 min, followed by 30 cycles of denaturation at 95 ºC for 0.5 min, primer annealing at 48.9 ºC for 0.5 min and extension at 72 ºC for 1.5 min. Final extension was done at 72 ºC for 7 min.

The PCR products were purified using the GelJet PCR purification kit (Thermo-scientific, Lithuania) according to the manufacturer's instructions. The purified PCR amplicon were visualised on 1% agarose gel as described previously. The DNA concentrations of the purified products were determined using a nanodrop (IMPLEN, Shimadzu) before subjected to sequencing.

DNA Sequencing and Sequence Analysis

The purified PCR products of each isolate were sequenced thrice on both strands by ABI Prism 3730xl DNA sequencer using ABI PRISM Dye Terminator Cycle Sequencing Ready Reaction kit (Perkin Elmer) to get precise consensus sequence. BioEdit™ software version 7.2 package (Hall, 1999) was used in editing, quality assurance trimming and analysing the consensus sequence between the three sets of forward and the reverse complement of the reverse sequences. The consensus sequence was then BLAST for highly similar organism sequence identity using the "blastn" algorithm from GenBank (http://www.ncbi.nlm.nih.gov/BLAST/). Isolate identities of 99% and above were considered the identity of the query organisms. Sequences of all isolates from each genus were BLAST with a reference sequence for comparison.

Molecular Evolutionary Genetics Analysis, MEGA (Tamura et al., 2007) software version 6.03 Beta (6131108) was used to construct the tree. The neighbour-joining algorithm was used to explore the phylogenetic tree (Saitou & Nei, 1987); the robustness of individual branches was estimated using bootstrapping with 1000 replications (Felsenstein, 1985).

A total of 35 isolates was included in the phylogenetic analysis depicted by neighbour-joining (Table 1). Twenty of the sequences were obtained from this study while 15 closely related available sequences were retrieved online from the GenBank database.

Table1
16S rDNA Gene of the Strains Used in Sequence and Phylogenetic Analyses

S/N	Strain	Accession number	Region	References
1	*Enterococcus faecalis*	CP008816	1629243-1630110	Minogue et al. (2014)
2	*Enterococcus faecalis*	CP008816	2056343-2057210	Minogue et al. (2014)
3	*Staphylococcus lugdunensis*	FR87027	2424570-2425475	Heilbronner et al. (2011)
4	*Staphylococcus lugdunensis*	FR87027	2476052-2476957	Heilbronner et al. (2011)
5	*Staphylococcus lugdunensis*	CP001837	2447081-2447986	Tse et al. (2010)
6	*Staphylococcus lugdunensis*	CP001837	2505017-2505922	Tse et al. (2010)
7	*Staphylococcus hominis*	FN393804	10-900	Unpublished
8	*Staphylococcus hominis*	EU337115	24-914	Bauer et al. (2009)
9	*Staphylococcus hominis*	FJ768458	15-905	Tothova et al. (2010)
10	*Staphylococcus hominis*	JQ795892	5-895	Unpublished

Table1 (*continue*)

11	*Staphylococcus hominis*	KJ147074	14-904	Unpublished
12	*Enterobacter cloacae*	CP008823	3604651-3605545	Unpublished
13	*Enterobacter cloacae*	CP008823	4730135-4731029	Unpublished
14	*Enterobacter cloacae*	CP008823	4390718-4391612	Unpublished
15	*Enterobacter cloacae*	CP008823	4649858-4650752	Unpublished
16	*Staphylococcus hominis*	KM392086	1-890	This study
17	*Staphylococcus hominis*	KM392085	1-890	This study
18	*Staphylococcus lugdunensis*	KM392088	1-905	This study
19	*Staphylococcus hominis*	KM392087	1-890	This study
20	*Staphylococcus hominis*	KM609184	1-890	This study
21	*Staphylococcus hominis*	KM609185	1-890	This study
22	*Enterobacter cloacae*	KM609192	1-894	This study
23	*Enterobacter cloacae*	KM392095	1-894	This study
24	*Enterobacter cloacae*	KM392093	1-894	This study
25	*Enterobacter cloacae*	KM392094	1-894	This study
26	*Enterococcus faecalis*	KM609186	1-867	This study
27	*Enterococcus faecalis*	KM392090	1-867	This study
28	*Enterococcus faecalis*	KM392089	1-867	This study
29	*Enterococcus faecalis*	KM392091	1-867	This study
30	*Enterococcus faecalis*	KM609187	1-867	This study
31	*Enterococcus faecalis*	KM609188	1-867	This study
32	*Enterococcus faecalis*	KM609189	1-867	This study
33	*Enterococcus faecalis*	KM609190	1-867	This study
34	*Enterococcus faecalis*	KM609191	1-867	This study
35	*Enterococcus faecalis*	KM392092	1-867	This study

Confirmatory PCR

After the molecular identification of the isolates, confirmatory PCR was performed using genus and/or specie specific primers (Table 2) to the identified isolates to double confirm the success and reliability of the bacterial identification.

Bacterial Accession Numbers

All sequences obtained in this study were deposited in the GenBank under the following accession numbers: KM392085, KM392086, KM392087, KM392088, KM392089, KM392090, KM392091, KM392092, KM392093, KM392094, KM392095, KM609184, KM609185, KM609186, KM609187, KM609188, KM609189, KM609190, KM609191 and KM609192.

Table 2
Primers Used for Confirmatory PCR

S/N	Name	Sequence (5′ 3′)	PCR product (bp)	Remark	Reference
1	E1	TCA ACC GGG GAG GGT	733	*Enterococci* genus specific primer	(Deasyt et al., 2000)
	E2	ATT ACT AGC GAT TCC GG			
2	FL1	ACTTATGTGACTAACTTAACC	360	*Enterococcus faecalis* species specific primer	(Jackson et al., 2004)
	FL2	TAATGGTGAATCTTGGTTTGG			
3	TstaG422 F	GGCCGTGTTGAACGTGGTCAAATCA	370	Staphylococcus genus specific primer	(Martineau et al., 2001; Morot-bizot et al., 2004)
	Tstag765 R	TNACCATTTCAGTACCTTCTGGTAA			
4	Hsp60-F	GGTAGAAGAAGGCGTGGTTGC	341	*Enterobacter cloacae* species hsp60 gene specific primer	(Morand et al., 2009)
	Hsp60-R	ATGCATTCGGTGGTGATCATCAG			

RESULTS AND DISCUSSION

Human milk was traditionally considered sterile; however, studies have shown that the fluid serves as a continuous supply of commensal, mutualistic and/or potentially probiotic bacteria to the infant gut. Staphylococci, Streptococci, Lactic acid bacteria and Bifidobacteria were reported to be the dominant species in human milk (Fernández et al., 2013).

Twenty bacterial isolates were identified in this study and their metabolic profile showed that all of the isolates were able to metabolise a wide variety of carbon sources and have the ability to survive in many environments. For example, D-Maltose, Sucrose, D-Turanose, α-D-Glucose and D-Fructose were metabolised by all of the bacteria identified. They vary in a wide range of growth requirements, including also the carbon sources they utilise. Most of the identified bacteria needed some additional growth factors for adequate growth. Pyruvate, alanine, arginine, aspartate, glutamate, histidine, serine and pectin are some examples of essential nutrients required by these bacteria, which may not be present in general growth media. Therefore, we used an enriched media for their growth; otherwise they can over-grow in mixed cultures. Probiotic characteristics including acid tolerance and *l*-lactate production as seen from the isolates were also observed as did Choi et al. (2006). Individual requirement differences are tabulated in Table 3.

Consistent with earlier studies, this study showed the genera *Enterococci* and *Staphylococci* were the most frequently isolated from human breast milk (Caroll et al., 1979; Eidelman & Szilagyi, 1979; El-Mohandes et al., 1993; Wright & Feeny, 1998; Heikkila & Saris, 2003). Among the 20

Table 3
Metabolic Profiles of the Bacteria Isolated

Carbon sources	*Staphylococcus hominis* (GP cocci)	*Enterococcus faecalis* (GP cocci)	*Enterobacter cloacae ssdissolvens* (GN ENT)
Dextrin	-	+	+
D-Maltose	+	+	+
D-Trehalose	+	+	+
D-cellobiose	-	+	+
Gentibiose	-	+	+
Sucrose	+	+	+
D-Turanose	+	+	+
D-Stachyose	-	-	+
D-Raffinose	-	-	+
α-D-Lactose	-	-	+
D-Melibiose	-	-	+
β-Methyl-D-Glucosidase	-	+	+
D-salicin	-	+	+
N-Acetyl-D-Glucosamine	+	-	+
N-Acetyl-β-D-Mannosamine	-	+	+
N-Acetyl-D-Galactosamine	-	+	+
N-Acetyl Neuraminic Acid	+	-	-
α-D-Glucose	+	+	+
D-Mannose	-	+	+
D-Fructose	+	+	+
D-Galactose	-	+	+
L-Rhamnose	-	-	+
Inosine	-	+	+
D-sorbitol	-	+	+
D-Mannitol	-	+	+
Myo-innositol	-	-	+
Glycerol	-	+	+
D-Glucose-6-PO_4	-	+	+
D-Fructose-6-PO_4	-	+	+
D-Serine	-	-	+
Glycyl-L-Proline	-	-	+
L-Alanine	-	-	+
L-Arginine	-	-	+
L-Aspartic Acid	-	-	+
L-Glutamic Acid	-	-	+
L-Histidine	-	-	+
L-Serine	+	+	+
Pectin	+	+	+

Table 3 (*continue*)

Carbon sources	*Staphylococcus hominis* (GP cocci)	*Enterococcus faecalis* (GP cocci)	*Enterobacter cloacae ssdissolvens* (GN ENT)
D-Galactoronic Acid	-	-	+
L-Galactoronic Acid Lactone	-	-	+
D-Gluconic Acid	-	-	+
D-Glucoronic Acid	-	+	+
Glucoronamide	-	-	+
Mucic Acid	-	-	+
D-Sacchartic Acid	-	-	+
D-Hydroxy-Phenylacetic Acid	-	-	+
Methyl Pyruvate	+	+	+
L-Lactic Acid	+	-	+
Citric Acid	-	+	+
L-Malic Acid	-	+	
Bromo-Succinic Acid	-	+	-
α-Keto-Butytic Acid	-	+	-
ϒ-Amino-Butryric Acid	-	-	-
Acetic acid	+	-	+
Formic Acid	-	-	+

+ = Ability to metabolise - =Unable to metabolise GP=Gram Positive

bacteria isolated, *E. faecalis* were 10 and *Staphylococci*, six. The genus *Staphylococcus* has species that are of concern in medical treatment; however, most of the detected *Staphylococci* (*S. hominis*) are known as residents of the normal bacterial flora in humans (Heikkila & Saris, 2003).

This present finding supports the view that commensal *Staphylococci* are part of the predominant bacterial species in breast milk (Heikkilä & Saris, 2003). This bacterium may have originated from the skin (Dubos et al., 2011), perhaps when it came into contact with milk during suckling or pumping. Some bacteria present in the maternal gut could reach the mammary gland during late pregnancy and lactation through a mechanism involving gut monocytes. Infrared photography has shown that a certain degree of retrograde flow back into the mammary ducts can occur during suckling (Fernández et al., 2013). This bacterial community may differ depending on the individual and the health status of the lactating women. Cabrera-Rubio et al. (2012) held the view that breast milk microbiome is by the mammary glands because the bacteria isolated during the weeks previous to labour, that is, before any kind of contact with the infant, were very similar to the bacterial species isolated from fresh milk obtained after childbirth.

E. faecalis is a common inhabitant of the gastrointestinal tracts of humans and is a highly diverse species that includes opportunistic pathogens, commensal, food-derived and probiotic strains. However, probiotic strains were genetically similar to those from diary products

(Buhnik-Rosenblau et al., 2013). It is a member of the lactic acid bacteria group and was found as the most frequently identified strain in this study (Table 5). Its origin in the milk remains unclear. Some reports suggest that these microorganisms and even Bifidobacteria might be brought to the lactating breast tissue through the endogenous trafficking of bacteria-loaded dendritic cells originated from intestinal mucosa (Dubos et al., 2011). Dendritic cells have been described to penetrate the intestinal epithelium to take up commensal bacteria from the gut lumen to reach the systemic circulation, and to retain even life bacteria for several days (Cabrera-Rubio et al., 2012). However, it has been reported that lactobacilli and enterococcal isolates present in human milk are genotypically different from those isolated in the skin, within a same bacterial species and a same host (Martín et al., 2003).

A chemical sensitivity assay obtained in this study showed that all of the isolates profiled were able to grow in harsh environments such as growth at low acidic conditions (pH 5 and 6), as well as in a salted environment: that is in the presence of 1% sodium lactate and 1%, 2% and 8% NaCl. Thus, these characteristics make them potential probiotic microorganisms. These characteristics can be compared with probiotics' ability to resist bile acid and stomach conditions. The isolates vary in resistance to common antibiotics. For example, *Enterobacter cloacae* isolates were found to be resistant to Lincomycin, Niaproof 4, Rifamycin SV and Vancomycin antibiotics while *Staphylococcus hominis* and *Enterococcus faecalis* are sensitive. The latter, which were reported to be commensals/probiotic, were found to be sensitive to a range of antibiotics; nonetheless they survived in unfavourable physical environments (Table 4).

Table 4
Chemical Sensitivity Assay of the Isolated Bacteria

Chemicals	*Staphylococcus hominis* (GP cocci)	*Enterococcus faecalis* (GP cocci)	*Enterobacter cloacae ssdissolvens* (GN ENT)
pH 6	+	+	+
pH 5	+	-	+
1% NaCl	+	+	+
2% NaCl	+	+	+
8% NaCl	+	+	-
1% Sodium lactate	+	+	+
Fusidic Acid	-	-	+
D-Serine	+	+	-
Troleandomycin	-	-	+
Rifamycin SV	-	-	+
Minocycline	-	-	-
Lincomycin	-	-	+
Guanidine HCl	-	+	+
Niaproof 4	-	-	+
Vancomycin	-	-	+
Tetrazollium violet	+	+	+
Tetrazollium blue	-	+	+

Table 4 (*continue*)

Chemicals	*Staphylococcus hominis* (GP cocci)	*Enterococcus faecalis* (GP cocci)	*Enterobacter cloacae ssdissolvens* (GN ENT)
Nalidixic Acid	+	+	-
Lithium Chloride	+	+	-
Potassium Telluite	+	+	-
Aztreonam	+	+	-
Sodium Butyrate	+	+	-

+ = Resistant - = Sensitive

Table 5
Bacterial Species Recovered from Breast Milk Samples

S/N	Sample no.	Incubation time (days)	Shapes of organism	Gram reaction	Bacterial species
1	1	2	Cocci	+ve	
2	2	4			
3	2a1		Cocci	+ve	*Enterococcus faecalis* KM609186
4	3	4			
5	3a1		Rods	+ve	
6	3a2		Cocci	+ve	*Staphylococcus hominis* KM609184
7	3b		Cocci	+ve	*Staphylococcus hominis* KM392086
8	4	3	Cocci	+ve	
9	5	4			
10	5a1		Cocci	+ve	*Enterococcus faecalis* KM392090
11	6	6	No growth		
12	7	6	No growth		
13	8	3			
14	8a2		Cocci	+ve	*Enterococcus faecalis* KM392089
15	9		Cocci	+ve	
16	10	3			
17	10a		Cocci	+ve	*Staphylococcus hominis* KM392085
18	10c		Cocci	+ve	*Staphylococcus hominis* KM609185
19	11	3	Rods	+ve	
20	12	4	Cocci	+ve	
21	13	3	Cocci	+ve	

Table 5 (*continue*)

S/N	Sample no.	Incubation time (days)	Shapes of organism	Gram reaction	Bacterial species
22	14	3	Cocci	+ve	
23	15	3	Cocci	+ve	
24	16	3	Rods	+ve	
25	17	4	Cocci	+ve	
26	18	4			
27	18g		Cocci	+ve	*Enterococcus faecalis* KM392091
28	18n		Cocci	+ve	*Staphylococcus lugdunensis* KM392088
29	19	4			
30	19b1		Cocci	+ve	*Enterococcus faecalis* KM609187
31	19b2		Cocci	+ve	*Staphylococcus hominis* KM392087
32	20	4	Cocci	+ve	
33	21	3	Cocci	+ve	
34	22	2			
35	22l		Cocci	+ve	*Enterococcus faecalis* KM609188
36	22n		Rods	-ve	*Enterobacter cloacae* KM392094
37	23	3	Cocci	+ve	
38	24	4			
39	24d		Rods	-ve	*Enterobacter sp.* KM609192
40	24i		Rods	-ve	*Enterobacter sp.* KM392095
41	24m		Rods	-ve	*Enterobacter sp.* KM392093
42	25	4			
43	25a1		Cocci	+ve	*Enterococcus faecalis* KM609189
44	26	5	Cocci	+ve	
45	27	2			
46	27b1		Cocci	+ve	*Enterococcus faecalis* KM609190
47	28	4			
48	29	2			
49	29a1		Cocci	+ve	*Enterococcus faecalis* KM609191
50	30	3			
51	30a2		Cocci	+ve	*Enterococcus faecalis* KM392092

Resistance to bile salts, tolerance to gastric acid and low pH conditions are indication of survival in the stomach and intestinal digestion indicating probiotic properties (Dunne et al., 2001). As reported previously (Nueno-Palop & Narbad, 2011), *E. faecalis* is one of the strains found in this study to possess these characteristics. It was the strain that showed the most adherence to human intestinal cells (Nueno-Palop & Narbad, 2011) and adherence is an effective property of potential biotherapeutics as it is a prerequisite for colonisation, making the organisms a good probiotic.

S. hominis is normally found on human skin and usually as a harmless commensal. It is a coagulase-negative member of the bacterial genus *Staphylococcus*. They are Gram-positive, spherical cells in clusters of usually 1-2 mm in diameter. On agar plates, colonies usually have wide edges and an elevated centre and are yellow-orange pigmented. As observed during our isolation and also reported in previous findings (Abdalla et al., 2013), this study found out that *S. hominis* was able to metabolise glucose, fructose, sucrose, trehalose, turanose, lactose, galactose, mannitol and mannose. Its optimal growth conditions were 28 to 40 °C, but good growth was still observed at 45 °C, NaCl around 7.5% (Abdalla et al., 2013). *S. hominis* differ phenotypically from other species in the *Staphylococcus* genus as it produces acid from trehalose, low tolerance of NaCl and the carbohydrate reaction pattern.

The issue of antibiotic resistance is of medical concern since most of the genes involved are often plasmid or transposon associated, thereby presenting a risk of horizontal gene transfer of such genes to pathogens. In line with Nueno-Palop & Narbad (2011), the present findings indicated that both *E. faecalis* and *S. hominis* were susceptible to common antibiotics, for example, vancomycin, Niaproof 4 and rifampicin. However, *E. cloacae* is of concern due to its antibiotic-resistant pattern.

Pathogens such as *Staphylococcus aureus* and *Streptococcus agalactiae*, have been reported in breast milk (Bingen et al., 1992; Le Thomas et al., 2001; Novak et al., 2000). However, such pathogens were regarded as rare contaminants of the breast milk of healthy lactating women (Caroll et al., 1979; West et al., 1979; Law et al., 1989; El-Mohandes et al., 1993). In this study, the isolation of *Enterobacter cloacae* from the milk of healthy women can be considered as a contamination of breast milk. The presence of maternal dietary fat during pregnancy and lactation greatly influences breast milk fatty acid content (Amusquivar et al., 2000; Scopesi et al., 2001). Maternal dietary and health conditions (especially in terms of infection) are very important to the nature of bacteria in the milk. Berlin et al. (1984) reported the presence of dietary caffeine in human milk shortly after its consumption.

The number of *E. cloacae* in this study was few, but if the numbers were very high in the breast milk it could have caused dissemination of multidrug resistance. This is because the isolate was able to resist the presence of common antibiotics such as rifamycin SV, lincomycin, vancomycin, troleandomycin, among others while also being able to metabolise a wide range of carbon sources, growth at low pH and withstand up to 8% NaCl similar to *E. faecalis* and *S. hominis*.

Biolog GenIII MicroPlate™ was developed originally for the identification of isolated microorganisms based on their substrate utilisation pattern. It is a 96-well microtiter plate containing tetrazolium violet with a 71-carbon source utilisation assay and 23 chemical

sensitivity assays in addition to positive and negative controls. Three species of bacteria (*E. faecalis*, *E. cloacae*, *S. hominis*) were phenotyped using this identification panel.

Human milk is generally accepted as the best source of nutrition for neonates. It contains all of the essential nutrients and growth factors that can protect infants from infections. Expressed human milk contains commensal bacteria (Heikkilä & Saris, 2003) and has the potential to replace fresh milk. In addition to nutritional support, breast milk provides bioactive constituents that both directly and indirectly enhance mucosal barrier function and shape immune development (Cabrera-Rubio et al., 2012). The species diversity and the importance of the normal bacterial flora have received little attention so far (Heikkilä & Saris, 2003). This study explored the commensals' potential probiotic bacterial diversity in expressed human milk of healthy lactating women in Peninsular Malaysia.

Human breast milk is a fluid that serves as a source of microbes and their growth factors. It regulates interactions of host-microbe (Cabrera-Rubio et al., 2012). Until the past decade, most reports on the bacteria in human milk have focused on pathogenic bacteria (Gregoret et al., 2013), probably due to its significance in breast milk for milk banks. However, the milk contains beneficial bacteria whose growth is supported by several factors such as lysozyme, lactoferrin and oligosaccharides (prebiotics), which is believed to have assisted in preventing infections (Cabrera-Rubio et al., 2012).

All genomic DNA gel bands viewed have greater or equal to 20,000 base pairs (bp) when compared to the bands of the DNA ladder (Thermo Scientific). PCR amplification using the 16S rDNA gene universal primer set generated amplicons of around 945bp in size (Figure 1A). This is in line with the results of a previous study (Emerenini et al., 2013). BLAST results of the sequences obtained in this study showed an identity query coverage percentage of 100% and the percentage identity was 99% and 100%.

The *Enterococcus faecalis* genus- and species-specific primer sets produced fragments of around 733bp and 360bp, respectively (Figure 1B), as reported by Deasyt et al. (2000) and Jackson et al. (2004). Efforts to get clear and sharper bands for both genus- and species-specific primers for *E. faecalis* proved abortive, with PCR programmes annealing at different temperatures ranging from 47^{o}C to 62^{o}C. All the isolates yielded the expected band sizes with specie-specific primers and so, all were considered *E. faecalis*.

The *Staphylococci* group identified by sequencing and phenotyping produced bands with genus-specific primers at an annealing temperature of 49^{o}C. Products of 370 bp were produced by confirmatory PCR carried out using the *Staphylococci* genus primer set (Figure 1C), which was in line with that reported by Martineau et al. (2001).

Three out of four isolates produced bands when the *Enterobacter* species was amplified using the hsp60 gene of *Enterobacter cloacae*, as reported by Morand et al. (2009) and produced approximately 341bp (Figure 1D). However, the one *Enterobacter* isolate that failed to produce a band may be of a different species.

All sequences obtained were grouped by their respective genera and blasted against a reference. *E. faecalis* group was blasted using *Enterococcus faecalis* ATCC 29212, with the complete genome isolated in the USA with Sequence ID: gb|CP008816.1 and Length: 2939973 base pairs. Our isolates were found to amplify position 1629207 to 1630144 of the reference

sequence. Multiple sequence alignment was performed by the ClustalW programme of the BioEdit™ software package version 7.2. The sequences were trimmed at position 1629243-1630110 of the reference sequence so that they all had the same number of bases. Therefore, a total of 867 base pairs was used in *Enterococcus faecalis* multiple sequence alignment (data not shown).

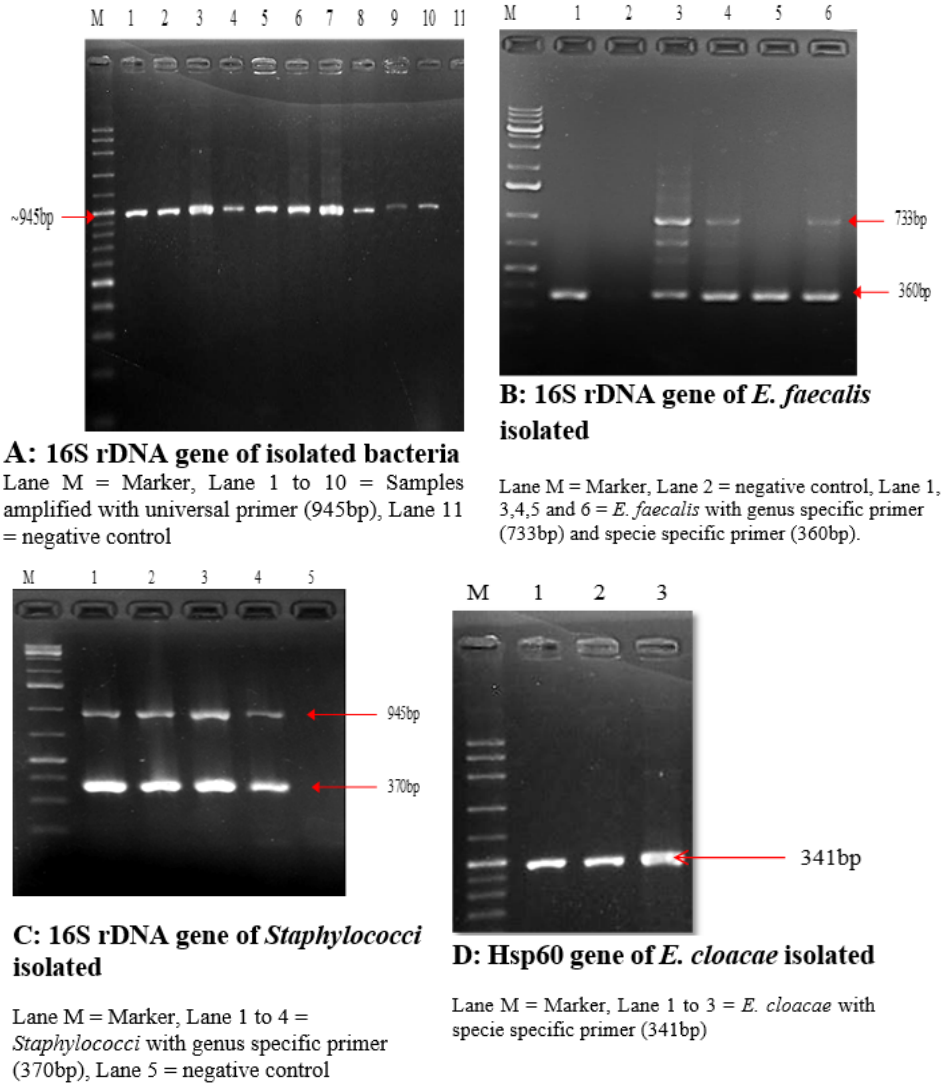

A: 16S rDNA gene of isolated bacteria

Lane M = Marker, Lane 1 to 10 = Samples amplified with universal primer (945bp), Lane 11 = negative control

B: 16S rDNA gene of *E. faecalis* isolated

Lane M = Marker, Lane 2 = negative control, Lane 1, 3,4,5 and 6 = *E. faecalis* with genus specific primer (733bp) and specie specific primer (360bp).

C: 16S rDNA gene of *Staphylococci* isolated

Lane M = Marker, Lane 1 to 4 = *Staphylococci* with genus specific primer (370bp), Lane 5 = negative control

D: Hsp60 gene of *E. cloacae* isolated

Lane M = Marker, Lane 1 to 3 = *E. cloacae* with specie specific primer (341bp)

Figure 1. PCR amplification of the isolated bacteria from human breast milk.

The *Enterobacter* group was blasted using *Enterobacter cloacae* ECNIH2 as the reference genome, the complete genome of which was also isolated in the USA with Sequence ID: gi|662712225, accession number CP008823 and length of 4852980 base pairs. Our isolates were found to amplify position 3604643 to 3605545 of the reference sequence. Multiple sequence alignment was performed by the ClustalW programme of the BioEdit™ software

package version 7.2. The sequences were trimmed at position 3604651 to 3605545 of the reference sequence so that they all had the same number of bases. Therefore, a total of 894 base pairs were used in the *Enterobacter* group for multiple sequence alignment (data not shown).

In the *Staphylococcus* genus, there were two strains: *S. lugdunensis* and *S. hominis*. *S. lugdunensis* was blasted against the complete genome of *Staphylococcus lugdunensis* N920143 with the sequence ID: gi|339893212, accession number FR870271 and length of 2595888 base pairs. Our isolate matched the reference at position 2424570 to 2425475. All of the sequences aligned at position 2424570 to 2425475 of *S. lugdunensis* (FR870271). The multiple sequence alignment included a total of 905 bases (data not shown).

Due to the lack of an available complete genome sequence of *Staphylococcus hominis*, the group was blasted against the *Staphylococcus* group (taxid: 90964). Our sequences were found to match 100% to *S. hominis* partial 16S ribosomal RNA with accession number KJ147074, which was 1511bp in length and had a sequence ID of gi|628823726 at region 4 to 944 base pairs. Multiple sequence alignment matched *S. hominis* (KJ147074) at 14 to 904; that is, a total of 890 base pairs were included in the alignments (data not shown).

The phylogenetic tree constructed (Figure 2) had two main clades, each containing an isolate relating closely to other isolates in the same genus. However, the *Staphylococcus* genus was divided into two distant clades. Each clade had a high bootstrap value (>80%). One of the clades contained *S. hominis* and *S. lugdunensis* from our isolates and the *S. lugdunensis* reference sequences, while the other clade contained our *S. hominis* sequence together with its reference sequence. The variations were also observed in the multiple sequence alignment results.

Phylogenetic analysis is a modern way of testing hypotheses about a descent of species from a common ancestor (Persing et al., 2011). Sequences that have related genomes are easily influenced to detailed reconstruction of the genome evolution (Makarova & Koonin, 2007). Phylogenetic tree construction works on principles proposed by Charles Darwin that all living organisms descended from a common ancestor and that struggles for existence make offspring dissimilar from their parents. Based on this, organisms can be classified in taxonomic hierarchy (Persing et al., 2011).

Rooted phylogenetic trees often allow prediction of descendent. A total of 890bp were analysed in Figure 2, with each genus assigned. The taxonomic assignment of the sequences showed that the composition of human breast milk is dominated by cocci. Every genus was grouped with its members from the same root. However, *Staphylococcus* genus was split into two distant clades with about 80% bootstrap. The clade that consisted of *S. hominis* alone was bootstrapped 100% whereas the other comprising both *S. hominis* and *S. lugdunensi* had 64% bootstrap value. This implies that although both are of the same genus and/or species, they have differences in their molecular characteristics that lead to their possible evolutional variation. These differences were reported in their phenotypic characteristics as well (Abdalla et al., 2013). The clade containing the two *Staphylococci* species together with *Enterococci* and *Enterobacter* appeared to have evolved earlier than the other clade because it has a shorter length to their common ancestor.

Lack of deposition of sequences of bacteria isolated from human breast milk to GenBank or other online databases limited the phylogenetic comparison of our isolates to those found in

human breast milk from other countries and regions of the world. Based on the results obtained as discussed herein, *E. faecalis* and *S. hominis* are the most frequently isolated species from the human milk.

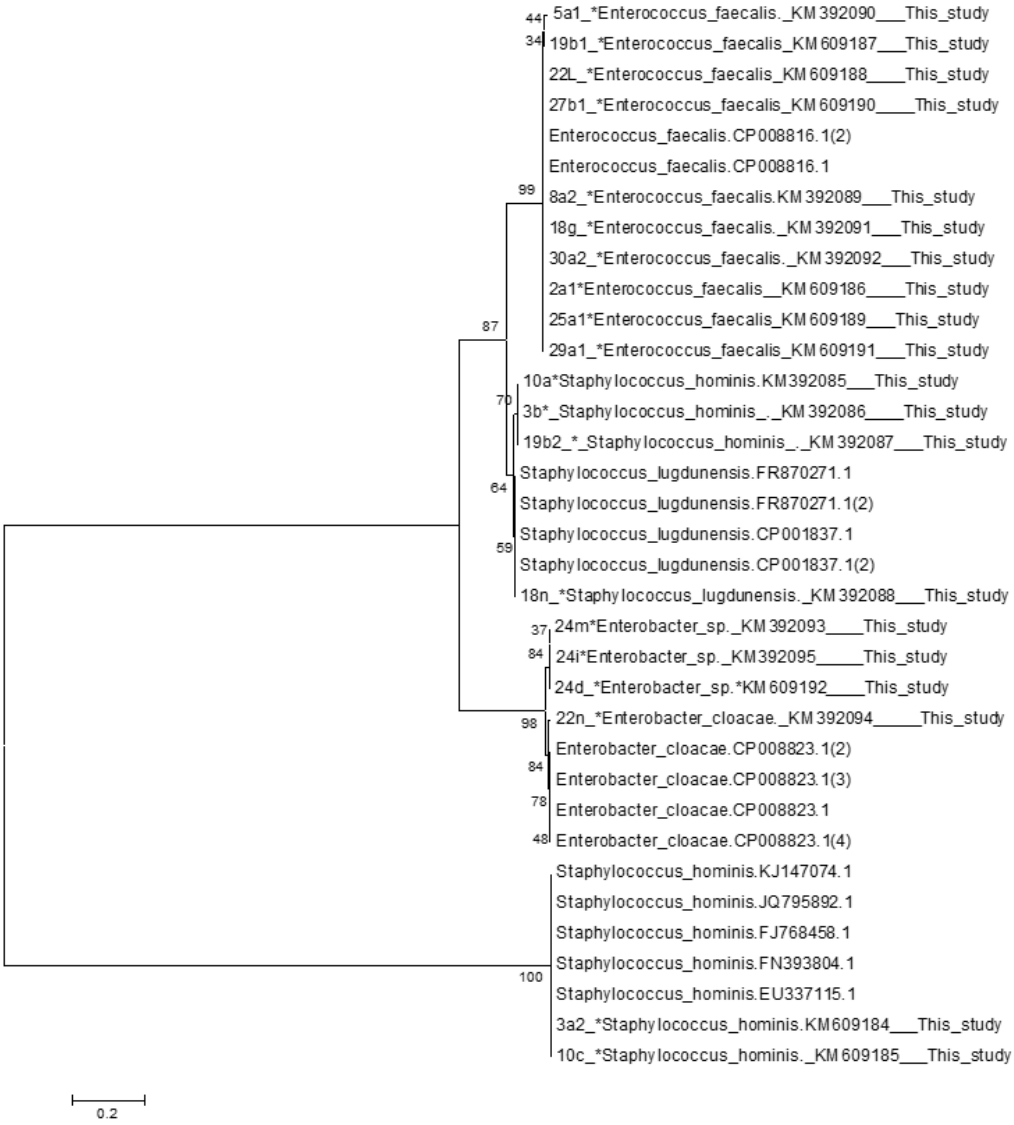

Phylogenetic tree showing the relative positions of identified isolates from human breast milk as inferred by the neighbour-joining method of partial 16SrDNA sequences. Bootstrap values for a total of 1000 replicates are shown at the nodes of the tree. References of the type strains used for comparison are given, as well as the accession numbers for all 16S rDNA sequences. Sequence divergence was at 0.2 scales.

Figure 2. Phylogenetic tree of 16S rDNA gene of bacteria isolated.

CONCLUSION

Three bacterial genera were successfully isolated and characterised from human breast milk using both phenotypic and molecular techniques. Based on the phenotypic characterisation, these isolates were found to metabolise a wide range of carbohydrates such as D-Maltose, Sucrose, D-Turanose, α-D-Glucose, D-Fructose, D-Mannose, D-Galactose, D-sorbitol and D-Mannitol. All the isolates were able to grow in acidic pH (5 and 6), 1% sodium lactate, 1%, 2% and 8% NaCl. The isolates' identities were further confirmed by molecular techniques, sequence and phylogenetic analyses. The knowledge of human milk commensal bacteria is limited especially in Malaysia. This study explored such commensal bacteria in expressed human milk of healthy lactating women. Isolation and identification of these bacteria from human milk served as the basis for further studies on benefit of these organisms towards human health such as in the area of biotherapeutics.

ACKNOWLEDGEMENTS

This study was funded by Fundamental Research Grants, Ministry of Higher Education, Malaysia, Vote number (5454244). We acknowledge the support of the Malaysian Society for Lactic Acid Bacteria during the sample collection exercise. We appreciate the effort and contributions of Faruku Bande (DVM) during sequence and phylogenetic analyses.

REFERENCES

Abdalla, N. M., Haimour, W. O., Osman, A. A., Sarhan, M. A., & Musaa, H. A. (2013). Antibiotics Sensitivity profile towards Staphylococcus hominis in Assir Region of Saudi Arabia. *Journal of Scientific Research*, *5*(1), 171-183.

Amusquivar, E., Ruperez, F. J., Barbas, C., & Herrera, E. (2000). Low arachidonic acid rather than alpha-tocopherol is responsible for the delayed postnatal development in offspring of rats fed fish oil instead of olive oil during pregnancy and lactation. *Journal of Nutrition*, *130*, 2855-2865.

Beasley, S. (2004). Isolation, identification and exploitation of lactic acid bacteria from human and animal microbiota. University of Helsinki, Finland.

Berlin, C. M., Denson Jr, H. M., Daniel, C. H., & Ward, R. M. (1984). Disposition of dietary caffeine in milk, saliva, and plasma of lactating women. *Pediatrics*, *73*(1), 59-63.

Bingen, E., Denamur, E., Lambert-Zechovsky, N., Aujard, Y., Brahimi, N., Geslin, P., & Elion, J. (1992). Analysis of DNA restriction fragment length polymorphism extends the evidence for breast milk transmission in Streptococcus agalaciae late-onset neonatal infection. *Journal of Infectious Diseases*, *165*, 569-573.

Buhnik-Rosenblau, K., Matsko-e, V., Danin-poleg, Y., Franz, C. M. A. P., Klein, G., & Kashi, Y. (2013). Biodiversity of Enterococcus faecalis based on genomic typing. *International Journal of Food Microbiology*, *165*, 27-34. doi:10.1016/j.ijfoodmicro.2013.04.009

Cabrera-Rubio, R., Collado, M. C., Laitinen, K., Salminen, S., Isolauri, E., & Mira, A. (2012). The human milk microbiome changes over lactation and is shaped by maternal weight and mode of delivery 1-4. *American Journal of Clinical Nutrition*, *96*, 544-551. doi:10.3945/ajcn.112.037382

Caroll, L., Osman, M., Davies, D. P., & McNeish, A. S. (1979). Bacteriological criteria for feeding raw breast-milk to babies on neonatal units. *Lancet*, *2*, 732-733.

Choi, S. S., Kim, Y., Han, K. S., You, S., Oh, S., & Kim, S. H. (2006). Effects of lactobacillus strains on cancer cell proliferation and oxidative stress in vitro. *Letters in Applied Microbiology.*, *42*, 452-458.

Deasyt, B. M., Real, M. C., Fitzgerald, G. F., Cogant, T. M., & Beresford, T. P. (2000). A rapid PCR based method to distinguish between Lactococcus and Enterococcus. *System and Applied Microbiology*, *23*, 510-522. doi:10.1016/S0723-2020(00)80025-9

Dubos, C., Vega, N., Carvallo, C., Navarrete, P., Cerda, C., Brunser, O., & Gotteland, M. (2011). Identification of Lactobacillus spp. in colostrum. *Archivos Latinoamericanos de Nutricion*, *61*(1), 66-68.

Dunne, C., O'Mahony, L., Murphy, L., Thornton, G., Morrissey, D., O'Halloran, S., … Collins, J. K. (2001). In vitro selection criteria for probiotic bacteria of human origin: Correlation with in vivo findings. *American Journal of Clinical Nutrition*, *73*, 386s-392s.

Eidelman, A. I., & Szilagyi, G. (1979). Patterns of bacterial colonization of human milk. *Obstetrics and Gynecology*, *53*, 550-552.

El-Mohandes, A. E., Keiser, J. F., Johnson, L. A., Refat, M., & Jackson, B. J. (1993). Aerobes isolated in fecal microflora of infants in the intensive care nursery: Relationship to human milk use and systemic sepsis. *American Journal of Infection Control*, *21*, 231-234.

El-Mohandes, A. E., Schatz, V., Keiser, J. F., & Jackson, B. J. (1993). Bacterial contaminants of collected and frozen human milk used in an intensive care nursery. *American Journal of Infection Control*, *21*, 226-230.

Emerenini, E. C., Afolabi, O. R., Okolie, P. I., & Akintokun, A. K. (2013). Isolation and molecular characterization of lactic acid bacteria isolated from fresh fruits and vegetables using nested PCR analysis. *British Microbiology Research Journal*, *3*(3), 368-377. Retrieved from www.sciencedomain.org

Felsenstein, J. (1985). Confidence limits on phylogenesis: An approach using the bootstrap. *Evolution*, *39*, 1596-1599.

Fernández, L., Langa, S., Martín, V., Maldonado, A., Jiménez, E., Martín, R., & Rodríguez, J. M. (2013). The human milk microbiota: Origin and potential roles in health and disease. *Pharmacological Research*, *69*(1), 1-10. doi:10.1016/j.phrs.2012.09.001

Fooks, L. J., Fuller, R., & Gibson, G. R. (1999). Prebiotics, probiotics and human gut microbiology. *International Dairy Journal*, *9*(1), 53-61. Retrieved from http://dx.doi.org/10.1016/S0958-6946(99)00044-8

Gregoret, V., Perezlindo, M. J., Vinderola, G., Reinheimer, J., & Binetti, A. (2013). A comprehensive approach to determine the probiotic potential of human-derived Lactobacillus for industrial use. *Food Microbiology*, *34*(1), 19-28. doi:10.1016/j.fm.2012.11.004

Hall, T. A. (1999). Bioedit: A user friendly biological sequence alignment editor and analysis program for windows 95/98/NT. *Nucleic Acid Symposium Series*, *41*, 95-99.

Heikkila, M. P., & Saris, P. E. J. (2003). Inhibition of Staphylococcus aureus by the commensal bacteria of human milk. *Journal of Applied Microbiology*, *95*(Huovinen 2001), 471-478. doi:10.1046/j.1365-2672.2003.02002.x

Holzapfel, W. H., Haberer, P., Snel, J., Schillinger, U., & Huis in't Veld, J. H. (1998). Overview of gut flora and probiotics. *International Journal of Food Microbiology*, *41*, 85-101.

Jackson, C. R., Fedorka-cray, P. J., John, B., & Barrett, J. B. (2004). Use of a genus- and species-specific multiplex PCR for identification of Enterococci. *Journal of Clinical Microbiology*, *42*(8), 3558-3565. doi:10.1128/JCM.42.8.3558

Kralj, S., van Geel-Schutten, G. H., Rahaoui, H., Leer, R. J., Faber, E. J., van der Maarel, M. J. E. C., & Dijkhuizen, L. (2002). Molecular characterization of a novel glucosyltransferase from Lactobacillus reuteri strain 121 synthesizing a unique, highly branched glucan with alpha-(1-->4) and alpha-(1-->6) glucosidic bonds. *Applied and Environmental Microbiology*, *68*(9), 4283-4291. doi:10.1128/AEM.68.9.4283-4291.2002

Law, B. J., Urias, B. A., Lertzman, J., Robson, D., & Romance, L. (1989). Is ingestion of milk-associated bacteria by premature infants fed raw human milk controlled by routine bacteriologic screening? *Journal of Clinical Microbiology*, *27*, 1560-1566.

Le Thomas, I., Mariani-Kurkdjian, P., Collignon, A., Gravet, A., Clermont, O., Brahimi, N., Gaudelus, J., … Bingen, E. (2001). Breast milk transmission of a panton-valentine leukocidin-producing Staphylococcus aureus strain causing infatile pneumonia. *Journal of Clinical Microbiology*, *39*, 728-729.

Lopez, I., Ruiz-larrea, F., Cocolin, L., Orr, E., Phister, T., Marshall, M., … Mills, D. A. (2003). Design and evaluation of PCR primers for analysis of bacterial populations in wine by denaturing gradient gel electrophoresis. *Applied and Environmental Microbiology*, *69*(11), 6801-6807. doi:10.1128/AEM.69.11.6801

Makarova, K. S., & Koonin, E. V. (2007). Evolutionary genomics of lactic acid bacteria. *Journal of Bacteriology*, *189*(4), 1199-1208. doi:10.1128/JB.01351-06

Martín, R., Heilig, H. G. H. J., Zoetendal, E. G., Jiménez, E., Fernández, L., Smidt, H. and, & Rodríguez, J. M. (2007). Cultivation-independent assessment of the bacterial diversity of breast milk among healthy women. *Research in Microbiology*, *158*(1), 31-37.

Martín, R., Langa, S., Reviriego, C., Maræn, M. L., Fernández, L., Xaus, J., A., & Rodríguez, J. M. (2002). Transferencia de bacterias lácticas del intestino de la madre al intestino del lactante a través de la leche materna. In *Actas Del II Congreso Español de Lactancia Materna, Sevilla*.

Martin, R., Olivares, M., Marin, M. L., Fernandez, L., Xaus, J., & Rodriguez, J. M. (2005). Probiotic potential of 3 Lactobacilli strains isolated from breast milk. *Journal of Human Lactation*, *21*, 8-17.

Martineau, F., Picard, O. I. S. J., Ke, D., Paradis, S., Roy, P. H., Ouellette, M., & Bergeron, M. G. (2001). Development of a PCR assay for identification of staphylococci at genus and species levels. *Journal of Clinical Microbiology*, *39*(7), 2541-2547. doi:10.1128/JCM.39.7.2541

Morand, P. C., Billoet, A., Rottman, M., Eyrolle, L., Jeanne, L., Tazi, A., … Dumaine, V. (2009). Specific distribution within the Enterobacter cloacae complex of strains isolated from infected orthopedic implants. *Journal of Clinical Microbiology*, *47*(8), 2489. doi:10.1128/JCM.00290-09

Nasiraii, L. R., Tabatabaie, F., Alaeddini, B., Noorbakhsh, R., Heravi, R. A., & Afsharian, S. (2011). Investigation of lactobacilli from mother's breast milk. *African Journal of Microbiology Research*, *5*(13), 1581-1585. Retrieved from http://www.academicjournals.org/ajmr

Novak, F. R., da Silva, A. V., Hagler, A. N., & Figueiredo, A. M. S. (2000). Contamination of expressed human breast milk with an epidemic multiresistant Staphylococcus aureus clone. *Journal of Medical Microbiology*, *49*, 1109-1117.

Nueno-Palop, C., & Narbad, A. (2011). Probiotic assessment of Enterococcus faecalis CP58 isolated from human gut. *International Journal of Food Microbiology*, *145*, 390-394. doi:10.1016/j.ijfoodmicro.2010.12.029

Nuraida, L., Palupi, N. S., Bastomi, R. R., Priscilia, D., & Nurjanah, S. (2012). Evaluation of probiotics properties of lactic acid bacteria isolated from breast milk and their potency as starter culture. *International Journal of Food, Nutrition and Public Health*, *5*(1), 33-60. Retrieved from http://www.worldsustainable.org

Olivares, M., Diaz-Ropero, M. P., Martin, R., Rodriguez, J. M., & Xaus, J. (2006). Antimicrobial potential of four Lactobacillus strains isolated from breast milk. *Journal of Applied Microbiology*, *101*, 72-79.

Persing, D. H., Tenover, F. C., Yi-Wei, T., Nolte, F. S., Hayden, R. T., & Belkum, V. (2011). *Molecular Microbiology: Diagnostic principles and practice.* (2nd ed.). Washington, DC: ASM Press.

Prentice, A. (1996). Constituents of human milk. *Food and Nutrition Bulletin*, *17*(4). Retrieved from http://unu.edu/unupress/food/8F174e/8F174E04 htm

Pridmore, R. O., Berger, B., Desiere, F., Vilanova, D., Baretto, C., Pittet, A. C., … Schell, M. A. (2004). The genome sequence of probiotic intestinal bacterium Lactobacillus johnsonii NCC533. In *Proceedings of the National Academy of Sciences of the USA* (Vol. 101, pp. 2512-2517). doi:10.1073/pnas.0307327101

Reid, G. (2001). Probiotic agents to protect the urogenital tract against infection. *American Journal of Clinical Nutrition*, *73*, 437S-443S.

Saitou, N., & Nei, M. (1987). The neighbor-joining method : A new method for reconstructing phylogenetic trees. *Molecular Biology*, *4*(4), 406-425.

Scopesi, F., Ciangherotti, S., Lantieri, P. B., Risso, D., Bertini, I., Campone, F., … Serra, G. (2001). Maternal dietary PUFAs intake and human milk content relationships during the first month of lactation. *Clinical Nutrition*, *20*, 393-397.

Tamura, K., Dudley, J., Nei, M., & Kumar, S. (2007). MEGA4: Molecular evolutionary genetics analysis (MEGA) software version 4.0. *Molecular Biology and Evolution*, *24*, 1596-1599.

Wagner, C. L. (2012). Human milk and lactation. *emedicine - medscape*. Retrieved from http://www.emedicine.medscape.com/article/1835675-overview#a0101

West, P. A., Hewitt, J. H., & Murphy, O. M. (1979). The influence of methods of collection and storage on the bacteriology of human milk. *Journal of Applied Bacteriology*, *46*, 269-277.

Wright, K. C., & Feeny, A. M. (1998). The bacteriological screening of donated human milk: Laboratory experience of British Paediatric Association's published guidelines. *Journal of Infection*, *36*, 23-27.

Pertanika J. Sci. & Technol. 24 (2): 371 - 379 (2016)

SCIENCE & TECHNOLOGY

Journal homepage: http://www.pertanika.upm.edu.my/

Coverage and Lifetime Optimization of WSN using Evolutionary Algorithms and Collision Free Nearest Neighbour Assertion

Vinodh P. Vijayan* and N. Kumar

Department of Computer Science and Engineering, Vels University, Chennai-600043, India

ABSTRACT

Multipath transmission of raw sensor signals is the customary technique used in the wireless sensor network to improve end-to-end delivery. However, this technique suffers significantly because of the occurrence of multiple copies of data at the destination and their collision. The Collision-Free Nearest Neighbour Assertion (CNNA) method with n-d tree structure improves the collision removal which, in turn, avoids duplicate packets, but load balancing among neighbouring nodes is an essential issue. Optimising network performance by considering various network parameters and load balancing the network demands a good evolutionary-based optimisation technique other than traditional algorithms. Optimisation techniques based on Particle Swarm Optimisation (PSO) and Genetic Algorithm (GA) are applied and compared against various network parameters in this work.

Keywords: Collision-Free Nearest Neighbour Assertion (CNNA), genetic algorithm (GA), multipath transmission, Particle Swarm Optimisation (PSO).

INTRODUCTION

Coverage, network-life time and end-to-end delivery are the three important parameters that decide the performance of a wireless sensor network (WSN). In WSN, network lifetime and coverage are dependent parameters, meaning there is a trade-off between these two parameters. Coverage can be simply improved by making more sensors active for a unit amount of time but this affects the life time of the sensor network. Similarly, in order to improve the average life time of the sensor network more sensors are needed to be in sleep mode for the maximum possible duration but this approach affects coverage of the network critically (Vijayan et al., 2015). The balancing of sensor coverage and network lifetime is a fundamental issue because of the dynamic nature of mission requirement. End-to-end delivery is also an important parameter because it ensures all fruitful messages reach the base station; this

Article history:
Received: 14 September 2015
Accepted: 15 March 2016

E-mail addresses:
vinodh.pvijayan@mangalam.in (Vinodh P. Vijayan),
kumar.se@velsuniv.ac.in (N. Kumar)
*Corresponding Author

ISSN: 0128-7680

demands multiple sensors to be active and a multipath transmission that ultimately affects network life time. So it is important to use good optimisation techniques to decide the optimal sensor scheduling that yields superior load balancing. The demand of the scheduling algorithm is purely on improving the pre-defined coverage and lifetime requirement. The dynamic nature of the application demands different coverage requirement but at the same time, lifetime parameters are always expected to be maximum. The proposed scheduling algorithm optimises coverage and life time based on the requirement by considering other network parameters like end-to-end delivery, throughput and load balancing etc. The type of sensor like static sensor or dynamic sensor requires different levels of attention in sensor scheduling because the requirement of coverage enhancement with a fixed number of static sensors cannot be solved using traditional techniques. Similarly, there are multiple mission requirements where the traditional algorithm fails, so an optimisation algorithm is needed that considers these multi-objective parameters for the best possible solution. Measurement coverage and life time are considered based on a spatial-temporal metric where the product of area and duration is calculated. In this work, we applied the collision-free Nearest Neighbour Assertion method in the inter-domain to improve the elimination of duplicate packets and energy, end-to-end delay, data loss etc. in WSN. The global measure of spatial-temporal coverage is taken from the average value of the individual local sites and such use of a network-wide metric guarantees global optimum solutions.

As the initial formulation of the problem confirms it is an NP hard optimisation problem, our objective was to optimise spatial temporal coverage by scheduling robotic sensors that use a centralised heuristic optimisation approach with the Nearest Neighbour Assertion method. As this is a classic problem of optimisation, coverage and lifetime measurement can be improved with the application of Genetic Algorithm (GA) (Vijayan et al., 2014) or Particle Swarm Optimisation (PSO). A comparison of the GA and PSO in this application context shows that each technique had its own strength according to context and configuration. However, challenges like creating initial populations, chromosome representation, selection of genetic operators etc. need to be solved in the implementation phase.

LITERATURE REVIEW

Robotic sensor coverage and lifetime optimising problems in a WSN has been discussed in detail. Convergent diversity like area coverage, point coverage and barrier coverage has been analysed precisely (Cardei & Wu, 2005). In coverage optimisation, most of the research focussed on minimising the number of wireless sensors without affecting coverage degree (e.g. 1-degree or k-degree) (Tian & Georganas, 2002; Wang et al., 2003) but these works did not consider network lifetime. A centralised scheduling algorithm can be used to activate sensors sequentially to ensure coverage and guarantee the O (logn) (Liu & Cao, 2010) factor of the improved network lifetime, where n is the total number of nodes. Further, application of a distributed scheduling algorithm improved the performance factor by O (logn*lognB), where B is the upper bound (Meguerdichian et al., 2001) of the initial battery. Connectivity is the other factor that needs research attention in WSN. For example, when coverage requirement could be satisfied, the conditions to achieve communication connectivity were derived (Kumar

et al., 2005). If coverage is not up to the expected level it needs to be improved e.g. partial coverage can be slightly improved by proper application of routing protocols (Kasbekar et al., 2011) that ensure delivery of data at the destination.

Major research works treat lifetime as an important objective and coverage and end-to-end delivery etc. as constraints that need the scheduling of robotic sensors for a unit amount of time to optimise total spatial-temporal coverage redundancy. Differences in problem formulation approaches are applicable based on the mission requirement for coverage or network life time.

THE OPTIMISATION OF NETWORK PARAMETERS AND LOAD-BALANCING PROCEDURE

In order to yield the optimum result, the robotic sensors need to cover a maximum area without compromising on life time of the network and other parameters like end-to-end delivery etc. In the implementation of the total network time 'T' is divided into 'L' number of cycles and the various sensors within each cycle are turned on based on the present coverage and battery life. The same procedure is repeated in each cycle and the sleep mode of the sensor is used in the same way the power-saving mode of 802.11 is used. The purpose of optimum scheduling is to identify the 'L' local schedule, which ensures maximum overall spatial-temporal coverage.

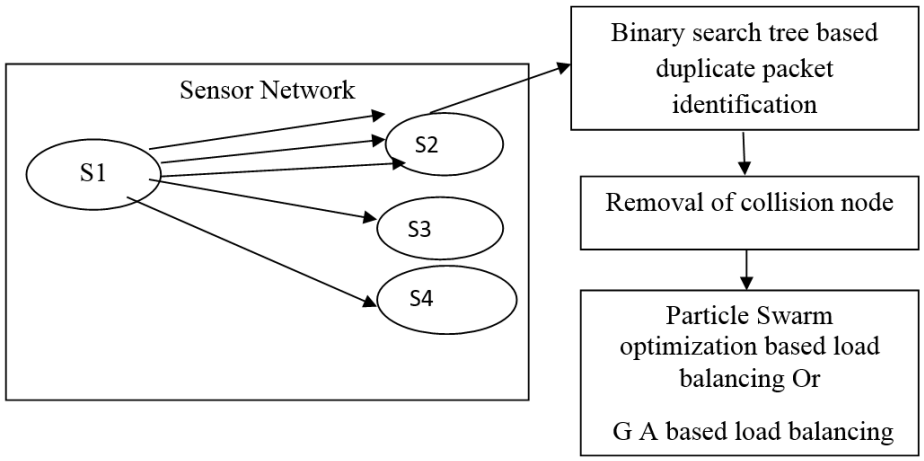

Figure 1. System architecture.

Here the initial step (Kumar et al., 2004) was to locate 'k' nearest neighbour sensor based on the distance or round-trip time in the wireless robotic sensor networks. Once the nearest neighbour list was identified a query would be sent to the nearest nodes and perimeter nodes around the query. A circle was formed around the query point and this space was further divided into subspaces of similar nature, with each subspace containing a perimeter node. Information from each subspace was collected through the perimeter node through a tree structure. Once the query was resolved the tree might be removed from the memory due to cost of maintenance.

The neighbour list created is used for Collision-Free Nearest Neighbour Assertion (CNNA) (Vijayan et al., 2016) and an n-d tree is created as shown in Figure 1. The focus is on locating

the nearest robotic sensor nodes; we assume the locations of robotic sensor nodes usually do not change during this time. Many researchers concentrate on the static environment (Zou & Chakrabarty, 2005; Kumar et al., 2004), but here the focus was on the dynamic environment tracked by the robotic sensor network. The object near a query point was located and the number of indexing schemes were proposed as dynamic object databases (Bai et al., 2006; Cardei et al., 2005).

Figure 1 clearly describes the segregation procedure with the aid of a flow chart. The nearest neighbour assertion method creates a neighbour list using the binary search technique and duplicate packets are removed based on the variance (Vijayan et al., 2016) value computed on each node, which is higher than a pre-defined threshold value (Liu et al., 2005). The evolutionary algorithms are now applied to the network to optimise network performance and parameters with the focus of load balancing.

The genetic optimisation procedure on the n-d data structure in the CNNA method undergoes genetic operations like initial population, selection, cross-over and mutation operation. Genetic operations with a weighted variance are used to optimise the load factor in a robotic sensor network with other network parameters. Challenges identified during the implementation are representation of chromosomes and selection of different genetic operators.

The GA-based optimisation technique is replaced by PSO and the performance measure is done. PSO is a robust stochastic optimisation technique based on the movement and intelligence of swarms, which literally try to improve the candidate solution. The inherent behaviour of PSO like separation, alignment, cohesion etc. are most appropriate for a WSN environment.

Procedures of the Global Version

The algorithm for PSO is as follows:

1. Initialise an array of the population of particles with random positions and velocities in D dimensions in the problem space.
2. Evaluate the fitness function in the D variables for each particle.
3. Compare each particle's fitness evaluation with its 'pbest'. If the current value is better than the 'pbest', save the current value as 'pbest' and let its location correspond with the current location in the 'D' dimensional space.
4. Compare the fitness evaluation with the population's overall previous best. If the current value is better than the 'gbest', save the current value as the 'gbest' to the current particle's array index and value.
5. Modify the velocity and position of the particle according to the following equations:

$$V_{id} = V_{id} + C_1 r_1 (P_{id} - X_{id}) + C_2 r_2 (P_{gd} - X_{id}) \quad [1]$$

$$X_{id} = X_{id} + V_{id} \quad [2]$$

The difference is that the basic principles applied to GA and PSO yield slightly different performance especially in different contexts.

METHOD AND RESULTS

The robotic sensor network is a distributed ad-hoc network comprising a large number of robotic sensor nodes equipped with capabilities of computing, storing and communicating. In this research simulation was done on Network Simulator 2 to evaluate the performance of the proposed collision-free Nearest Neighbour method with GA and PSO in the inter-domain. In the simulation, n robotic sensors were deployed in an area of 20 X 20 square metres with random motion enabled; the value of n varied from 100 to 800. The sensing range was 1 unit unless, otherwise specified. The scenarios were identified such that the application requirement made it difficult to achieve coverage and lifetime. Both homogeneous and heterogeneous cases of battery states were considered. In the homogeneous scenario, every node had the same battery/ network lifetime ratio, but in the heterogeneous scenario the battery life factor of each sensor node was considered different with value.

Result Analysis of CCNA with Optimisation Technique Applied

In order to analyse and infer the characteristics and functionality of the CNNA method with GA or PSO, we quantitatively simulated performance by considering a network size of 1000 * 1000 with simulation time varying from 100 to 800 (m/s). The routing protocol used was Dynamic Source Routing (DSR) Protocol and we compared the outcomes of the results achieved with the Genetic Optimisation (GO) algorithm and Particle Swarm Optimisation (PSO). The simulation results using NS2 simulator were compared and analysed using tabulated values and graphical form as given below. Table 1 shows the measured values that are evident for effectiveness of Genetic Optimisation algorithm and Particle Swarm Optimisation to support transient performance. The results were measured to obtain the collision-removal rate and comparison was made between the two techniques.

Table 1
Measure of Collision-Removal Rate & Measure of Load-Balancing Efficiency

Node Density	Collision Removal Rate (bps)		Load Balancing Efficiency in Terms of Load Balancing Factor (%)	
	CNNA with GA	CNNA with PSO	CNNA with GA	CNNA with PSO
100	2.105	2.055	48.15	43.10
200	3.472	3.172	51.25	46.20
300	3.750	3.650	57.35	52.30
400	4.025	4.045	61.15	56.10
500	5.275	5.125	64.24	41.59
600	4.135	4.225	53.45	62.60
700	9.105	9.035	70.05	65.00
800	11.255	11.150	71.08	66.03

Figure 2 shows that the Collision-Free Nearest Neighbour Assertion (CNNA) method provided a higher collision removal rate but it was comparable to both GA and PSO. The improved result was due to the application of collision-free nearest neighbour assertion

methods that efficiently identified duplicate packets created for a time period using n-d data structure with binary tree search. The n-d data structure identified the collision node using the binary tree, which ultimately reduced duplicate packets in the network and the node overhead in processing duplicate packets.

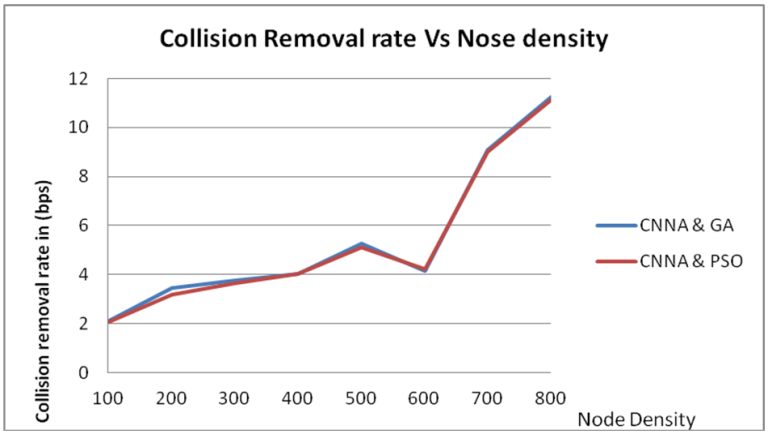

Figure 2. Impact of collision-removal rate on CNNA.

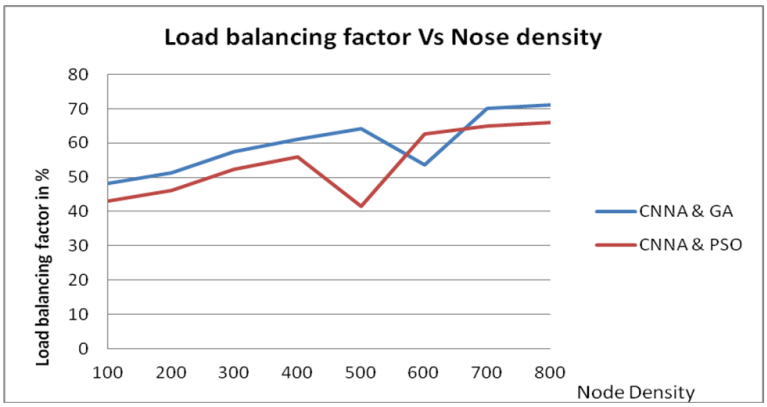

Figure 3. Impact of load-balancing efficiency with GA and PSO.

Figure 3 shows the load-balancing efficiency of both optimisation techniques. This result also proves that the effectiveness of both algorithms was comparable and that they performed equally well.

The comparison of the packet delivery ratio against the varying number of nodes for both GA and PSO was measured and tabulated as shown in Table 2. Figure 4 plots the packet delivery ratio of the two different optimisation techniques applied. It can be inferred from the graph that both GA and PSO provide a good packet delivery ratio with CNNA.

Table 2
Measure of Packet Delivery Ratio & Measure of Throughput.

Packet Delivery Ratio (%)			Throughput in %		
Node density	CNNA with GA	CNNA with PSO	Time	CNNA with GA	CNNA with PSO
100	30.25	36.35	100	66.3	32.35
200	32.45	42.44	200	59.1	37.48
300	38.56	48.52	300	58.2	42.55
400	42.35	52.35	400	52.0	58.42
500	45.55	55.45	500	66.33	62.59
600	55.45	60.45	600	70.53	70.25
700	34.45	45.25	700	65.23	70.38
800	72.35	72.45	800	66.70	70.45

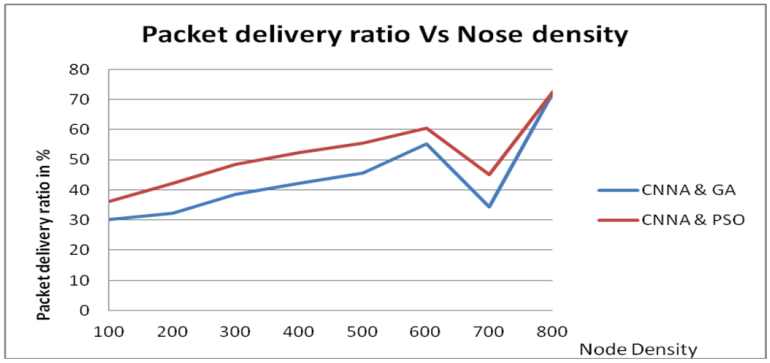

Figure 4. Impact of packet delivery ratio on varied node density.

The second part of Table 2 shows the measured value of the throughput against time and the corresponding graph plotted in Figure 5. It is evident from Figure 5 that the GA with CNNA is a good technique in the early stages of simulation while the PSO with CNNA performs well in the later stages of simulation.

From the various results obtained it can be inferred that the difference in performance between GA and PSO in different contexts is due to the operational principle difference of these techniques. Due to the strength of genetic operators like cross-over and mutation GA could bring an effective solution in the early period of network time. However, PSO operates with a previous value and memory and it can perform well once the solution is closer or in the later stage of the network.

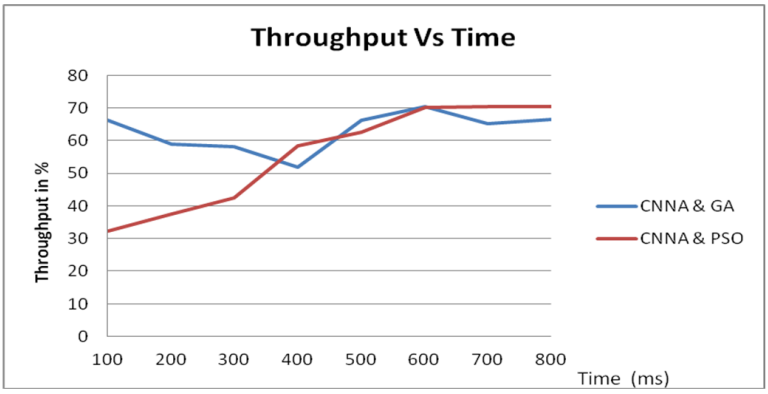

Figure 5. Impact of throughput on varying network time.

CONCLUSION

The application of Genetic Algorithm and Particle Swarm Optimisation in a wireless sensor network with Collision-Free Nearest Neighbour Assertion (CNNA) method is an effective technique for finding optimal sensor scheduling. The CNNA method eliminates duplicate packets in a network, which is generated due to multipath transmission. In this work, the optimisation technique solved the problem of load balancing in the network. The results proved that both GA and PSO performed equally well in collision removal, load balancing and packet delivery ratio for a dynamic network with a varying number of nodes. The results also proved that the throughput of the GA applied network was higher in the early stages of the scheduling and the throughput of the PSO applied network was higher in the later stages of scheduling. The performance difference was due to the operational difference of the optimisation techniques, where the GA produced higher fitness value initial populations quickly due to cross-over and mutation operations and due to the inherent nature of PSO i.e. it could operate on the existing values with large memory, performing well with later populations.

REFERENCES

Bai, X., Kumar, S., Xuan, D., Yun, Z., & Lai, T. H. (2006, May). Deploying wireless sensors to achieve both coverage and connectivity. In *Proceedings of the 7th ACM International Symposium on Mobile Ad Hoc Networking and Computing* (pp. 131-142). ACM.

Cardei, M., Thai, M. T., Li, Y., & Wu, W. (2005, March). Energy-efficient target coverage in wireless sensor networks. In *INFOCOM 2005. 24th Annual Joint Conference of the IEEE Computer and Communications Societies. Proceedings IEEE* (Vol. 3, pp. 1976-1984). IEEE.

Cardei, M., & Wu, J. (2005). Energy-Efficient coverage problems in wireless ad hoc sensor networks. *Journal of Computer Communications, 29*(4)*,* 413-420.

Kasbekar, G. S., Bejerano, Y., & Sarkar, S. (2011). Lifetime and coverage guarantees through distributed coordinate-free sensor activation. *IEEE/ACM Transactions on Networking, 19*(2), 470-483.

Kumar, S., Lai, T. H., & Arora, A. (2005, August). Barrier coverage with wireless sensors. In *Proceedings of the 11th Annual International Conference on Mobile Computing and Networking* (pp. 284-298). ACM.

Kumar, S., Lai, T. H., & Balogh, J. (2004, September). On K-coverage in a mostly sleeping sensor network. In *Proceedings of the 10th Annual International Conference on Mobile Computing and Networking* (pp. 144-158). ACM.

Liu, C., & Cao, G. (2010, March). Distributed monitoring and aggregation in wireless sensor networks. In *INFOCOM, 2010 Proceedings IEEE* (pp. 1-9). IEEE.

Liu, H., Wan, P., Yi, C. W., Jia, X., Makki, S. A. M., & Pissinou, N. (2005, March). Maximal lifetime scheduling in sensor surveillance networks. In *INFOCOM 2005. 24th Annual Joint Conference of the IEEE Computer and Communications Societies. Proceedings IEEE* (Vol. 4, pp. 2482-2491). IEEE.

Meguerdichian, S., Koushanfar, F., Potkonjak, M., & Srivastava, M. B. (2001). Coverage problems in wireless ad-hoc sensor networks. *Proceedings of the IEEE INFOCOM*.

Tian, D., & Georganas, N. D. (2002, September). A coverage-preserving node scheduling scheme for large wireless sensor networks. In *Proceedings of the 1st ACM International Workshop on Wireless Sensor Networks and Applications* (pp. 32-41). ACM.

Vijayan, V. P., & Gopinathan, E. (2014, August). Improving Network Coverage and Life-Time in a Cooperative Wireless Mobile Sensor Network. In *Fourth International Conference on Advances in Computing and Communications (ICACC), 2014* (pp. 42-45). IEEE.

Vijayan V. P., & Gopinathan E. (2015). Neuro-Genetic hybrid optimization for multi objective wireless sensor networks. *International Journal of Applied Engineering Research, 10*(22), 42897-42901.

Vijayan V. P., & Gopinathan E. (2016, January). Design of collision-free nearest neighbor assertion and load balancing in sensor network system. In *Procedia Computer Science, 70,* (pp. 508-514). Proceedings of the 4th International Conference on Eco-friendly Computing and Communication System .

Wang, X., Xing, G., Zhang, Y., Lu, C., Pless, R., & Gill, C. (2003, November). Integrated coverage and connectivity configuration in wireless sensor networks. In *Proceedings of the 1st International Conference on Embedded Networked Sensor Systems* (pp. 28-39). ACM.

Zou, Y., & Chakrabarty K., Aug. (2005). A distributed coverage and connectivity centric technique for selecting active nodes in wireless sensor networks. *IEEE Trans. Computers, 54*(8), 978-991.

Pertanika J. Sci. & Technol. 24 (2): 381 - 392 (2016)

SCIENCE & TECHNOLOGY

Journal homepage: http://www.pertanika.upm.edu.my/

Data Gathering Protocol for Reducing Energy Utilisation in a Wireless Sensor Network

Biju Paul* and N. Kumar

Department of Computer Science and Engineering, Vels University, Chennai-600043, India

ABSTRACT

Energy is a main issue in wireless sensor networks (WSN) that function on limited power supplies like batteries. Minimisation of energy utilisation is a promising area of research in WSN. However, energy utilisation of partitioning data still remains a demanding issue. With the objective of reducing the energy utilisation partitioning multi-hop wireless communications, the Energy-Efficient Traffic Renovate Partitioning (EETRP) method is proposed in this paper. The network traffic partitioning method, phantom partitioning, is an efficient technique for practical conditions. The partitioning using double cut methods yields desirable results with significant reduction in energy utilisation. Renovating by the EETRP method provides enhanced data gathering by means of centroid mean point gathering. Crucial sites are recognised and connectivity is reestablished in data aggregation. The results prove that the EETRP method achieves significant improvement in performance over state-of-the-art methods in terms of network-connectivity rate, data-gathering accuracy, network-traffic rate, energy-utilisation rate, node-renovating efficiency and network-partitioning time.

Keywords: Energy-efficient traffic renovate partitioning, partition gaps, phantom partitioning, wireless sensor networks

INTRODUCTION

A wireless sensor network is defined as the group of sensor nodes with one or more base stations. Sensor nodes generate and process through intermediate sensor nodes to base stations. Recent research has developed a capable technique to reduce communication energy utilisation in renovating partitioned nodes. The Connectivity-Based Data Collection (CBDC) algorithm detailed by Abdullah et al. (2014) used the connectivity between sensor nodes to establish the route of the mobile sink to suit its path limit and reduce the number of multi-hop communications. However, it utilised a large volume of energy. Ant Colony Optimisation

Article history:
Received: 14 September 2015
Accepted: 15 March 2016

E-mail addresses:
bijuathappadath@gmail.com (Biju Paul),
kumar.se@velsuniv.ac.in (N. Kumar)
*Corresponding Author

ISSN: 0128-7680

for Data Aggregation (DAACA) as explained by Lin et al. (2012) was used to reduce energy consumption and increase network lifetime. However, the data-gathering efficiency was not at the required level.

Sheetalrani (2014) described an energy-balanced data-gathering routing algorithm that was designed based on the principles of physics. An energy-balanced routing protocol sent data packets to the sink through dense energy areas for preserving the nodes with low residual energy. However, it failed to send the packets by eliminating loops. A cross-layer energy efficient protocol (Munish et al., 2015) decreased the energy utilisation of sensor nodes at the Network, MAC and physical layers of the protocol stack. However, the results for the network and MAC layer were not verified and validated.

Mohamad and Seyed (2014) took an energy-efficient approach based on a genetic evolutionary algorithm for preserving coverage and connectivity where the sensor node had many numbers of sensing ranges and transmission ranges. However, the renovating efficiency remained an unsolved issue. A layer-based topology control scheme for long-term hybrid WSNs (Ikjune et al., 2015) had both battery-powered and energy-harvesting nodes. Each node chose its own layer with the available energy to balance energy levels and preserve network connectivity. However, the scheme took a long time to renovate. The Combine-Skip-Substitute (CSS) scheme used by He et al. (2013) is a good technique with minimum data collection delay in WSN while the Energy-efficient Routing Algorithm to Prolong Lifetime (ERAPL) (Zhu et al., 2010) increased network lifetime when energy utilisation was efficiently managed. In ERAPL, a data-gathering sequence (DGS) was employed to remove mutual transmission and loop transmission between the nodes built, and each node sent out traffic to the links in the DGS. However, an overhead was required to swap the messages among the sink and the nodes.

Our objectives in this research work were threefold. Initially, we introduced the phantom-partitioning method to locate the affected areas to change the range of mobile elements and renovate the network structure derived from inter-partition gaps. Secondly, the method attained high data gathering efficiency by relating the centroid mean point gathering method derived from Euclidean distance. Lastly, double-cut-based partitioning contributed to reduce energy usage in a dynamic sensor environment.

LITERATURE REVIEW

The deterministic model of data collection suffers from many demerits and at the same time, the probabilistic approach of data aggregation improves data collection efficiency. A probabilistic model of data aggregation using path scheduling gives improved performance to the Cell-Based Path Scheduling (CPS) algorithm (Ji et al., 2014). However, CPS does not solve the security issues that could be raised in sensor networks. A hybrid approach of using the centralised heuristic approach with a distributed parallel optimisation (POP) (Liu & Cao, 2011) gives improved data rate against time. However, this hybrid model is not so feasible in the face of practical implementation procedures. Performance improvement in a critical mission with a distributed approach and improved scalability, collision removal etc. were focussed on a conflict-free time slot allocation mechanism (Lin et al., 2011) but this technique did not consider the position of the various sensors involved in data collection.

Ozlem et al. (2011) reported that multi-frequency scheduling could be used to deal with issues related to many interference and channel modes. Even though the problem of data with a static nature was considered, the problem with dynamic data remained unsolved. An efficient data collection scheme by a ferry node was planned by Mariam et al. (2015) with a significant result in the ferry path. The performance of the selecting cluster heads was derived from their residual energy and distance from the ferry path. However, it was not used for a nonlinear route to attain enhanced results. A distributed data compression framework (Lee & Lee, 2013), however, used the broadcasting feature of the wireless medium to increase energy efficiency. However, data compression was not considered.

ENERGY-EFFICIENT TRAFFIC- RENOVATE PARTITIONING

The design and details of the traffic-renovate partitioning method, which offers energy efficiency during data collection in WSN, is discussed here. The key goal of the proposed work was to renovate the structure of the network, and with the help of a renovated network structure, the EETRP method executed an effective data-gathering process with optimised utilisation of energy. Renovation was done based on the position of the mobile node. The process of partitioning the wireless sensor network structure is described in Figure 1.

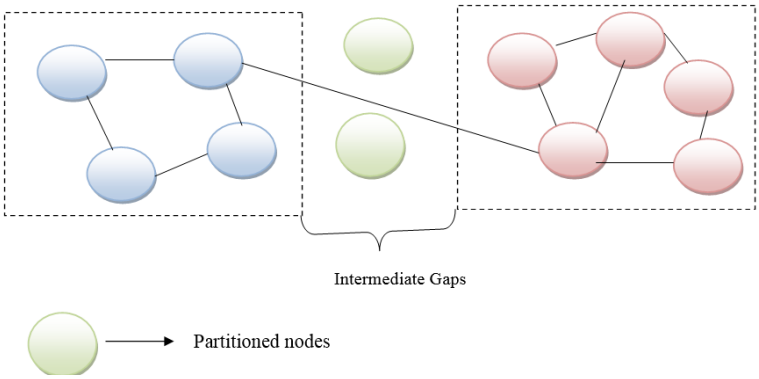

Figure 1. Node partitioned in wireless sensor network structure.

Figure 1 describes node partitioning. The intermediate gaps connecting the partitioned nodes are recognised by means of phantom partitioning. Phantom partitioning in the EETRP method represents spectral-based damaged and partitioned nodes recognised in the wireless sensor network structure. The traffic network structure discovers the route path connectivity with the double cut. The double cut in the EETRP method is employed in order to divide or cut the network structure into two divisions and then balance the partitioned limits with less energy utilisation. The bisected path discovers the safer route in a sensor network with help of the EETRP.

The renovated network structure functions as an efficient data-gathering system using the centroid mean point gathering method. The method is executed after addressing the network traffic problem using the EETRP method. The partitioned nodes are added into the suitable

group in the renovated network structure. The data gathering is executed using the centroid mean computation value. The renovated network structure for data gathering executed by the centroid mean point gathering method is explained in Figure 2.

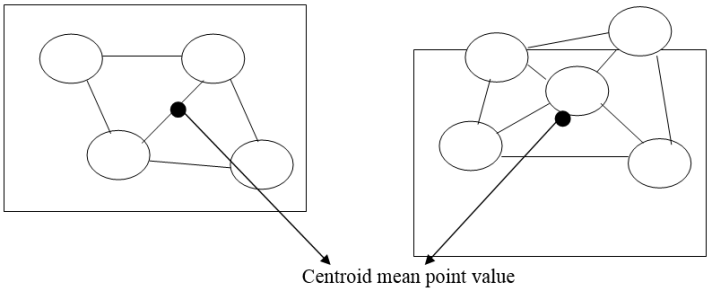

Figure 2. Renovated wireless sensor network structure in EETRP for data gathering.

The centroid mean point in the EETRP method is calculated by Euclidean distance. The centroid-based technique divides the structure into 'n' different zones and the data collection is done at the centre point. The EETRP method makes use of mobile sensor nodes to identify the partitioned nodes. The partitioned node gap inside the traffic network structure is recognised by phantom partitioning. Phantom partitioning utilises the double cut in the EETRP method to balance the limits. The balanced limits eliminate the partitioned node and renovate the sensor network structure. The renovated network structure utilises the centroid mean point gathering method to improve the data-gathering rate. The framework of the Energy Efficient Traffic Renovate Partitioning (EETRP) method is explained in Figure 3.

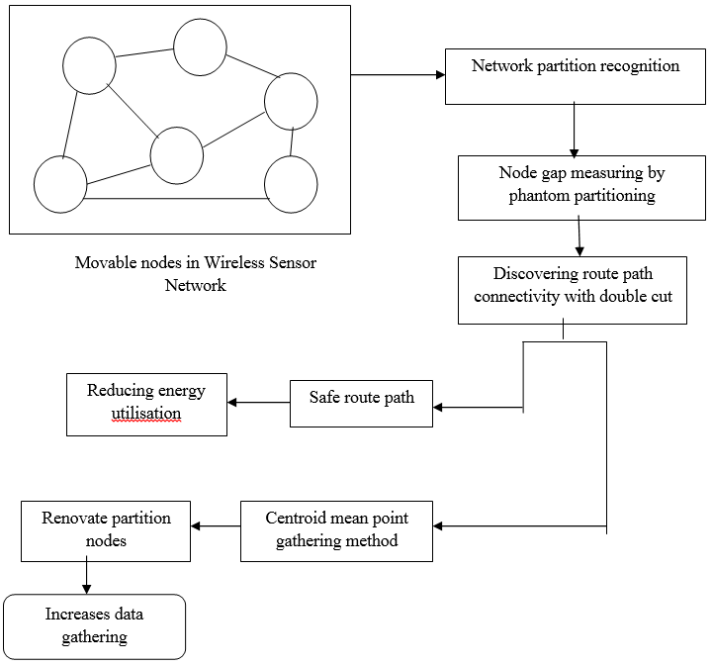

Figure 3. Architecture diagram of EETRP method.

Finally, the renovated network structure, now without any traffic, executes data gathering derived from the estimation of the centroid mean point.

Partitioned Node-Gap Calculation

The gap between the partitioned nodes in the sensor network structure is calculated to renovate the nodes with less energy utilisation. Consider a wireless sensor network with vertex 'v' and edges 'e' on the two integers 'p' and 'q'. The $v_k \in$ v is such that:

$$Number\ of\ node\ partitioned = \sum_{k=1}^{p} F_m\,(v_k) \quad [1]$$

In Eqn (1), F_m denotes the degree of membership function on the vertex 'v_k'. All the partitioned nodes are added together and form the point '1' to integer 'p'. The partitioned nodes are represented in Figure 1. Eigen vector value is used to identify the gap between the partitioned nodes. Eigen vector points are a non-zero vector matrix, where the matrix multiplication results in constant multiple points in EETRP method. The vector point is automated as:

$$p * \overrightarrow{v_k} = \lambda * v_k \quad [2]$$

v_k is the vector point on integer 'p' and 'λ' represents the constant multiple points. The Eigen vector with the continuous vector space functions computes the distance between the partitioned nodes in the sensor network. The continuous vector space function is explained as:

$$f_c(p,q) = \lambda * e^{\lambda(p,q)} \quad [3]$$

$f_c(a,b)$ on integer 'p' and 'q' uses the Eigen value multiple constants for calculation on a larger network zone. The algorithmic step on the partitioned node-gap calculation in the EETRP method is explained as:

Input: vertex 'v', edges 'e', two integers 'p' and 'q', Eigen vector 'λ', partitioned nodes 'n'
Output:
// **Partitioned Node Distance Computation**
Begin
Step 1: Membership function degree on partitioned node is calculated by Eqn (1) on all the vector points
Step 2: Recognise distance gap by Eigen vector and calculate vector points using Eqn (2) with constant multiple points
Step 3: Calculate continuous vector space function to reduce energy consumption using Eqn (3)
End

The step-wise explanation is given for the distance-gap calculation on all partitioned nodes in the sensor network structure of changeable mobile range numbers.

Balancing Limits Through Double Cut

The balancing limits (B_L) by the double cut in the EETRP method is given by:

$$B_L = \frac{1}{p}\left|(p * v_k) - |v|\right| \leq q \quad [4]$$

Eqn (4) uses the vector v_k within the network structure to renovate the network set-up. The balancing limit is less than the integer value 'q' so the partitioned nodes are eliminated and the renovated structure is designed in the EETRP method. The renovated network with a traffic-free mobile element structure recognises the efficient connectivity between the sensor nodes.

Centroid Mean Point Gathering Method

In order to estimate the centroid mean point gathering on all 'n' zones in the sensor network structure by means of the EETRP method, the partitioned nodes are maintained in the corresponding group for the sake of fruitful data collection.

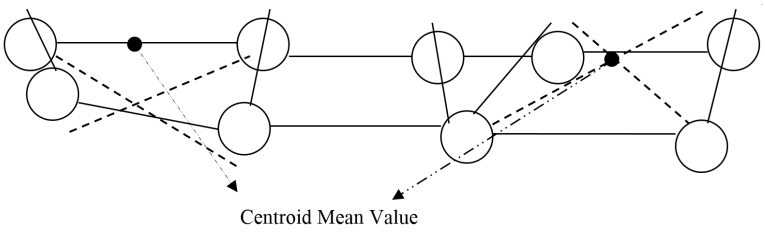

Figure 4. Centroid mean point collection method.

Figure 4 describes the Centroid Mean Point Collection method. The method renovates the partition nodes, which help to increase the data-gathering rate.

RESULTS

The environment was simulated in NS2 with a sensor field size of 900m X 900m. Simulation was done using a configuration of 100 sensor nodes, while the routing protocol initialised was DSR, the speed of the sensor was 30 m/s and random motion was enabled.

The Energy Efficient Traffic Renovate Partitioning (EETRP) method was compared with the existing the Ant Colony Algorithms for Data Aggregation (DAACA) method and the Connectivity-Based Data Collection (CBDC) method with regards to factors such as network-connectivity rate, data-gathering accuracy, network-traffic rate, energy-utilisation rate, node-renovating efficiency and node-partitioning time.

Energy-Utilisation Rate (EUR)

The energy-utilisation rate is defined as the amount of energy consumed for partitioning the nodes by double-cut-based partitioning to create a safe route path. It is measured in terms of percentage (%).

Table 1
Tabulation for Energy-Utilisation Rate

Number of Sensor Nodes	Energy-Utilisation Rate (%)		
	DAACA	CBDC	EETRP
10	35	40	29
20	38	43	33
30	41	47	36
40	45	51	39
50	48	54	44
60	52	57	49
70	55	60	53

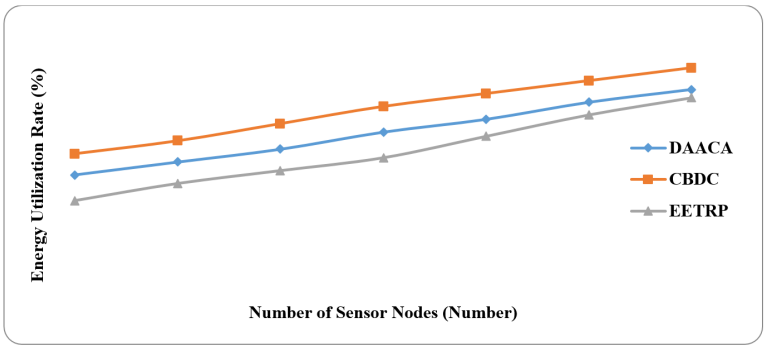

Figure 5. Performance of energy-utilisation rate with respect to sensor nodes.

A performance analysis for energy-utilisation rate with respect to movable sensor nodes was carried out with the existing DAACA and CBDC. The energy-utilisation rate for increasing the number of movable sensor nodes in the range of 10 to 70 was used in a wireless sensor network. The simulation results are shown in Figure 5. It can be seen that when the number of movable sensor nodes increased, the energy-utilisation level also increased; however, this development was achieved using the proposed EETRP method. The Research in Energy Efficient Traffic Renovate Partitioning (EETRP) method utilised 12.01% less energy than the Ant Colony Algorithms for Data Aggregation (DAACA) method and 25.97% less energy than the Connectivity-Based Data Collection (CBDC) method.

Node-Renovating Efficiency

Node-Renovating Efficiency is defined as the rate at which the nodes in the networks get renovated exactly after the partitioning of the nodes. It is measured in terms of percentage (%).

Table 2
Tabulation for Node-Renovating Efficiency

Number of Sensor Nodes	Node-Renovating Efficiency (%)		
	DAACA	CBDC	EETRP
10	70	60	78
20	73	63	81
30	75	67	84
40	78	71	87
50	81	75	89
60	84	78	91
70	86	82	94

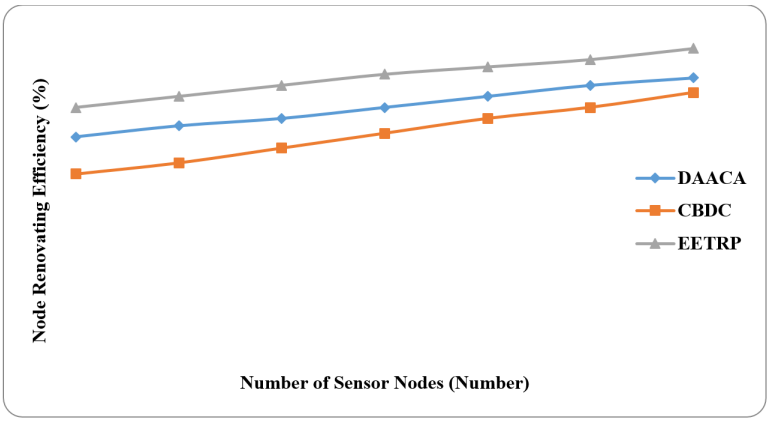

Figure 6. Performance of node-renovating efficiency with respect to sensor nodes.

A performance analysis for node-renovating efficiency with respect to movable sensor nodes was carried out with the existing DAACA and CBDC. Node-renovating efficiency for increasing the number of movable sensor nodes in the range of 10 to 70 was measured in a wireless sensor network. The simulation results are shown in Figure 6. It can be seen that when the number of movable sensor nodes increased, node-renovating efficiency also increased although growth was attained by means of the proposed EETRP method. The Research in Energy Efficient Traffic Renovate Partitioning (EETRP) method had 9.48% greater node-renovating efficiency than the Ant Colony Algorithms for Data Aggregation (DAACA) method and 18.10% greater node-renovating efficiency than the Connectivity-Based Data Collection (CBDC) method.

Data-Gathering Accuracy

Data-gathering accuracy is defined as the degree to which the data are exactly collected. It is measured in terms of percentage (%).

Table 3
Tabulation for Data-Gathering Accuracy

Number of Sensor Nodes	Data-Gathering Accuracy (%)		
	DAACA	CBDC	EETRP
10	75	69	84
20	77	72	86
30	78	73	89
40	80	75	91
50	82	76	93
60	83	79	94
70	86	81	95

A performance analysis for data-gathering accuracy with respect to movable sensor nodes was carried out using the existing DAACA and CBDC methods. The data-gathering accuracy for an increasing number of movable sensor nodes in the range of 10 to 70 was measured in a wireless sensor network. The simulation results are shown in Figure 7.

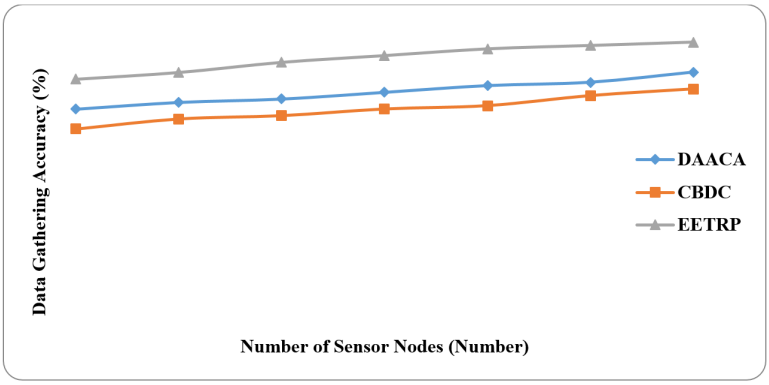

Figure 7. Performance of data-gathering accuracy with respect to sensor nodes.

It can be seen that when the number of movable sensor nodes increased, the data-gathering accuracy also increased, although growth was attained by means of the proposed EETRP method. The Research in Energy Efficient Traffic Renovate Partitioning (EETRP) method had 11.23% greater data-gathering accuracy than the Ant Colony Algorithms for Data Aggregation (DAACA) method and 16.95% greater data-gathering accuracy than the Connectivity-Based Data Collection (CBDC) method.

Node-Partitioning Time

Node-partitioning time is defined as time taken to partition the nodes in an efficient manner. It is measured in terms of milliseconds (ms).

Table 4
Tabulation for Node-Partitioning Time

Number of Sensor Nodes	Node-Partitioning Time (ms)		
	DAACA	CBDC	EETRP
10	20	23	13
20	24	25	16
30	26	29	18
40	27	31	21
50	29	35	24
60	31	37	25
70	33	40	29

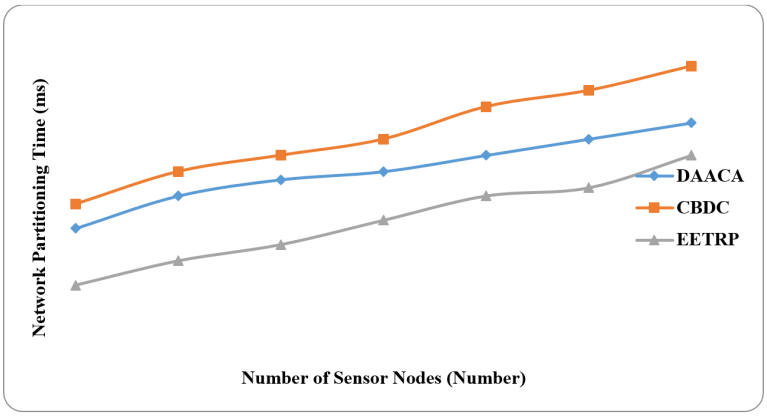

Figure 8. Performance of node-partitioning time with respect to sensor nodes.

A performance analysis for node-partitioning time with respect to movable sensor nodes was carried out using the existing DAACA and CBDC methods. The node-partitioning time for increasing the number of movable sensor nodes in the range of 10 to 70 was measured in a wireless sensor network. The simulation results are shown in Figure 8. It can be seen that when the number of movable sensor nodes increased, the node-partitioning time also increased, although the development was achieved using the proposed EETRP method. The Research in Energy Efficient Traffic Renovate Partitioning (EETRP) method took 33.64% less node-partitioning time than the Ant Colony Algorithms for Data Aggregation (DAACA) method and 55.16% less node-partitioning time than the Connectivity-Based Data Collection (CBDC) method.

CONCLUSION

The issue of data-gathering efficiency in a wireless sensor network was solved using the Energy Efficient Traffic Renovate Partitioning (EETRP) method, which also reduced energy utilisation during renovation of nodes. The mobile nodes were used to reduce energy during transmission

in a mobile environment, which also improved data-gathering efficiency. We also examined the process of minimum energy utilisation during renovation into data-gathering efficiency and attained optimality for these contentious ideas. Three important methods were designed; they are termed as phantom partitioning for changing the range of mobile elements in a wireless sensor network structure for recognising the exact positioning of partitioned nodes that use the double-cut structure for efficient energy utilisation, resulting in data gathering by the Centroid Mean Point Collection method for movable sensor nodes. The performances results showed that the proposed EETRP method presented a higher level of data collection efficiency and also reduced energy utilisation compared to state-of-the-art methods.

REFERENCES

Abdullah I. A., Khaled D. M., Haitham A. A., & Ziad A. A. (2014, June). Connectivity-Based data gathering with path-constrained mobile sink in wireless sensor networks. *Journal of Wireless Sensor Network, 6*(6), 118-128.

Chi Lin , Wu, G. Xia, F., Li, M., Lin Yao , & Pei, Z. (2012, November). Energy efficient ant colony algorithms for data aggregation in wireless sensor networks. *Elsevier, Journal of Computer and System Sciences, 78*(6), 1686-1702.

He, L., Pan, J., & Xu, J. (2013, July). A progressive approach to reducing data collection latency in wireless sensor networks with mobile elements. *IEEE Transactions on Mobile Computing, 12*(7), 1308-1320.

Ji, S., Raheem B., & Cai, Z. (2014, March). Snapshot and continuous data collection in probabilistic wireless sensor networks. *IEEE Transactions on Mobile Computing, 13*(3), 626-637.

Lee, S., & Lee, H. (2013, July). Energy-Efficient data gathering scheme based on broadcast transmissions in wireless sensor networks. *The Scientific World Journal*, 1-7.

Lin, C. K., Zadorozhny, V. I., Prashant V. K., Park, H. H. & Lee, C. G. (2011, February 17). A distributed and scalable time slot allocation protocol for wireless sensor networks. *IEEE Transactions on Mobile Computing, 10*(5), 505-518.

Liu, C., & Cao, G. (2011, February 17). Spatial-Temporal coverage optimization in wireless sensor networks. *IEEE Transactions on Mobile Computing, 10*(4), 1-9.

Mariam A., Khaled S., Klaithem A., & Mohammed A-H. (2015). Ferry-Based data gathering in wireless sensor networks with path selection. *Elsevier, Procedia Computer Science, 52,* 286-293.

Mohamad N., & Seyed M. J. (2014, April). Energy efficient approach based on evolutionary algorithm for coverage control in heterogeneous wireless sensor networks. *International Journal of Computer Science, Engineering and Information Technology, 4*(2), 1-8.

Munish G., Paramjeet S., & Shveta R. (2015, July). Optimizing physical layer energy consumption for reliable communication in multi-hop wireless sensor networks. *Indian Journal of Science and Technology, 8*(7), 1-7.

Ozlem D. I., Amitabha G., Bhaskar K., & Krishnakant C. (2011, November 21). Fast data collection in tree-based wireless sensor networks. *IEEE Transactions on Mobile Computing, 11*(1), 1-15.

Sheetalrani R. K. (2014, January). Enhancing energy efficiency in WSN using energy potential and energy balancing concepts. *International Journal of Computer Science and Business Informatics, 13*(1), 1-10.

Yoon, I., Dong, K. N., & Shin, H. (2015, March). Energy-Aware hierarchical topology control for wireless sensor networks with energy-harvesting nodes. *International Journal of Distributed Sensor Networks,* 1-13.

Zhu, Y., Wua, W., Jian Pan , & Tang, Y. (2010, March 15). An energy-efficient data gathering algorithm to prolong lifetime of wireless sensor networks. *Elsevier, Computer Communications, 33*(5), 639-647.

Pertanika J. Sci. & Technol. 24 (2): 393 - 396 (2016)

SCIENCE & TECHNOLOGY

Journal homepage: http://www.pertanika.upm.edu.my/

Case Report

18F-FDG-PET CT Features of Colo-Colic Intussusceptions in Patient with Colonic Carcinoma

Fathinul Fikri, A. S.[1]*, Noraini Sarina, A.[1], Shahrin, S.[2] and Abdul Jalil, N.[1]

Centre for Diagnostic Nuclear Imaging, Universiti Putra Malaysia, 43400 Serdang, Selangor, Malaysia

Department of Diagnostic Imaging, KPJ Rawang Specialist Hospital, Jalan Rawang, Bandar Baru Rawang, 48000 Rawang, Selangor

ABSTRACT

Colo-colic intussusception is a rare manifestation of a primary tumour in an adult patient. This article aims to document the rarity of colo-colic intussusception features on the 18 FDG- PET-CT in a patient with primary colonic carcinoma. An 18 FDG-PET-CT was performed for the purpose of pretreatment staging of a colonic carcinoma in a 61-year-old man following a diagnostic colosnoscopic biopsy. He presented with abdominal distension and peri-rectal bleeding for a month. The fused 18 F-FDG PET-CT image revealed an FDG-avid mass in the left hemicolon showing a rim of FDG avidity denoting the head of intussusceptum. There are also multiple FDG-avid nodules seen along the anti-mesenteric colonic fat suspicious for lymph nodes metastasis. Debulking of tumour revealed a mucinous adenocarcinoma of colon with a metastatic lymph node. 18 FDG PET-CT features of intussusception in colonic carcinoma have never been described before. It can potentially become a preferred diagnostic tool in delineating a potential tumour mass within the intussusceptions that help improve prognosis in patients with malignancy

Keywords: Colonic carcinoma, synchronous tumour, adult intussusception, colo-colonic intussusceptions, FDG PET-CT

INTRODUCTION

Intussusception occurs when one loop of bowel (intussusceptum) telescopes into an adjacent segment (intussuscipiens). Intussusception is rarely found in adults, with only approximately 5% of all intussusceptions occurring in adults, often associated with a malignant lead point (Young et al., 2006).

Article history:
Received: 13 July 2015
Accepted: 21 August 2015

E-mail addresses:
ahmadsaadff@gmail.com (Fathinul Fikri, A. S.),
surihatiku.sn@gmail.com (Noraini Sarina, A.),
dr_shahrinrad@yahoo.com (Shahrin, S.)
drimaging@yahoo.com (Abdul Jalil, N.)
*Corresponding Author

ISSN: 0128-7680

More than one half of large-bowel intussusceptions are associated with malignant lesions with the incidence of primary cancers in the colon at about 2 to 5% (Chien-Chih et al., 2013). Affected adults are rarely present with intestinal obstruction (Gayer et al., 2002).

At large diagnostic work of the intussusception is by conventional imaging technique i.e. abdominal radiography, barium enema, upper gastrointestinal series and ultrasound following further evaluation of the suspected intestinal obstruction. Computed Tomography (CT) is a routine examination as it will clearly demonstrate the site of intussusceptions given its compatibility in visualising a gaseous structure. In addition, CT could delineate a complex sausage-shaped mass, the 'target' lesion, consisting of the outer intussuscipiens and the central intussusceptum (Gayer et al., 2002). There is often an eccentric area of fat density within the mass representing the intussuscepted mesenteric fat, and the mesenteric vessels are often visible within it (Gayer et al., 2002). Furthermore, a rim of oral contrast medium may at times be noted encircling the intussusceptum conforming along the opposing walls of the intussusceptum and the intussuscipiens.

The Positron Emission Tomography-Computed Tomography (PET/CT) utilising Flurodeoxyglucose (FDG) is a sensitive imaging tool in localising mass lesions. Aside from its role in preoperative evaluation of tumours, the PET-CT feature of intussusceptions has never been reported to our best knowledge. We document a PET-CT feature of a rare case of the colo-colonic intussuception secondary to colonic cancer.

CASE REPORT

A 61-year-old man presented with an altered bowel habit for for months associated with constitutional symptoms and tenesmus. On physical examination, there appeared to be a vague mass in the left lumbar region. Diagnostic colonoscopy revealed a friable obstructing tumour of approximately 70-cm distance from the anal verge. An FDG PET-CT of the whole body revealed an FDG-intense mass at the descending colon proximally measuring about 6 cm x 4c m x 5.7c m in diameter with a claw-like FDF-avidity at the proximal descending colon for which the correlated CT revealed a bowel-telescoping, denoting the site of intussusception (Figure 1). There was also a focus of FDG avidity at the peri-colonic area suspected of hosting a metastatic lymph node.

The patient underwent a left hemicolectomy and omentectomy. Intraoperative findings showed an obstructive colon tumour with intussuseption at the splenic flexure with dilated proximal colon. There were also multiple lymph nodes seen along the mesentery and omentum with minimal ascites without peritoneal involvement. An intussusseption at the tumour growth of the splenic flexure was confirmed.

Histologically, the tumour was a moderately differentiated mucinous adenocarcinoma which had invaded the muscular layer with only one adjacent pathological lymph node metastasis (T3N1M0) modified Dukes C1. Surgical resection with adjuvant chemotherapy was planned for the patient.

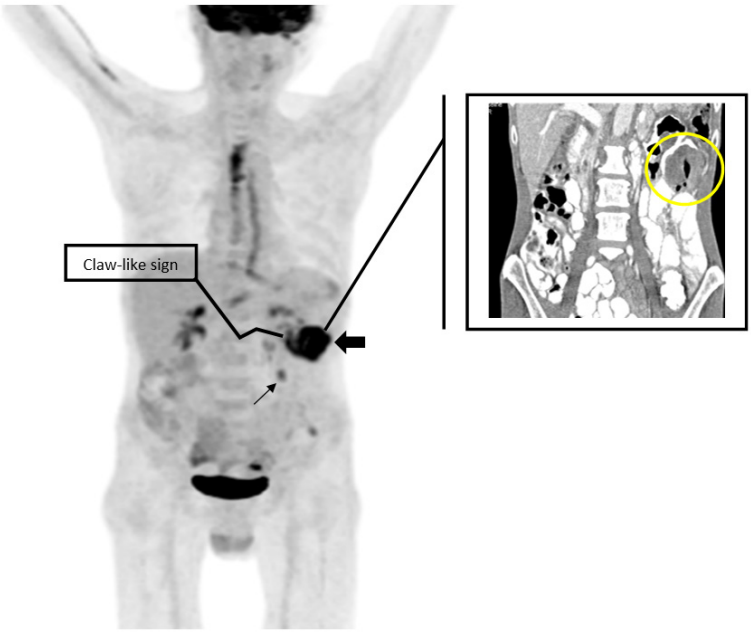

Figure 1. Maximum intensity projection (MIP) image of the FDG PET-CT showing an FDG-avid mass (SUVmax: 8.9) (arrow head) with a claw-like FDF-avidity (wall of the opposing inflammatory walls of the intussusceptum and the intussuscipiens) at the proximal descending colon (blue arrow). The correlated CT image revealed the site of intusseption (telescoping of the bowel lumen). There is also a focal FDG uptake lesion (long arrow) suggestive of lymph node metastasis.

DISCUSSION

In nearly two thirds of adult patients with colo-colonic tumours, intussusception is strongly associated with a malignant lead point (Gayer et al., 2002). Typically, adults presented with chronic complaints such as intermittent crampy abdominal pain, nausea or bloody stools. In this case, the patient presented with altered bowel habits associated with constitutional symptoms. The erect plain radiograph is not specific to characterise the intususseption aside from revealing evidence of air-fluid levels and the dilated colonic segment proximal to the intussuseption. A recent Best Evidence Topic report found that the sensitivity of plain radiology ranges from 36 to 90% and a specificity of 45-90% (Broomfield., 2008). Routinely, single contrast barium enema is more popular in neonatal intussusception. Air, water-soluble or barium contrast enemas are diagnostic approaches with significant therapeutic values, with reduction rates between 70% and 90%, which characterises the intussuseption as a coiled-spring contrast fill. (Daneman et al., 2005). The patient underwent 18F-FDG PET-CT for pre-operative staging following a detection of mass lesion in the descending colon on the colonoscopy, which revealed an FDG-avid mass in the descending colon with suspicion of mesenteric lymph node metastasis. Peculiarly in our case, the nature of the leading cause for an intussusception was poorly defined on the corroborated CT images. The sensitivity of CT scans to correctly diagnose intussusception has been reported from 71.4%-87.5% while its specificity in adults has been reported to be 100% as verified by the subsequent surgery (Erkan et al., 2005).Therefore, a long intestinal

tube visualised in the centre of the colon may not be readily distinguished as an interposition of a malignant mass (Gayer et al., 2002).

With the use of FDG PET-CT scanning in this case, the increased FDG activity of the lead mass confirmed the site of the primary tumour origin. The increased FDG avidity could also be attributable to infection of the intussusception, for which inflammatory cells constitute a major portion of increased FDG accumulation in tumour tissue (Chamroonrat et al., 2010). The claw-like FDG avidity seen at the intussusceptum is likely the hallmark of the opposing inflammatory walls of the intussusceptum and the intussuscipiens. These case documented that 18-FDG-PET-CT can be utilised as a tool for detection of intussusception given its superiority in delineating an infective focus and the detection of primary colonic carcinoma (Fathinul et al., 2013).

CONCLUSION

18-FDG-PET-CT features of intussusception in colonic carcinoma have never been described before. It can potentially become a preferred diagnostic tool in delineating a potential tumour mass within the intussusceptions, which will help improve prognosis in patients with malignancy.

REFERENCES

Broomfield, D. (2008). Best evidence topic report. Role of plain abdominal radiograph in the diagnosis of intussusception. *Emergency Medicine Journal, 25,*106-107.

Chien-Chih Y., Sheng-Chuan H., Chih-Pin C., & Yung-Hsi K. (2013). Synchronous triple carcinoma of the colon and rectum. *World Journal of Surgical Oncology, 11,* 66.

Daneman A., & Navarro O. (2004). Intussusception. Part 2: An update on the evolution of management. *Pediatric Radiology, 34*(2), 97-108.

Gayer G., R. Zissin, A. S., Papa M., & Hertz M. (2002). Adult intussusception a CT diagnosis. *British Journal of Radiology, 75*(890)*,* 185-190.

Chamroonrat, W., Cheng, G., Servaes, S., & Zhuang, H. (2010). Intussusception incidentally detected by FDG-PET/CT in a pediatric lymphoma patient. *Annal of Nuclear Medicine, 24*(7), 555-558.

Erkan, N., Haciyanli, M., Yildirim, M., Sayhan, H., Vardar, E., & Polat, A. F. (2005). Intussusception in adults: An unusual and challenging condition for surgeons. *Internal Journal Colorectal Disease 20*(5)*,* 452-456.

Fathinul, F., Nordin, A. J., & Lau, F. W. (2013). 18[F] FDG-PET/CT is a useful molecular marker in evaluating tumour aggressiveness; A revised understanding of an in-vivo FDG PET imaging that alludes the alteration of cancer biology. *Cell Biochemistry and Biophysic, 66*(1), 37-43.

Young, H. K, Michael, A. B., & Mukesh, G. H. (2006). Adult intestinal intussusception: CT appearances and identification of a causative lead point. *Radiographics, 26*(3), 733-44.

Pertanika J. Sci. & Technol. 24 (2): 397 - 401 (2016)

SCIENCE & TECHNOLOGY

Journal homepage: http://www.pertanika.upm.edu.my/

Case Report

Pattern of Calcification on CT and FDG-PET of a Rare Perineural Mantle Cell Lymphoma: A Potential of Non-Histological Imaging Marker

Fathinul Fikri, A. S.[1]*, Ramdave Shakher[2] and Abdul Jalil, N.[1]

[1]*Centre for Diagnostic Nuclear imaging, Universiti Putra Malaysia, 43400 Serdang, Selangor, Malaysia*

[2]*PET centre, Moorabbin Hospital, Monash Health, East Benthleigh, Victoria, Australia*

ABSTRACT

The presence of calcification in a particular FDG-avid soft tissue lesion may at times present uncertainty regarding the clinical course of the disease pathology. Calcific deposits are not specific for either benign or malignant aetiologies (Brant et al., 2010). Altered glucose metabolism with associated calcification may underpin underlying aggressive pathophysiology with necrosis as sequelae. Mantle Cell Lymphoma (MCL) is a subtype of non-Hodgkin's lymphoma. It is a rare B-cell NHL that is prevalent in men over the age of 60. The disease may be aggressive but it can also behave in a more indolent fashion in some patients. MCL comprises about 5% of all NHLs. The disease is called Mantle Cell Lymphoma because the tumour cells originally come from the 'mantle zone' of the lymph node (Zhou et al., 2004). Pretreatment Hodgkin's lymphoma with calcification may masquerade as other second primary pathologies, e.g. extraosseous osteosarcoma or myositis ossificans (Apter et al., 2002; Korek-Amorosa et al., 1974). A calcified perineural lymphoma prior to treatment is exceedingly rare and calcification usually occurs one to five years after chemotherapy or radiation therapy with an incidence of 2% (Apter et al., 2002). This case documents how the manifestation of a rare malignant perineural mantle cell lymphoma may be indistinguishable from other pathological entities based on its pattern of distribution in a combined FDG- PET-CT study.

Keywords: Mantle Cell Lymphoma, PET-CT, FDG, calcification, perineural

Article history:
Received: 14 July 2015
Accepted: 15 September 2015

E-mail addresses:
ahmadsaadff@gmail.com (Fathinul Fikri, A. S.),
sramdave@gmail.com (Ramdave Shakher),
drimaging@yahoo.com (Abdul Jalil, N.)
*Corresponding Author

ISSN: 0128-7680

CASE REPORT

A 71-year-old female, who presented with chronic cough with associated dyspnea and constitutional symptoms, underwent 18F-FDG-PET-CT for investigation of a

suspicious pulmonary nodule found on a CT scan. Her symptoms persisted in spite of antibiotic treatment. On examination, she looked pale and had pulmonary rhonci on auscultation. Biochemical results were unremarkable. FDG-PET-CT revealed numerous FDG-avid pulmonary nodules, FDG-avid nodal disease above and below the diaphragm and extra-nodal disease in the left thigh soft tissue with suspicion of stage IV lymphoma (Figure 1). The left thigh FDG avidity (standardised uptake value: SUV of 14.5) was associated with dystrophic peripheral rim calcification (Figure 2). Biopsy of the lymph node and the left thigh lesion confirmed a diagnosis of Mantle Cell Lymphoma (MCL)

Peripheral rim calcification of an FDG-avid lesion in a florid lymphomatous disease may masquerade as other concomitant second pathologies e.g. extraosseous sarcoma or a benign lesion e.g. myositis ossificans. There are two types of CT pattern of calcification: dystrophic and metastatic. Typically, in an aggressive tumour, associated dystrophic calcification commonly results from necrosis in an unchecked altered cellular glucose metabolism (Apter et al., 2002). Such infarction typically occurs in histologically aggressive lymphoma e.g. Mantle Cell (Korek-Amorosa et al., 1974; Ishikawa et al., 1999). This is likely to represent a dystrophic process when bulky tumours outgrow their blood supply. In this case, the untreated lymphomatous deposit in the perineural region featuring as peripheral rim calcification indicated the likelihood of a malignant feature on the CT scan (Henry, 2012). On the one hand, the dystrophic calcific deposition in MCL is peculiar to its aggressive nature as opposed to the now common calcification in post-treatment lymphoma. On the other hand, the basis of metastatic calcification manifested by a raised serum calcium level is not demonstrated in this patient (Apter et al., 2002).

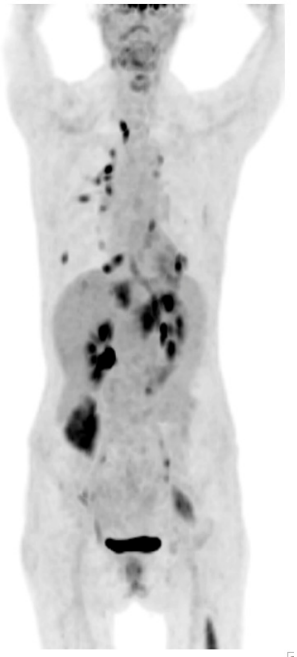

Figure 1. Multiple image projection (MIP) PET image showing numerous FDG-avid nodal diseases above and below diaphragm with an extranodal avid disease in the left mid-thigh.

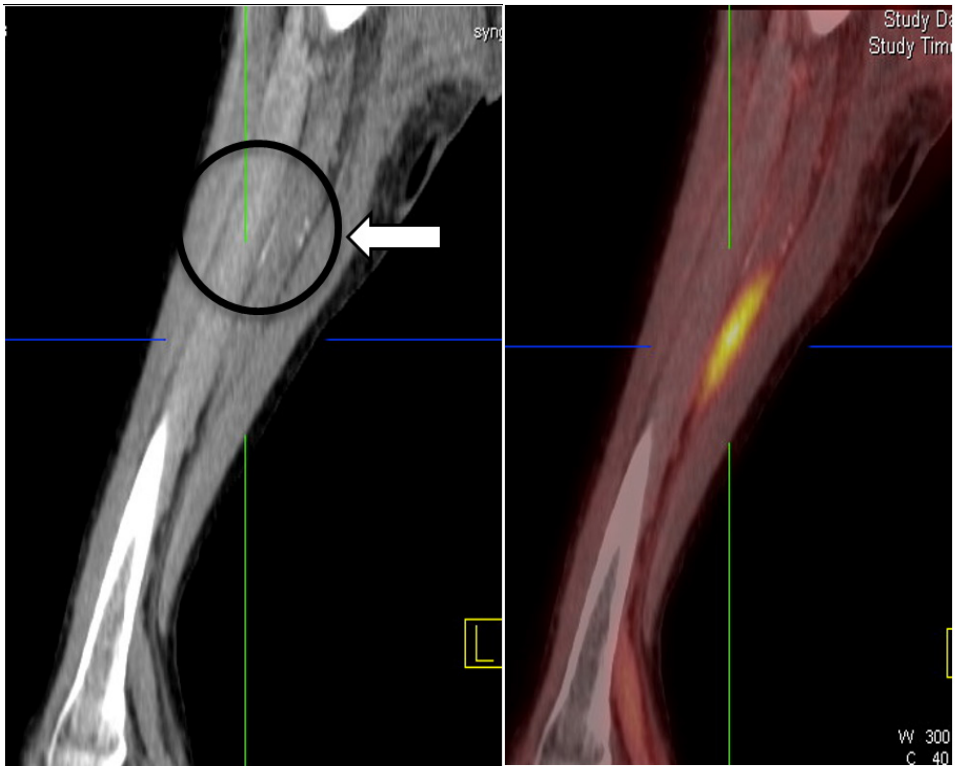

Figure 2. Coronal non-contrasted CT and coronal fused PET-CT images showing an elongated FDG-avid mid-thigh soft tissue lesion (SUVmax: 14.5; value>2.5 is significant) with adjoining dystrophic peripheral rim calcification (arrowed).

The dystrophic rim calcification shown on the CT scan with FDG avidity has been described in myositis ossificans, with a potential resemblance to the features shown in this case. The calcification is the result of mineralisation of the mature lamellar bone, which occurs after 4 to 6 weeks of trauma (Brant et al., 2010). Nevertheless, by virtue of the previous surgical history of non-traumatic bodily harm, potential second pathology of myositis ossificans was unlikely.

Extraskeletal osteosarcoma on the combined FDG PET-CT may also resemble the pattern of disease in this case. It is a rare malignant neoplasm that produces osteoid or unmineralised bone in soft tissues without an attachment to bone or periosteum (McAuley et al., 2012). Clinically, this patient denied any history of an enlarging soft tissue mass, which is not always accompanied by pain.

The dystrophic peripheral rim calcification of a soft tissue lesion on the FDG-PET-CT is otherwise non-specific for MCL with an aggressive malignant tendency resulting from the necrosis. The index of suspicion of MCL is rendered high when dystrophic calcification is seen with the adjoining FDG-avid masses along the nodal chain. Other diagnostic methods include CT and fine needle biopsy with a sensitivity of 37% and 63-100%, respectively (Dong et al., 2001). Multiparametric MRI exploiting diffusion-weighted sequences have been shown to improve lesion detection by 47% compared to conventional MRI sequences, which renders differentiation of benign from malignant pathology an adjunct to the FDG-PET-CT (Gu Ji

et al., 2011; McAuley et al., 2012). The cytologic features of MCL have yet to be directly correlated with the FDG-PET-CT in the altered glucose metabolism, for which the latter would potentially serve as a non-invasive imaging marker for the suspicion of the diagnosis (Fathinul et al., 2014). More correlative studies of this cell line is needed to ascertain the significant correlative pathological imaging features. Magnetic Resonance Imaging (MRI)/ PET would also be important to further associate the soft tissue characterisation adjunct to the CT (Nagata, 2005).

CONCLUSION

The recognition of the disease distribution pattern on the combined 18-FDG-PET-CT is potentially important in suspecting the likelihood of an underlying disease when a typical calcific pattern of pathology is indeterminate. This could potentially become a non-histological imaging marker for the rare perineural Mantle Cell Lymphoma.

REFERENCES

Apter, S., Avigdor, A., Gayer, G., Portnoy, O., Zissin, R., & Hertz, M. (2002). Calcification in lymphoma occurring before therapy: CT features and clinical correlation. *American Journal of Roentgenology, 178*(4), 935-938.

Brant, W., & Helms, C. (2010). Skeletal "don't touch" lesions. *Fundamentals of Diagnostic Radiology* (4th ed.). p. 1078. Philadelphia: Lipppincott Williams & Wilkins.

Dong, H. Y., Harris, N. L., Preffer, F. I., & Pitman, M. B. (2001). Fine-needle aspiration biopsy in the diagnosis and classification of primary and recurrent lymphoma: a retrospective analysis of the utility of cytomorphology and flow cytometry. *Modern Pathology, 14*(5), 472-481.

Fathinul Fikri, Nordin, A. J., & Lau, E. F. (2014). 18[F] FDG-PET/CT is a useful molecular marker in evaluating tumour aggressiveness: A revised understanding of an in-vivo FDGPET imaging that alludes the alteration of cancer biology. *Cell Biochemistry and Biophysic, 55*(5), 631-640.

Gu, J., Chan, T., Zhang, J., Leung, A. Y., Kwong, Y. L., & Khong, P. L. (2011). Whole-body diffusion-weighted imaging: the added value to whole-body MRI at initial diagnosis of lymphoma. *American Journal of Roentgenology, 197*(3), W384-W391.

Henry, G., Camila, M., & Andrei, I. (2012). Demonstration of peripheral nerve root involvement by non-Hodgkin's lymphoma on 18F-FDG PET/CT. *European Journal of Nuclear Medicine and Molecular Imaging, 39*(4), 729-730.

Hutchings, M., Loft, A., Hansen, M., Pedersen, L. M., Berthelsen, A. K., Keiding, S., ... & Specht, L. (2006). Position emission tomography with or without computed tomography in the primary staging of Hodgkin's lymphoma. *Haematologica, 91*(4), 482-489.

Ishikawa, T., Kobayashi, Y., Omoto, A., Adachi, Y., Nakagawa, S., Kaneko, T., ... & Kondo, M. (1999). Calcification in untreated non-Hodgkin's lymphoma of the jejunum. *Acta haematologica, 102*(4), 185-189.

Korek-Amorosa, J., Scheinman, H. Z., Clemett, A. R., Amorosa, L. F., & McKenna, P. J. (1974). Hypercalcaemia and extensive lymph-node calcification in a patient with Hodgkin's disease prior to therapy. *The British Journal of Radiology, 47*(564), 905-907.

Mc Auley, G., Jagannathan, J., O'Regan, K., Krajewski, K. M., Hornick, J. L., Butrynski, J., & Ramaiya, N. (2012). Extraskeletal osteosarcoma: spectrum of imaging findings. *American Journal of Roentgenology, 198*(1), W31-W37.

Nagata, S., Nishimura, H., Uchida, M., & Hayabuchi, N. (2005). Usefulness of diffusion-weighted MRI in differentiating benign from malignant musculoskeletal tumors. *Nihon Igaku Hoshasen Gakkai zasshi. Nippon Acta Radiologica, 65*(1), 30-36.

Zhou, Y., Wang, H., Fang, W., Romaguer, J. E., Zhang, Y., Delasalle, K. B., ... & Wang, M. (2008). Incidence trends of mantle cell lymphoma in the United States between 1992 and 2004. *Cancer, 113*(4), 791-798.

Pertanika J. Sci. & Technol. 24 (2): 403 - 410 (2016)

PERTANIKA JOURNALS

SCIENCE & TECHNOLOGY

Journal homepage: http://www.pertanika.upm.edu.my/

A Combined Meshless RBF-FDTD Method for the Analysis of Transient Electromagnetic Fields

Khalef, R.[1]*, Benkhawa, L.[2], Grine, F.[2], Benhabiles, M. T.[2] and Riabi, M. L.[2]

[1]Doctoral School of Technology and Space Applications, Faculty of Technology Sciences, Department of Electronic, Laboratory of Electromagnetism and Telecommunications, University of Constantine1, Algeria, Road Ain El Bay, 25000, Constantine, Algeria

[2]Faculty of Technology Sciences, Department of Electronic, Laboratory of Electromagnetism and Telecommunications, University of Constantine1, Algeria, Road Ain El Bay, 25000, Constantine, Algeria

ABSTRACT

A Meshless Time Domain Method is used in the local support domain to solve Maxwell's equations for one-dimensional transient electromagnetic problems. The approach is based on a combination of the Meshless Radial Basis Functions and the Leapfrog time-stepping scheme for the Finite-Difference approximation of the first order partial derivatives. A comparison is performed between the conventional FDTD and RBF's with Gaussian, Wendland-C4 Compactly Supported RBF (CSRBF) and Inverse Multi-Quadric (IMQ) basis functions. The numerical results showed that the proposed method provides an accurate solution for transient electromagnetic problems.

Keywords: Finite-Difference-Time-Domain, Local Support, Meshless method, Compact support RBF, Inverse Multi-Quadric, Transient Electromagnetic Field

INTRODUCTION

During the last decade, several methods have been proposed to solve Maxwell equations in complex radiating structures, without the use of finite element meshes. Such Meshless approaches distinguish four main methods based on a Galerkin variational formulation:

- √ The Moving Least-Squares approximations, which regroup fundamentally the Diffuse Element Method DEM, and the Element Free Galerkin Method EFGM (Cingoski et al., 1998).

Article history:
Received: 17 February 2016
Accepted: 22 April 2016

E-mail addresses:
kh.rostom@gmail.com (Khalef, R.),
benkhaouadj@yahoo.fr (Benkhawa, L.),
faroukgrine@umc.edu.dz (Grine, F.),
mt.benhabiles@umc.edu.dz (Benhabiles, M. T.),
ml.riabi@yahoo.fr (Riabi, M. L.)
*Corresponding Author

ISSN: 0128-7680

√ The Reproducing Kernel Method RKM, or Smooth Particle Hydrodynamics (Belytschko et al., 1996).

√ Methods constructed from a purely polynomial interpolation, Point Interpolation Method PIM (Liu & Gu, 1999), (Lima et al., 2012).

√ Mixed methods coupling radial basis functions, either with a moving least square approximation (Kansa, 1990; Kansa, 1992; Fasshauer , 2007; Liu & Gu, 2005), or with a polynomial interpolation (Viana et al., 2006; Wang & Liu, 2001; Wendland, 1995).

The purpose of this paper is to apply the explicit Meshless RBF (Radial Basis Function) method, with three types of local support of basis functions, namely Gaussian, Wendland – C4 CSRBF and IMQ, to solve time domain Maxwell equations in one dimension. The rationale for this project is to check the stability problems related with last basis functions in local support domain and to provide the best solutions for the analysis of transient electromagnetic problems. Additionally, the RBF method is very economical in terms of computation time and programming burden in comparison with the conventional Finite-Difference Time-Domain (FDTD) method. The present research also attempts to shed light on the errors of the FDTD method.

The present project is structured as follows. The first section provides a brief overview of the RBF method with a description of the shape function with its derivative; the local support domain will be presented in the same section. Section three is equated to the time domain equations for the electromagnetic field in one dimension and the criterion of stability condition of time. Section four discusses the use of 1-D electromagnetic case to estimate the accuracy and efficiency of the proposed method by comparing the results of the proposed method with that of the FDTD, and the RBF with global support basis function at (Lai et al., 2008) with regard to the PEC boundary conditions and time-exponential current excitation. The last section presents a general conclusion about the results of the present study.

THE MESHLESS METHOD BASED ON RBF

The RBF approximation function $\boldsymbol{u^h(x)}$ can be expressed as follows:

$$\boldsymbol{u^h(x) = \sum_{I=1}^{N} \varphi_I(x).\, a_I \ , \ \forall\, x \ \in R^d} \qquad [1]$$

where $\boldsymbol{\varphi_I(x) = \varphi(\|x - x_I\|)}$ is the radial basis function centred at the collocation nodes $x_1, x_2, \ldots,$ $x_N \in \boldsymbol{R^d}$, $\boldsymbol{a_I}$ are unknown coefficients to be computed and represents the Euclidean distance between test points x and node points x_I.

In order to determine the coefficients $\boldsymbol{a_I}$ we force the interpolation to pass through all the N collocation points, resulting in

$$\boldsymbol{u^h(x) = \varphi^T A^{-1} u_e = N(x) u_e} \qquad [2]$$

where $\boldsymbol{u_e = [u(x_1), u(x_2), \ldots, u(x_N)]^T}$,

$$\boldsymbol{A} = \begin{bmatrix} \boldsymbol{\varphi_1(x_1)} & \boldsymbol{\varphi_2(x_1)} & \dots & \boldsymbol{\varphi_N(x_1)} \\ \boldsymbol{\varphi_1(x_2)} & \boldsymbol{\varphi_2(x_2)} & \dots & \boldsymbol{\varphi_N(x_2)} \\ \vdots & \vdots & \ddots & \vdots \\ \boldsymbol{\varphi_1(x_N)} & \boldsymbol{\varphi_2(x_N)} & \cdots & \boldsymbol{\varphi_N(x_N)} \end{bmatrix}_{\boldsymbol{NxN}} \quad [3]$$

and $\boldsymbol{N(x)} = [\boldsymbol{N_1}, \dots, \boldsymbol{N_J}, \dots, \boldsymbol{N_N}]$is the matrix of shape function, that is to satisfy the delta function property. The vector $\boldsymbol{u_e}$ holds the field values at *N* node locations in the surrounding domain of influence around *x*.

Figure 1 represents the local support domain.

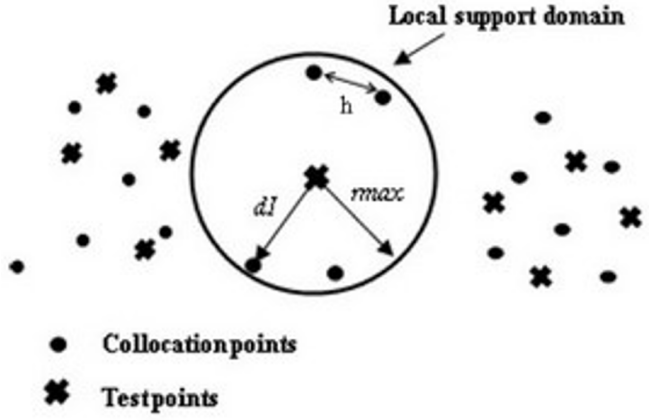

Figure 1. Schematic Illustration of the Local Support Domain with Radius $r_{max,}$ Average Node Distance *h* and Distance d_I between Collocation Points and Test Points

In this work, the formula $\boldsymbol{u^h(x)}$can be any component of the electric and magnetic fields, the spatial derivatives of electric and magnetic fields needed to solve Maxwell's equations. The partial derivative of $\boldsymbol{u^h(x)}$ is only related to shape function matrix. Where, the first – order derivative of this function in *x* direction can be expressed as (Lai et al., 2008):

$$\frac{\boldsymbol{\partial u^h(x)}}{\boldsymbol{\partial x}} = \frac{\boldsymbol{\partial N(x)}}{\boldsymbol{\partial x}} \quad [4]$$

where

$$\frac{\partial N(x)}{\partial x} = \left[\frac{\partial \varphi_1(x)}{\partial x}, \frac{\partial \varphi_2(x)}{\partial x}, \dots, \frac{\partial \varphi_N(x)}{\partial x}\right] \quad [5]$$

THE TIME DOMAIN FIELD FORMULATION IN ONE DIMENSION

The one-dimensional transient electromagnetic problem in a homogenous isotropic medium is tackled as a *TEM* wave. According to Cartesian coordinates, the wave is polarised along the y direction, and it propagates along the *x* direction. Consequently, the problem is independent of the z variable, and Maxwell's set reduces to only two equations where the time derivatives in RBF meshless method can be approximated by central differences in leapfrog time stepping

scheme similar to FDTD method. The resulting explicit discretisation formulation of those equations can be derived by the following equations (Kaufmann et al., 2012):

$$H_{z,i}^{n+\frac{1}{2}} = H_{z,i}^{n-\frac{1}{2}} - \frac{\Delta t}{\mu}\left[\sum_{j=1}^{nAs} \partial x \; N_{E,i}^{j} \; E_{y,j}^{n}\right] \quad [6]$$

$$E_{y,i}^{n+1} = E_{y,i}^{n} - \frac{\Delta t}{\varepsilon}\left[\sum_{j=1}^{nAs} \partial x \; N_{H,i}^{j} \; H_{z,j}^{n+\frac{1}{2}} + J_{y}^{n+\frac{1}{2}}\right] \quad [7]$$

where *i* is the current node locations, *n* is the time step and *j* the index in local support domain in Figure 1. An acceptable time-step Δt for the stability of leapfrog scheme is derived from the Neumann condition as $\Delta t \leq d_{\min i}\sqrt{\mu\varepsilon}$, where $d_{min,i}$ is the shortest distance between any two collocations points in the domain (Shaterian et al., 2012).

NUMERICAL EXAMPLE

In order to confirm the proposed method, comparison of simulation results was carried out between the Meshless RBF with three types of basis function (Gaussian, Wendland-C4 CSRBF, IMQ) and the FDTD on a 1-D perfect electric conductor. The tangential electric field component must be zero at the boundary collocation points with each time-step update (Lai et al., 2008):

In Figure 2, the distribution of collocation points and test points is uniform. We suppose that N_x is the number of collocation points and that n_x is the test points whereas, *h* is the distance between two successive collocation points.

The computation region is one-metre long, the current excitation point is at J_P *(x = 0.35m)* and the measurement point is at *obs1(x = 0.85m)* (Lai et al., 2008).

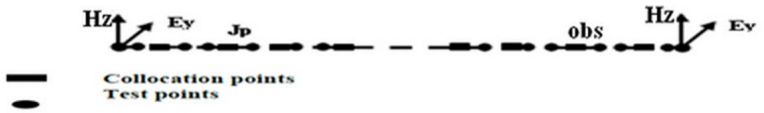

Figure 2. Distribution of collocation and test points in one dimension

The excitation source is a Gaussian pulse. Accordingly; we used three kinds of basis functions with a local support domain, namely Gaussian, Wendland-C4 CSRBF, and IMQ.

The Gaussian pulse of excitation is expressed by:

$$J_y(t) = exp\left[-(\frac{t-t_0}{T})^2\right] \quad (\text{A/m}^2) \quad [8]$$

where: t_0=3x10^{-9} (s), T=0.5x10^{-9} (s)

In the present study, the following three types of radial basis functions (Gaussian, Wendlend-C4 CSRBF and IMQ) are expressed by:

$$\varphi_I(x) = \exp\left(-s.r_I^2\right) \quad [9]$$

$$\varphi_I(x) = \left[1 - \left(\frac{r_I}{\delta}\right)\right]^6 \left[3 + 18\left(\frac{r_I}{\delta}\right) + 35\left(\frac{r_I}{\delta}\right)^2\right] \quad [10]$$

$$\varphi_I(x) = \frac{1}{\sqrt{1+(e.r_I)^2}} \qquad [11]$$

where s, δ and e are the shape parameters of the above basis functions successively.

And $r_I = \frac{d_I}{r_{max}}$, where r_{max} represents the local support domain radius at collocations points x_I, $d_I = \|x_I - x\|$ is the distance between the test points and the collocations points.

Based on the analysis in this section, it can be inferred that the number of collocation points N_x represents the number of electric field *E*-points, and the number of test points n_x represents the number of magnetic field *H*-points. In the electromagnetic computation, the shape parameters *s* in the Gaussian function, δ in the Wendland-C4 function and *e* in the IMQ function, have to be adjusted carefully in order to achieve a sum of shape functions equal to unity and subsequently to ensure the stability of the computational scheme. In the following, we will choose their parameters to obtain the best results.

RESULTS AND DISCUSSION

The input data used for the computation of the plots presented in Figures 3-5are N_x=101, n_x=100, *rmax= 1.1.h.* Figure 3 shows a comparison of the results for the E_y component in the observation point *obs1* for the effective odd oscillations 20 periods in PEC boundary condition between:

1. Three different types of local support basis functions, Gaussian, Wendland-C4 CSRBF, and IMQ, for which we obtained identical results.
2. For RBF method and the traditional FDTD method, we had obtained the same results.
3. The same as the previously obtained result from RBF-FDTD method with the data from (Lai et al., 2008), Figure 3-5-a and we found them similar, although the radial basis function from (Lai et al., 2008), is of global support, and the number of collocation and test points differs (Lai et al., 2008).

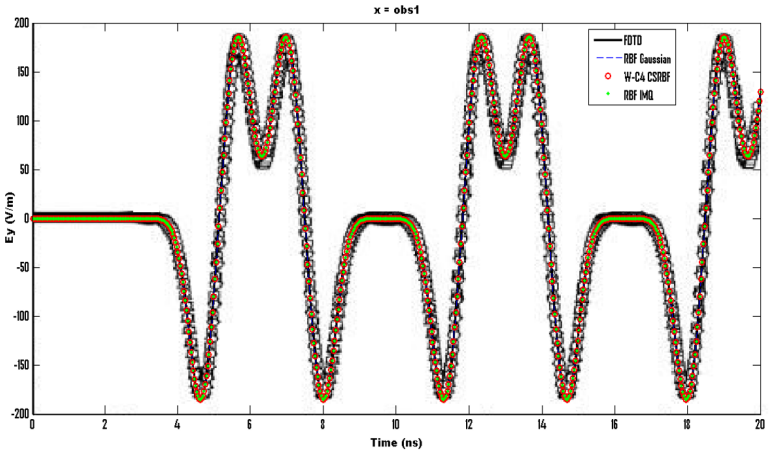

Figure 3. E_y at observation point obs1 using PEC boundary condition

Figure 4 shows that on one hand, a comparison of the spatial profiles of propagation computed respectively to RBF method at three types of local support with each and on the other hand, the same results of RBF method with the FDTD method at t=10ns, t=15ns and t=20ns where identical results were obtained.

In order to show consistency in the computing scheme for long term time arguments as well as for both the RBF Method and the FDTD, the spatial distribution of E_y are plotted in Figure 5 at *t*= 150 ns, where the comparison showed identical results. The results obtained by RBF-FDTD was compared with the results shown in Figure 6 from Lai et al. (2008) are identical.

Through this comparison, the choice of the type of support and the number of points do not affect completely the results obtained.

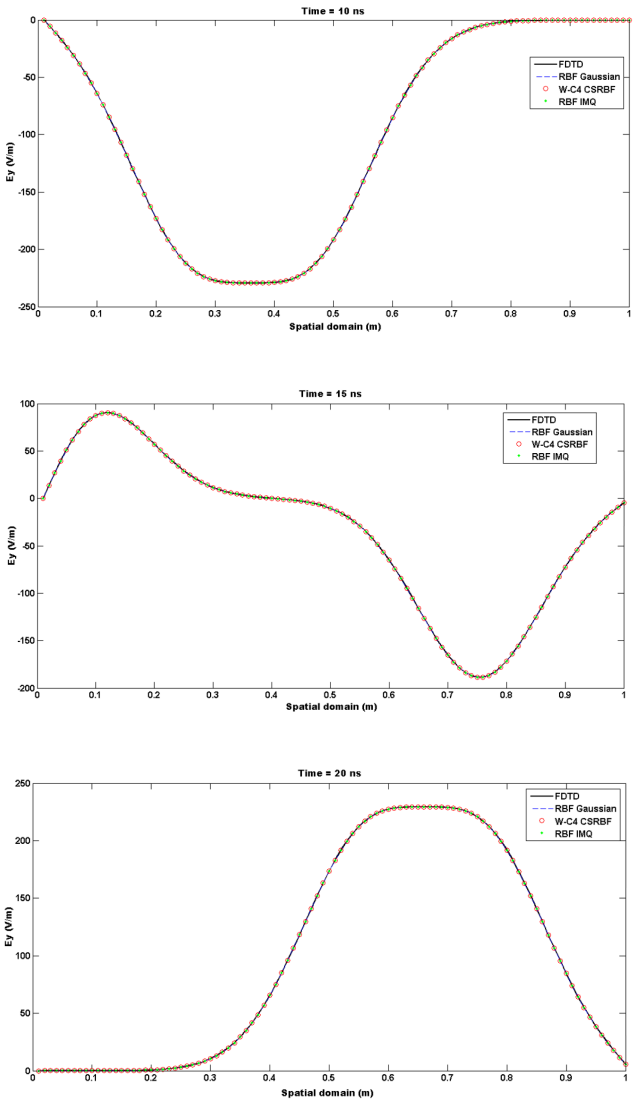

Figure 4. Evolution of E_y spatial profiles for FDTD and RBF method at t=10 ns (a), t=15ns (b) and t=20 ns (c), using PEC boundary condition.

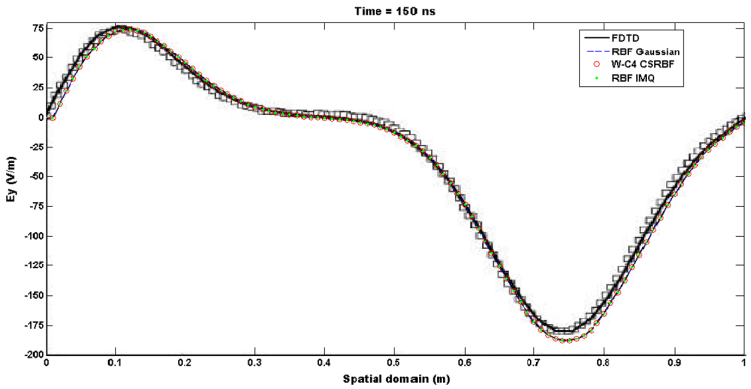

Figure 5. E_y spatial profiles given by RBF- FDTD method at t= 150ns, using PEC boundary condition.

CONCLUSION

In this research, a comparison was performed between the conventional FDTD and RBF methods with radial basis functions. The numerical results showed that the numerical stability of the proposed method is related to the radius of a local support domain and the shape parameters of basis functions. Yet, the construction of the shape function matrix in local RBF method is more complex than that of the global RBF method. Moreover, the use of locally Gaussian and CSRBF basis function is more complex than that of the IMQ; otherwise, the previous basis functions have a problem of stability . In order to eliminate the instability programming process of the above two basis functions, each node in the local support must have its own suitable parameter. It was found that the use of RBF method is very economical in terms of computation time and programming burden.

REFERENCES

Belytschko, T., Krongauz, Y., Organ, D., Fleming, M., & Krysl, P. (1996). Meshless methods: an overview and recent developments. *Computer Methods in Applied Mechanics and Engineering, 139*(1), 3-47.

Cingoski, V., Miyamoto, N., & Yamashita, H. (1998). Element-free Galerkin method for electromagnetic field computations. *Magnetics, IEEE Transactions on, 34*(5), 3236-3239..

Fasshauer, G. E. (2007). *Meshfree approximation methods with MATLAB (Vol. 6)*. World Scientific Co Pte.Ltd.

Kansa, E. J. (1990). Multiquadrics—A scattered data approximation scheme with applications to computational fluid-dynamics—II solutions to parabolic, hyperbolic and elliptic partial differential equations. *Computers and Mathematics with Applications, 19*(8), 147-161.

Kaufmann, T., Yu, Y., Engström, C., Chen, Z., & Fumeaux, C. (2012). Recent developments of the meshless radial point interpolation method for time-domain electromagnetics. *International Journal of Numerical Modelling: Electronic Networks, Devices and Fields, 25*(5-6), 468-489.

Lai, S. J., Wang, B. Z., & Duan, Y. (2008). Meshless radial basis function method for transient electromagnetic computations. *Magnetics, IEEE Transactions on, 44*(10), 2288-2295.

Lima, N. Z., Fonseca, A. R., & Mesquita, R. C. (2012). Application of local point interpolation method to electromagnetic problems with material discontinuities using a new visibility criterion. *IEEE Transactions on Magnetics, 48*(2), 615.

Liu, G. R., & Gu, Y. T. (1999) *A point Interpolation Method*. In the proceeding of 4th Asia-pacific Conference on Computational Mechanics. pp. 1009- 1014.

Liu, G. R., & Gu, Y. T. (2005). An Introduction to Meshfree Methods and their Programming. *Springer;* Dortrecht, The Netherlands.

Shaterian, Z., Kaufmann, T., Fumeaux, C. (2012). *Impact of different Node Distributions on Meshless Radial Point Interpolation Method in Time-Domain Electromagnetic Simulations*. Proceeding of APMC, Taiwan.

Viana, S. A., Rodger, D., & Lai, H. C. (2006). Application of the local radial point interpolation method to solve eddy-current problems. *IEEE transactions on magnetics, 42*(4), 591-594.

Wang, J. G., & Liu, G. R. (2002). A point interpolation meshless method based on radial basis functions. *International Journal for Numerical Methods in Engineering, 54*(11), 1623-1648.

Wendland, H. (1995). Piecewise polynomial, positive definite and compactly supported radial functions of minimal degree. *Advances in computational Mathematics, 4*(1), 389-396.

Pertanika J. Sci. & Technol. 24 (2): 411 - 422 (2016)

SCIENCE & TECHNOLOGY

Journal homepage: http://www.pertanika.upm.edu.my/

High Capacity Video Steganography Technique in Transform Domain

Hemalatha, S.*, U. Dinesh Acharya and Renuka, A.

Department of Computer Science and Engineering, Manipal Institute of Technology, Manipal University, Manipal - 576104, India

ABSTRACT

Steganography is one of the techniques used for secure transmission of secret information. The secret information is concealed in a carrier and transmitted. Video steganography uses video signals to hide the secret information. The objective of this paper is to hide large volumes of secret data in video files. In the proposed technique, AVI video files are used as the carrier. Video files containing audio are split to get video and audio frames. Video frames are like still images and so, can be used for image steganography. When audio is extracted from the video, it is like an audio file and it can also be used for steganography. This leads to the high capacity steganography, since both video and audio frames are used as the carrier. When a small video clip is read, thousands of video and audio frames will also become available. The secret data can be image, audio or text. In this proposed work, secret image and audio signals are hidden in the video file.

Keywords: Capacity, Integer Wavelet Transform, Peak Signal to Noise Ratio, Structural Similarity Index Metric, Video Quality Metric (VQM), Video steganography

INTRODUCTION

Steganography is the science of secret communication. The secret information to be communicated is hidden in another carrier and transmitted. In video steganography a video clip can be a carrier. A video stream consists of many images and audio frames. All these frames can be used to hide the secret information, so, any image and/or audio steganography techniques can be used with video steganography too. Video steganography gives flexibility of selective frame steganography to increase the security of the system or it can use the whole video for hiding huge amounts of data so that the hiding capacity is much higher in the case of video. Compressed video formats

Article history:
Received: 17 February 2016
Accepted: 22 April 2016

E-mail addresses:
hema.shama@manipal.edu (Hemalatha, S.),
dinesh.acharya@manipal.edu (U. Dinesh Acharya),
renuka.prabhu@manipal.edu (Renuka, A.)
*Corresponding Author

ISSN: 0128-7680

however, are challenging because during compression the hidden information may be lost. The most commonly used codec for video is H.264/AVC. The underlying coding structure can be modified to hide data but in this case, only a small amount of data can be hidden securely. Other possible ways of data hiding in video are hiding in motion vectors or macro blocks (Sadek et al., 2014; Tew & KokSheik, 2014).

Compared with image steganography, video steganography is harder to be tested by the attacker because random frames or audio tracks can be selected for the hiding process and for the attacker it is difficult to guess the sequence of frames or audio tracks. There are many attacks for videos such as lossy compression, change of frame rate, frames interchanging and addition or deletion of frames during video processing among others. The challenge in video steganography is to make the steganography technique resistant to these attacks.

Three important characteristics of steganography are invisibility or imperceptibility, robustness and security. Invisibility or imperceptibility is the ability to be unseen by human eye. Robustness is the aptitude of the steganography to resist operations such as filtering, cropping, rotation, and compression. If the hidden information is not detected by third party, then the system is said to be secure. Even if it is suspected, it should be impossible to detect the hidden information by the third party.

Capacity is another important factor to be considered in steganography. It is the amount of information that can be hidden relative to the size of the cover object without reducing the quality of the cover object. Usually, it is specified as the number of bits per bytes or kilobytes. The more information the cover can carry the better it is. Large embedded information however, degrades the quality of the steganography (referred to as stego henceforth) significantly. This means that when capacity is increased, the security decreases and vice versa

Steganography can be in spatial domain or in transform domain. In spatial domain techniques, actual sample values are modified to hide the secret information. These techniques are less resistant to signal processing operations. In transform domain, the actual sample values are transformed to some other domain like frequency domain or time-frequency domain. The transformed coefficients are then modified to hide the secret information. Transform domain techniques are robust against signal processing operations (Sadek et al., 2014).

In this paper, a transform domain video steganography technique is proposed. Integer Wavelet Transform (IWT) is used to transform the video and audio frames into time-frequency domain. The IWT is a type of wavelet transform which maps integer to integers and can be used to transform digital signals.

MATERIALS AND METHODS

A study (Su et al., 2013) proposed high volume of data embedding in compressed video files in H.264/AVC format. The process is too complex and it achieved only 10% of the capacity of the video file size. Since in this process the size of the stego file increases, it is prone to suspicions about hidden data. Some researchers (Gujjunoori & Amberker, 2013) have proposed a data embedding technique for MPEG-4 video using HVS characteristics in DCT domain to improve the capacity while maintaining good visual quality. Tamer Shanableh (2014) proposed two approaches. The message bits are hidden using modulation of the quantisation scale of a

constant bitrate video in the first approach. A payload of one message bit per macro-block is achieved. In the second approach, a second order multivariate regression is used. The regression model is then used by the decoder to predict the values of the hidden message bits. This also did not improve the capacity.

A few researchers (Xu et al., 2014) have attempted to hide data in the encrypted H.264/AVC video, but it will not increase the security level of data hidden. A study (Yao et al., 2014) proposed a motion vector based steganography by defining embedding distortion. But it increased the bit rate which is not appreciated in steganography. Other researchers (Gaj et al., 2015), proposed a watermarking technique for H.264/AVC video which resists rotation, scaling and translation attacks by embedding the watermark in the moving objects of the video. Quality of a video is measured using many metrics. Peak Signal to Noise Ratio is the most widely used metric. Pinson and Wolf (2004, 2011) discovered a new standardised method for objectively measuring video quality, namely Video Quality Metric or VQM. Winkler and Wang, 2009) and Tew & KokSheik (2014) also suggested that VQM is one of the best metrics to measure the video quality.

All the above compressed video steganography papers did not achieve good payload capacity. Compared with the size of the video, the capacity was too low. The capacity can be improved if the information is hidden in many frames. But selection of frames which can resist compression is the challenge. The proposed method is explained below.

Video files containing audio are split to get video and audio frames. Video frames are like still images and so can be used for image steganography. When audio is extracted from the video it is like an audio file and it can also be used for steganography. When a small video clip is read, thousands of video and audio frames become available. All these frames can be used for steganography. The stego video file however, cannot resist compression, even though the other attacks such as RST attack, addition and deletion of frames can be handled efficiently. When the RST attack is applied, the secret data is not lost since it is applied to the entire frame. To handle frame deletion or addition, random frames are selected as per random number generator and secret information is hidden in duplicates. Pseudo Random Number Generator (PRNG) principle is used to select the frames. Only the seed has to be exchanged between sender and receiver. The first two prime factors of the seed are discovered. Sum of these two prime factors gives the first frame number where the secret data is hidden; then for the next two continuous frames, same secret data are hidden. This procedure is repeated three times in the frames at an offset of sum of the prime factors. For example, if 10 is the seed then 2 and 5 are its first two prime factors. Their sum is 7. Secret data is hidden in the continuous frames 7, 8 and 9. Then in the frames 16, 17 and18 (because 9+7=16) and in frames 25, 26 and 27 (because 18+7=25) same data are hidden. At the receiver, data is extracted from all these frames and checked for majority similarity. There is no chance of losing all such frames. Thus, any addition or deletion of frames can be handled.

The audio frame size is small and the first frame always contains silent period. Hence, except for the first frame, all other frames are combined to hide secret audio. The secret audio is hidden in duplicate to resist frame loss.

Secret information is hidden in the video frames using Integer Wavelet Transform (IWT). The IWT decomposes the image into four sub bands LL, LH, HL and HH. The low frequency

LL sub band contains the most significant features and the high frequency sub bands contain less significant features. Thus, if the secret information is an image, only LL sub band will be hidden and during extraction, the secret image is constructed using only LL sub band. When IWT is applied to audio signals, it is converted into approximate or low frequency components and detail or high frequency components. Detail components are not significant. So to hide secret audio in audio frames, only approximate components are hidden and it is possible to reconstruct the secret audio using only approximate components.

Experimentation is done in MATLAB 8.2. The embedding and extracting procedures are explained in the following sections. The MATLAB functions used in this proposal are listed in the Appendix.

Embedding Procedure:

Input:

- Cover video *C.avi*
- Secret images *S1.jpg and S2.jpg.*
- Secret audio *S3.wav.*

Output: Stego video, *G.avi.*

Method:

1. Read cover video *C.avi* and get video and audio frames. Store audio frames in '*a*' and video frames in '*im*'.
2. Get the frame numbers as per the PRNG and hide the secret image in duplicates. Separate out Red Green and Blue components from the selected frames. Two secret images are hidden in one frame: one in Blue component and the other in Green component. Hiding procedure in the frame is explained in the following steps.
3. Obtain IWT of Blue and Green components to get four sub bands in each as BLL, BHL, BLH and BHH, GLL, GHL, GLH and GHH.
4. Obtain IWT of the secret images *S1* and *S2* to get four sub bands of each as sLL1, sHL1, sLH1 and sHH1, sLL2, sHL2, sLH2 and sHH2.
5. Hide the low frequency sub band of the secret image *S1* by replacing the coefficients in BHH band. Also, hide the number of coefficients hidden.

   for i=1 to size(sLL1) ***do***

   begin

   BHH(i) = sLL1(i)

   end.
6. Hide the low frequency sub band of the secret image *S2* by replacing the coefficients in GHH band along with the number of coefficients hidden.

   for i=1 to size(sLL2) ***do***

begin

GHH(i) = sLL2(i)

end.

7. Obtain the inverse IWT to get Blue and Green components
8. Integrate the R, G and B components into a single image frame
9. Add the frame to the video in the correct location.

The secret audio is hidden as follows:

10. Except for the first frame, all other audio frames are combined.
11. Obtain IWT of the combined audio frames and secret audio *S3* to get approximation (CA) and detail coefficients (CD).
12. Obtain the binary of approximation coefficients of the secret audio and duplicate the bits 3 times.
13. Hide the duplicated secret bits in the 3^{rd}, 4^{th} and 5^{th} bit planes of the detailed coefficients of the cover.
14. Obtain the inverse IWT of the cover to get the stego audio samples and then convert into frames. Add the frames to the audio in the correct location.
15. Store the video and audio frames in the AVI format in the uncompressed form to get stego video *G.avi*.

Extracting Procedure:

Input: Stego video *G.avi*

Output:

- Secret images *S1.jpg.* and *S2.jpg*.
- Secret audio *S3.wav*.

Method:

1. Get the frame numbers as per the PRNG and extract the required video and audio frames from the stego video. The hidden secret images are extracted as follows:
2. Decompose the extracted video frames into Blue and Green components.
3. Obtain IWT of Blue and Green components and get the secret image sizes.
4. Extract the low frequency sub bands of the secret images hidden in the high frequency sub bands of Blue and Green components of all the selected frames. The size of the low frequency sub band is one fourth of the secret image size since 'haar' transform is used.

for i=1 to (secret size)/4

begin

newSLL1(i) = gHH1(i)

newSLL2(i) = gHH2(i)

end// gHH1 and gHH2 are the HH sub band of the Blue and Green components of the stego frame respectively. The size of the two secret images are taken as same.

5. For the extracted low frequency sub bands of the secret images, obtain the inverse IWT by considering zeroes as high frequency components to get secret images
6. Extract all the duplicates of the secret images similarly. The corresponding secret images must be compared for majority similarity and that will be selected as the secret image. Thus obtain the secret images *S1* and *S2*.

The secret audio is extracted as follows:

7. Except for the first frame, combine all the audio frames and obtain the IWT to get approximate and detail coefficients.
8. Extract the 3rd, 4th and 5th bits of detail coefficients as per the number of secret bits hidden.
9. Form the bits into three groups and perform the majority evaluation and obtain the secret coefficients. These are the approximate coefficients of the secret audio.
10. Perform inverse IWT for these approximate coefficients, considering detailed coefficients as zeros to get the secret audio *S3*.

RESULTS AND DISCUSSION

Figure 1 shows one of the frames. The frame size is 240 X 320. Figure 2 shows the secret images. The stego frame and the extracted secret images are shown in Figure 3.

Figure 1. One of the frames from the video
Source: downloaded from MirchiFun.com in January 2015.

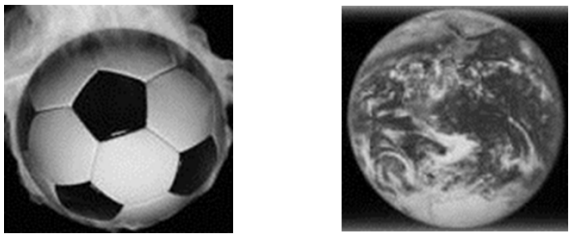

(a) (b)

Figure 2. Secret images : (a) football, (b) earth
Source: downloaded from Google in June 2013

(a)

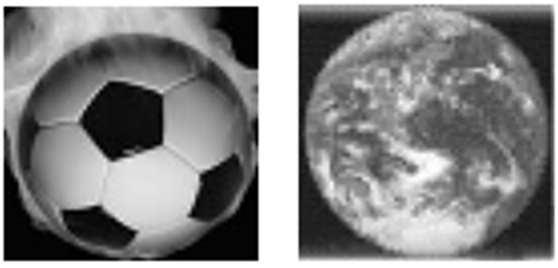

(b) (c)

Figure 3. Stego frame and Extracted images: (a) stego frame (b) extracted football (c) extracted earth

The quality of the stego video is measured using Video Quality Metric (VQM). The VQM (Pinson & Wolf, 2004) is developed by the Institute for Telecommunication Science (ITS) which is used as an objective measurement to evaluate the quality of the video. It measures the perceptual effects such as blurring, unnatural motion, noise and colour distortion among

others and combines them into a single metric. The VQM has a high correlation with subjective video quality assessment and it has been accepted by American National Standards Institute (ANSI) as an objective video quality standard. Hence, VQM is a better quality metric than Peak Signal to Noise Ratio (PSNR).

The ITS has developed a video quality metric (BVQM) software tool that performs automated batch processing of multiple video clips to objectively assess their video quality (Pinson & Wolf, 2011). The processed video clips are calibrated and the VQM is calculated. This tool is used to measure VQM. The VQM ranges between '0' and '1'. If it is '0', that indicates no difference between the original and the stego video meaning it is of good quality. '1' indicates a fully distorted video.

The extracted secret image quality is measured using PSNR and Structural Similarity Index Metric (SSIM). The PSNR is a simple statistics error metric which objectively quantifies the error signal. With PSNR, greater values indicate greater similarity. It is given by equation [1].

$$PSNR = 10 \times log_{10}\left(\frac{MAX^2}{MSE}\right) \quad [1]$$

where *MAX* = maximum value, MSE = Mean Square Error as given by equation [2].

$$MSE = \frac{1}{M \times N}\sum_{i=1}^{M}\sum_{j=1}^{N}\|O(i,j) - D(i,j)\|^2 \quad [2]$$

O(i,j) is original pixel and *D(i,j)* is stego pixel. *M X N* is the size of image. It is expressed in decibels (dB).

The SSIM is an objective image quality metric and is superior to traditional PSNR which estimates the perceived errors, whereas SSIM considers image degradation as perceived change in structural information. The SSIM is given by equation [3].

$$SSIM = \frac{(2\times\bar{x}\times\bar{y}+C1)(2\times\sigma_{xy}+C2)}{(\sigma_x{}^2+\sigma_y{}^2+C2)\times(\bar{x}^2+\bar{y}^2+C1)} \quad [3]$$

where $C1 = (k_1L)^2$, and $C2 = (k_2L)^2$ are two constants used to avoid null denominator. L is the dynamic range of the pixel values (typically this is $2^{\#\text{ bits per pixel}}$ -1). $k_1 = 0.01$ and $k_2 = 0.03$ by default.

The dynamic range of SSIM is between -1 and 1. The maximum value of 1 will be obtained for identical images. Equation [3] can be written as the product of three terms: M1, M2 and M3.

$$M1 = \frac{2\times\bar{x}\times\bar{y}+C1}{\bar{x}^2+\bar{y}^2+C1}. \quad [4]$$

$$M2 = \frac{2\times\sigma_x\times\sigma_y+C2}{\sigma_x{}^2+\sigma_y{}^2+C2} \quad [5]$$

$$M3 = \frac{\sigma_{xy}+\mathrm{C3}}{\sigma_x{}^*\sigma_y+\mathrm{C3}} \quad [6]$$

where $C3 = \frac{C2}{2}$.

M1 indicates luminance distortion, M2 indicates contrast distortion and M3 indicates structural distortion (Wang et al., 2004); Sasi varnan et al., 2011).

The extracted secret audio is evaluated using Signal to Noise Ratio (SNR) and Squared Pearson Correlation Coefficient (SPCC). The SNR is a term that refers to the measurement of the level of an audio signal compared to the level of noise that is present in that signal. It is expressed in decibels (dB). A larger SNR value indicates a better quality. It is given by equation [7].

$$\text{SNR} = 10\log_{10}\left(\frac{\frac{1}{N}\sum_{i=0}^{N} xi^2}{MSE}\right) \quad [7]$$

The recommended SNR for audio signal is above 30dB.

The SPCC is based on correlation of samples. The high value of SPCC indicates a good quality of the output signal. Its range is between 0 and 1. It is given by equation [8].

$$SPCC = \left[\sum \frac{(x-\bar{x})(y-\bar{y})}{\sqrt{\sum(x-\bar{x})^2}\sqrt{\sum(y-\bar{y})^2}}\right]^2 \quad [8]$$

where x, y, $\bar{x}$ and $\bar{y}$ are the cover signal, stego signal, average of the cover signal and average of the stego signal, respectively (Ballesteros & Moreno, 2013).

Table 1 shows the performance metrics for the stego video and extracted secret images and secret audio. When the payload is increased, the quality of the stego is reasonably good even with six secret images and 40000 secret audio samples. The quality of the extracted secret audio however, decreases and if the payload is further increased, the extracted secret audio will be distorted. Table 2 shows performance against RST attack. A rotation of 3 degrees is applied to all the stego frames and then scaled to the original size. It is possible to extract the secret image and audio with reasonable performance metrics. Table 3 compares the proposed video steganography algorithm with the research outcome of other video steganography. Since VQM is not calculated in those papers, the comparison is done in terms of PSNR with reference to payload capacity percentage. The results show that the proposed technique has better metrics than the others.

CONCLUSION

This paper proposes a high capacity video steganography technique using AVI video files as cover object. The secret information is hidden in the cover video frames, instead of hiding in the Meta data or macro block as found in the literature. The audio frames are also used for information hiding. The experimental results show that the technique is robust and secure.

Table 1
Performance Metrics

Cover video	Secret images (gray scale) and Secret audio	Stego	Extracted image		Extracted audio	
		Average VQM	PSNR in dB	SSIM	SNR in dB	SPCC
C.avi	Two images with size 128X128 and 20000 secret audio samples	0.0001	S1:36.2 S2:36.1	S1:0.9949 S2:0.9053	30.1	0.9235
	Four images with size 128X128 and 32768 secret audio samples	0.0002	S1:36.2 S2:36.1 S3:35.9 S4:32.4	S1:0.9949 S2:0.9053 S3:0.9894 S4:0.8812	28.5	0.8906
	Six images with size 128X128 and 40000 secret audio samples	0.0041	S1:36.2 S2:36.1 S3:35.9 S4:32.4 S5:36 S6:34.4	S1:0.9949 S2:0.9053 S3:0.9894 S4:0.8812 S5:0.9907 S6:0.9355	25	0.7536

Table 2
Performance Against RST Attack

Cover video	Secret images (gray scale)	Stego	Extracted image		Extracted audio	
		VQM	PSNR in dB	SSIM	SNR in dB	SPCC
C.avi	Two images with size 128X128 and 20000 secret audio samples	0.0591	S1:29 S2:30.5	S1:0.7940 S2:0.8105	29.5	0.7985

Tabel 3
Performance Comparison of Proposed Video Steganography Algorithm with That of Other Related Published Work

Algorithm	Payload capacity in %	PSNR in dB
Su et al. (2013)	14.5	36.5
Gujjunoori & Amberker (2013)	3.1	25.0
Liu et al. (2013)	2.0	36.0
Proposed	17.6	34.0

REFERENCES

Ballesteros, L. D. M., & Moreno, A. J. M. (2013). Real-time, speech-in-speech hiding scheme based on least significant bit substitution and adaptive key. *Computers and Electrical Engineering, 39*(4), 1192–1203.

Gaj, S., Patel, A. S., & Sur, A. (2015, January 23). Object based watermarking for H.264/AVC video resistant to rst attacks. *Multimedia Tools and Applications,* 1-28. doi: 10.1007/s11042-014-2422-3.

Gujjunoori, S., & Amberker, B. B. (2013). DCT based reversible data embedding for MPEG-4 video using HVS characteristics. *Journal of information security and applications, 18*(4), 157 -166.

Liu, Y., Li, Z., Ma, X., & Liu, J. (2013). A robust data hiding algorithm for H.264/AVC video streams. *The Journal of Systems and Software, 86*(8), 2174– 2183

Pinson, M. H., & Wolf, S. (2011). *Batch Video Quality Metric (BVQM) User's Manual.* Handbook series, U. S. Department of Commerce, National Telecommunications and Information Administration.

Pinson, M. H., & Wolf, S. (2004). A New Standardized Method for Objectively Measuring Video Quality. *IEEE Transactions on Broadcasting, 50*(3), 312-322.

Sadek, M. M., Khalifa, A. S., & Mostafa, M. G. (2014, March 20). Video steganography: a comprehensive review. *Multimedia Tools and Applications, 74*(17), 7063-7094. doi: 10.1007/s11042-014-1952-z.

Sasi varnan, C., Jagan, A., Kaur, J., Jyoti, D., & Rao, D. S. (2011). Image Quality Assessment Techniques in Spatial Domain. *International Journal of Computer Science and Technology, 2*(3), 177-184.

Shanableh, T. (2014). Data Hiding in MPEG Video Files Using Multivariate Regression and Flexible Macroblock Ordering. *IEEE transactions on information forensics and security, 7*(2), 455-464.

Su, P. C., Lu, M., & Wu, C. (2013). A practical design of high-volume steganography in digital video files. *Multimedia Tools and Applications, 66*(2), 247–266.

Tew, Y., & KokSheik, W. (2014). An Overview of Information Hiding in H.264/AVC Compressed Video. *IEEE Transactions on Circuits and Systems for Video Technology, 24*(2), 305-319.

Wang, Y. (2006). Survey of Objective Video Quality Measurements. *EMC Corporation Hopkinton, MA 01748, USA*, pp.1-7.

Wang, Z., Bovik, A. C., Sheikh, H. R., & Simoncelli, E. P. (2004). Image Quality Assessment: From Error Visibility to Structure Similarity. *IEEE Transactions on Image Processing, 13*(4), 600-612.

Winkler, S. (2009). Video Quality Measurement Standards –Current Status and Trends. *Proc. 7th International Conference on Information, Communications & Signal Processing*, (pp. 1-5).

Xu, D., Wang, R., & Shi Yun, Q. (2014). Data Hiding in Encrypted H.264/AVC Video Streams by Codeword Substitution. *IEEE Transactions on Information Forensics and Security, 9*(4), 596-606.

Yao, Y., Zhang, W., Yu, N., & Zhao, X. (2014, September 3). Defining embedding distortion for motion vector-based video steganography. *Multimedia tools and Applications*. doi: 10.1007/s11042-014-2223-8

APPENDIX

Following MATLAB functions are used in the experimentation:

To read video file *C.avi* and to get number of video frames *n*:

VideoFreader=vision.VideoFileReader('*C.avi*')

vid=VideoReader('*C.avi*') (Sadek, Khalifa, & Mostafa, 2014)

n= vid.NumberOfFrames

To extract audio and image frames (*a* and *im*) from the video:

for i=1 to *n* do

begin

[I, Audio] =step(VideoFreader)

a{i}=Audio

im{i}=I

end

To decompose an image *B* into four sub bands *BLL, BHL, BLH, BH* using IWT:

LS = liftwave('haar','Int2Int')

[*BLL,BHL,BLH,BHH*] = lwt2(double(*B*), LS)

To get back the image *B,* inverse IWT is applied as follows:

B=ilwt2(*BLL, BHL, BLH, BHH*, LS)

To obtain the IWT of audio frame *a*:

[*CAc, CDc*] = lwt(double(*a*), LS)

To get back the audio frame, inverse IWT is applied as follows:

a= ilwt (*CAc, CDc*, LS)

To write video and audio frames (*im* and *a*) into a video file *G. avi* (*n* is the total no. of frames):

VideoFwriter=vision.VideoFileWriter('*G.avi*')

for i=1to *n* do

begin

step(VideoFwriter,*im*{i},*a*{i})

end.

Pertanika J. Sci. & Technol. 24 (2): 423 - 438 (2016)

SCIENCE & TECHNOLOGY

Journal homepage: http://www.pertanika.upm.edu.my/

The Heat Transfer Performance of Gold/Water Nanofluid Flows in Minitube using Thermal Lattice Boltzmann Method

Ahmed A. Hussien[1]*, Mohd Z. Abdullah[2], Mohd A. Al-Nimr[3], N. M. Yusop[1], C. Nuntadusit[4] and M. H. Elnaggar[5]

[1]School of Mechanical Engineering, Engineering Campus, Universiti Sains Malaysia, 14300 Nibong Tebal, Penang, Malaysia

[2]School of Aerospace Engineering, Engineering Campus, Universiti Sains Malaysia, 14300 Nibong Tebal, Penang, Malaysia

[3]Department of Mechanical Engineering, Jordan University of Science and Technology, Irbid 22110, Jordan

[4]Department of Mechanical Engineering, Faculty of Engineering, Prince of Songkla University, HatYai, Songkla, Thailand 90112

[5]Engineering Department Palestine Technical College-Deir EL-Balah Gaza Strip, Palestine

ABSTRACT

One of the best ways to enhance heat transfer coefficient is by improving thermal properties of the working fluid. Gold/water nanofluid flow through horizontal minitube with very low Reynolds number was simulated by using Thermal Lattice Boltzmann Method (TLBM) under uniform heat flux boundary condition. The effect of different volume fraction of nanoparticles on the heat transfer coefficient was studied and compared with the base fluid (water). The results were verified using Finite Volume Method (FVM). The results showed enhancement of heat transfer coefficient when using gold/water nanofluid and this enhancement depends on the volume concentration of Gold nanoparticles. The maximum enhancement was 18% with 0.03 volume concentration.

Keywords: Convective heat transfer, Gold nanoparticles, Nanofluids, TLBM, Axisymmetric, Laminar flow

Article history:
Received: 17 February 2016
Accepted: 22 April 2016

E-mail addresses:
ahmed.a.a.hussien@gmail.com (Ahmed A. Hussien),
mezul@eng.usm.my (Mohd Z. Abdullah),
malnimr@just.edu.jo (Mohd A. Al-Nimr),
menadiah@eng.usm.my (N. M. Yusop),
chayut@me.psu.ac.th (C. Nuntadusit),
mohdhn@yahoo.com (M. H. Elnaggar)
*Corresponding Author

ISSN: 0128-7680

INTRODUCTION

Nowadays, conventional fluid with the addition of ultrafine particles in nanometer size makes a difference in enhancing heat transfer exchange in many applications which emit high heat flux, such as MEMS/NEMS systems, high performance electronic device,

solar cells and many applications that need high performance cooling systems (Hussien et al., 2016; Verma & Tiwari, 2015) . These nanoparticles have thermal conductivity of a hundred times more than conventional fluid. This means that the thermal and rheological properties will be changed upon the addition of nanoparticles to the fluid even at a very low amount (*Zhou* et al., 2012). Moreover, the change depends on the size, shape and the material of the nanoparticles (Anoop et al., 2009; Ji et al., 2011) . Many experimental research have been conducted to identify the physical properties of nanofluids and compared with existing models as described in nanofluids cases (Mostafizur et al., 2015; Solangi et al., 2015) . Besides that, the nanoparticles are continuously in the stage of development by introducing new materials (hybrid nanoparticles), shapes and sizes (Sarkar et al., 2015; Tian et al., 2015) .

So far, the literature survey conducted by researchers have created roles for very small channels to increase the heat transfer coefficient. It is desirable for high heat transfer rate and that is the reason why the contact surface area is higher out of the volume.

Many experimental investigations performed so far have concerned mainly with the study of nanofluids with micro/minichannels for developing a new generation of cooling systems. For instance, Jung et al. (2009) found enhancing the heat transfer up to 30% in their experimental study of AL_2O_3/water nanofluid in rectangle microchannels. Meanwhile, Nitiapiruk et al. (2013) studied TiO_2/water nanofluids in rectangle microchannels experimentally and their results showed that enhancing heat transfer coefficient depends on the volume concentration of the nanoparticles. Nazari et al. (2014) experimented with the performance of the CPU cooling performance by using nanofluids. They used two types of nanoparticles (Al_2O_3 and CNT) dispersant in (water and EG) with various particle concentrations in their experiment. Their results showed 13% maximum enhancement in convection heat transfer which occurred when they used CNT nanoparticles. They also concluded that the maximum enhancement can be achieved when the optimum concentration of nanoparticles and flow rate is taken into consideration.

Recently, numerical simulations of testing the enhancement of heat transfer performance when using nanofluids in micro/minichannels were taken into account for avoiding experimental fabrication efforts and saving time and money. Jang and Choi (2006) investigated numerically Cu/water and diamond/water nanofluids in rectangle microchannels heat sink. The enhancement in thermal performance was about 10%. In another study, J. Li and Kleinstreuer (2008) worked numerically to find out CuO/water nanofluid in trapezoidal microchannels leading to extra pressure drop with the enhancement of heat transfer. Mohammed et al. (2011) tested six different types of nanofluids (Al_2O_3, Ag, CuO, diamond, SiO_2 and TiO_2)/water in triangular microchannels numerically and based on their observation, the peak thermal performance and less pressure drop can be utilised using Diamond and Ag /water nanofluids. Salman et al. (2012) studied convection heat transfer of (Al_2O_3, CuO,SiO_2, ZnO) / EG nanofluids flow through circular microchannel with different nanoparticle sizes and volume concentrations. Their results revealed significant effects on the Nusselt number, velocity, wall shear stress and pressure drop with the change of size and concentration of the nanoparticles. Mohammadian et al. (2014) studied the performance of counter flow microchannel heat exchanger when using Al_2O_3–water nanofluid numerically. They used different nanoparticle volume concentrations

and sizes. The results pinned that the highest thermal performance can be achieved using the highest concentration and the smallest particle size.

Some researchers prefer the minichannel when using nanofluids by for two main reasons: the cost of fabrication and less of pressure drop (Shenoy et al., 2011). Ijam and Saidur (2012) studied the cooling performance of the heat sink by using the SiC–water and TiO_2– water in the minichannel. They found out that the improvement was between 7–12%. Liu and Yu (2011) investigated experimentally convective heat transfer Al_2O_3/water nanofluid flow inside circular minichannel (Di= 1.09 mm) in different flow types of laminar and transition and turbulence. Their results revealed that the laminar flow caused greater enhancement compared with the transition and turbulent flow with pressure drop penalty while the conventional correlations can be used in the laminar regime. Vafaei and Wen (2012) studied the Al_2O_3/water nanofluid flow inside circular minichannel (Di= 510 μm). The enhancement of the heat transfer coefficient reached 40% for higher flow rate. In addition, Al_2O_3/water nanofluid with rectangle minichannels heat sink was investigated experimentally by Ho et al. (2014) with the hydraulic diameter at 1.2 mm. Ijam et al. (2012) investigated (Al2O3, TiO2)/water nanofluids flow through rectangle minichannels heat sink. Hassan et al. (2013) concluded that nanofluids with laminar flow in minichannels are a superior coolant when compared between the circular minichannel (Di=3mm) and microchannel (Di=50 μm) with Al_2O_3/water nanofluid.

Many types of nanofluids have been studied so far for high thermal conductivity of metal nanoparticles, such as Au, Ag, Cu, Al, which made it highly demanding for being the perfect coolant in the recent market. However, very few researches have been concerned with the convection of heat transfer performance on gold/water nanofluid. Sabir et al. (2015) studied experimentally the characteristics of convection heat transfer of gold nanofluid with very low volume concentrations and their results detected up to 30% of enhancement in heat transfer coefficient. On the other hand, Patel et al. (2003) detected 9% thermal conductivity enhancement in their experimental research when they used Au/water nanofluid, while Tsai et al. (2004) revealed that using gold/water nanofluid reduced the thermal resistance of the heat pipes.

In the past few years, researchers have started using the **Thermal Lattice Boltzman Method** (TLBM), which is considered as a very effective method to simulate many problems for fluid and thermal flow (Sidik & Razali, 2014). Sheikholeslami et al. (2013) applied TLBM to figure the magnetic field effect to concentric annuals filled by A_2O_3/H_2O nanofluid. In another research, Karimipour et al. (2015) used TLBM the force convection of Cu/H_2O nanofluid flow inside the microtube in very low Reynolds number with slip wall flow boundary condition.

This article focuses on the enhancement of heat transfer coefficient by using gold/water nanofluid flow inside the minitube with different volume concentrations using TLBM.

GEOMETRY MODELING AND GOVERNING EQUATIONS

The continuity, 2-D Navier-Stokes and energy equations will be used to describe the flow velocities and temperature distributions in the whole region. Figure 1 shows the computational domain, the axial and radial axis (z, r) respectively, and the uniform heat flux (q") which will be exposed to the outer surface of the minitube. According to Kandlinkar classifications

(Kandlikar, 2006), the channel that has hydraulic diameter from 200μm to 3mm is considered minichannel, whereas the minitube diameter is 2.1 mm with wall thickness of 0.45 mm.

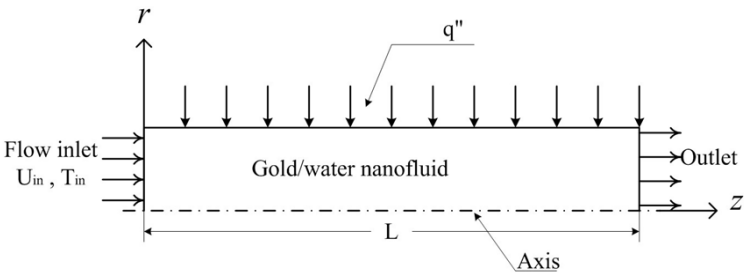

Figure 1. Schematic diagram

The governing equations are:

$$\frac{1}{r}\frac{\partial}{\partial r}(vr)+\frac{\partial u}{\partial z}=0 \quad [1]$$

$$u\frac{\partial u}{\partial z}+v\frac{\partial u}{\partial r}=-\frac{1}{\rho}\frac{\partial p}{\partial z}+\vartheta\left(\frac{\partial^2 u}{\partial z^2}+\frac{\partial^2 u}{\partial r^2}+\frac{1}{r}\frac{\partial u}{\partial r}\right) \quad [2]$$

$$u\frac{\partial v}{\partial z}+v\frac{\partial v}{\partial r}=-\frac{1}{\rho}\frac{\partial p}{\partial r}+\vartheta\left(\frac{\partial^2 v}{\partial z^2}+\frac{\partial^2 v}{\partial r^2}+\frac{1}{r}\frac{\partial v}{\partial r}-\frac{v}{r^2}\right) \quad [3]$$

$$u\frac{\partial T}{\partial z}+v\frac{\partial T}{\partial r}=\frac{\vartheta}{P_r}\left(\frac{\partial^2 T}{\partial z^2}+\frac{\partial^2 T}{\partial r^2}+\frac{1}{r}\frac{\partial T}{\partial r}\right) \quad [4]$$

where u, v are the velocity components in z and r directions respectively.

The following assumptions will be considered:

- Continuum.
- Newtonian fluid.
- Incompressible.
- Constant viscosity, density, and thermal conductivity.
- Negligible gravity force.
- Negligible nuclear, electromagnetic and radiation energy transfer

NUMERICAL METHOD

Nanofluids Treatment

In this paper, we used gold-water nanofluid as homogenous working fluid. The physical and thermal properties of the nanofluid were calculated from the properties of water and gold as shown in Table 1.

Table 1
The Properties of Water and Gold nanoparticles at T=313.15K (Bergman et al., 2011)

	ρ (kg m^{-3})	C_p (J kg^{-1} K^{-1})	μ (kg m^{-1} s^{-1})	K (W m^{-1} K^{-1})
Water	992.22	4178	0.0006532	0.6305
Gold nanoparticles	19300	126	-	318

The general formulas for fluid-solid mixture was used to find the density and specific heat capacity of the nanofluids:

$$\rho_{nf} = (1-\varphi)\rho_f + \varphi\rho_p \quad [5]$$

$$(c_p\rho)_{nf} = (1-\varphi)(c_p\rho)_f + \varphi(c_p\rho)_p \quad [6]$$

Batchelor's model (Batchelor, 1977) was used to calculate the effective viscosity of nanofluids:

$$\mu_{eff} = (1+2.5\phi+6.2\phi^2)\mu_{bf} \quad [7]$$

The effective thermal conductivity was calculated by using the Hamilton and crosser model (Hamilton & Crosser, 1962):

$$k_{eff} = k_{bf}\frac{k_p+(n-1)k_{bf}+(n-1)(k_p-k_{bf})\phi}{k_p+(n-1)k_{bf}-(k_p-k_{bf})\phi} \quad [8]$$

where the kinematic viscosity is $v = \mu/\rho$, the prandtl number is $P_r = c_p\mu/k$ and the thermal diffusivity is $\alpha = v/P_r$.

According to Hamilton and Crosser (1962), increasing the volume concentration caused an increase in the thermal conductivity and the viscosity in the crosser model and Batchelor's model, as can be seen in Figure 2.

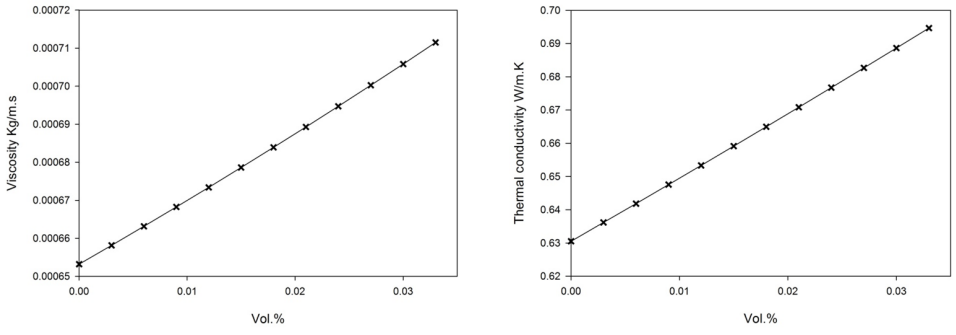

(a) (b)

Figure 2. The effect of the nanoparticles volume concentrations on the (a) viscosity and (b) thermal conductivity

Lattice Boltzmann Methods

Numerical simulations are considered over experimental at the situations where it becomes tedious to collect data from setup. Numerical methods are preferable because experimental setup needs very high treatment care, special tools and expensive instruments. Thus, the Thermal Lattice Boltzman Method (TLBM) has become a very significant research technique in mini/ microchannels with nanofluids (Yang & Lai, 2011). In this study, TLBM was used for the analysis of fluid flow and heat transfer in minitube, with uniform heat flux.

The idea of Lattice Boltzmann Method (LBM) is to take advantage of micro-scale and macro-scale by considering a collection of particles as a unit, which is called the meso-scale. For instance, LBM is connected between the entropy of a system with time and the change in macroscopic variables. It can predict the macroscopic behaviour by studying the distribution functions which is in a general probability of finding particles in Lattice Unite at a certain time f(r,c,t) and g(r,c,t) respectively.

Halliday et al. (2001) were the first to explore the energy equation in axisymmetry by LGK approximation with selected source terms. Later, many models studied the axisymmetric flow such as those by Lee et al. (2006), Reis and Phillips (2008), Guo et al. (2009) and J. G. Zhou (2011).

In this paper, Zhou's model (J. G. Zhou, 2011) was used to define the source terms in the D2Q9 LB Model, the distribution function of nine velocities were formulated as:

$$f_\alpha(\boldsymbol{x}+e_\alpha\Delta t, t+\Delta t) = \omega_\alpha f_\alpha^{eq}(\boldsymbol{x},t) + (1-\omega_\alpha) f_\alpha(\boldsymbol{x},t) + w_\alpha\theta\Delta t + \frac{\Delta t}{\forall e^2} e_{\alpha i} F_i \quad [9]$$

the source terms θ and F_i are defined as: $\theta = \frac{-\rho u_r}{r}$, and $F_i = \frac{-\rho u_i u_r}{r} - \frac{2\rho\nu u_i}{r}\delta_{ir}$ respectively. where f_α is the distribution functions, $\boldsymbol{x}$ is the position vector $\boldsymbol{x} = \boldsymbol{x}(z,r)$, ω_α the effective relaxation time depends on the position, *i* index represents *z* and *r*. The other parameters of the D2Q9 model are shown in Table 2.

Table 2
D2Q9 LBM Model Variables (Mohamad, 2011)

C_s^2	A	$e_{\alpha i}$	w_α
	0	(0,0)	4/9
1/3	1,2,3,4	$(\cos\frac{\alpha-1}{2}\pi, \sin\frac{\alpha-1}{2}\pi)$	1/9
	5,6,7,8	$\sqrt{2}(\cos(\frac{\alpha-5}{2}\pi+\frac{\pi}{4}), \sin(\frac{\alpha-5}{2}\pi+\frac{\pi}{4}))$	1/36

The equilibrium distribution function can be formulated as:

$$f_\alpha^{eq} = w_\alpha\rho\left(1 + \frac{e_{\alpha i}\mathbf{u}_i}{C_s^2} + \frac{1}{2}\frac{e_{\alpha i}e_{\alpha j}\mathbf{u}_i\mathbf{u}_j}{C_s^4} + \frac{1}{2}\frac{\mathbf{u}_i\mathbf{u}_j}{C_s^2}\right) \quad [10]$$

The distribution functions give the density and the velocity as:

$$\rho(\boldsymbol{x},t) = \sum_{\alpha} f_{\alpha}(\boldsymbol{x},t) \quad [11]$$

$$\mathbf{u}_{\mathrm{i}} = \frac{1}{\rho}\sum_{\alpha} \mathrm{e}_{\alpha \mathrm{i}} f_{\alpha}(\boldsymbol{x},t) \quad [12]$$

Peng et al. (2003) proposed the first axisymmetric flow in TLBM by solving the temperature distribution with finite difference method. The hybrid model was then used to solve the thermal and vorticity stream function (Sheng Chen et al., 2009).

In recent times, the dual lattice form has been used to recover thermal energy equation by new distribution function g(x,t) with f(x,t) (Wang et al., 2007; Q. Li et al., 2009; Zheng et al., 2010). In this paper, D2Q4 thermal model was used for solving the temperature distributions, which in turn helps to reduce the computational efforts over D2Q9 thermal model (Djebali et al., 2008). In this model, the scalar distribution function can be derived from the following formulation:

$$g_{\gamma}\left(\boldsymbol{x} + e_{\gamma}\Delta t, t + \Delta t\right) = \omega_{\gamma} g_{\gamma}^{eq}(\boldsymbol{x},t) + \left(1 - \omega_{\gamma}\right) g_{\gamma}(\boldsymbol{x},t) + w_{\gamma}\Delta t\ (1 + 0.5\omega_{\gamma}) \quad [13]$$

where:

$S = \frac{\alpha}{r}\frac{\partial T}{\partial r}$, $\omega_{\gamma} = \frac{1}{\tau_g}$ and the relation between thermal diffusivity $\boldsymbol{\alpha}$ and thermal relaxation time τ_g is $\boldsymbol{\alpha} = \frac{\tau_g - 0.5}{\mathbf{2}}\frac{\Delta \boldsymbol{x}^{\mathbf{2}}}{\Delta \boldsymbol{t}}$. The equilibrium distribution $\mathrm{g}_{\gamma}^{\mathrm{eq}}(\mathrm{x},\mathrm{t}) = \mathrm{w}_{\gamma}\mathrm{T}\left(1 + \frac{\mathrm{e}_{\gamma \mathrm{i}}\mathrm{u}_{\mathrm{i}}}{\mathrm{C}_{\mathrm{s}}^{2}}\right)$, where $\mathrm{C}_{\mathrm{s}}^{2} = \frac{1}{2}$, $\mathrm{w}_{\gamma 1-4} = \frac{1}{4}$ and $\mathrm{e}_{\gamma \mathrm{i}}$ as shown in Fig. 3.

The macroscopic temperature is obtained similarly as that of flow distribution functions:

$$\mathrm{T} = \sum_{\gamma} \mathrm{g} + \frac{\Delta \mathrm{t}}{2}\mathrm{S} \quad [14]$$

Boundary conditions

After the streaming process, f_1, f_5, f_8 *and* g_1 are unknown at the inlet and for outlet its f_3, f_6, f_7 *and* g_2. N`ow at the wall, f_4, f_8, f_7 *and* g_4 and at the axis f_2, f_5, f_6 *and* g_{12} as shown in Figure 3.

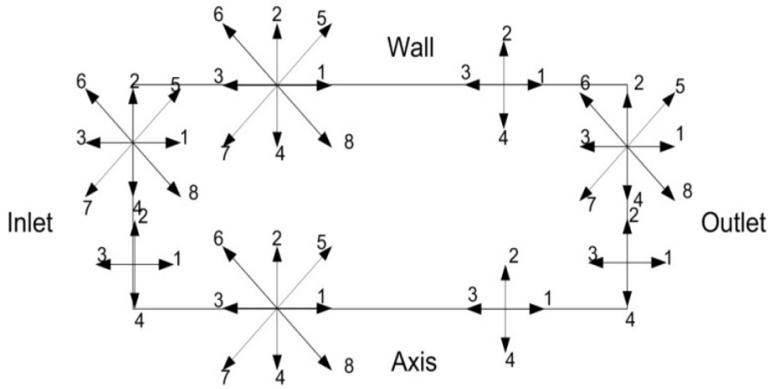

Figure 3. Distribution functions at the boundaries for D2Q9-D2Q4 flow thermal model

Applying boundary conditions helps to locate the unknown distribution functions. For a boundary condition with nonzero velocity, the inlet flow in the west side is known, so the bounce-back scheme is obviously invalid. The Zou and He (Zou & He, 1997) boundary condition for known inlet velocity was used, whereas for constant inlet temperature, $\mathbf{T_0}$ was divided to scalar distribution function and hence, the macroscopic and microscopic boundary conditions are:

$$z = 0 \begin{cases} u_z = U_0 \\ u_r = 0.0 \\ T_i = T_0 \end{cases} \rightarrow \begin{cases} \rho_w = \frac{1}{1-U_0}[f_0 + f_2 + f_4 + 2(f_3 + f_6 + f_7)] \\ f_1 = f_3 + \frac{2}{3}\rho_w U_0 \\ f_5 = f_7 - \frac{1}{2}(f_2 - f_4) + \frac{1}{6}\rho_w U_0 \\ f_8 = f_6 - \frac{1}{2}(f_2 - f_4) + \frac{1}{6}\rho_w U_0 \\ g_1 = (w_1 + w_3)T_0 - g_3 \end{cases} \quad [15]$$

For constant heat flux at the wall, the bounce back boundary (Shiyi Chen et al., 1996) condition was used to the flow distribution function, and constant temperature gradient for scalar distribution functions is expressed as (Tarokh et al., 2013):

$$r = R \begin{cases} u_r = 0.0 \\ u_z = 0.0 \\ -k\frac{\partial T}{\partial r} = q_0^{"} \end{cases} \rightarrow \begin{cases} f_4 = f_2 \\ f_7 = f_5 \\ f_8 = f_6 \\ g_4 = (w_2 + w_4)\frac{q_0^{"}}{k} - g_2 + \sum_1^4 g \end{cases} \quad [16]$$

Simple forward finite's difference scheme was used to define the unknown distribution function around the central axis as shown in Eq. (17).

$$r = 0 \begin{cases} \frac{\partial u}{\partial r} = 0 \\ \frac{\partial T}{\partial r} = 0 \end{cases} \longrightarrow \begin{cases} f^1_{\alpha=0-9} = f^2_{\alpha=0-9} \\ g^1_{\gamma=1-4} = g^2_{\gamma=1-4} \end{cases} \quad [17]$$

As outlet density and velocity are unknown, it is assumed that velocity at the point before last lattice is the outlet velocity and the same procedure of inlet boundary condition is applied (Mohamad, 2011). For thermal distribution function, the extrapolation was used to define the unknown value.

Figure 4 shows the sequence steps for each time step to solve BKG-LBM D2Q9-D2Q4 flow thermal models until convergence (Mohamad, 2011).

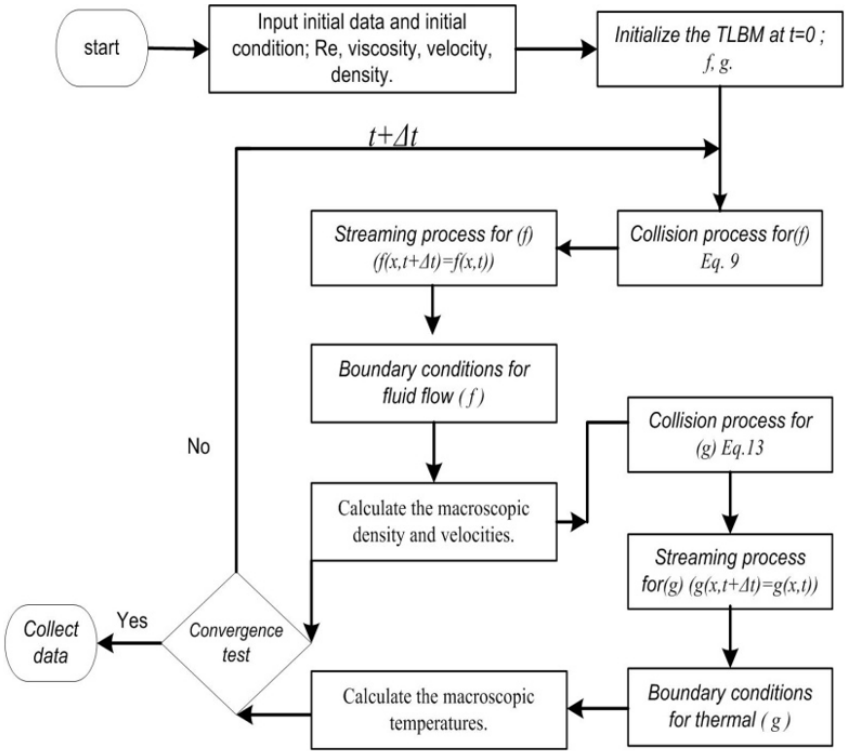

Figure 4. The TLBM steps

DISCUSSION

In this simulation, the uniform heat flux was applied at the surface of the tube $q''_0 = 6000\ {}^{W}/_{m^2}$, with low Reynolds number $(\mathrm{Re} = 50)$ for all process fluids. In total, four different volume concentrations of gold nanoparticles were used to perform the experiment, namely 0.1,0.5,1 and 3% volume concentrations. The enhancement of heat transfer coefficient through axial distance was studied by using a 2.1 mm diameter minitube and 27cm axial length.

Thus, the local heat transfer coefficient was calculated by applying the Newton law:

$$h(z) = \frac{q_0^{"}}{(T_w(z) - T_m(z))} \quad [18]$$

where T_{wi} is the temperature of the inner wall surface and $T_m(z)$ is the mean temperature in the z location and can be predicted by using the following formulae:

$$T_m(z) = \frac{\int_0^R \rho u T \, dr}{\rho_m u_m} \quad [19]$$

ρ_m , u_m is the mean density and the mean axial velocity in the same axial point respectively:

$$\theta(z, r) = \frac{T(z,r) - T_m(z)}{q^{"} l / k} \quad [20]$$

The results of D2Q9-D2Q4 TLBM showed acceptable values as compared with commercial CFD package. From Figure 5 and Figure 6, it can be easily confirmed that wall temperature along the axial direction and cross section temperature distribution in different axial locations are almost matching respectively.

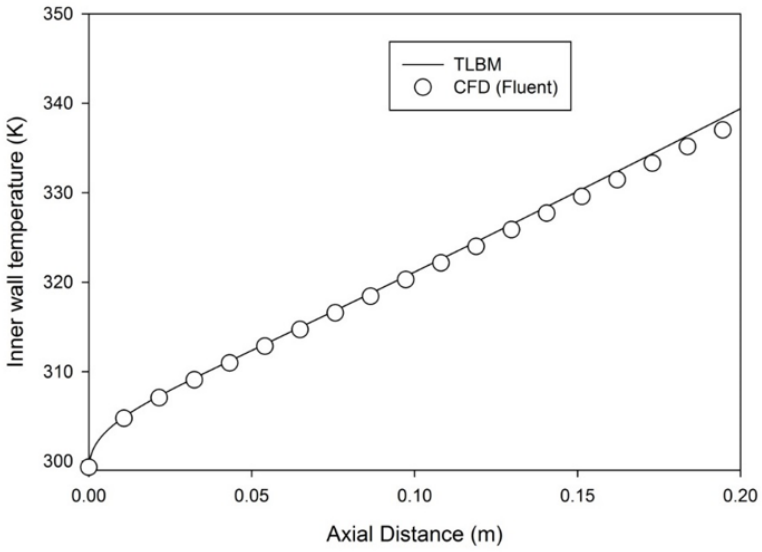

Figure 5. The Inner wall temperature along the axial direction for water

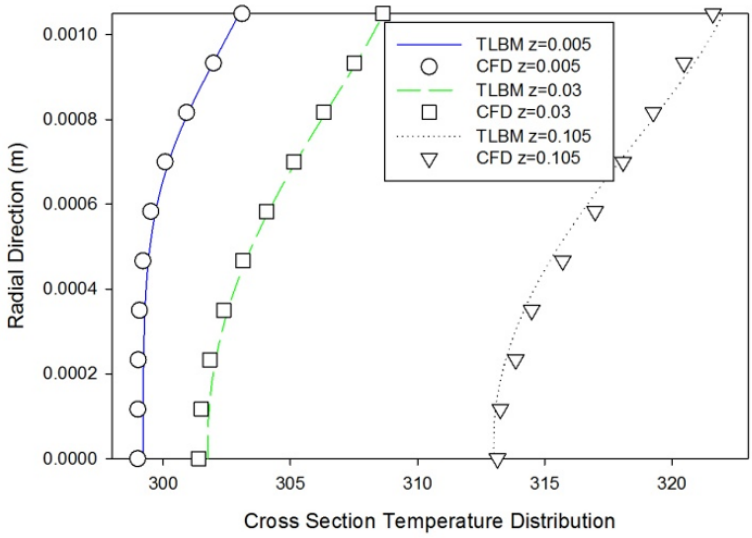

Figure 6. Temperature distribution for different axial locations

Figure 7 shows the dimensionless inner wall temperature $\theta_{w,}$ with reference to Eq.20 along the axial distance ranges from 0 - 0.27m. This curve indicates that the increase in volume concentration of nanoparticles will decrease the dimensionless wall temperature. This is due to the increase in effective thermal conductivity of the nanofluids, which in turn improves the heat transfer along the radial direction. This relation can be seen especially in the fully developed regions.

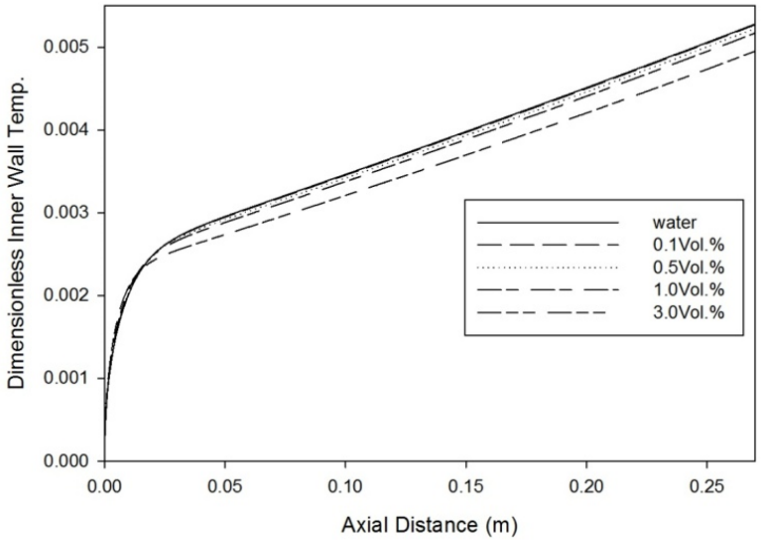

Figure 7. The dimensionless inner wall temperature variation with different nanoparticles volume concentration

Figure 8 shows heat transfer coefficient along axial direction by considering volume concentrations of gold nanoparticles. It can be seen that heat transfer coefficient increases with the increase in concentration of the gold/water nanofluid. Now comparing results with that of water, we found out that there is an enhancement of 18% for 3.0vol.% gold/water nanofluid. Hence, for very low concentration of 0.1vol.%, the enhancement was around 1%. With these figures, a much large enhancement was seen at the beginning of the developing region.

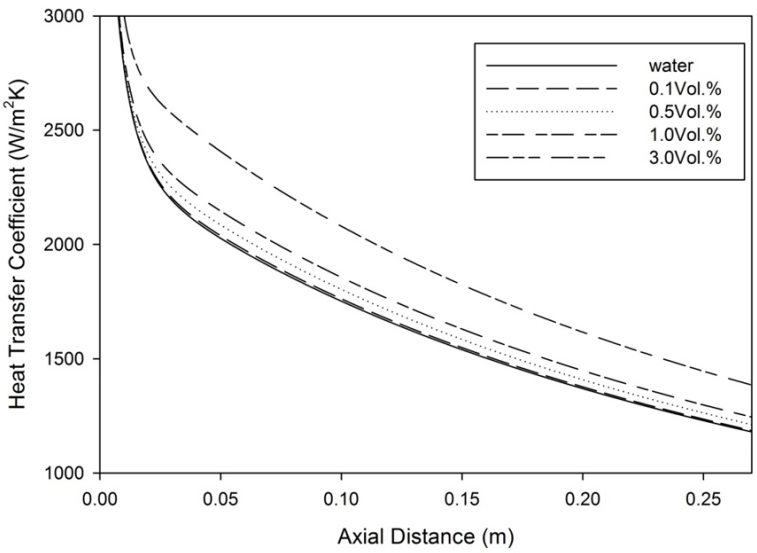

Figure 8. The heat transfer coefficient variation with different volume concentrations of nanoparticles

The average Nusselt number increases with the increase in volume concentration of gold nanoparticle, as shown in Figure 9. The results show very low enhancement in average Nusselt number which is due to the enhancing of nanofluids thermal conductivity. The maximum developing value of Average Nusselt number in comparing water is 7% for 3.0vol.% gold/water nanofluid.

The major advantage of using nanofluids will not only boost effective thermal conductivity but also drastically enhance viscosity. For example, the velocity of the 3.0vol.% gold/water nanofluid is about 30% less than the velocity of water at the same Reynolds number. This shows that the reduction in the mean velocity causes more heat carrier.

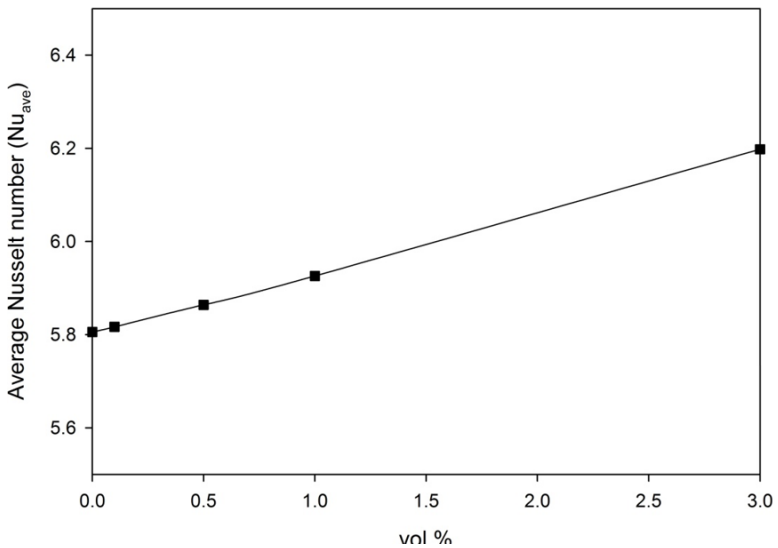

Figure 9. Average Nusselt number variation with different volume concentrations of nanoparticles

Nowadays, research on gold/water nanofluid is rarely seen, thus more experimental research must be carried out in this area for a comprehensive understanding.

CONCLUSION

The Thermal Lattice Boltzmann Method (D2Q9-D2Q4 TLBM) has been used to simulate the force convection heat transfer by using gold/water nanofluid with different volume concentrations through minitube. The results pinned that heat transfer coefficient enhances with gold/water nanofluid over pure water. Furthermore, the enhancement depends on the volume concentration of the gold nanoparticles proportionally. From this study, the maximum enhancement was 20% for 0.03 volume concentration of gold/water nanofluid compared with water. The enhancement of the heat transfer coefficient was due to the effective thermal conductivity and effective viscosity. From this study, it has been observed that there is a shortage in the investigation of gold/water nanofluid and its effects in enhancing heat transfer coefficient experimentally.

ACKNOWLEDGEMENTS

The first author would like to thank Universiti Sains Malaysia (USM) for the financial support provided for a PhD student through the USM fellowship.

REFERENCES

Anoop, K., Sundararajan, T., & Das, S. K. (2009). Effect of particle size on the convective heat transfer in nanofluid in the developing region. *International Journal of Heat and Mass Transfer, 52*(9), 2189-2195.

Batchelor, G. (1977). The effect of Brownian motion on the bulk stress in a suspension of spherical particles. *Journal of Fluid Mechanics, 83*(01), 97-117.

Bergman, T. L., Incropera, F. P., & Lavine, A. S. (2011). *Fundamentals of heat and mass transfer*: John Wiley & Sons.

Chen, S., Martinez, D., & Mei, R. (1996). On boundary conditions in lattice Boltzmann methods. *Physics of Fluids (1994-present), 8*(9), 2527-2536.

Chen, S., Tölke, J., & Krafczyk, M. (2009). Simple lattice Boltzmann subgrid-scale model for convectional flows with high Rayleigh numbers within an enclosed circular annular cavity. *Physical Review E, 80*(2), 026702.

Djebali, R., Pateyron, B., El Ganaoui, M., & Sammouda, H. (2008). Axisymmetric high temperature jet behaviours based on a lattice Boltzmann computational method. Part I: Argon Plasma.

Guo, Z., Han, H., Shi, B., & Zheng, C. (2009). Theory of the lattice Boltzmann equation: lattice Boltzmann model for axisymmetric flows. *Physical Review E, 79*(4), 046708.

Halliday, I., Hammond, L., Care, C., Good, K., & Stevens, A. (2001). Lattice Boltzmann equation hydrodynamics. *Physical Review E, 64*(1), 011208.

Hamilton, R., & Crosser, O. (1962). Thermal conductivity of heterogeneous two-component systems. *Industrial and Engineering Chemistry Fundamentals, 1*(3), 187-191.

Hassan, M., Sadri, R., Ahmadi, G., Dahari, M. B., Kazi, S. N., Safaei, M. R., & Sadeghinezhad, E. (2013). Numerical study of entropy generation in a flowing nanofluid used in micro-and minichannels. *Entropy, 15*(1), 144-155.

Ho, C., Chen, W.-C., & Yan, W.-M. (2014). Correlations of heat transfer effectiveness in a minichannel heat sink with water-based suspensions of Al 2 O 3 nanoparticles and/or MEPCM particles. *International Journal of Heat and Mass Transfer, 69*, 293-299.

Hussien, A. A., Abdullah, M. Z., & Moh'd A, A.-N. (2016). Single-phase heat transfer enhancement in micro/minichannels using nanofluids: Theory and applications. *Applied Energy, 164*, 733-755.

Ijam, A., & Saidur, R. (2012). Nanofluid as a coolant for electronic devices (cooling of electronic devices). *Applied Thermal Engineering, 32*, 76-82.

Ijam, A., Saidur, R., & Ganesan, P. (2012). Cooling of minichannel heat sink using nanofluids. *International Communications in Heat and Mass Transfer, 39*(8), 1188-1194.

Jang, S. P., & Choi, S. U. (2006). Cooling performance of a microchannel heat sink with nanofluids. *Applied Thermal Engineering, 26*(17), 2457-2463.

Ji, Y., Wilson, C., Chen, H.-h., & Ma, H. (2011). Particle shape effect on heat transfer performance in an oscillating heat pipe. *Nanoscale Research Letters, 6*(1), 1-7.

Jung, J.-Y., Oh, H.-S., & Kwak, H.-Y. (2009). Forced convective heat transfer of nanofluids in microchannels. *International Journal of Heat and Mass Transfer, 52*(1), 466-472.

Kandlikar, S. G. (2006). Effect of liquid-vapor phase distribution on the heat transfer mechanisms during flow boiling in minichannels and microchannels. *Heat Transfer Engineering, 27*(1), 4-13.

Karimipour, A., Nezhad, A. H., D'Orazio, A., Esfe, M. H., Safaei, M. R., & Shirani, E. (2015). Simulation of copper–water nanofluid in a microchannel in slip flow regime using the lattice Boltzmann method. *European Journal of Mechanics-B/Fluids, 49*, 89-99.

Lee, T., Huang, H., & Shu, C. (2006). An axisymmetric incompressible lattice Boltzmann model for pipe flow. *International Journal of Modern Physics C, 17*(05), 645-661.

Li, J., & Kleinstreuer, C. (2008). Thermal performance of nanofluid flow in microchannels. *International Journal of Heat and Fluid Flow, 29*(4), 1221-1232.

Li, Q., He, Y., Tang, G., & Tao, W. (2009). Lattice Boltzmann model for axisymmetric thermal flows. *Physical Review E, 80*(3), 037702.

Liu, D., & Yu, L. (2011). Single-phase thermal transport of nanofluids in a minichannel. *Journal of Heat Transfer, 133*(3), 031009.

Mohamad, A. A. (2011). *Lattice Boltzmann method: fundamentals and engineering applications with computer codes*: Springer Science & Business Media.

Mohammadian, S. K., Seyf, H. R., & Zhang, Y. (2014). Performance Augmentation and Optimization of Aluminum Oxide-Water Nanofluid Flow in a Two-Fluid Microchannel Heat Exchanger. *Journal of Heat Transfer, 136*(2), 021701.

Mohammed, H., Gunnasegaran, P., & Shuaib, N. (2011). The impact of various nanofluid types on triangular microchannels heat sink cooling performance. *International Communications in Heat and Mass Transfer, 38*(6), 767-773.

Mostafizur, R., Saidur, R., Aziz, A. A., & Bhuiyan, M. (2015). Thermophysical properties of methanol based Al 2 O 3 nanofluids. *International Journal of Heat and Mass Transfer, 85*, 414-419.

Nazari, M., Karami, M., & Ashouri, M. (2014). Comparing the thermal performance of water, Ethylene Glycol, Alumina and CNT nanofluids in CPU cooling: Experimental study. *Experimental Thermal and Fluid Science, 57*, 371-377.

Nitiapiruk, P., Mahian, O., Dalkilic, A. S., & Wongwises, S. (2013). Performance characteristics of a microchannel heat sink using TiO 2/water nanofluid and different thermophysical models. *International Communications in Heat and Mass Transfer, 47*, 98-104.

Patel, H. E., Das, S. K., Sundararajan, T., Nair, A. S., George, B., & Pradeep, T. (2003). Thermal conductivities of naked and monolayer protected metal nanoparticle based nanofluids: Manifestation of anomalous enhancement and chemical effects. *Applied Physics Letters, 83*(14), 2931-2933.

Peng, Y., Shu, C., Chew, Y., & Qiu, J. (2003). Numerical investigation of flows in Czochralski crystal growth by an axisymmetric lattice Boltzmann method. *Journal of Computational Physics, 186*(1), 295-307.

Reis, T., & Phillips, T. N. (2008). Numerical validation of a consistent axisymmetric lattice Boltzmann model. *Physical Review E, 77*(2).

Sabir, R., Ramzan, N., Umer, A., & Muryam, H. (2015). An experimental study of forced convective heat transfer characteristic of gold water nanofluid in laminar flow. *Science International, 27*(1).

Salman, B., Mohammed, H., & Kherbeet, A. S. (2012). Heat transfer enhancement of nanofluids flow in microtube with constant heat flux. *International Communications in Heat and Mass Transfer, 39*(8), 1195-1204.

Sarkar, J., Ghosh, P., & Adil, A. (2015). A review on hybrid nanofluids: Recent research, development and applications. *Renewable and Sustainable Energy Reviews, 43*, 164-177.

Sheikholeslami, M., Gorji-Bandpy, M., & Ganji, D. (2013). Numerical investigation of MHD effects on Al 2 O 3–water nanofluid flow and heat transfer in a semi-annulus enclosure using LBM. *Energy, 60*, 501-510.

Shenoy, S., Tullius, J., & Bayazitoglu, Y. (2011). Minichannels with carbon nanotube structured surfaces for cooling applications. *International Journal of Heat and Mass Transfer, 54*(25), 5379-5385.

Sidik, N. A. C., & Razali, S. A. (2014). Lattice Boltzmann method for convective heat transfer of nanofluids–A review. *Renewable and Sustainable Energy Reviews, 38*, 864-875.

Solangi, K. H., Kazi, S. N., Luhur, M. R., Badarudin, A., Amiri, A., Sadri, R., ... & Teng, K. H. (2015). A comprehensive review of thermo-physical properties and convective heat transfer to nanofluids. *Energy, 89*, 1065-1086.

Tarokh, A., Mohamad, A., & Jiang, L. (2013). Simulation of conjugate heat transfer using the lattice Boltzmann method. *Numerical Heat Transfer, Part A: Applications, 63*(3), 159-178.

Tian, J., He, Z., Xu, T., Fang, X., & Zhang, Z. (2015). Rheological Property and Thermal Conductivity of Multi-walled Carbon Nanotubes-dispersed Non-Newtonian Nanofluids Based on an Aqueous Solution of Carboxymethyl Cellulose. *Experimental Heat Transfer* (in press).

Tsai, C., Chien, H., Ding, P., Chan, B., Luh, T., & Chen, P. (2004). Effect of structural character of gold nanoparticles in nanofluid on heat pipe thermal performance. *Materials Letters, 58*(9), 1461-1465.

Vafaei, S., & Wen, D. (2012). Convective heat transfer of aqueous alumina nanosuspensions in a horizontal mini-channel. *Heat and Mass Transfer, 48*(2), 349-357.

Verma, S. K., & Tiwari, A. K. (2015). Progress of nanofluid application in solar collectors: A review. *Energy Conversion and Management, 100*, 324-346.

Wang, J., Wang, M., & Li, Z. (2007). A lattice Boltzmann algorithm for fluid–solid conjugate heat transfer. *International Journal of Thermal Sciences, 46*(3), 228-234.

Yang, Y.-T., & Lai, F.-H. (2011). Numerical study of flow and heat transfer characteristics of alumina-water nanofluids in a microchannel using the lattice Boltzmann method. *International Communications in Heat and Mass Transfer, 38*(5), 607-614.

Zheng, L., Shi, B., Guo, Z., & Zheng, C. (2010). Lattice Boltzmann equation for axisymmetric thermal flows. *Computers and Fluids, 39*(6), 945-952.

Zhou, J. G. (2011). Axisymmetric lattice Boltzmann method revised. *Physical review E, 84*(3), 036704.

Zhou, M., Xia, G., Chai, L., Li, J., & Zhou, L. (2012). Analysis of flow and heat transfer characteristics of micro-pin fin heat sink using silver nanofluids. *Science China Technological Sciences, 55*(1), 155-162.

Zou, Q., & He, X. (1997). On pressure and velocity boundary conditions for the lattice Boltzmann BGK model. *Physics of Fluids (1994-present), 9*(6), 1591-1598.

Pertanika J. Sci. & Technol. 24 (2): 439 - 449 (2016)

SCIENCE & TECHNOLOGY

Journal homepage: http://www.pertanika.upm.edu.my/

Flapping Membrane Wing: A Prediction towards Inter-Domain Flight

Abas, M. F.[1], Aftab, S. M. A.[1], Rafie, A. S. M.[1], Yusoff, H.[2] and Ahmad, K. A.[1]*

[1]Department of Aerospace Engineering, Faculty of Engineering, Universiti Putra Malaysia, 43400 UPM Serdang, Selangor, Malaysia

[2]Faculty of Mechanical Engineering, Universiti Teknologi MARA Pulau Pinang, 13500 Permatang Pauh, Pulau Pinang, Malaysia

ABSTRACT

The purpose of this research is to gain initial knowledge and to predict the sustainability of an all-weather Micro-Aerial-Vehicle (MAV). The observed parameters are: the maximum coefficient of lift, C_L and the changes in C_L after impact, the fluctuation of C_L upon entering simulated rain environment, and length of stability recovery in terms of time and flapping cycle, t and t/T, at flapping frequencies of 8, 16, and 24 Hz, at t/T = 3/8 and 7/8. At 24 Hz, the increase in peak C_L value after impact of entering rain environment is 0.59. The average fluctuations in C_L occurred when entering the rain environment are 410.263. The stability recovery time recorded is 0.006 seconds. Small birds (especially hummingbirds) have a very high flapping frequency that enables them to efficiently withstand external disturbances caused by nature and to instantly adapt to new environments.

Keywords: Membrane wing, flapping, flat plate, inter-domain, flapping stability, simulated rain

INTRODUCTION

The DARPA (The Defense Advanced Research Projects Agency) defines Micro-Aerial-Vehicle (MAV)as an aerial vehicle that has; a maximum wingspan of 15cm. Producing a small size flapping vehicle inspired by biomimetics of birds has been a very challenging feat, even more when designing a flapping vehicle that has a size of an insect. There are a lot of factors and variables to consider, and a lot more to be discovered. As MAV has a very short wingspan, lift and thrust production are limited to the ability of the MAV's wings to manipulate airflow in its surroundings to counter any shortcomings.

Article history:
Received: 17 February 2016
Accepted: 22 April 2016

E-mail addresses:
firdausabas12@gmail.com (Abas, M. F.),
syedaftab2020@gmail.com (Aftab, S. M. A.),
shakrine@upm.edu.my (Rafie, A. S. M.),
ham_mid2003@hotmail.com (Yusoff, H.),
aekamarul@upm.edu.my (Ahmad, K. A.)
*Corresponding Author

ISSN: 0128-7680

External disturbance is also a potential factor in determining the reliability of a certain MAV, with larger concerns when attempting to achieve and produce an all-weather MAV (a MAV that could be operated under any weather condition).

One of the simplest ways to produce enough lift and thrust force for a very short wingspan is to reduce its aspect ratio (AR). Tsai and Fu (2005) have proven that a wing with AR of 3 can produce lift equivalent to a wing with AR of 8 given the right chord length and flight speed. Referring to the external disturbance factor, Warrick et al . (2005) discovered that hummingbird wing motion exhibits a figure-eight pattern and is highly adaptive to accommodate the challenges posed by wind gust. To top it off, AeroVironment (http://www.avinc.com/) uses a hummingbird-like flapping wing design that can withstand a 2 m/s wind gust from the side without drifting more than 1m.

On the other hand, Lee et al. (2011) discovered that longitudinal flight dynamics of a bio-inspired ornithopter with a reduced-order aerodynamics model and wing flexibility effects showed robustness towards external disturbances due to its trimmed flight dynamic characteristics. Niu et al. (2012), Lee et al. (2008), and Kim et al. (2005) conducted a preliminary study of three-dimensional aerodynamics, experimental evaluation of aerodynamic model, and a comparative study of rigid and flexible wing in flapping motion respectively. Combes and Dudley (2009) have discovered that bees have the ability to overcome external disturbances as well by means of wing-body interactions to regain aerodynamic stability. Lian et al. (2003) reported that the advantage of a flexible membrane wing is that it can adapt to wind gust and provide a smoother flight platform, which has been proven experimentally by Shyy et al. (1997). Furthermore, Shyy et al. (2013) have compiled all of his researches with a special subtopic addressing the effects of wind gust on hovering aerodynamics.

Limited research has been done on the other effects of external disturbances on flapping wing aerodynamics, such as rain, snow, and sandstorm due to the high complexity and difficulty of mimicking those environments and the vast amount of variables and unknowns to consider. The purpose of this research is to gain initial knowledge and to predict the sustainability of an all-weather MAV. In this research, a flat wing is simulated to flap through two different domains, from actual atmospheric air plunging through simulated “rainy” environment. An initial prediction on the effects of rain on flapping wing aerodynamic forces will be simulated by applying an assumption - rain environment is treated as modified water vapour environment with mixture density, ρ_{mix} and viscosity, μ_{mix}. The maximum coefficient of lift, C_L and the changes in C_L after impact, the fluctuation of C_L upon entering simulated rain environment, and length of stability recovery in terms of time and flapping cycle, t and t/T, will be observed for 8, 16, and 24 Hz flapping frequencies, *f*. The nomenclature associated in this research is shown in Table 1.

Table 1
Nomenclature

Symbol	Quantity	SI Units
$y(t)$	wing motion with respect to time	m
h_a	flapping amplitude	m
Fh	flapping oscillating frequency	Hz
T	time	s
φ_h	phase angle	°

[a]SI Units: s = seconds, m = meter, Hz = Hertz, ° = Degree angle

METHODOLOGY

Simulation Model

In this research, a rectangular flat plate wing has been considered for simplicity. The chord length of the wing, c is 5cm, the half wingspan length is 7.5cm, and the thickness is 0.03cm. The domain of the simulation is created using three-dimensional "C-mesh". The dimensions are 32.5c in length, 12.5c in width, and 25c in height. Two test domains were created, one with structured mesh "casing" to capture the boundary layer effects and increase the accuracy of the simulation as shown in Fig. 1a, and the other one without the structured mesh casing as shown in Fig. 1b. Both test domains have similar cell count; 633862 and 642544, with the former being the test domain with the structured mesh casing. The structured mesh casing has been set to move with the flapping motion of the membrane wing.

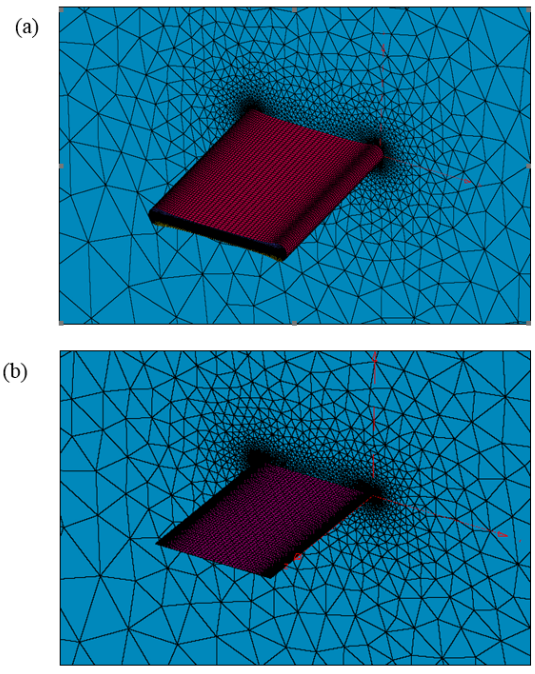

Figure 1. Membrane wing with structured mesh casing (a) and without structured mesh casing (b).

As shown in Figure 2, the movement of the structured mesh casing does not interfere with the pressure distribution on the wing and it has been observed that this domain produces faster simulation results compared with the one without the structured mesh casing by approximately one hour. The mesh was done using Pointwise V17.3R1 (2015) while simulation of the test domains were done using Ansys Fluent 15.0 (2013).

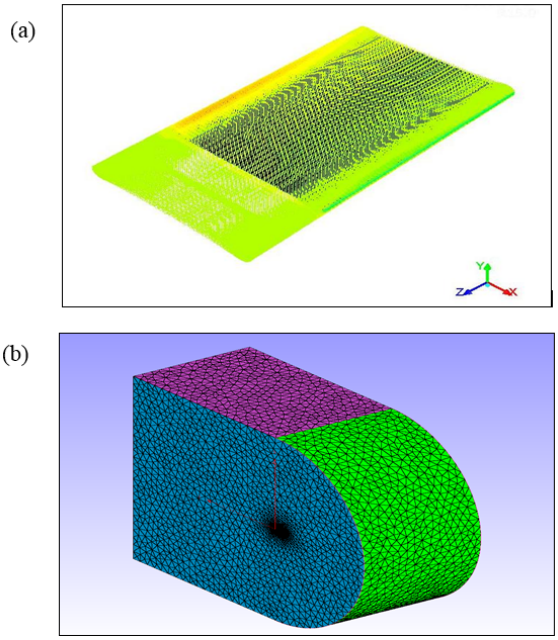

Figure 2. High pressure value at leading edge of membrane wing (a) and the 3D simulation domain (b).

The simulation was been done under unsteady (transient) conditions, utilising SIMPLE pressure-velocity coupling scheme, with pressure and momentum solver set to 2nd order upwind under spatial discretisation criteria. A simple harmonic function (pure flapping) was adopted for the membrane wing flapping motion.

$$y(t) = h_{\alpha}cos(2\pi f_h t+\varphi_h)$$

where h_{α} is the flapping amplitude (30˚) and is defined positive upwards, $2\pi f_h$ is the flapping angular frequency, f_h is the flapping oscillating frequency (8, 16, 24 Hz), and φ_h is the phase angle of the flapping motion (15˚). The flapping flight velocity was set to 10 m/s. The impact of rain environment will be initiated at two different instances, t/T = 3/8 and t/T = 7/8 as shown in Figure 3.

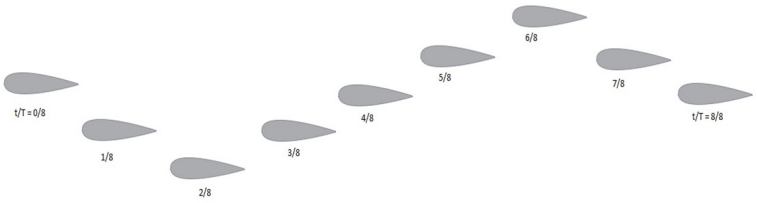

Figure 3. Visualisation of wingtip position viewed at normal of wingtip surface.

Validation of Model

The simulation of the flapping membrane wing in this research was validated using Tsai and Fu (2015) and Shi-Ming Huang (2004). Figure 4 below shows the comparison of the validation test case of the flapping membrane wing at 24 Hz flapping frequency. All calculations and comparisons are done with respect to the second flapping cycle to ensure optimum data accuracy.

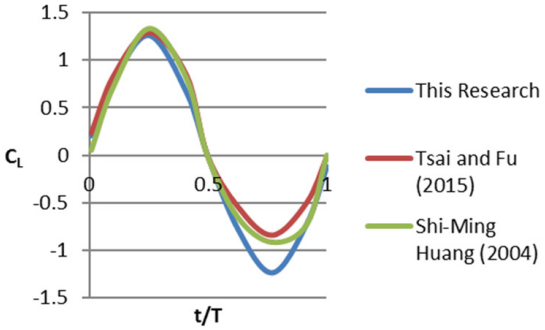

Figure 4. Validation case of flapping membrane wing at 24 Hz; this research, Tsai and Fu (2015), and Shi-Ming Huang (2004).

Rain Condition Prediction

To mimic a rainy environment, an assumption was made; rain particles were treated as modified water vapour particles with mixture density, ρ_{mix} and viscosity, μ_{mix}, since no published method or equation is currently available dedicated solely on calculating the actual density and viscosity of rainy atmosphere. Therefore, the following equations, as proposed by Davidson (1993) and Brokaw (1968), will be used to predict the density and viscosity of dry air-water vapour mixture:

$$D = \left(\frac{P}{Rd * T}\right)\left(1 - \frac{0.378 * Pv}{P}\right)$$

where

D = Density
P = Pd + Pv = Total air pressure
Pd = Pressure of dry air
Pv = Pressure of water vapour
$7Rd$ = Gas constant for dry air = 287.05 J/kg˚K
$7T$ = Temperature = 288.15 ˚K

Pressure of water vapour, Pv can be obtained using the following equation:

$$Es = c0\left(10^{\frac{c1*Tc}{c2+Tc}}\right)$$

where
As = Saturation pressure of water vapour
Tc = Temperature in ˚C
c0 = 6.1078
c1 = 7.5000
c2 = 237.3000

To predict the viscosity of dry air-water vapour mixture, the following equation was adopted:

$$\mu_{mix} = x_{dry\ air}\mu_{dry\ air} + x_{water\ vapor}w_{ave\ vapour}$$

where
μ_{mix} = viscosity of dry air-water vapour mixture
$x_{dry\ air}$ = mole fraction of dry air
$x_{water\ vapour}$ = mole fraction of water vapour
$\mu_{dry\ air}$ = viscosity of dry air
$\mu_{water\ vapour}$ = viscosity of water vapour

Using all the equations above, the value of dry air-water vapour mixture's density, ρ_{mix} will be set to 1.2378 kgm^{-3} and the value of dry air-water vapour mixture's viscosity, μ_{mix} will be set to $1.597x10^{-5}$ *kgm-1s-1*.

RESULTS AND DISCUSSION

Maximum coefficient of lift, C_L before and after impact

In this research, the maximum achievable coefficient (peak value) of lift, C_L during upstroke and downstroke was observed for membrane wing with flapping frequency of 8 Hz, 16 Hz, and 24 Hz, before and after the impact of crossing from atmospheric air into the simulated rain environment. The peak CL for all three of the flapping wing frequencies is as shown in Figure 5.

For flapping frequency of 8 Hz, the peak C_L value stabilises at an average value of ±0.405 and for flapping frequency of 16 Hz, the peak C_L value stabilises at an average value of ±0.891. Meanwhile for flapping frequency of 24 Hz, the peak C_L value stabilises at an average value of ±1.266. These peak C_L values achieved stability after the second flapping cycle within the air domain before entering the simulated rain domain. As mentioned in the methodology section above, peak C_L values are taken from the second flapping cycle to ensure optimum accuracy. These stabilised peak C_L values agree with the simulation results produced by Tsai and Fu (2015) and Shi-Ming Huang (2004).

After entering the rain environment and immediately after the peak C_L values regained stability, a slight increase in peak C_L values for all three flapping frequencies was observed.

At t/T = 3/8 impact position, an increase of peak C_L values of approximately 0.21, 0.53, and 0.56 were observed at 8, 16, and 24 Hz respectively. Meanwhile at t/T = 7/8 impact position, a slightly larger increase in peak C_L values were recorded as compared to the increase in peak C_L values at t/T = 3/8, which yielded an increase of peak C_L values of approximately 0.23, 0.57, and 0.62 at 8, 16, and 24 Hz respectively.

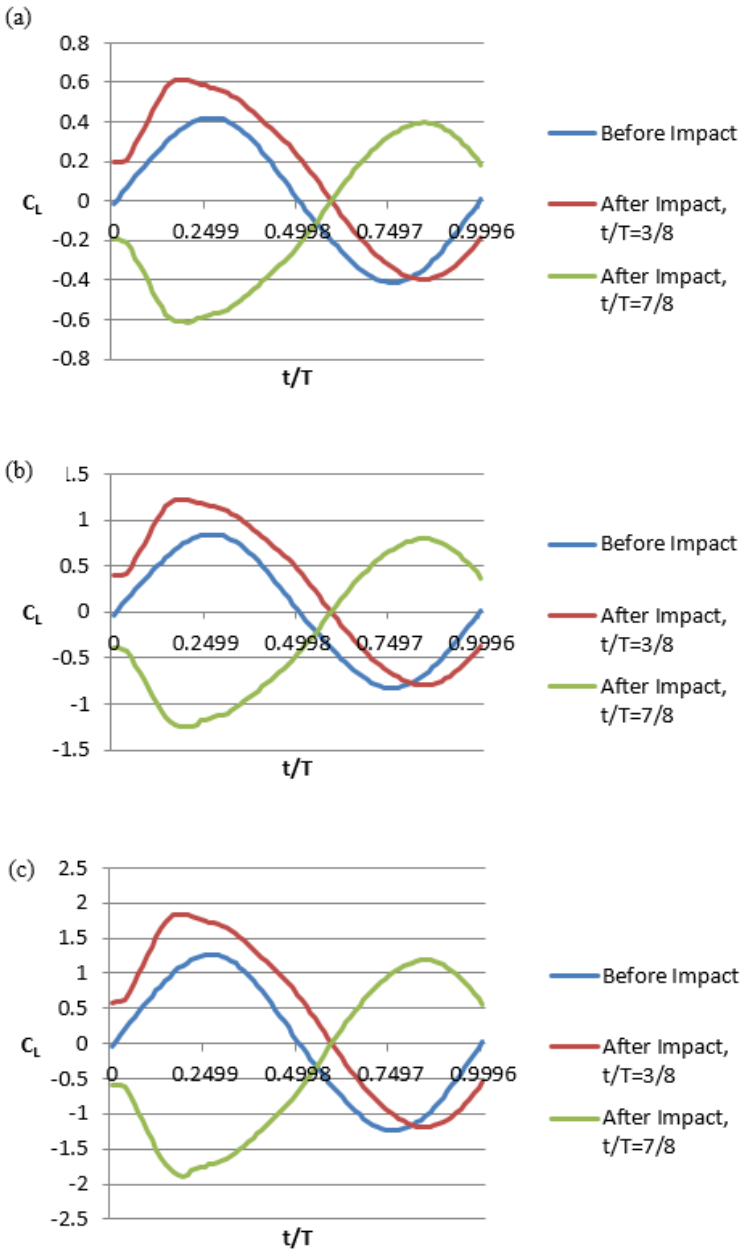

Figure 5. Peak C_L before and after impact of rain environment; 8 Hz (a), 16 Hz (b), 24 Hz (c)

Impact of rain domain

The effects of rain domain are applied at the t/T = 3/8 and t/T = 7/8 positions. Figure 6 a-c shows the fluctuations of C_L that occur upon impact at the boundary between air domain and rain domain. The maximum fluctuations of C_L are recorded for flapping frequency on 8, 16 and 24 Hz.

At t/T = 3/8, C_L fluctuation that occurred at flapping frequency of 8 Hz reached up to 140.505, which is more than 346 times the maximum value of stabilised C_L. For flapping frequency of 16 Hz, C_L fluctuated up to 261.031 and flapping frequency of 24 Hz recorded C_L fluctuation up to 409.522, which was more than 292 and 323 times the maximum value of stabilised C_L for 16 Hz and 24 Hz respectively.

At t/T = 7/8, it can be observed that the maximum value of C_L fluctuations is similar to its t/T = 3/8 position counterpart. Flapping frequency of 8 Hz recorded a maximum value of C_L fluctuation of up to -140.997 ("-" sign indicates downstroke direction). Meanwhile flapping frequencies of 16 Hz and 24 Hz recorded a maximum value of C_L fluctuation of up to -260.374 and -411.003 respectively. Therefore, we can safely assume that the values C_L fluctuation at t/T = 7/8 are the same in magnitude with t/T = 3/8 (less than 10 percent difference) but in different direction (caused by upstroke and downstroke motions).

It is observed that fluctuations occurred more than a 100 folds more than the recorded stabilised C_L. With this much amplification of peak C_L, aerodynamic instability will definitely occur during the flapping flight. The fluctuation of peak C_L only happens within a narrow time frame of 0.0035 to 0.0195 seconds. Within that short window of opportunity, a flapping wing MAV must be able to adapt and regain aerodynamic stability in order to maintain air superiority.

Stability Recovery

As mentioned in the previous section, a flapping wing MAV needs to be able to adapt towards any form of peak C_L fluctuations within an instance to maintain aerodynamic stability. It is important for us to understand and estimate the period of time a flapping wing MAV takes to regain stability of its flapping wing peak C_L value in order to produce a sustainable all-weather MAV. As shown in Figure 7a-b, the length of stability recovery in terms of time and flapping cycle, t and t/T, are observed for 8, 16, and 24 Hz flapping frequencies at t/T = 3/8 and t/T = 7/8 impact positions.

At impact position t/T = 3/8, a flapping membrane wing that flaps at 8 Hz recovers its stabilised peak C_L value in 0.016 seconds, which is equivalent to 1.375 flapping cycle where as a flapping wing that flaps at 16 Hz recovers its stabilised peak C_L value in 0.011 seconds, which is equivalent to 1.4375 flapping cycle. Flapping at 24 Hz, a flapping membrane wing recovers its stabilised peak C_L value in 0.006 seconds, which is equivalent to 1.625 flapping cycle.

At impact position t/T = 7/8, the time and flapping cycle taken by a flapping membrane wing that flaps at 8 Hz, 16 Hz, and 24 Hz to recover stabilised peak C_L values are equivalent to its counterpart at impact position t/T = 3/8. With this results, we can conclude that a flapping wing MAV that flaps at 24 Hz is able to adapt to the impact of entering the simulated rain environment the fastest with only 0.006 seconds of recovery time.

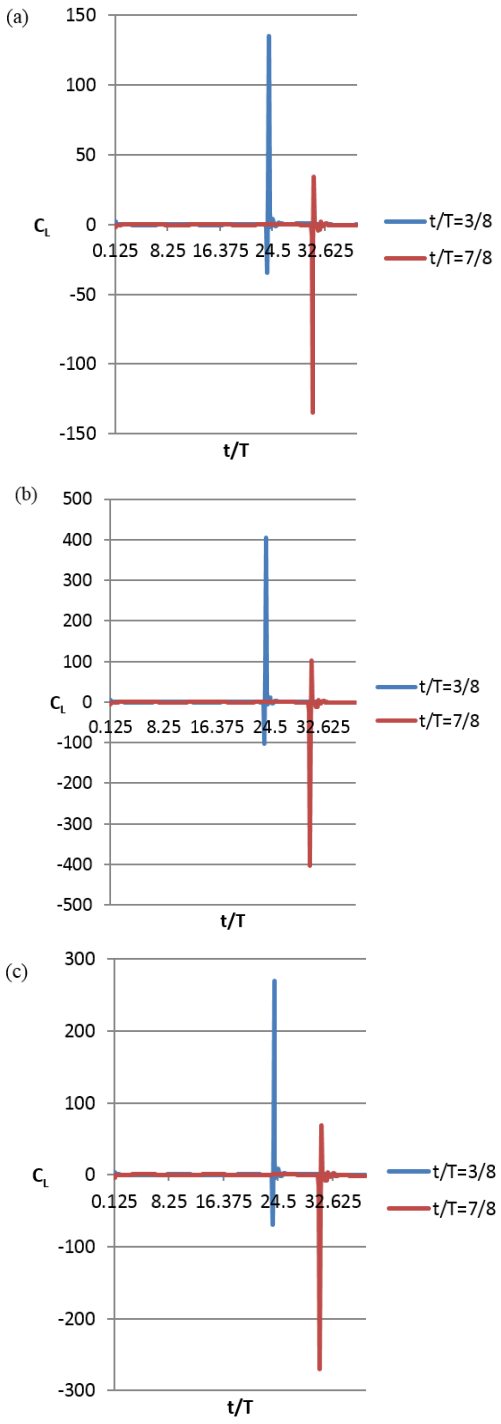

Figure 6. Fluctuation at 8 Hz (a), 16 Hz (b), and 24 Hz (c)

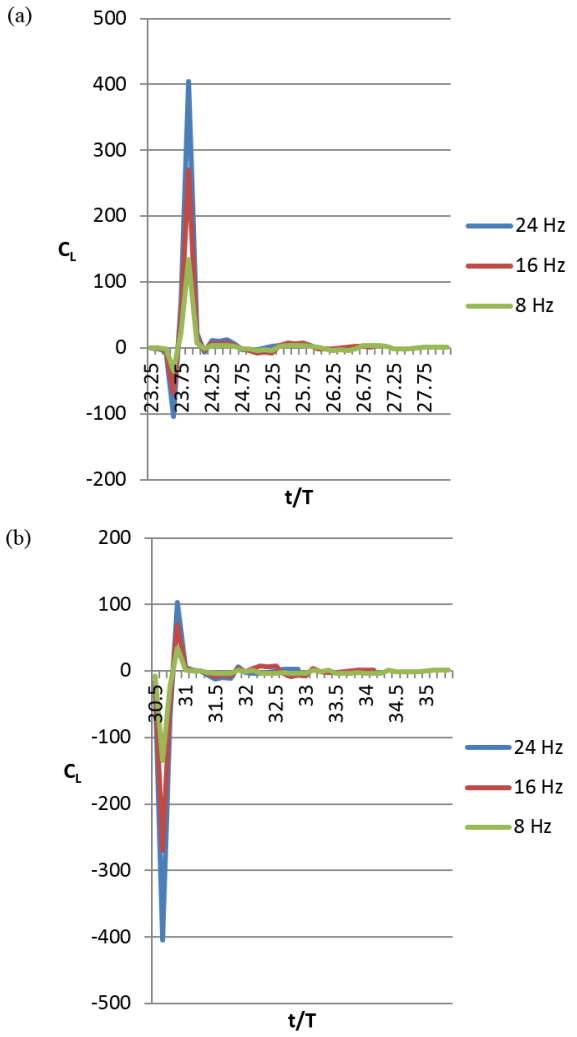

Figure 7. Stability recovery period at t/T = 3/8 (a) and t/T = 7/8 (b) at 8 Hz, 16 Hz, and 24 Hz

CONCLUSION

In this research, a flapping membrane wing has undergone impact of inter-domain flight from atmospheric air into a simulated rain environment at an impact position of t/T = 3/8 and 7/8. Three flapping frequencies, 8 Hz, 16 Hz, and 24 Hz have been considered for this research. As a conclusion, at 8 Hz flapping frequency, the increase in peak C_L value after impact of entering rain environment is the lowest among the three flapping frequencies, which is only by an average of 0.22. The fluctuations that occurred are also the lowest among the three flapping frequencies, up to an average of 140.751. At 8 Hz flapping frequency, the stability recovery time recorded is 0.016 seconds, which is the longest stability recovery time among the three flapping frequencies.

At 24 Hz flapping frequency, the increase in peak C_L value after impact of entering rain environment is the highest, which is by an average of 0.59. The fluctuations that occurred are also the highest, up to an average of 410.263. At 24 Hz flapping frequency, the stability recovery time recorded was 0.006 seconds, which is the shortest stability recovery time among the three flapping frequencies. The results of this research can very well explain as to why small birds (especially hummingbirds) have a very high flapping frequency. It is to enable them to efficiently withstand external disturbances caused by nature and to instantly adapt to new environments.

REFERENCES

Brokaw, R. S. (1968). *Viscosity of Gas Mixtures* (Report No. NASA TN D-4496). Washington D. C.: National Aeronautics and Space Administration.

Combes, S. A., & Dudley, R. (2009). Turbulence-driven instabilities limit insect flight performance. *Proceedings of the National Academy of Sciences, 106*(22), 9105-9108..

Davidson, T. A. (1993). *A Simple and Accurate Method for Calculating Viscosity of Gaseous Mixtures* (Report No. RI9456). USA: Bureau of Mines.

Huang, S. M. (2004). *Numerical simulation of flow over a flapping wing* (Doctoral dissertation). National Cheng Kung University, Tainan City, Taiwan.

Kim, Y. J., Choi, H. C., & Kim, K. H. (2005). The comparative study of rigid wing and flexible wing in flapping motion. *AIAA Atmospheric Flight Mechanics Conference and Exhibit*, Paper No. 2005-6336.

Lee, J. S., Kim, D. K., Lee, J. Y., & Han, J. H. (2008). Experimental evaluation of a flapping-wing aerodynamic model for MAV applications. *SPIE 15th Annual Symposium Smart Structures and Materials*, *6928*(69282M), 1-8.

Lee, J. S., Kim, J. K., Kim, D. K., & Han, J. H. (2011). Longitudinal flight dynamics of bioinspired ornithopter considering fluid-structure interaction. *Journal of Guidance, Control, and Dynamics*, *34*(3), 667-677.

Lian, Y., Shyy, E., Viieru, D., & Zhang, B. (2003). Membrane wing aerodynamics for micro air vehicles. *Progress in Aerospace Sciences*, *39*(6), 425-465.

Niu, Y. Y., Liu, S. H., Chang, C. C., & Tseng, T. I. (2012). A preliminary study of the three-dimensional aerodynamics of flapping wings. *Journal of Applied Science and Engineering*, *15*(3), 257-263.

Shyy, W., Aono, H., Kang, C. K., & Liu, H. (2013). *An Introduction to Flapping Wing Aerodynamics*. New York, NY: Cambridge University Press.

Shyy, W., Jenkins, D. A., & Smith, R. W. (1997). Study of adaptive shape airfoils at low Reynolds number in oscillatory flow. *American Institute of Aeronautics and Astronautics Journal*, *35*(9), 1545-1548.

Tsai, B. J., Fu, Y. C. (2005). Design and aerodynamic analysis of a flapping-wing micro aerial vehicle. *Aerospace Science and Technology*, *13*(7), 383-392.

Warrick, D. R., Tobalske, B. W., & Powers, D. R. (2005). Aerodynamics of the hovering hummingbirds. *Nature, 435*(7045), 1094-1097.

Pertanika J. Sci. & Technol. 24 (2): 451 - 463 (2016)

PERTANIKA JOURNALS

SCIENCE & TECHNOLOGY

Journal homepage: http://www.pertanika.upm.edu.my/

CFD Investigation of Transonic Axial Compressor Rotor Blade at Various Off-Design Conditions

Pauline Epsipha*, Mohammad, Z. and Kamarul, A. A.

Department of Aerospace Engineering, Engineering Faculty, Universiti Putra Malaysia, Selangor, 43400, Selangor, Malaysia

ABSTRACT

Flow separation over blade surfaces is an important parameter and its reduction or elimination can improve better aerodynamic performance, efficiency and stall margin. In this work, numerical investigation has been carried out to study the flow separation and performance analysis of a transonic axial compressor rotor blade at off-design operating conditions. The off-design cases studied comprised of compressor operation at 80%, 90%, 100% and 105% on the on-design rotational speed. The results are validated with experimental work from literature. Additionally, 3D flow visualisations and performance parameters were examined in detail to understand the blade to blade relative mach number distributions and shock front created by the model. Finally, the benefits of unsteady simulation on axial compressor blade performance predictions were examined.

Keywords: Compressor rotor blade, Numerical investigation, Flow separation, Off-design cases, Shock front, Efficiency

INTRODUCTION

In recent years, in the field of turbo machinery and aero-engine, transonic axial flow compressors have played important role to attain higher pressure ratios which help in increasing the efficiency and reducing the size and weight of the engine. The increase in pressure ratio at every single stage of compressor counts the reciprocating results on operational and fuel cost. Thus, progress in the performance chart of the compressors plays a crucial part in research as well engine manufacturing.

The flow field which progresses inside a transonic axial compressor is particularly complicated and puts forth huge challenges on compressor designers. Critical flow challenges such as secondary flows, shock waves, shock/

Article history:
Received: 17 February 2016
Accepted: 22 April 2016

E-mail addresses:
paul.totty89@gmail.com (Pauline Epsipha),
mzuber@upm.edu.my (Mohammad, Z.),
aekamarul@upm.edu.my (Kamarul, A. A.)
*Corresponding Author

ISSN: 0128-7680

boundary layer interactions, and flow separation over the blade surfaces decrease the efficiency and encourage energy losses (Cumpsty, 1989; Law & Wadia, 1993; Denton & Xu, 1998).

Various experimental and numerical investigations of transonic compressors have been carried out since 1960 (Chen et al., 1991; Freeman & A., 1992). As transonic compressors paved the way for investigation over supersonic compressors, various researches of its kind have been conducted over the past decades. A significant number of researches were carried out for new development in design (Reid & Moore, 1978; Strazisar, 1985), which in turn gave a wider perspective over the loss mechanisms (Strazisar, 1985; Hah & Reid, 1991). These deeper understanding later emerged as concepts for active and passive techniques to decrease the loss (Cumpsty, 1989; Denton & Xu, 1998; Calvert et al., 2003) and increase the efficiency and stall margin.

According to Biollo (Biollo & Benini, 2013), in transonic axial flow compressors, the typical value achieved for the rotor inlet relative flow at the tip is Mach = 1.3. And the total pressure ratio achieved for high efficiency transonic axial flow compressors (civil aviation) is in the order of 1.7-1.8 along with the tip speed of 450 m/s and high stage loading in the order of 1.0. Despite a decade of research on it, the concept of further performance enhancement in transonic compressor is still under investigation.

The primary goal of this research is to investigate the flows within the transonic axial flow compressor rotor blade across a wide range of off-design operating conditions. The off-design cases studied comprised compressor operation at 80%, 90%, 100% and 105% at on-design rotational speed. The opportunity to study the flow separation and performance of rotor blade would provide a broad understanding of its reduction/elimination capacity and thereby improve efficiency and stall margin.

NASA ROTOR 37

The NASA rotor 37 is an isolated low aspect ratio inlet rotor for an axial core compressor. This rotor is a transonic compressor with a tip speed of 454 m/s and produces a relatively high pressure ratio of 2.1 (Denton, 1997). This 'blind' test case study is widely used in many research programmes, which intends to study the flow and aerodynamic parameters at transonic speed level. Initially, it was designed and tested at NASA lewis research centre without any inlet guide vanes for four related axial flow compressor stage. These stages were tested for a wide range of design parameters especially aspect ratio and pressure ratio by Reid and Moore (1978). A more detailed performance parameters of this rotor 37 were reported by Reid and Moore (1980, 1982). The rotor was again tested in a single-stage compressor facility at NASA Glenn by Suder (Kenneth & Celestina, 1996; Kenneth, 1997; Suder et al. 1995) and by various researchers. Table 1 shows the design parameters for the Rotor 37 and Figure 1 shows the meridional view of NASA Rotor 37 (Benini et al., 2011).

Table 1
Aerodynamic design parameters

Number of blades	37
Blade type	Multiple Circular Arc
Rotational Speed	17188.7 rpm
Inlet hub-tip diameter ratio	0.7
Blade aspect ratio	1.19
Tip solidity	1.29
Tip clearance	0.0356 cm (0.45% of blade span)
Tip speed	454 m/s
Adiabatic efficiency	0.877
Design pressure ratio	2.106
Design mass flow rate	20.19 kg/s
Choked mass flow rate	20.93 kg/s

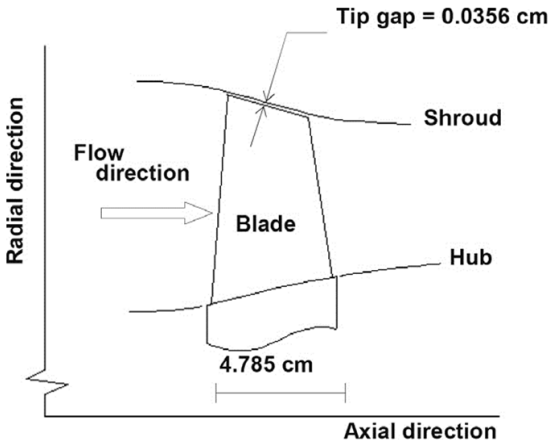

Figure 1. Meridional view of NASA Rotor 37 (Benini et al., 2011)

TURBULENCE THEORY

Navier–Stokes equations

The Navier-Stokes equations describing the flow of compressible gases are a non-linear set of partial-differential equations (PDEs) governing the conservation of mass, momentum and energy of the gaseous motion.

The conservation of mass equation (Continuity Equation) in tensor notation can be formulated as:

$$\frac{\partial \rho}{\partial t} + \frac{\partial}{\partial x_i}\left(\rho\, u_i\right) = 0$$

where ρ and u_i are gas density and flow velocity respectively. In tensor notation, the momentum equation that represents the Navier-stokes equation is:

$$\frac{\partial}{\partial t}(\rho u_i) + \frac{\partial}{\partial x_j}(\rho u_i u_j + p\delta_{ij} - \tau_{ij}) = \rho f_i$$

where *P* and τ_{ij} are gas pressure and mean rate of stress tensor respectively and f_i is the acceleration of the gas due to body forces.

Reynolds-averaged Navier–Stokes (RANS) equations

The Reynolds-averaged Navier–Stokes (RANS) equations are the oldest form of time averaged equation for turbulence modelling. In turbulent flow, even in a steady state, all the variables tend to fluctuate with time. Reynolds (1895) introduced the idea that the turbulent flow total variable (U) can be expressed as the sum of the mean ($\bar{u}$) and fluctuating variable (u'). The $\bar{u}$ (overbar) represents the time averaged quantity as:

$$U(t) = \bar{u} + u'(t)$$

This decomposition equation can be substituted for all the variables in the flow (u, v, w, P, ρ). RANS describing the time-evolution of the mean flow quantities Ui and P can be written as:

$$\frac{\partial U_i}{\partial t} + Uj\frac{\partial U_i}{\partial x_j} + \frac{1}{\rho}\frac{\partial P}{\partial x_i} = \frac{1}{\rho}\frac{\partial}{\partial x_j}(\bar{\tau}_{ij} + \lambda_{ij})$$

where $\bar{\tau}_{ij}$ is fluid stress tensor which is evaluated in terms of the mean flow quantities and λ_{ij} is the Reynolds or turbulent stress tensor which is given as:

$$\lambda_{ij} = -\rho\overline{u'_\iota u'_\jmath}$$

Shear-Stress Transport model

Predicting the flow separation from a smooth surface is considered as one of the main issues in turbulence modelling. Standard two equations do not have the capability to predict the amount of flow separation under adverse pressure gradient conditions. Hence, several advanced turbulence models were developed for this application. One such model is known as Shear Stress Transport (SST) turbulence model, which is a combination of k-ε and k-ω models.

The turbulence model used in this computation is k-ω based Shear-Stress-Transport (SST) model which was designed to give a highly accurate prediction of the onset and the amount of flow separation under adverse pressure gradients by the inclusion of transport effects into the formulation of the eddy-viscosity. This results in a major improvement in terms of flow separation predictions.

The turbulent eddy viscosity is computed from the turbulent kinetic energy and turbulent frequency as:

$$\mu_T = {}^{\rho k}/_{\omega}$$

METHODOLOGY

A steady state simulation was carried out for 80, 90, 100 and 105% design speed of the rotor 37 using ANSYS CFX and the resultant flow field was further investigated along with an overall performance map. The results obtained from the numerical analysis were compared with the experimental data for validation purposes. It should be noted that no stage approach has been carried out but only a rotor was used in the frozen approach.

Modelling and Mesh Generation

The data points for the rotor model and the computational domain were collected as a .curve and .inf (bladegen files), where it is interlinked to the ANSYS Turbo grid meshing tool. Figure 2 shows the 3D model of the rotor along with the flow domain in the entire compressor. The meshing of the domain with blade is made using ANSYS Turbo grid package. *y*+ value for the generated mesh near the wall zones are maintained at 2 which is as per the turbulence modelling requirements. Thus, the discretisation of the structured grid with around 1,800,000 cells was generated. A single passage simulation is modelled and numerically solved with an assumption that the flow is periodic within the passage. Figure 3 shows the picture of discretised rotor model with flow domain.

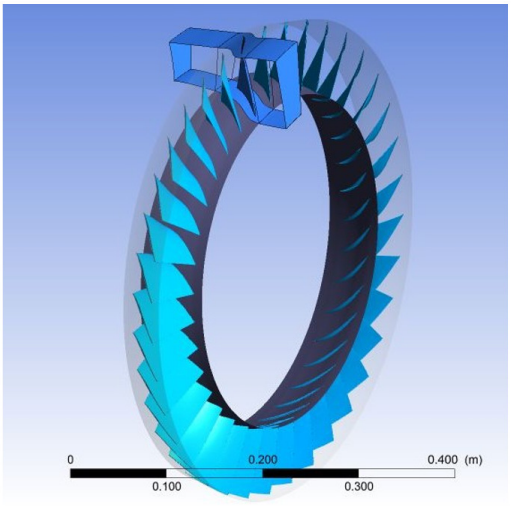

Figure 2. Rotor alone model

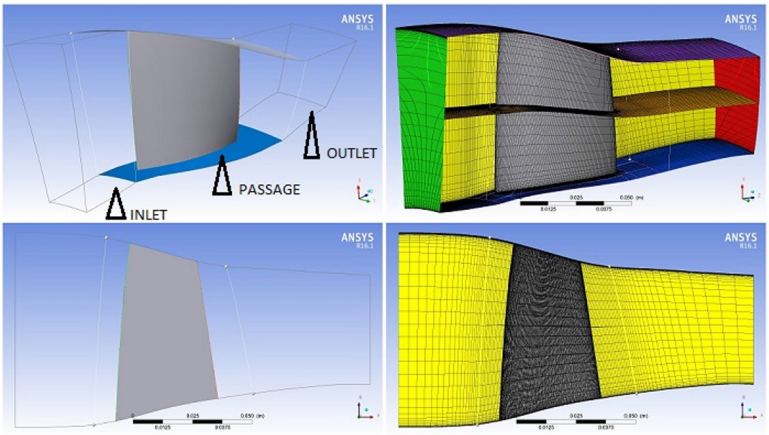

Figure 3. Meshed Rotor model

Flow Analysis

The flow analyses were carried out using a commercial CFD package. The ANSYS CFX executes 3D Reynolds-averaged Navier-stokes equations based on the finite volume numerical method. The flow fluid was assumed to be an Ideal gas, having constant specific heats. K-ω Shear Stress Transport (SST) turbulence model was equipped for the present study which is governed by adverse pressure gradients. This model is not able to capture the fine vortex micro structures development We neglect the necessity as it is not of primary concern. To confirm that results are independent of the mesh, grid dependency tests were carried out for Y+ values as 1, 2, 5 and total of around 1,800,000 cells were taken into account for the final domain.

The walls of the domain were assumed to be adiabatic and hydraulically smooth which is specified as no slip condition. It indicates that the fluid sticks to the wall and moves with the same velocity as the wall (if it is moving). For validation purposes, calculations were run at the design speed of the rotor (1800 rad/s). The boundary conditions of total pressure and total temperature were imposed at the inlet (P_{inlet} = 101330 Pa, T_{inlet} = 288.15 K) to recreate the experimental boundary conditions.

As an outlet condition, the static pressure was imposed as a mass-averaged value, in order to find the Design mass flow and choked mass flow condition at On-design speed. The turbulent intensity was fixed to a 5% value. The rotor was run at frozen rotor condition in order to make a smooth flow inside the domain. For every steady simulation, the convergence criteria (RMS residuals) was inflicted as 1 x 10^{-6}. Figure 4 shows the boundary conditions applied to the flow domain.

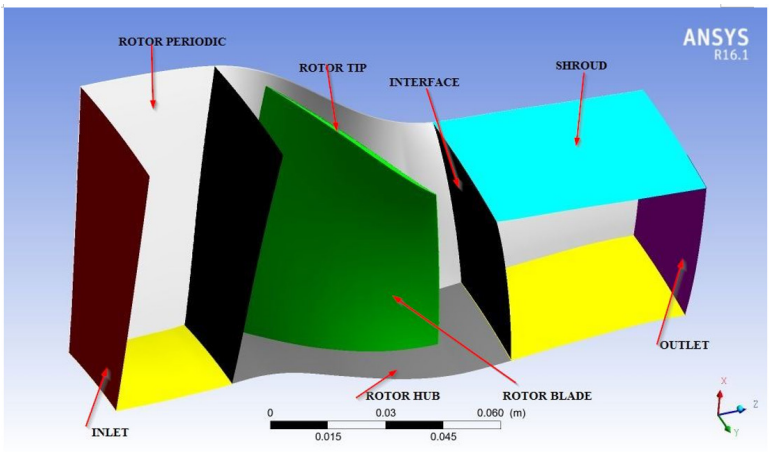

Figure 4. Flow domain boundary conditions.

Validation of Numerical Results

Validation processes were carried out upon the on-design rotor speed (1800 rad/s) and the numerical results were plotted against experimental results of baseline compressor performance extracted from Suder et al. (1995). The primary performance measure investigated is total pressure ratio which is ratio between exit pressure and inlet pressure. Figure 5 shows graph for total pressure ratio and adiabatic efficiency against the various mass flow rate condition. The percentage error calculated were 1.24% and 1.61%. Through the plotted graph, it is witnessed that computed results which are below than 5% are in good agreement with the experimental data at on-design speed.

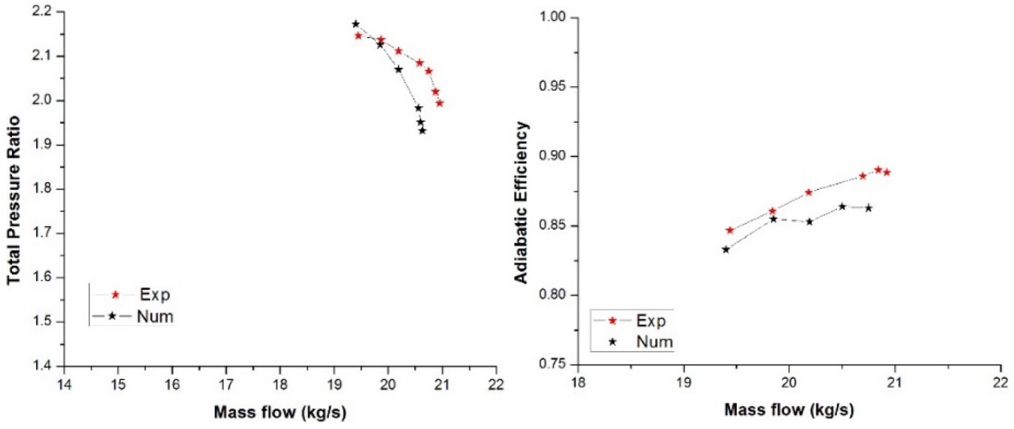

Figure 5. Performance characteristics of design speed (1800rad/s)

RESULTS AND DISCUSSION

The comparative performance map of the baseline compressor at on- design speed and off-design speed is shown in Figure 6. Total pressure ratio and adiabatic efficiency against the mass flow rate were plotted in the performance map below. The red plots indicate experimental case results while the black plots indicate the numerical case of the baseline rotor. As the on-design speed is validated properly with a percentage error of 1.24% and 1.61%, the off-design speed of 90% experimental values were ignored. It is monitored that among the off/on design conditions, the flow follows the consistent patterns and the highest efficiency occurred at on-design speed. The flow physics of the compressor rotor for different off-design conditions were studied using velocity vectors, mach number contours and velocity streamlines as mentioned below.

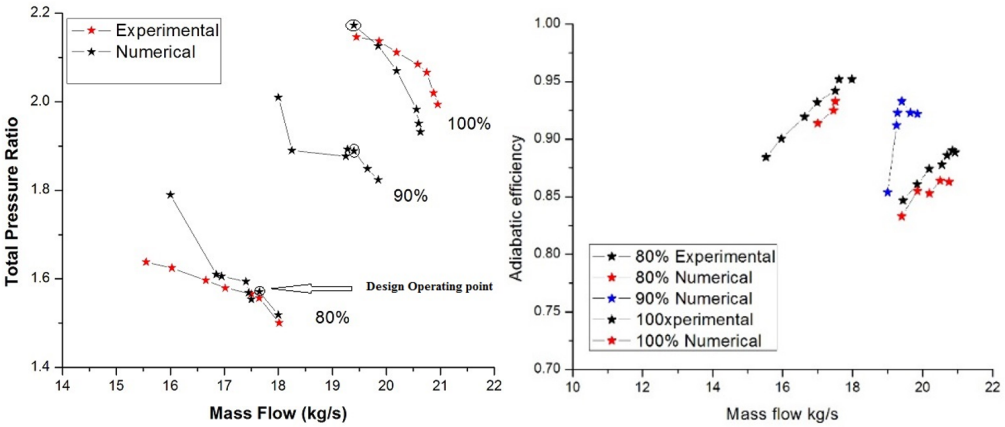

Figure 6. Overall Performance characteristics

Mach number

Figure 7 shows the comparative mach number contours computed along the on-design speed and varied off design conditions. Concerning the calculated flow field, the plots were computed at 70% span blade to blade mach number. It is observed that a strong shock front was created and flow separation was combined along the flow at the suction side of the rotor blade at 100% and 105% design speed. While in the 90%, the formation of shock and flow separation region was much weaker compared to previous flows.

In 80% design speed, the flow was much smoother and flow separation was almost unnoticed. With the help of a well captured model, the reduction in shock strength is seen to directly affect the pressure ratio reduction which disturbs the efficiency of the compressor rotor. It also indicates the fact that blade boundary layer and its interaction have been properly captured by the numerical simulation. Table 2 indicates the relative inlet mach number for each speed.

Table 2
Variation of Inlet Mach number for various speed

% speed	M_{rel} at hub	M_{rel} at tip
80	0.91	1.15
90	0.94	1.29
100	1.02	1.33
105	0.97	1.45

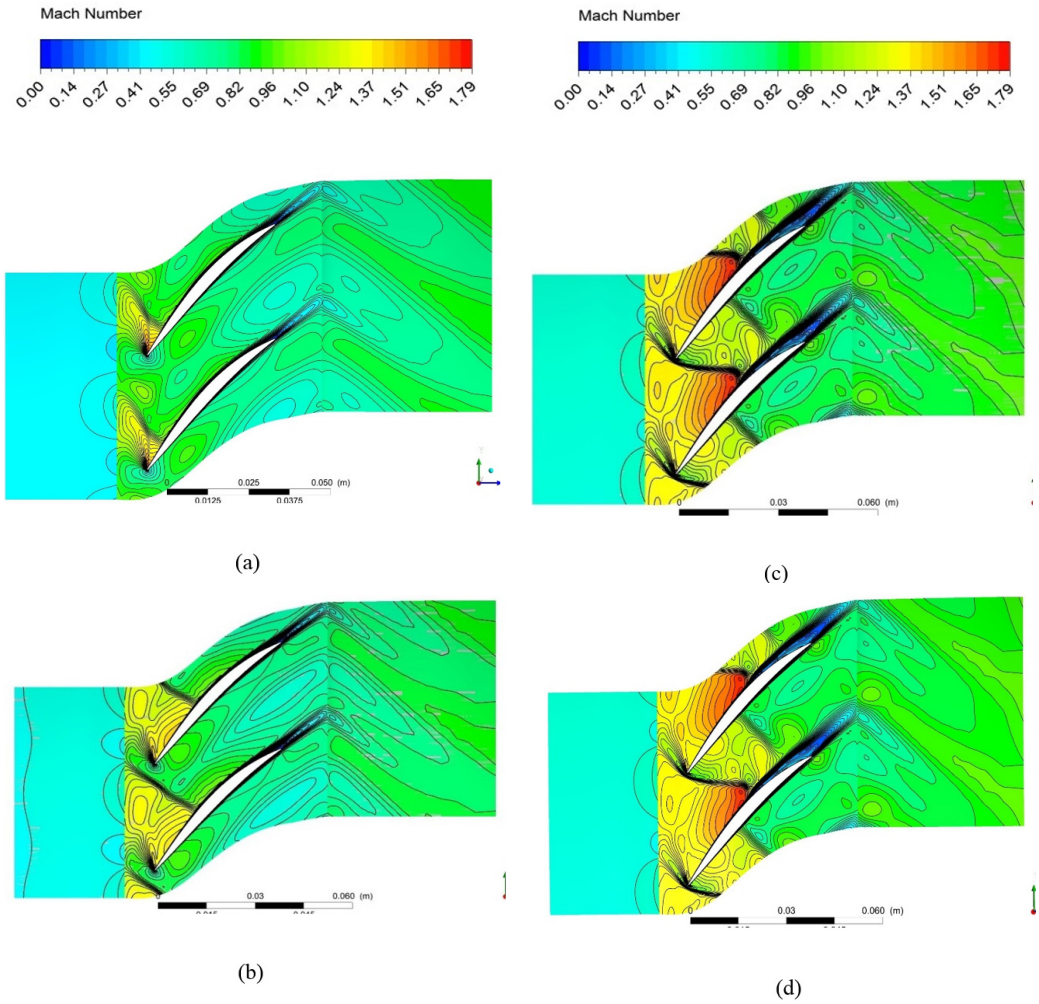

Figure 7. Comparative Mach number contours at 70% span at various off design conditions, (a) 80% (b) 90% (c) 100% (d) 105%

Velocity

Figure 8 displays the comparative velocity vector plots for peak efficiency condition at baseline rotor's on/off design compressor speed. Vector plots are plotted at the 95% span of blade to blade view for the velocity distribution over the different operating conditions. As shown in the contour, high velocity is observed at the inlet condition which produces shock front where

it gets reduced from the blade surface at trailing edge because of the flow separation. Though there is a difficulty to produce the well-defined tip clearance vortex pattern, its shock interaction with the flow is captured reasonably well.

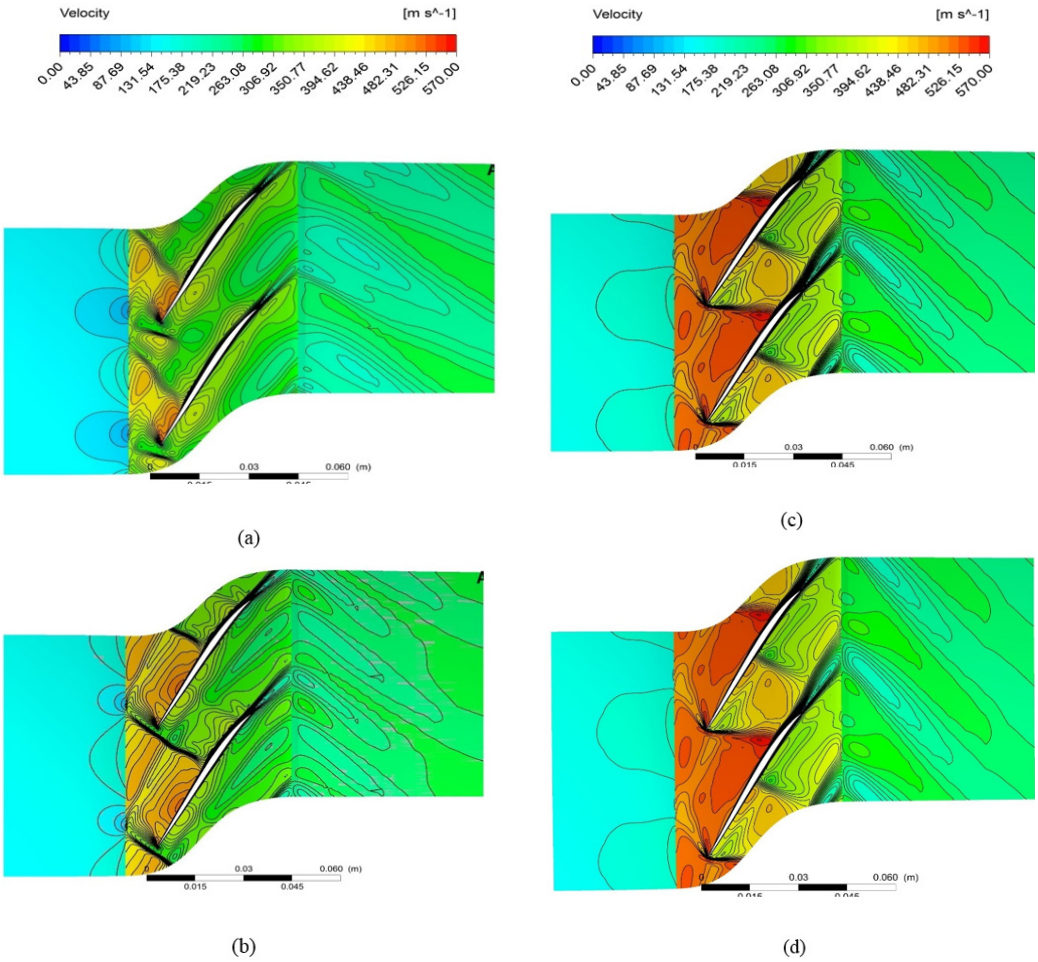

Figure 8. Comparative Velocity plot at 95% span at Various off design conditions, (a) 80% (b) 90% (c) 100% (d) 105%

Streamline

Figure 9 shows the comparative detailed streamline patterns in suction side of the rotor for various design speed at maximum efficiency condition. The streamlines discharged from the leading edge and the separation line are created at the suction side boundary. The 3D streamline patterns indicate fairly well the internal flow conditions created at suction of the rotor span. A form of flow disruption were created because of the shock and the flow separation near the trailing edge which were also captured in the blade to blade mach number contour as seen in Figure 7. Also for the off-design condition at maximum efficiency state, clearly reveals that there is less flow separation created compared with the on-design speed.

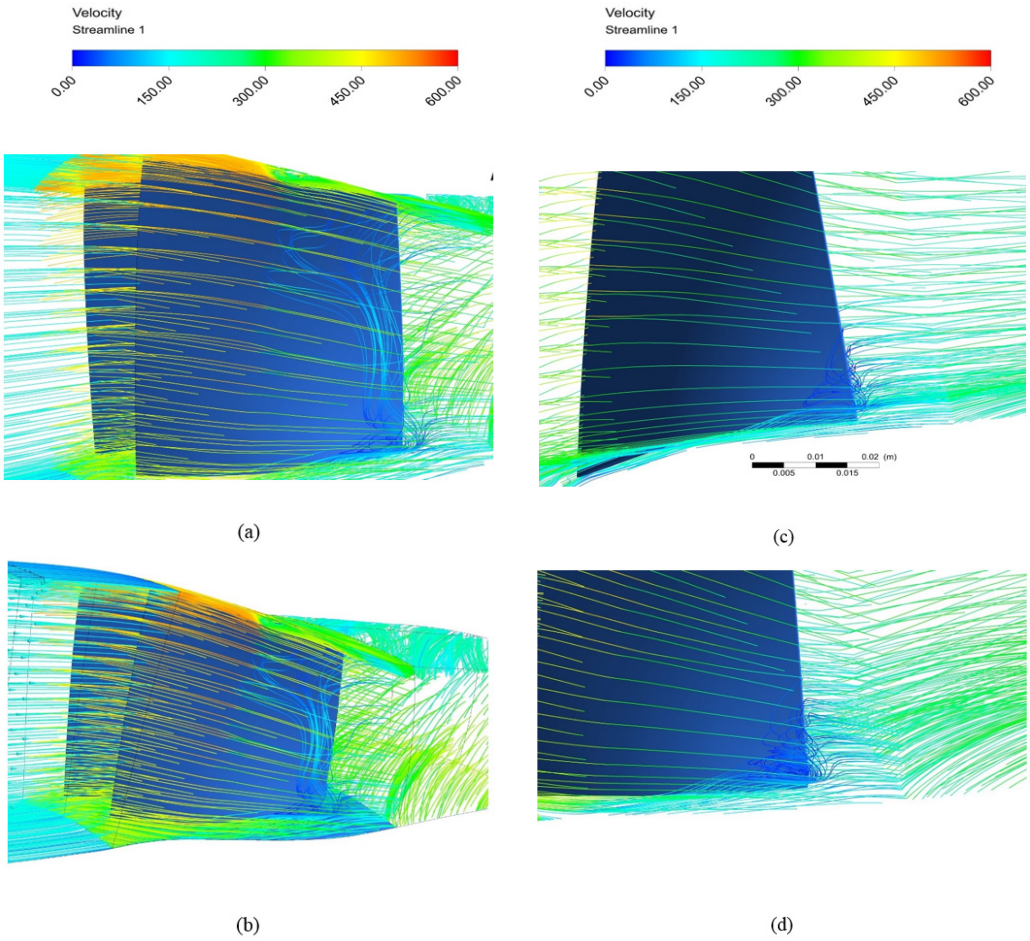

Figure 9. Comparative streamlines on the maximum efficiency rotor state at various off design conditions (a) 105% (b) 100% (c) 90% (d) 80%

CONCLUSION

A computational flow steady analysis for a transonic axial flow compressor rotor at on-design speed (1800 rad/s) and various off design conditions at 80%, 90% and 105% was carried out. The flow pattern analysis was conducted for the mach number distribution, velocity vector and streamline patterns to provide a detailed conclusion. The purpose of this paper was to study the flow and performance parameters for better understanding over the off-design condition. A weak flow separation condition was observed in mach number contour at the off design conditions at 80% and 90% compared with 100% and 105% design speed. It was found that the efficiency of the rotor has a direct impact from the shock front created. Thus, there is a reduction in efficiency due to the poorly produced shock front in 80% and 90% design speed along with a big pressure ratio difference. Even though the velocity condition at 105% design speed looks better than on-design speed (1800 rad/s), due to unstable flow condition along various mass flow rate, reduced efficiency was noted which negatively impacts the efficiency.

ACKNOWLEDGEMENTS

The first author would like to thank Universiti Putra Malaysia (UPM) for providing funds through the UPM GP –IPM/2014/9444000 grant.

REFERENCES

Benini, E., Biollo, R., & Ponza, R. (2011). Efficiency enhancement in transonic compressor rotor blades using synthetic jets: A numerical investigation. *Applied Energy*, *88*(3), 953–962. http://doi.org/10.1016/j.apenergy.2010.08.006

Biollo, R., & Benini, E. (2013). Recent advances in transonic axial compressor aerodynamics. *Progress in Aerospace Sciences*, *56*, 1–18. http://doi.org/10.1016/j.paerosci.2012.05.002

Calvert, W. J., Emmerson, P. R., & Moore, J. M. (2003). Design, Test and Analysis of a High-Pressure-Ratio Transonic Fan. In *Volume 6: Turbo Expo 2003, Parts A and B* (pp. 417–427). ASME. http://doi.org/10.1115/GT2003-38302

Chen, G. T., Greitzer, E. M., Tan, C. S., & Marble, F. E. (1991). Similarity Analysis of Compressor Tip Clearance Flow Structure. *Journal of Turbomachinery*, *113*(2), 260. http://doi.org/10.1115/1.2929098

Cumpsty, N. A. (1989). *Compressor aerodynamics*. *Compressor Aerodynamics*. Longman Scientific & Technical. Retrieved from http://www.amazon.com/Compressor-Aerodynamics-N-Cumpsty/dp/1575242478/ref=pd_sim_b_2

Denton, J. D. (1997). Lessons from rotor 37. *Journal of Thermal Science*, *6*(1), 1–13. http://doi.org/10.1007/s11630-997-0010-9

Denton, J. D., & Xu, L. (1998). The exploitation of three-dimensional flow in turbomachinery design. *Proceedings of the Institution of Mechanical Engineers -- Part C -- Journal of Mechanical Engineering Science*, *213*(2), 125–137. http://doi.org/10.1243/0954406991522220

Freeman, C., & A., C. N. (1992). Method for the prediction of supersonic compressor blade performance. *Journal of Propulsion and Power*, *8*(1), 199–208.

Hah, C., & Reid, L. (1991). A viscous flow study of shock-boundary layer interaction, radial transport, and wake development in a transonic compressor, *114*(July 1992). http://doi.org/10.1115/1.2929177

Law, C. H., & Wadia, A. R. (1993). Low Aspect Ratio Transonic Rotors: Part 1—Baseline Design and Performance. *Journal of Turbomachinery*, *115*(2), 218–225. http://doi.org/10.1115/1.2929226

Moore Royce, D., & Reid, L. (1982). Performance of Single stage Axial Transonic Compressor with rotor and stator as pect ratios of 1.19 and 1.26 Respectively and with design pressure ratio of 1.82. *Nasa Technical Paper*, (November 1978), 105. http://doi.org/NASA-TP-1338

Reid, L., & Moore, R. D. (1978). Design and overall performance of four highly loaded, high speed inlet stages for an advanced high-pressure-ratio core compressor. Retrieved from http://ntrs.nasa.gov/search.jsp?R=19780025165

Strazisar, a. J. (1985). Investigation of flow phenomena in a transonic fan rotor using laser anemometry. *Journal of Engineering for Gas Turbines and Power*, *107*(2), 427. http://doi.org/10.1115/1.3239743

Suder, K. L. (1997). Blockage Development in a Transonic, Axial Compressor Rotor. http://doi.org/10.1115/1.2841741

Suder, K. L., & Celestina, M. L. (1996). Experimental and Computational Investigation of the Tip Clearance Flow in a Transonic Axial Compressor Rotor. *J. Turbomach.*, *118*(2), 218–229. http://doi.org/10.1115/1.2836629

Suder, K. L., Chima, R. V., Strazisar, a. J., & Roberts, W. B. (1995). The Effect of Adding Roughness and Thickness to a Transonic Axial Compressor Rotor. *Journal of Turbomachinery*, *117*(4), 491. http://doi.org/10.1115/1.2836561

Pertanika J. Sci. & Technol. 24 (2): 465 - 473 (2016)

SCIENCE & TECHNOLOGY

Journal homepage: http://www.pertanika.upm.edu.my/

On the Extension of Moving Particle Method for Flow Computation in Irregular Flow Domain

Ng, K. C.[1]*, Sheu, T. W. H.[2] and Hwang, Y. H.[3]

[1]Center of Fluid Dynamics (CFD), Department of Mechanical Engineering, Universiti Tenaga Nasional, Jalan IKRAM-UNITEN, 43000 Kajang, Selangor, Malaysia

[2]Center for Advanced Studies in Theoretical Sciences (CASTS), National Taiwan University, Taipei, Taiwan

[3]Department of Marine Engineering, National Kaohsiung Marine University, Kaohsiung 805, Taiwan

ABSTRACT

A new numerical scheme based on the particle method, namely the Moving Particle Pressure Mesh (MPPM) method, has been previously developed by the authors to address the limitation of the conventional Moving Particle Semi-implicit (MPS) method in simulating incompressible flow. In this paper, we shall investigate on a more practical way to extend our MPPM method to handle complex geometry, i.e. by employing an embedded unstructured mesh system to cope with an arbitrarily-complex flow domain. No-slip boundary condition is modelled via placing a series of fixed particles at the wall boundaries, negating the use of ghost particles which are difficult to generate. In order to verify our numerical procedure, the vortex-shedding process behind a cylinder is computed and it is found the numerical result is agreeable with the reference solution.

Keywords: Moving Particle Semi-implicit (MPS), Moving Particle Pressure Mesh (MPPM), CFD, incompressible flow, unstructured mesh, semi-Lagrangian

INTRODUCTION

The original Moving Particle Semi-implicit (MPS) method was developed by Koshizuka and Oka (1996) to simulate incompressible flow. One of the main advantages of MPS is that the convective term (i.e. the non-linear term in Navier-Stokes equation) is discretised in the Lagrangian manner which can circumvent the issue of convective instability as commonly found in the Eulerian scheme (e.g. finite-volume method, see Ng et al., 2006a, 2006b, 2007, 2008; Ng 2009). To date, the MPS method has been extensively used in various engineering applications, such as breaking

Article history:
Received: 17 February 2016
Accepted: 22 April 2016

E-mail addresses:
nkching@uniten.edu.my (Ng, K. C.),
twhsheu@ntu.edu.tw (Sheu, T. W. H.),
yhhwang@mail.nkmu.edu.tw (Hwang, Y. H.)
*Corresponding Author

ISSN: 0128-7680

wave (Koshizuka et al. 1998; Lee et al. 2011), two-phase flow (Chen et al. 2010), mixing problem (Ng et al. 2013; Ng & Ng 2013) and many others.

While realising the fact that the computational domain for practical fluid flow problem is geometrically complex, we have notified that the original MPS scheme poses a few problems while treating complex flow boundary. First, the information related to proper reinforcement of a uniform initial particle number density (commonly denoted as n_0) throughout the flow field involving an arbitrarily complex flow boundary, is rather limited. Second, the current treatment of no-slip wall boundary condition (e.g. mirror/ghost particles) on complex flow boundary is cumbersome (Akomoto, 2013).

We have previously worked on a possible way to partially address the problems mentioned above. In our previous work, namely the Moving Particle Pressure Mesh (MPPM) method (Hwang 2011; Ng et al. 2014), we have made use of an embedded pressure mesh to resolve the continuity equation, thereby negating the use of particle number density. However, owing to the Cartesian nature of the embedded pressure mesh in MPPM, we are able to consider only the simple flow problem (i.e. rectangular flow domain). In spite of this, we realise that this problem can be resolved by employing a more robust pressure mesh system (e.g. unstructured mesh) to cope with the complex domain.

In the current work, we shall report on our recent numerical results obtained based on the unstructured pressure mesh. A typical flow past a cylindrical bluff body will be considered and the numerical results will be validated with the well-established numerical results published in the renowned *Journal of Fluid Mechanics* (Zovatto & Pedrizzetti, 2001).

MATHEMATICAL MODEL AND NUMERICAL METHODS

Governing Equation

The 2D incompressible flow equations, which consist of the continuity and momentum equations, are solved in the current work:

$$\nabla \bullet \vec{u} = 0 \qquad [1]$$

$$\rho \frac{D\vec{u}}{Dt} = -\nabla P + \mu \nabla^2 (\vec{u}) \cdot \qquad [2]$$

Numerical Methods

Eqns. (1&2) are solved by using the fractional-step method. The velocity of a fluid particle i at time level n+1 can be computed via:

$$\vec{u}_i^{n+1} = \vec{u}_i^n + \frac{\Delta t}{\rho_i}\left(\mu_i \nabla^2 (\vec{u})_i^n - \nabla P_i^{n+1}\right), \qquad [3]$$

and the new position of the particle i can be updated as:

$$\vec{r}_i^{n+1} = \vec{r}_i^n + \Delta t \vec{u}_i^{n+1} . \qquad [4]$$

Eqn. [4] is mainly adopted to address the convective effect of fluid flow in particle-based method.

As seen from Eqn. [3], the viscous term and pressure gradient term are treated in an explicit and implicit manner respectively. In order to ensure the divergence-free velocity condition as enforced in Equation [1], the pressure term must be corrected accordingly via the Pressure Poisson Equation (PPE):

$$\frac{\Delta t}{\rho_M}\nabla^2 P_M^{n+1} = \nabla \bullet \vec{u}_M^{\,*} . \qquad [5]$$

Here, the superscript * denotes the intermediate time level, a state where the fluid flow velocity is obtained by considering only the viscous term (i.e. neglecting the effect of pressure gradient term in Eqn. [3]). The subscript *M* indicates mesh level, indicating that Eqn. [5] is solved on the mesh level (i.e. pressure mesh) instead, which is in contrast with Eqn. [3]. In the current work, Eqn. [5] is discretised on an unstructured mesh system. Once the correct pressure field is obtained at the mesh level, the particle's velocity is corrected corresponding to the pressure gradient. Meanwhile, the face velocities at the mesh level can be correspondingly corrected to ensure divergence-free condition. It is worth to mention here that in MPPM, the pressure and velocity are stored in a staggered mesh manner, following the philosophy of the classical Marker and Cell (MAC) method. The numerical details of MPPM method can be found in our previous work (Hwang, 2011).

RESULT

The method has been applied to solve the incompressible flow pass through a non-rectangular body. A cylindrical bluff body of diameter D = 0.2m is considered in this case, whereby it is contained in a flow channel of length L = 10.5m. The distance apart between the top and bottom walls (i.e. width of the channel W) is 1.0m. The inflow x-velocity profile is assumed to be parabolic (which yields an averaged inflow velocity U = 1.0m/s). For this particular flow case where the origin is placed at the lower left corner of the flow domain (refer to Figure 1), the inflow x-velocity profile is:

$$u(y) = 6(y - y^2), \qquad [6]$$

while the inflow y-velocity is zero. Mass balance is ensured via specifying the same velocity profile at the outlet.

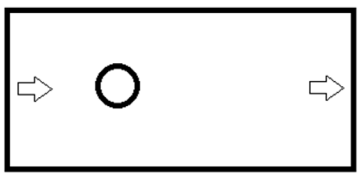

Figure 1. Schematic diagram of the problem involving flow passing through a cylinder (of diameter D = 0.2m) placed in the middle of the flow channel of length L = 10.5m and W = 1.0m. The distance between the inlet and the cylinder centre is 3.0m

The flow Reynolds number is defined as $Re = U.W/\upsilon$, where υ is the kinematic viscosity of the fluid. An unstructured quadrilateral mesh consisting of 16704 elements is used to discretise the flow domain, while the flow particles (necessary to solve the momentum equation, see Eqn. (3)) are placed at the centroid of the quad-mesh initially. In order to model the no-slip boundary condition at the wall, fluid particles with fixed velocity (i.e. u=v=0.0) are placed along the wall segment, without the necessity to employ the ghost/mirror particles. The implementation of boundary condition without introducing ghost particles have been discussed in Ng et al. (2015). Figure 2 shows the initial layout for the unstructured pressure mesh and fluid particles of this flow problem.

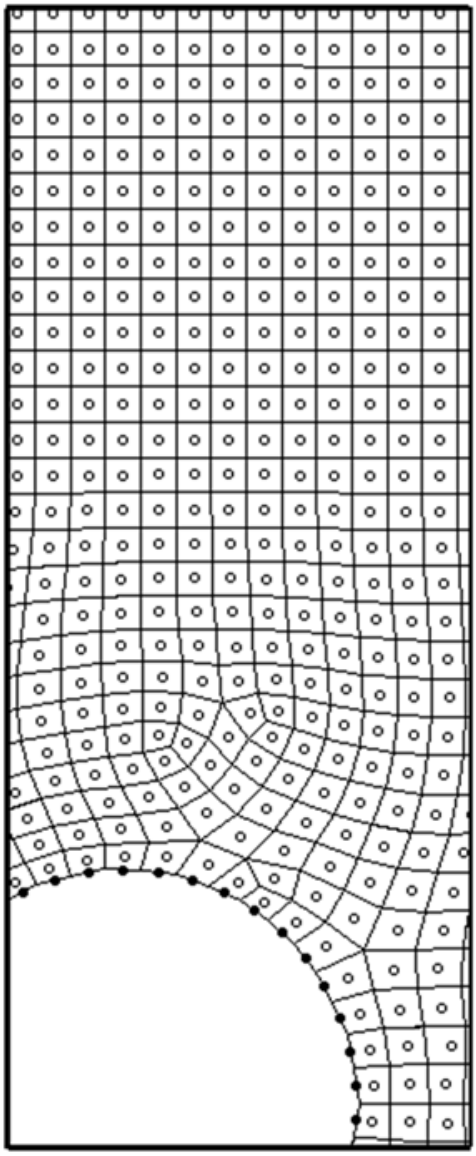

Figure 2. The pressure mesh in the vicinity of the cylinder body. Fixed wall particles (solid black circles) are placed along the cylinder body without the necessity of employing ghost/mirror particles

In order to initiate the flow instability, a skewed inflow x-velocity profile is introduced within a short time frame $0 < t < 0.1$ s, defined as:

$$u(y) = \begin{matrix} 1.5 & y < 0.5 \\ 0.5 & y \geq 0.5 \end{matrix}. \quad [7]$$

This skewed inflow velocity profile is crucial to hasten the occurrence of vortex shedding behind the cylinder, if any. For this unsteady simulation, we have adopted a Courant number of 0.5.

Two flow cases (Re = 240 and Re = 1000) have been considered in the current work. For the case of Re = 240, a relatively mild vortex shedding process behind the cylinder can be observed from the vorticity plot reported in Figure 3(a). The y-velocity plot is shown in Figure 4, indicating that the shedding is intensified while the Reynolds number is increased to 1000. Figure 5 reports the spatial distribution of static pressure at t=80s. It is interesting to note the smoothness of the static pressure field computed from our particle method, which is hardly attainable by employing the conventional MPS methods.

In order to validate the shedding frequencies of the flow cases, the y-velocity values at point located at 1.0m downstream from the cylinder centroid are numerically measured. Results are shown in Figure 6. It is found that the period (T) is 0.844s and 0.679s for Re = 240 and Re = 1000, respectively. Our numerical results are very close to that reported in Zovatto and Pedrizzetti (2001), i.e. 0.85s (for Re = 240) and 0.67s (for Re = 1000). As observed from Figure 6, as Re increases, the shedding frequency increases (decrease of T).

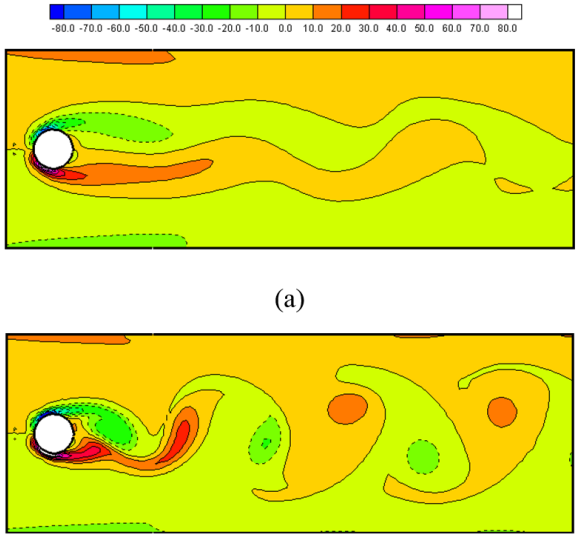

Figure 3. Vorticity [s^{-1}] plot for (a) Re = 240 and (b) Re = 1000. Negative vorticity values are marked with dashed lines. t = 80s

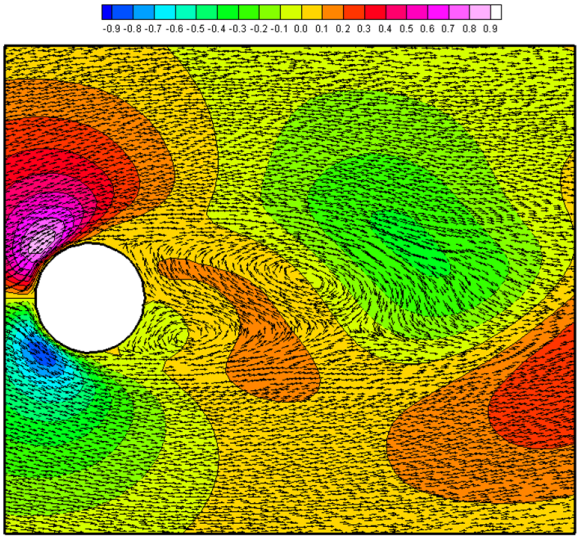

(a)

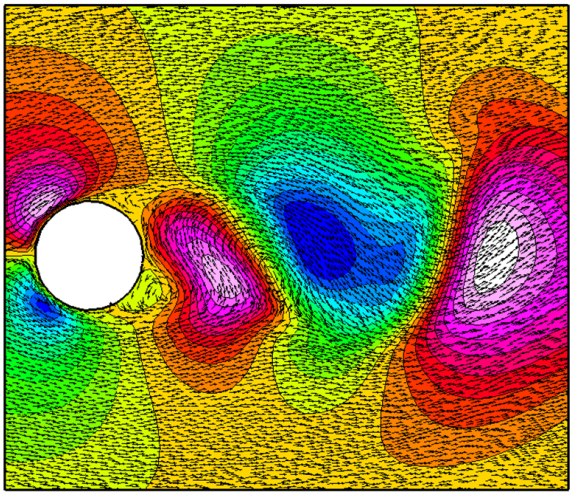

(b)

Figure 4. *y*-velocity [m.s^{-1}] plot for (a) *Re* = 240 and (b) *Re* = 1000. *t* = 80s. The velocity vectors are positioned at the centroid of the flow particles

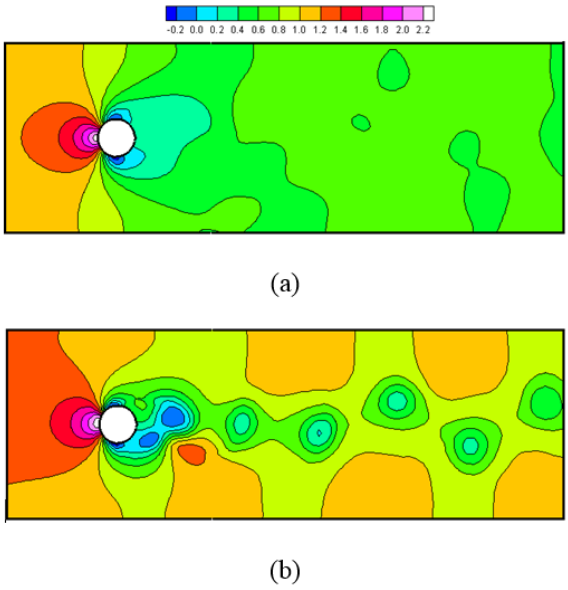

Figure 5. Static pressure [Pa] plot for (a) *Re* = 240 and (b) *Re* = 1000. *t* = 80s

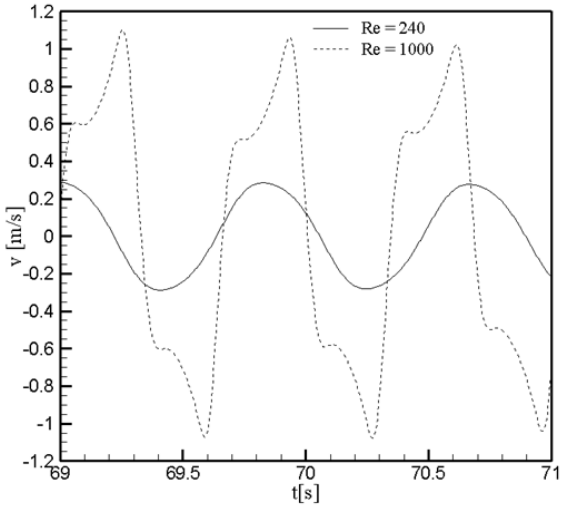

Figure 6. Time evolution of *y*-velocity at point located 1.0 m downstream from the cylinder centroid at different Reynolds number

CONCLUSION

In the current work, we have implemented an unstructured pressure mesh system as a solution to extend our previous MPPM particle method to solve an incompressible fluid flow problem in a non-rectangular flow domain. Although data structure is relatively complex compared with that of our original MPPM solver which employed a Cartesian mesh to resolve the continuity equation, we find that our current method is robust and it has a great potential to resolve industrial flow problems involving very complex flow domains. Combined with the inherited

benefits of moving particles used to resolve the convective term, we foresee that this method is accurate in computing flow at high *Re* (convection-dominated flow).

A few interesting problems have been observed during the course of our study. Generally, the total execution time of most of the particle methods (including our current one) is relatively longer compared with the conventional Eulerian scheme, mainly due to the CPU time spent to process the scattered moving particles. Also, the order of accuracy of the discretisation method of the diffusion (or viscous) term is highly dependent on the instantaneous locations of the fluid particles, which may diminish the overall accuracy of the flow solver. As such, we are currently considering ways to shorten the overall execution time of the flow solver by parallelisation (via OPENMP and GPU). A more proper way to discretise the viscous term must be sought as well.

ACKNOWLEDGEMENTS

We acknowledge with gratitude the financial support provided by the Ministry of Education, Malaysia (Fundamental Research Grant Scheme Ref. No: FRGS/2/2013/TK01/UNITEN/02/1) and the Ministry of Science, Technology and Innovation (MOSTI), Malaysia (Project No: 06-02-03-SF0258) .

REFERENCES

Akimoto, H. (2013). Numerical simulation of the flow around a planning body by MPS method. *Ocean Engineering*, *64*, 72-79.

Chen, R., Tian, W., Su, G. H., Qiu, S., Ishiwatari, Y., & Oka, Y. (2010). Numerical investigation on bubble dynamics during flow boiling using moving particle semi-implicit method. *Nuclear Engineering and Design*, *240*(11), 3830-3840.

Hwang, Y. H. (2011). A moving particle method with embedded pressure mesh (MPPM) for incompressible flow calculations. *Numerical Heat Transfer, Part B*, *60*(5), 370-398.

Koshizuka, S., & Oka, Y. (1996). Moving-Particle Semi-implicit method for fragmentation of incompressible fluid. *Nuclear Science and Engineering*, *123*(3), 421-434.

Koshizuka, S., Nobe, A., & Oka, Y. (1998). Numerical analysis of breaking waves using the moving particle semi-implicit method. *International Journal for Numerical Methods in Fluids*, *26*(7), 751-769.

Lee, B. H., Park, J. C., Kim, M. H., & Hwang, S. C. (2011). Step-by-step improvement of MPS method in simulating violent free-surface motions and impact loads. *Computer Methods in Applied Mechanics and Engineering, 200*(9), 1113-1125.

Ng, K. C., Yusoff, M. Z., & Ng, E. Y. K. (2006a). Multigrid solution of Euler equations using high-resolution NVD differencing scheme for unstructured meshes. *Progress in Computational Fluid Dynamics, an International Journal, 6*(7), 389-401.

Ng, K. C., Yusoff, M. Z., & Ng, E. Y. K. (2006b). Parametric study of an improved GAMMA differencing scheme based on normalized-variable formulation for low-speed flow with artificial compressibility technique. *Numerical Heat Transfer, Part B: Fundamentals, 50*(6), 561-584.

Ng, K. C., Yusoff, M. Z., & Ng, E. Y. K. (2007). Higher-order bounded differencing schemes for compressible and incompressible flows. *International Journal for Numerical Methods in Fluid*s, *53*(1), 57-80.

Ng, K. C., Ng, E. Y. K., Yusoff, M. Z., & Lim, T. K. (2008). Applications of high-resolution schemes based on normalized variable formulation for 3D indoor airflow simulations. *International Journal for Numerical Methods in Engineering*, *73*(7), 948-981.

Ng, K. C. (2009). A collocated finite volume embedding method for simulation of flow past stationary and moving body. *Computers and Fluids, 38*(2), 347-357.

Ng, K. C., & Ng, E. Y. K. (2013). Laminar mixing performances of baffling, shaft eccentricity and unsteady mixing in a cylindrical vessel. *Chemical Engineering Science*, *104*, 960-974.

Ng, K. C., Ng, E. Y. K., & Lam, W. H. (2013). Lagrangian simulation of steady and unsteady laminar mixing by plate impeller in a cylindrical vessel. *Industrial and Engineering Chemistry Research*, *52*(29), 10004-10014.

Ng, K. C., Hwang, Y. H., & Sheu, T. W. H. (2014). On the accuracy assessment of Laplacian models in MPS. *Computer Physics Communications*, *185*(10), 2412-2426, 2014.

Ng, K. C., Hwang, Y. H., Sheu, T. W. H., & Yu, C. H. (2015). Moving Particle Level-Set (MPLS) method for incompressible multiphase flow computation. *Computer Physics Communications, 196*, 317-334.

Zovatto, L., & Pedrizzetti, G. (2001). Flow about a circular cylinder between parallel walls. *Journal of Fluid Mechanics*, *440*, 1-25.

Pertanika J. Sci. & Technol. 24 (2): 475 - 482 (2016)

PERTANIKA JOURNALS

SCIENCE & TECHNOLOGY

Journal homepage: http://www.pertanika.upm.edu.my/

Split-Disk Properties of Kenaf Yarn Fibre-Reinforced Unsaturated Polyester Composites using Filament Winding Method

Misri, S.[1], Ishak, M. R.[1,2,4]*, Sapuan, S. M.[2,3,4] and Leman, Z.[3]

[1]Department of Aerospace Engineering, Universiti Putra Malaysia, 43400 UPM Serdang, Selangor, Malaysia

[2]Aerospace Manufacturing Research Centre (AMRC), Universiti Putra Malaysia, 43400 UPM Serdang, Selangor, Malaysia

[3]Department of Mechanical and Manufacturing Engineering, Universiti Putra Malaysia, 43400 UPM Serdang, Selangor, Malaysia

[4]Laboratory of Biocomposite Technology, Institute of Tropical Forestry and Forest Products (INTROP), Universiti Putra Malaysia, 43400 UPM Serdang, Selangor, Malaysia

ABSTRACT

There are many contributions from synthetic fibres in the world of industrial composites over the years. However, they contain hazardous properties to humans causing irritation when exposed to the skin and eye. Inhalation of fibrous synthetic can cause lung cancer with its deadly effects. There have been studies and researches conducted on natural fibres to replace synthetic fibres as it is believed the latter are more environmental-friendly and pose less health risks to humans. The aim of this study was to investigate hoop tensile properties of the composite hollow shaft for different winding angles and PVC reinforcement produced via the filament winding technique. For this purpose, split-disk tests (according to ASTM D-2290 standard) were performed for the specimens produced with two different winding angles such as 45° and 90° winding angle. By determining the hoop tensile strength and modulus of these specimens, the effects of filament-winding processing parameter in winding angle were evaluated. Experiments successfully showed that the mechanical properties such as tensile properties of kenaf yarn fibre reinforced unsaturated polyester hollow tube at 90° and 45° winding angle with and without PVC. The value was 15% for the different winding angles and 25% for the different winding angles with and without PVC. The results indicate that 90° fibre winding angle kenaf yarn fibre unsaturated polyester with PVC has the highest hoop tensile strength compared with other composite specimens. The experiments concluded that the orientation on fibre angle has a significant impact on the hoop tensile strain, hoop tensile modulus and hoop tensile strength properties.

Keywords: Split-disk tests, filament winding, composite tube, hoop tensile strength, hoop modulus of elasticity

Article history:
Received: 17 February 2016
Accepted: 22 April 2016

E-mail addresses:
sairizal.misri.84@gmail.com (Misri, S.),
mohdridzwan@upm.edu.my (Ishak, M. R.),
sapuan@upm.edu.my (Sapuan, S. M.),
zleman@upm.edu.my (Leman, Z.)
*Corresponding Author

ISSN: 0128-7680

INTRODUCTION

In the world of composites, there are many natural fibres that have not yet been explored for the sake of commercial purposes . Synthetic fibre composites have many bad side effects on human health and the environment. As a result, many researchers have studied natural fibre composites with the hope that natural fibre composites may reduce the usage of synthetic fibre in composite. Before discussing further on how natural fibres can contribute to the world of composite, below is a brief overview of bio-composites. What is a bio-composite? Bio-composites or natural fibres are made up of resin and reinforced by natural fibres. Natural fibres can be categorised into three different types: = bast fibre, leaf fibre, and seed fibre (Suddel, 2008).

Kenaf is categorised as bast fibre in natural fibre. There are many studies that have been conducted on kenaf and its composites (Alkbir et al., 2014; Misri et al., 2015;). Kenaf is a fibre plant which has been grown for several thousand years for its food and fibre sources, especially in east-central Africa. It is also a common wild plant in Asia. Kenaf has been a source of textile fibre to produce products such as rope, twine, bag and rugs. Kenaf is a promising source of raw material fibre for pulp, paper and other fibre products, and has been introduced since World War II (WWII) in China, USSR, Thailand, South Africa, Egypt, Mexico and Cuba.

Lehtiniemi et al., (2011) studied the use of natural fibre yarn reinforcement composites such as flax fibre made from filament winding process. Filament winding process of fibre reinforced thermosetting resin and can used to make simple components such as pipes, tubes and rods such as those found in sailboard masts, lamp posts, and fishing rods or high tech components such as high pressure vessels, and aerospace components (Hernández-Moreno et al., 2008; Abdalla et al., 2007; Zhou et al., 2009). Shaw-Stewart (1985) reported that complicated tubes can be made from a series of joined filament wound tubes to develop a space frame. Synthetic fibres such as glass and carbon are the main fibres used for filament winding process. Studies on the winding process employing natural fibre composites however, are very limited.

METHODOLOGY

Materials

There are four types of fabricated specimens. The first specimen is ±45° kenaf yarn fibre reinforced unsaturated polyester (UP) composite without PVC. The second specimen was 90° kenaf unsaturated polyester (UP) composite without PVC. The third specimen consists of ±45° kenaf unsaturated polyester (UP) composite with PVC while the fourth specimen consists of 90° kenaf unsaturated polyester (UP) composite with PVC.

Fabrication

An advanced composite material is made up of a fibrous material embedded in a resin matrix and usually laminated with fibres oriented in alternating directions to give the material strength and stiffness. The strength and stiffness of a composite build-up depend on the orientation sequence of the plies. A proper selection of ply orientation in advanced composite materials is necessary to provide a structurally efficient design. The part may require 90° plies to react to the axial loads, ±45° plies to react to the shear loads and 90° plies to react to the side loads.

In filament winding, a bundle of continuous filaments is wound on mandrel. For hoop winding and polar winding filaments, they are wound together in one direction. For helical winding filaments, they are wound together in two directions. The directions are determined by given winding angles in Figure 1 (a) and Figure 1 (b).

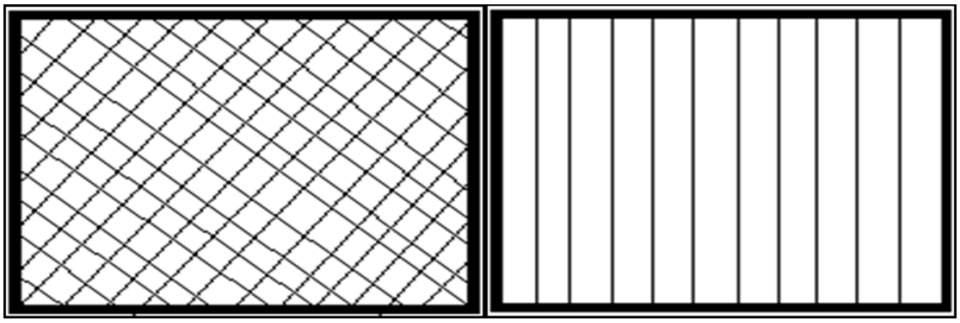

(a) (b)

Figure 1. (a) ±45° Winding Angle, and (b) 90° Winding Angle

Split Disk Method

The current experimental test to study the mechanical properties of kenaf yarn fibre reinforced unsaturated polyester hollow tubes uses 4 sets of specimens. The orientation at 90° and 45° winding angle with and without PVC were done according to ASTM D2290 standard. The ASTM D2290 standard determines the comparative apparent tensile strength of most plastic products using a split disk test fixture tested under defined conditions and test machine speed. Extruded and moulded thermoplastic piping is also covered in this test. Data from this test are useful for research and development, quality control specification and design. This test method covers the determination of the comparative apparent tensile strength of most plastic products utilising a split disk test fixture when tested under defined conditions of pre-treatment, temperature, humidity and test machine speed. In a split-disk tensile test, tension forces are applied as shown by the arrow in Figure 2. The internal diameter of the kenaf yarn fibre hollow composite was 90 mm and the length was 35 mm. The thickness of kenaf yarn fibre hollow composite was 4.5–5.5 mm. The mandrel was a PVC cylinder with a diameter of 90 mm.

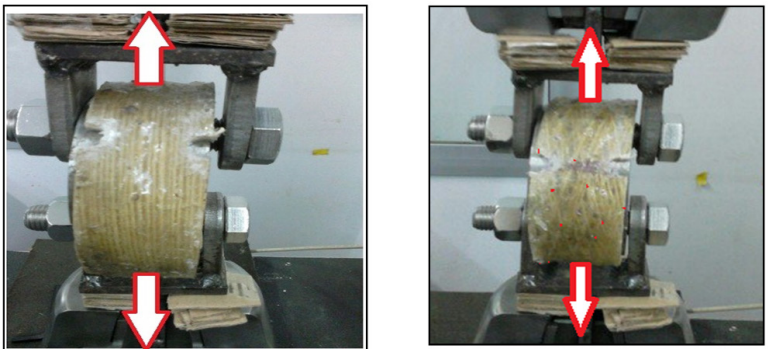

Figure 2. 90° and ±45° Fibre winding angle kenaf with PVC when given load (direction of load)

Equation for Hoop Tensile Strength and Hoop Tensile Modulus

The hoop tensile strength of the specimens was calculated using the following equation:

$$\sigma_{hts} = \frac{P_m}{2.A_m} \quad [1]$$

where:

σ_{hts} : Hoop tensile strength, MPa

P_m : Maximum load, N

A_m : Cross-sectional area of crack composite sections, mm^2

Obtained strain and calculated stress data were then used to plot hoop tensile of stress-strain curve for kenaf yarn hollow tube composites. The plotted curves were analysed to obtain the hoop tensile modulus elasticity of the kenaf yarn hollow tube composites specimens. Then, the slopes of the linear portion of the curve were determined. After that, fitting a straight line to the linear portion of the curve and the least square method was done. Therefore:

$$E_{htm} = \frac{d\sigma}{d\varepsilon} \quad [2]$$

where:

E_{htm} : Hoop tensile modulus of elasticity, GPa.

$d\sigma / d\varepsilon$: Slope of the linear portion of the stress – strain curve from kenaf composite analysis.

RESULTS AND DISCUSSION

By conducting the tensile test experiment, it can determine the stress-strain curve. From the stress-strain graph, it can be examined whether the material is brittle or ductile. The hoop tensile properties such as hoop tensile strength, hoop tensile modulus and hoop tensile strain could be determined from the stress-strain graph. This experiment was conducted to investigate the hoop tensile strength, hoop tensile modulus and hoop tensile strain of the specimen and to differentiate the tensile properties between kenaf reinforced unsaturated polyester with and without PVC as a composite material with different 90° and ±45° fibre winding angle. Figure 3 shows the tensile stress-strain behaviour of kenaf reinforced hollow tube in filament winding technique.

From the graph, it can be observed that composite materials with 90° kenaf fibre winding angle have the highest hoop tensile strength compared with the other specimens. It clearly shows that at 90° orientation of kenaf fibre winding angle with PVC, the hoop tensile strength value has increased. This was followed by ±45° kenaf fibre winding angle with PVC (142.79 MPa), pure kenaf 90° winding angle (119.72 MPa), ±45° kenaf fibre winding angle (98.13 MPa) and PVC of 59.67 Mpa. Emrah (2004) compared the hoop tensile strengths of specimens having different winding angle hollow fibre composite. The result shows the 90º winding angle has the highest hoop tensile strength compared with the lower winding angle. It shows a similar trend with the current study where lower winding angle gives lower hoop tensile properties. This is because the failure fibre direction for 90º winding angle is parallel to the direction of loading. The lowest strength values were obtained for the fibre direction in 90º winding angle where the failure fibre direction is perpendicular to the direction of loading.

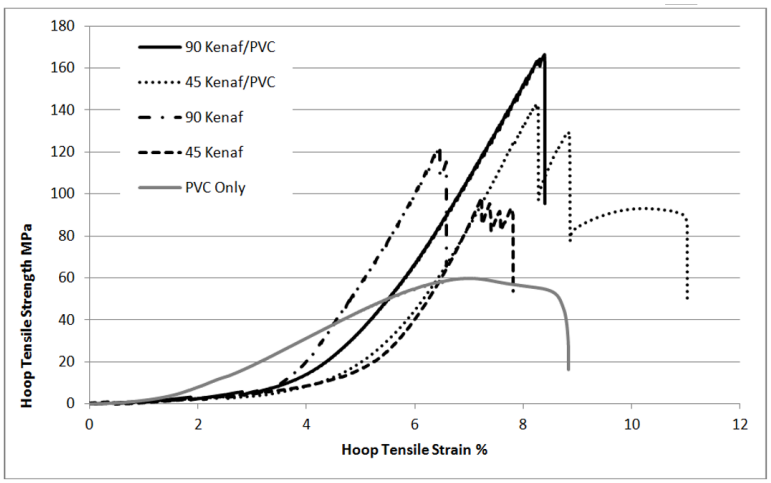

Figure 3. Hoop tensile of stress-strain curve for kenaf yarn hollow tube composites

The hoop tensile strength of the kenaf fibre composite with different type of winding angle and specimens are shown in Figure 4. The highest hoop tensile strength values were obtained for the specimens having the 90º winding angle with PVC due to the fact that they have two layers. The first layer is kenaf yarn composite and the second layer is the PVC hollow tube. Reinforcing it with PVC increases the strength of structure fibre hollow tube composite. The lowest strength values were obtained for the specimens having only PVC. The results for the specimens having ±45º winding angles show decreased ability of the kenaf fibre to absorb stress from the matrix during failure. Thus, as shown in Figure 4, when the winding angle decreases, the values of hoop tensile strength specimens also decrease.

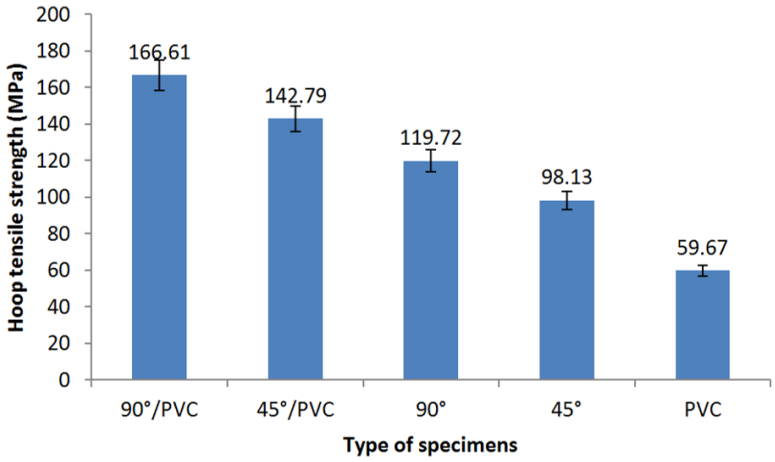

Figure 4. Hoop tensile strength graph of kenaf yarn filament wound hollow tube

Another substantial property that can be extracted from the tensile stress-strain behaviour is hoop tensile modulus. The hoop tensile modulus is the capability of a material to persist deformation in tension. Theoretically, the higher the hoop tensile modulus is, the stiffer the

materials. It means that the tensile modulus affects the stiffness property of the material (Ishak, 2009). Figure 5 shows the results of tensile modulus kenaf yarn fibre reinforced unsaturated polyester hollow composite with different fibre winding angle, with PVC and without PVC. The results shown in Figure 5 clearly indicate that ±45º kenaf reinforced unsaturated polyester without PVC has the higher hoop tensile modulus compared with other composite samples whereas PVC has the lowest hoop tensile modulus. The ±45º was increased and so, the composite becomes stiffer compared with 90º winding angle of composite. Thus, it is clear that different winding angle has a different effect on the mechanical properties of composites.

The fractured kenaf yarn fibre in this hollow composite was observed to exhibit brittle fracture as well, suggesting that the arrangement of the 90º winding angle kenaf fibre has decreased the ability of the kenaf fibre to absorb stress from the matrix during failure and contributed to the decreasing hoop tensile modulus and hoop tensile strain failure of the composites. At the ±45º winding angle kenaf yarn fibre hollow composite, only a few fibre de-bonding occurred during the failure of the unsaturated polyester composites.

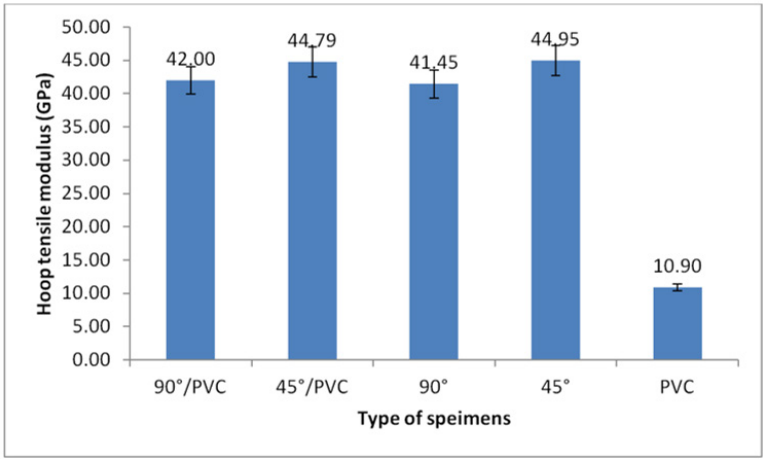

Figure 5. Hoop tensile modulus graph of kenaf filamen wound hollow tube

By studying the hoop tensile strain, the ductility of a material can be determined where a higher hoop tensile strain indicates a higher ductility of the material. The result of hoop tensile strain for 90º and ±45º winding angle kenaf yarn fibre reinforced unsaturated polyester with and without PVC are shown in Figure 6. It has been shown that ±45º kenaf yarn fibre composite with PVC has the highest value of hoop tensile strain compared with other samples. The Figure 6 below also show the same behaviour between two types of winding angles such as 90º and ±45º. The ±45º winding angle kenaf yarn composite was higher than the 90º winding angle; it has been shown that the ±45º winding angle improves the hoop tensile strain of kenaf yarn fibre composite. The effect of winding angles and the different layers are depicted in Figure 6. Generally, the in plane tensile modulus for winding angle 45° is higher than 90°. It is a well-known fact the maximum tensile strain occurs at 45° from hollow of loading. It means that it can withstand more tensile and this is clearly seen in Figure 6. These have been supported by Cho and Lee (1998) and in a large scale test of a hybrid aluminium/composite drive shaft for passenger car.

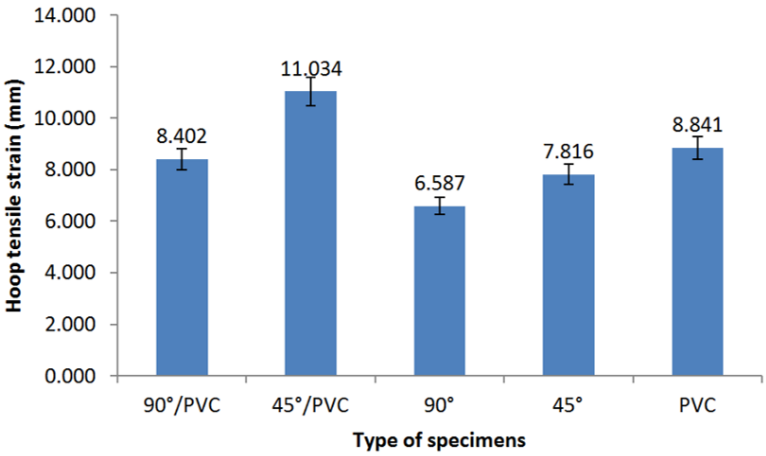

Figure 6. Hoop tensile strain graph of kenaf filamen wound hollow tube

The winding angle fibre composite plays a major role in determining the fibre strength. It is because the force is exerted by the composite and will be distributed to the fibre so the winding angle is very important for load distribution. In general, it is known that fibre winding angles are related to mechanical properties, especially in unidirectional fibrous composites (Baosheng et al., 2010).

CONCLUSION

From the experiments, the mechanical properties such as hoop tensile properties of 90° and ±45° winding angle kenaf yarn fibre reinforced unsaturated polyester hollow tube composites with and without PVC are successfully determined. The results of the experiments concluded that the winding angle fibre has a significant impact on the hoop tensile strain, hoop tensile modulus and hoop tensile strength. This is because they have different winding angle fibre and effect the mechanical properties of composites. When the loads were further increased in testing, the crack grew in the composite and penetrated the fibres at the interface, showing the brittle fracture perpendicular to the load direction in composite. This proves that winding angle fibre has a significant impact on improving the mechanical properties of the material. Adding a kenaf yarn fibre composite using the filament winding technique will increase the material structure. In this experiment, PVC is used as a mandrel for kenaf yarn fibre composite and also to improve the strength of the kenaf yarn fibre composite. The results showed that the 45°winding angle has a higher value for hoop tensile strain and hoop tensile modulus to crack the wound of winding single yarn kenaf fibre composite compared with 90º winding angle.

ACKNOWLEDGEMENTS

The authors wish to thank the Ministry of Education, Malaysia, for providing the scholarship MyPhD to the principal author. Thanks are also extended to Universiti Putra Malaysia for providing a research grant: Research Universiti Grant Scheme (RUGS) with vote number

9301200. The authors wish to thank Professor Y. Ando of Kyushu Institute of Technology Kyushu Institute of Technology for his contribution.

REFERENCES

Abdalla, F. H., Mutasher, S. A., Khalid, Y. A., Sapuan, S. M., Hamouda, A. M. S., Sahari, B. B., & Hamdan, M. M. (2007). Design and fabrication of low cost filament winding machine. *Journal of Material and Design, 28*(1), 234-239.

Alkbir, M. F. M., Sapuan, S. M., Nuraini, A. A., & Ishak, M. R. (2014). Effect of geometry on crashworthiness parameters of natural kenaf fibre reinforced composite hexagonal tubes. *Journal of Material and Design, 60*, 85–93.

Baosheng, R., Noda, J., & Goda, K. (2010). Effects of fibre orientation angles and fluctuations on the stiffness and strength of sliver-based green composites. *Journal of Society of Materials Science Japan, 59*(7), 567-574.

Cho, D. H., & Lee, D. G. (1998). Manufacturing of co-curing aluminium composite shafts with compression during co-curing operation to reduce residual thermal stresses. *Journal of Composite Materials*, *32*(12), 1221-1241.

Emrah, S. E. (2004). *Experimental investigation for mechanical properties of filament wound composite tubes. Master of Science*. The graduate school of Natural and Applied Sciences of Middle East Technical University.

Hernández-Moreno, H., Douchin, B., Collombet, F., Choqueuse, D., & Davies, P. (2008). Influence of winding pattern on the mechanical behavior of filament wound composite cylinders under external pressure. *Composites Science and Technology, 68*(3), 1015–1024.

Ishak, M. R. (2009). *Mechanical Properties of Treated and Untreated Woven Sugar Palm Fibre-Reinforced Unsaturated Polyester Composites*. (Master of Science Thesis dissertation). Universiti Putra Malaysia, Malaysia.

Lehtiniemi, P., Dufva, K., Berg, T., Skrifvars, M., & Järvelä, P. (2011). Natural fiber-based reinforcements in epoxy composites processed by filament winding. *Journal of Reinforcement Plastic Composite, 30*, 1947-1955.

Misri, S., Sapuan, S. M., Leman, Z., & Ishak, M. R. (2015). Torsional behaviour of filament wound kenaf yarn fibre reinforced unsaturated polyester composite hollow shafts. *Material and Design, 65*, 953–960.

Shaw-Stewart, D. (1985). Filament winding-Materials and Engineering. *Materials and Design, 6*(3), 140-144.

Suddell, B. (2008). Industrial fibres: recent and current developments. *Proceedings of the Symposium on Natural Fibres*, *44*, 71–82.

Zhou, W., Qi, S., Ai, T., Zhao, H., Zhang, M., Li, W., & Lau, E. (2009). Toughened Epoxy Resin Matrix for a Membrane Shell by Wet Filament Winding. *Journal of Applied Polymer Science, 111*(1), 255–263.

Pertanika J. Sci. & Technol. 24 (2): 483 - 491 (2016)

SCIENCE & TECHNOLOGY

Journal homepage: http://www.pertanika.upm.edu.my/

Using *Tracker* to Engage Students' Learning and Research in Physics

Eddy Yusuf[1,2]

[1]*Department of Civil Engineering, Pembangunan Jaya University, Jl. Cendrawasih Raya B7/P, Bintaro Jaya, Sawah Baru, Ciputat, Tangerang Selatan 15413, Indonesia*

[2]*IPH Schools, Jl. Raya Kedung Baruk 112-114, Surabaya, Indonesia*

ABSTRACT

Information and communication technologies (hardware and software), have become an important part in classroom learning because they allow diversity in learning styles and make learning more flexible. This study focuses on *Tracker,* a free video analysis and modeling software, which offers an alternative route to discuss concepts that are otherwise difficult to grasp. Using the popular game, *Angry Birds*, we demonstrate the ongoing research on the application of *Tracker* in three cases: 1) motion of exploding projectile, 2) free fall with air resistance, and 3) calibration of a home-made spectrometer. Findings reveal that such visualizations can offer an alternative way to explain concepts that are otherwise rather difficult to grasp in Physics. Findings from these experiments open up exciting possibilities on the need for future research in more advanced research themes like determining diffusion coefficient and absorption spectra of materials.

Keywords: Tracker, parabola, momentum conservation, air resistance, spectrometer, physics

INTRODUCTION

Technologies have become an integral part of classrooms these days; they serve not only as an alternative way to make active learning in classroom but also as a tool to deliver concepts more clearly (Kozma, 2003; Freeman, et al., 2014). The technologies cover a wide range of spectrums, including, but not limited to, mobile apps, tablets, and computer software. Recent developments have embraced using social media to teach Physics in classrooms (Page, 2015).

In this paper, we focus on *Tracker* (Brown, 2015), an image and video analysis software, which is suitable as a teaching aid to deliver Physics concepts in classrooms. The power of *Tracker* lies in the fact that one is able to visualize the concept in question in

Article history:
Received: 8 December 2015
Accepted: 22 April 2016

E-mail address:
yusuf.eddy@fulbrightmail.org (Eddy Yusuf)

ISSN: 0128-7680

real time. We have picked two concepts that are often misunderstood by the students (the law of momentum conservation in exploding projectile and the effect of air resistance on falling objects) and we demonstrate how *Tracker* is employed to help students understand those concepts. We also investigate using a simple exercise in calibrating a home-made spectrometer using *Tracker* and discuss how *Tracke*r can be used to deliver advanced concepts beyond high school level.

EXPLODING PROJECTILE

Consider the motion of a projectile under gravity. Ignoring the effect of air resistance, the projectile will have a trajectory of a parabola. Let us assume at some point the projectile explodes into several fragments. A typical problem of this sort involves finding the trajectories of these fragments after the explosion happens. If we consider the earth-projectile system, then there is no external force acting on the system and total momentum is conserved. i.e. $\boldsymbol{P}_i = \boldsymbol{P}_f$, where $\boldsymbol{P}_i$ is the initial momentum of the projectile + earth and $\boldsymbol{P}_f$ is the total momentum of the fragments + earth after the explosion. The fact that the earth is much more massive than the projectiles, allows us to ignore the earth's recoil effect and consider it stationary. Thus the trajectory of the center of mass of the fragments after the explosion would follow the trajectory of the original projectile if there had not been any explosion (Thornton & Marion, 2003).

The calculation for this problem is straightforward: by applying the center of mass theorem or conservation of momentum, one can easily solve the exploding projectile problem (Holics, 2011). However, the formal machinery may pose challenges to the students' understanding so that they may fail to fully grasp the concept behind it. One of the approaches to circumvent the difficulty in understanding concepts in Physics is through visualization (Robinett, 1995; Dori & Belcher, 2005; Cataloglu, 2006). We revisit this classic problem and use the popular game "Angry Bird" (Google Play, 2015) to visualize the physics of exploding projectiles. We focus on The Blues (Angry Birds Wiki, 2015) which have the property of splitting into three birds. We record The Blues in action and use *Tracker* to extract the coordinates of the bird(s) before and after explosion for analysis.

A snapshot of the tracker window which consists of three major components is shown in Figure 1. The left side of the window is where the user uploads the video and performs the analysis which includes setting the coordinate system, determining the scale, and tracking the object. The right side of the window allows the user to choose what parameters/variables to plot. The numerical values of the variables are given in the table below the plot. The red symbols on Figure 1 mark the traces of the objects from which the coordinates are recorded.

Tracker allows us to visualize the conservation of momentum in the exploding projectile problem process. We show that $(P_i)_x = \left(P_f\right)_x$ and $(P_i)_y = \left(P_f\right)_y$, where $\boldsymbol{P}_i = m\boldsymbol{v}$ and the final momenta of the birds are

$$\left(P_f\right)_x = m_1(v_1)_x + m_2(v_2)_x + m_3(v_3)_x$$
$$(P_f)_y = m_1(v_1)_y + m_2(v_2)_y + m_3(v_3)_y,$$

where we assume that the original bird splits into three birds with equal mass. Figure 2 shows the momentum per unit mass of the bird before the explosion (black) and the total momentum per unit mass after the explosion (blue) as calculated from the above equations. Had there not

been any explosion, the original bird would have the momentum per unit mass as shown in orange. By comparing the total momentum per unit mass after the explosion (blue) and the momentum of the bird if there had not been any explosion (orange), one can verify that the momentum is indeed conserved in the process. The momentum per unit mass of the individual birds after explosion is also shown in the figure (red, green, yellow) for completeness.

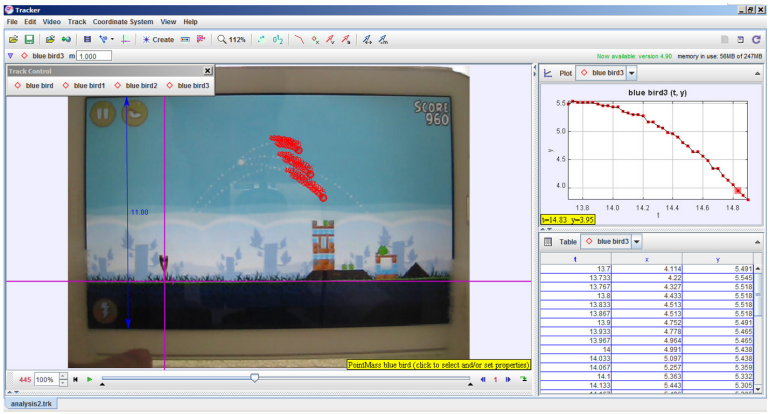

Figure 1. Tracking the coordinates of the bird(s) from which relevant quantities are extracted and calculated. We define the frame of reference (purple lines) along with the calibration measurement (blue line) to allow us to extract and record the data. The red marks show that the birds are tracked by *Tracker*. The Top panel shows the trajectory of the original bird before explosion and the bottom panel shows the trajectories of the birds after explosion. The user can choose the plots and numerical values to show at the right side of the window as shown in the figure above.

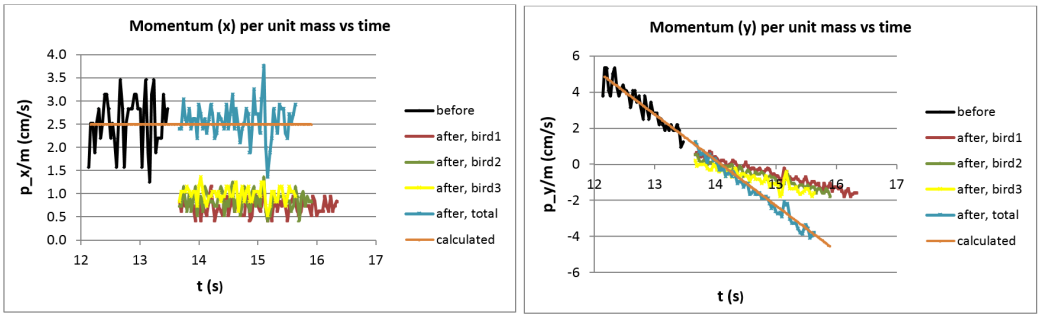

Figure 2. Momentum analysis of The Blues before and after the explosion along the $\boldsymbol{x}-$(top panel) and $\boldsymbol{y}-$(bottom panel) which demonstrates the conservation of momentum. The momentum per unit mass if there had not been any explosion (black and orange) matches the total momentum of the 3 birds after explosion (blue), indicating that momentum is conserved. The momentum per unit mass of the three birds after explosion, from which the total momentum is calculated, are shown in red, green, and yellow.

The trajectories of The Blues before (black) and after explosion (red, green, and yellow) are shown in Figure 3. The top (bottom) panel of Figure 3 shows the horizontal (vertical) position of the birds. We show the trajectory of the center of the mass after the explosion (blue) by performing weighted average. We also plot the calculated trajectory of the original bird if

there had not been any explosion (orange). The analysis clearly shows that the trajectory of the center of mass after the explosion agrees with the calculated trajectory of the original bird if there had not been any explosion.

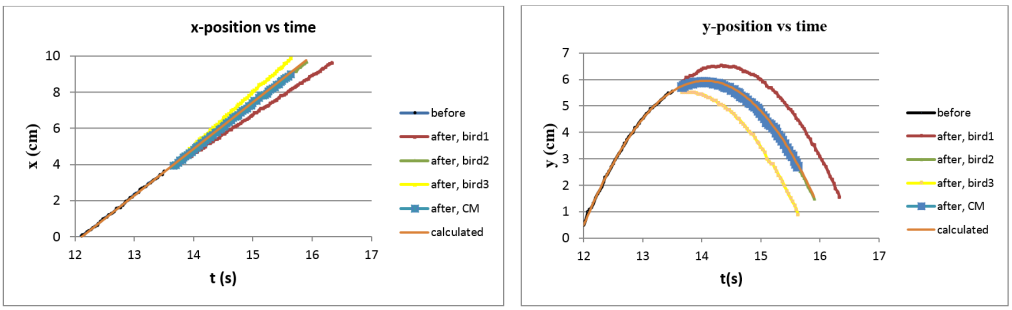

Figure 3. The trajectories of The Blues before (black) and after (red, green, and yellow) the explosion: the horizontal position (top panel) and vertical position (bottom panel) as the function of time. We assume that a single blue bird splits into three birds (bird1, bird2, bird3) with equal masses after the explosion. The trajectory of the center of mass (blue) after the explosion is obtained by averaging the trajectories of the individual birds (red, green, and yellow). The calculated trajectory if there had not been any explosion is shown in orange. The analysis confirms that the trajectory of the bird if there had not been any explosion (orange) follows those of the center of mass of the birds (blue).

Here we have shown how visualizations can offer an alternative way to explain concepts that are otherwise rather difficult to grasp. We use a simple and free tool and combine it with a popular game to discuss the application of momentum conservation and center of mass in the exploding projectile problem.

THE PHYSICS OF FALLING OBJECTS

In this section we discuss the physics of falling objects under gravity. The equivalence between inertial and gravitational mass (Pendrill, et al., 2014) implies that, in the absence of air resistance, all objects will fall with the same acceleration, i.e. gravity. A hammer and feather will fall at the same time dropped from the same height in a vacuum, or on the Moon (NSSDCA, 2008). The situation changes when one considers the drag force which arises from air resistance. The drag force will oppose the motion of the falling objects and will change the kinematics.

We contrast the cases where the effect of air resistance is negligible and is important. In the absence of air resistance, where the only force acting on an object is the force of gravity, the vertical position is quadratic with time and the vertical velocity is linear with time. The presence of air resistance is usually modeled by a velocity-dependent force, $f = bv$, at low speeds (Landau & Lifshitz, 1959). The parameter $\boldsymbol{b}$ is a constant which depends on the surface area of the object and v is the instantaneous velocity at a particular time. The velocity of the falling object, with mass m, in the presence of air resistance will then be given (Alonso & Finn, 1992):

$$v(t) = \frac{mg}{b}\left[1 - e^{-bt/m}\right];$$

at short times, the force of air resistance is small and plays little role in modifying the kinematics; the object obeys the kinematics of free fall. As time increases, the force of air resistance grows and opposes gravity, thus decreasing the effective acceleration. At long times, the velocity of the object saturates (terminal velocity) because the force of air resistance balances the force of gravity. The vertical position is no longer quadratic in time but grows linearly with time.

We performed a simple experiment to see how air resistance affects the motion of falling objects. We used two sheets of tissue paper, one tightly crumpled and another one loosely crumpled, as the objects, dropped them separately from a height of approximately 3 meters, and recorded the motions. *Tracker* was used to analyze the motions of the tissue papers. This is shown in Figure 4.

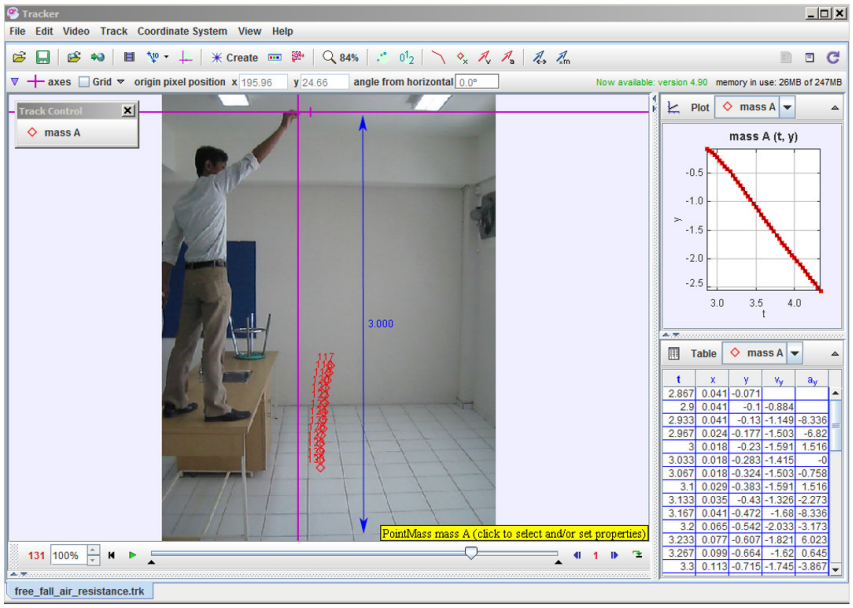

Figure 4. Video analysis of a sheet of tissue paper dropped from a certain height above the floor. We set up the frame of reference (purple lines) and calibration (blue line) to enable data collection of the motion. Red symbols are the tracked data in the motion. The right panel shows the plotted graph on a vertical position along with the numerical values on the table below it.

The result of the analysis is presented in Figure 5. The effect of air resistance is small for the tightly-crumpled tissue paper and thus it serves as a model for free fall situations where an object falls under the sole influence of gravity. The position and velocity are plotted in Figure 5 in red symbols. The time dependence of the position and velocity agree with that of theoretical description: quadratic in time for the position and linear in time for the velocity. The effect of air resistance on the loosely-crumpled tissue paper is large. The position and velocity exhibit time dependence consistent with the description of an object falling under gravity and opposed by the force of air resistance. At short times, the position and velocity agree with those of free fall, while at long times, the position is linear with time and the velocity saturates, a hallmark

of terminal velocity. This simple exercise can bring a new level of understanding about the physics of falling objects in the absence and presence of air resistance.

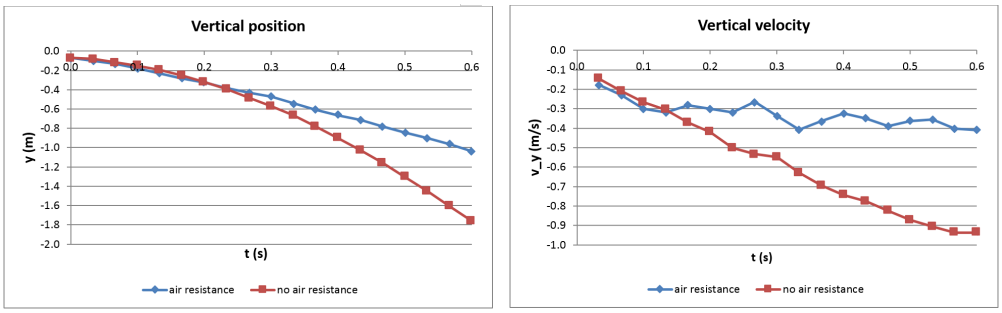

Figure 5. The position (top panel) and velocity (bottom) of falling objects in the absence (red) and presence (blue) of air resistance. When the effect of air resistance is negligible (red), the object follows free-fall kinematics where the object is falling under the sole influence of gravity: the position grows quadratically in time while the velocity grows linearly in time. When the effect of air resistance is large, the position grows linearly with time while the velocity is linear with time at short times and saturates at long time, a clear demonstration of the strong interplay between the force of gravity and force of air resistance.

CALIBRATION OF A HOME-MADE SPECTROMETER

In the last example, we show how to use *Tracker* to calibrate a home-made spectrometer based on known spectra of a mercury lamp (Philips Lighting, 2015). The spectrometer was made from household items such as cardboard, an unused mouse pad which was used as the entrance slit, and an old CD which served as the diffracting grating. Figure 6 demonstrates the calibration process and result. The calibration process is as follows: we used the entrance slit (white line on top panel of Figure 6) as the frame of reference from which the distance (in pixels) to the known spectra is measured. To determine the distance to the spectral lines, we used the line profile feature in *Tracker* to measure the spectral intensities along the line; the peaks in the observed intensity were marked as the distance to the said spectrum. Correlating the known wavelengths of the spectra with distance gave us the calibration curve shown in the bottom panel of Figure 6.

Equipped with the calibration curve, one can extract unknown wavelengths of observed spectra of a light source. We applied this to a commercial mosquito repellant lamp. Figure 7 shows the image of the observed spectra of such a light source which has 3 sharp lines. The calibration curve given in Figure 6 allowed us to extract the wavelengths of the spectra. The result is shown in Table 1. It is unfortunate that the commercial mosquito repellant light does not provide any information on the wavelengths of the emitted light. Thus it is not possible to compare our finding with the real wavelengths.

Table 1
The extracted wavelengths of the spectra of a commercial mosquito repellant lamp

Distance from entrance slit (pixels)	Calculated λ (nm)
665	384.6
838	507.2
888	542.6

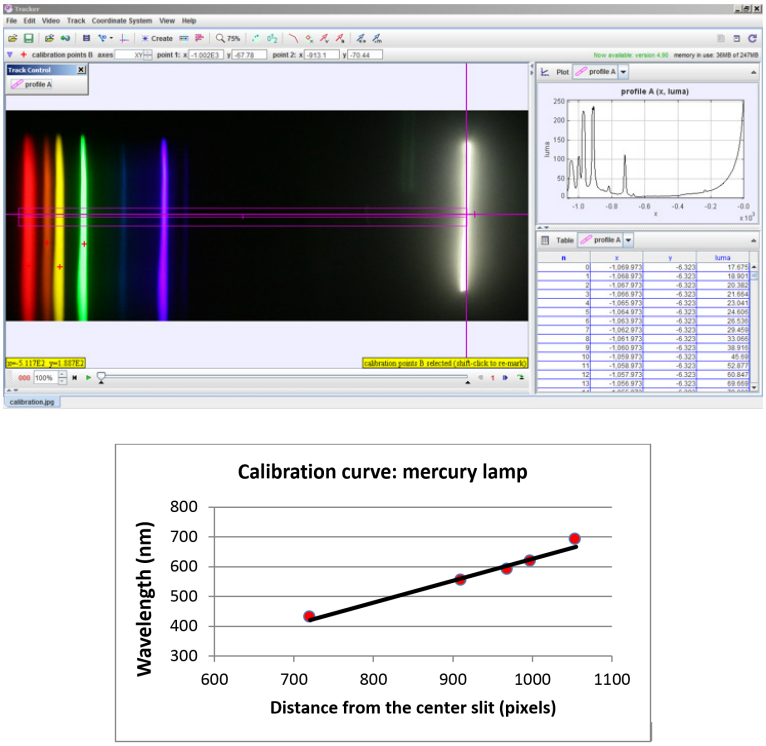

Figure 6. Calibrating a home-made spectrometer using a mercury lamp with known spectra. The top panel shows the tracker window where the calibration involves two processes: 1) setting up the coordinate system and 2) placing calibration points at spectral lines with known wavelength. The calibration points mark the distance (measured in pixels) from the reference point, which is taken as bright white line at the right. The bottom panel shows the calibration curve for the mercury lamp which is done by correlating the distance from the reference point with the known wavelength.

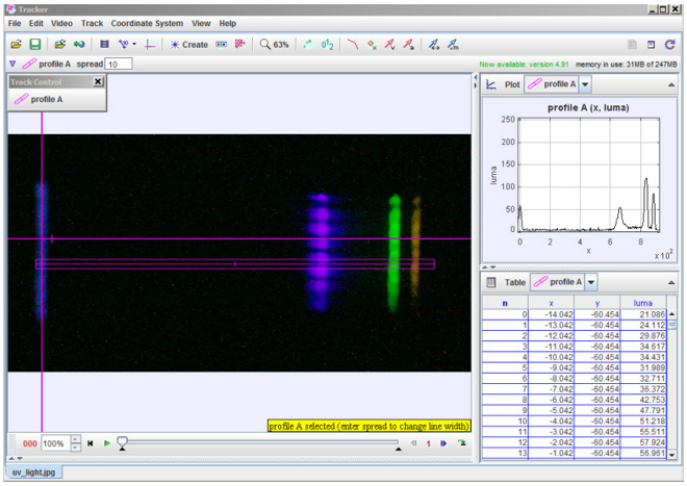

Figure 7. Measuring the unknown wavelengths of the spectra of a commercial mosquito repellant lamp. The entrance slit is used as a reference from which the distance to the spectra is measured. By comparing the measured distance with the calibration curve in Figure 6, one can extract the wavelengths of the observed spectra.

CONCLUSION

In this work we show how *Tracker* offers visualizations of concepts that are otherwise rather difficult to grasp. We discuss the application of *Tracker,* an image and video analysis software, in two different settings: mechanics and optics. In mechanics, *Tracker* was used to analyze videos of an exploding projectile, modeled by The Blues in the Angry Bird game, and a falling object in the presence of air resistance. The concepts of momentum conservation, center of mass, and terminal velocity in these exercises are presented by combining experiments, calculations, and visualizations. In optics, a home-made spectrometer was calibrated using *Tracker* by analyzing still images of the known spectra of a mercury lamp. The calibrated spectrometer can be used to extract wavelengths of unknown spectra. This simple exercise opens up an opportunity to introduce advanced concepts in modern Physics, such as energy band gap, at high school levels.

In the future, we would like to bring *Tracker* into the classrooms. One of the goals of this future study is to study the effectiveness of using visualizations in delivering Physics concepts. *Tracker* can also be used to study advanced topics beyond conventional topics in classrooms. For example, diffusion dynamics is one of the topics that is not typically offered at high school level; nevertheless we believe that students will be able study and grasp the concept using *Tracker.* Thus *Tracker* opens up wide range of possibilities for further (advanced) works.

REFERENCES

Alonso, M., & Finn, E. J. (1992). *Physics*. Amsterdam: Addison-Wesley.

Angry Birds Wiki. (2015). Retrieved October 1, 2015 from Jay, Jake, and Jim: http://angrybirds.wikia.com/wiki/Jay,_Jake,_and_Jim

Brown, D. (2015). *Tracker, Video Analysis and Modeling Tool*. Retrieved October 1, 2015 from http://physlets.org/tracker/

Cataloglu, E. (2006). Open Source Software in Teaching Physics: A Case Study on Vector Algebra and Visual Representations. *Turkish Online Journal of Educational Technology, 5*(1), 68-74.

Dori, Y. J., & Belcher, J. (2005). How Does Technology-Enabled Active Learning Affect Undergraduate Students' Understanding of Electromagnetism Concepts? *Journal of the Learning Sciences, 14*(2), 243-279.

Freeman, S., Eddy, S. L., McDonough, M., Smith, M. K., Okoroafor, N., Jordt, H., & Wenderoth, M. P. (2014). Active learning increases student performance in science, engineering, and mathematics. *Proceeding of the National Academy of Sciences, 111*(23), 8410-8415.

Google Play. (2015). Retrieved October 1, 2015, from Angry Birds: https://play.google.com/store/apps/details?id=com.rovio.angrybirds&hl=en

Holics, L. (2011). *300 Creative Physics Problems with Solutions.* London: Anthem Press.

Kozma, R. B. (2003). Technology and Classroom Practices. *Journal of Research on Technology in Education, 36*(1), 1-14.

Landau, L. D., & Lifshitz, E. M. (1959). *Fluid Mechanics*. Addison-Wesley.

NSSDCA. (2008). Retrieved October 1, 2015 from The Apollo 15 Hammer-Feather Drop: http://nssdc.gsfc.nasa.gov/planetary/lunar/apollo_15_feather_drop.html

Page, K. (2015). Using Social Media in A High School Physics Classroom. *Physics Teacher, 53*, 184.

Pendrill, A.-M., Ekström, P., Hansson, L., Mars, P., Ouattara, L., & Ryan, U. (2014). The equivalence principle comes to school—falling objects and other middle school investigations. *Physics Education, 49*(4), 425-430.

Philips Lighting. (2015). Retrieved October 1, 2015, from High Pressure Mercury HPL-N 80W: http://www.lighting.philips.com/main/prof/lamps/high-intensity-discharge-lamps/hpl-high-pressure-mercury/hpl-n/928051007360_EU/product/downloads

Robinett, R. (1995). Visualizing the solutions for the circular infinite well in quantum and classical mechanics. *American Journal of Physics, 64*(4), 440-446.

Thornton, S. T., & Marion, J. B. (2003). *Classical Dynamics of Particles and Systems.* Brooks Cole.

Pertanika J. Sci. & Technol. 24 (2): 493 - 506 (2016)

SCIENCE & TECHNOLOGY

Journal homepage: http://www.pertanika.upm.edu.my/

Automatic Tags Generation in Folksonomy for Learning Resources Reuse and Sharing

Ching Chieh Kiu

School of Computing and IT, Taylor's University, 47500 Subang Jaya, Selangor, Malaysia

ABSTRACT

With the proliferation of Web 2.0 technologies, folksonomy which is also known as social tagging or collaborative tagging is widely used by learners to annotate and categorize their learning resources. In a folksonomy system, the tags are added by learners to the learning resources, hence the tags are often ambiguous, overly personalised and imprecise. In addition, conjugated words, compound words and nonsense words may be used in tagging and shared among a group of learners. This has resulted in an uncontrolled and chaotic set of tagging terms that cause learning resources searching, reuse and sharing to become ineffective. In this paper, we present a content-based approach which automatically generates tags from a learning resource using Part-Of-Speech Tagging and K-Means Clustering techniques. The generated tags are more precise and unambiguous which can improve learning resources searching, reuse and sharing among learners.

Keywords: Folksonomy, clustering, K-Means, Part-of-Speech, collaborative tagging, learning content reuse, learning content Sharing, learning process, automatic tagging

INTRODUCTION

With the increasing popularity of Web 2.0 technologies, folksonomies (a method for collecting, organizing and creating tags) are emerging to allow learners to categorise and annotate learning content through collaborative tagging or social tagging systems. In social tagging systems, learners freely choose their own vocabulary, so-called tags, by adding explicit meaning which may come from inferred understanding of the learning contents. In this way folksonomies provide a new mechanism for learners to retrieve their learning resources via tag clouds (unstructured navigations). In addition, the mechanism also enables the learning resources to be shared and reused with their peers in an e-learning environment. The example of learning resources uploaded and tagged by learners with freely chosen tags

Article history:
Received: 8 December 2015
Accepted: 22 April 2016

E-mail addresses:
kiuchingchieh@gmail.com, chingchieh.kiu@taylors.edu.my
(Ching Chieh Kiu)

ISSN: 0128-7680

and their tag clouds are depicted in Figure 1. Tag clouds display the most popular tags. The bigger the font size of a tag, the more learning resources are indexed with the tag.

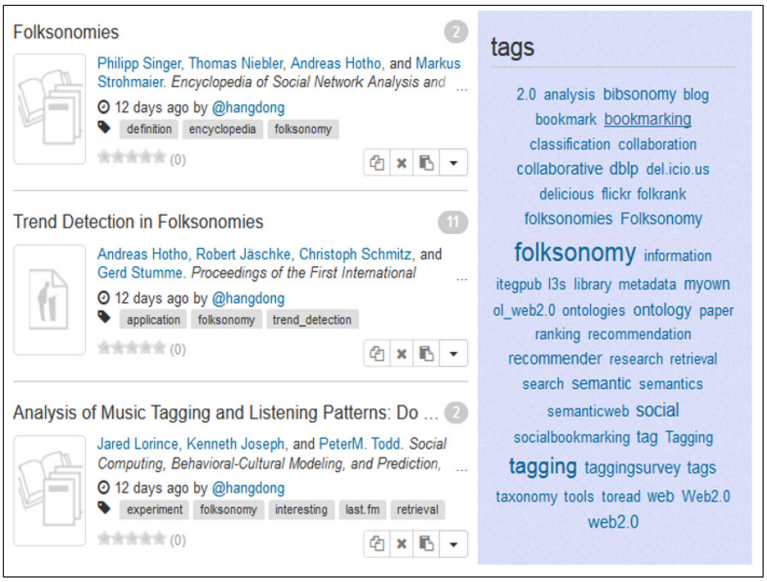

Figure 1. Example of Learning Resources Tagged by Learners and Their Tag Cloud

Since learners personally assign tags to the learning resources, the tags are often ambiguous, overly personalised and imprecise. In addition, learners may use acronyms words, conjugated words, compound words and nonsense words to tag their learning resources and these tags may be shared among a group of learners in collaborative learning environments. This has resulted in uncontrolled and chaotic sets of tagging terms (uncontrolled vocabularies) that cause learning resources retrieval, reuse and sharing among learners to become ineffective and inefficient (Macgregor & McCulloch, 2006; Koren, 2010; Gueye et al., 2014;). Hence, the use of controlled vocabularies to tag learning resources should be prominent prior to knowledge sharing and reuse in a collaborative learning environment (Lau et al., 2015).

In a social tagging system, there are three typical approaches of tag recommendation for annotating learning resources as listed below:

1.) Content-based tagging approach – recommends a tag to a user based on items with similar content in the user's profile. Relies on the content of the documents (Figure 2(a) & Figure 2(b)).

2.) Collaborative-based tagging approach – recommends a tag to a user based on tags used by similar users. Relies on the tagging behaviour of similar users (Figure 2(c)).

3.) Hybrid or combined approaches.

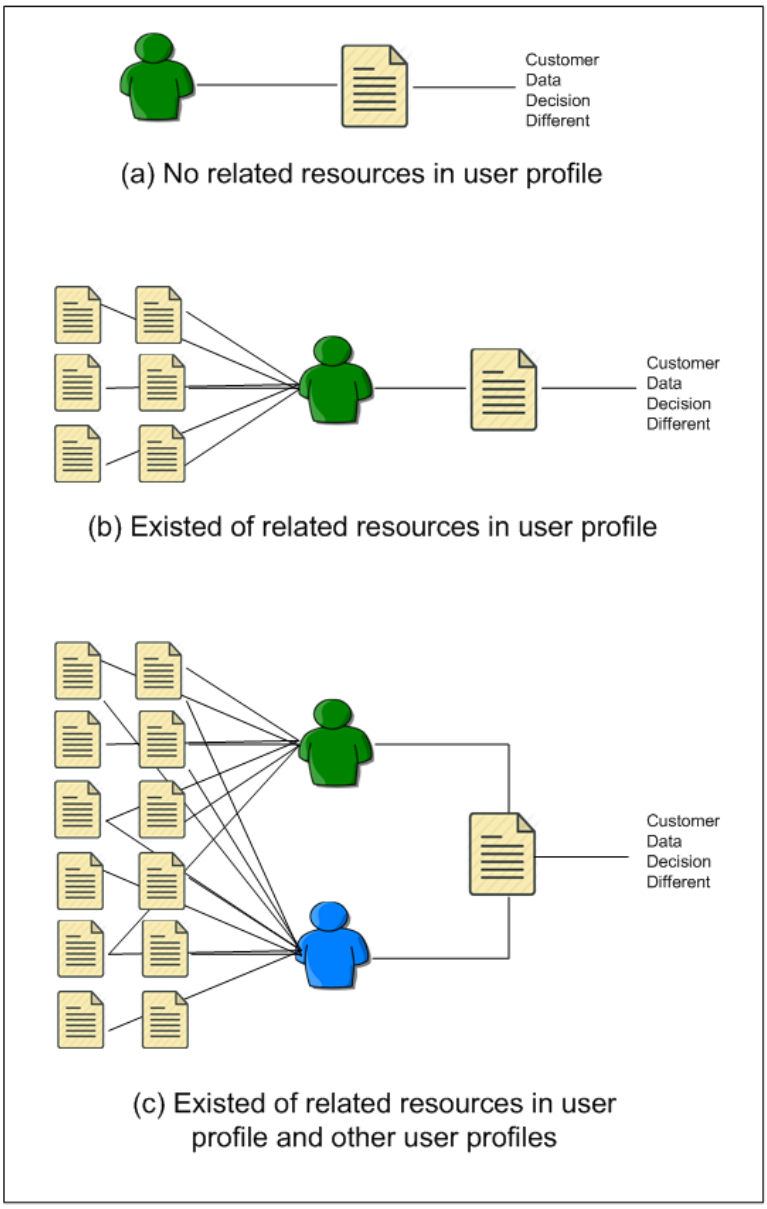

Figure 2. Tag Recommendation Approaches of Tagging System

Automatic tag recommendations can ease the task of learners when annotating new resources. The majority of the tag recommendation approaches assume that a learning resource posting by a learner already exists in the system (prior knowledge) (Jaschke et al., 2007) as depicted in Figure 2(b) and Figure 2(c). In the case where there is no prior knowledge and a learner posts for the first time, the tag recommendation needs to rely on the content of a learning resource to provide good recommendations for unseen resources (Lipczak, 2008; Lu et al., 2009; Tatu et al., 2008; Hassan et al., 2009) as shown in Figure 2(a).

This paper addresses the limitation of uncontrolled vocabularies and the absence of prior knowledge in tagging a learning resource by presenting a content-based approach to automatically generate social tags (controlled vocabularies) from a learning resource using Part-Of-Speech Tagging and K-Means Clustering techniques. The generated social tags from a learning content itself are regarded as controlled vocabularies, hence they are more precise and unambiguous social tags to use for tagging learning resources. The searching, reuse and sharing on the learning resources among learners becomes more effective and efficient through the generated social tags.

The paper is organized as follows: In next section, we discuss related work. Following section explains methodologies for tag generation which comprise folksonomy, part-of-speech tagging and k-means clustering. The framework for automatic tag generation is presented in next section. An example of the results of a simulation to illustrate the framework algorithm is provided in following section. Lastly, the paper is concluded with conclusions and future work.

RELATED WORK

Automatic tag recommendations can reduce people's tagging effort and encourage them to use more tags to annotate resources in a folksonomy system. Therefore, the annotated learning resources can be easily retrieved, shared and reused among people in the folksonomy system. Tags provide new information to resources over original contents (Bischoff et al., 2008; Zhang & Ge, 2015; De Caro et al., 2016), hence tags enhance the capability to discover relevant resources via existing search engines (Heymann et al., 2008; Wei et al., 2016). Furthermore, automatic tag recommendations lighten the task of users while annotating a new resource when prior tag information is not available.

Most of the tag recommendations rely on prior tag information (Sigurbjornsson & Zwol, 2008; Jaschke et. al., 2007; Symeonidis et al., 2008). However, if prior tag information is not available, then the contents of the posted resource need to be relied upon. For folksonomy systems, contents of resources are textual and unstructured in nature, hence appropriate text and natural language processing techniques are required to overcome them (Hassan et. al., 2009). In addition, clustering techniques have been used to handle parsing of document spaces in summarizing large set of documents (Kogan et al., 2006; Kiu & Eric, 2011) for information retrieval and post recommendation in collaborative tagging systems (Begelman et al., 2006; Shepitsen et al., 2008; Lau et. al., 2015).

As discussed in previous section, social tagging systems mainly can be categorized into two approaches, the content-based tagging approach and collaborative-based tagging approach. In this section, content-based tagging for folksonomy systems proposed by Lipczak (2008), Tatu et. al. (2008), Heymann et. al. (2008), Hassan et. al. (2009) and Lu et. al. (2009) are discussed.

Lipczak (2008) proposed a method to extract the terms in the title of a post, and then to expand the set using a tag co-occurrence database. The result is filtered with the poster's tagging history. Meanwhile, Tatu et. al. (2008) used terms from several fields including URL and title to build post and user based models. Natural language processing is used to normalize terms from various sets before recommending them.

Heymann et. al. (2008) developed content-based tag recommendation using a supervised learning method. Page text, anchor text, surrounding hosts and available tag information are formulated as training data. They trained a classifier for each tag they wanted to predict. However, the time required to train the classifiers for each tag becomes substantial when the number of distinct tags increases. For little tag information associated with documents, an association rules mining is used to generate the tag set of the document.

Hassan et. al. (2009) implemented a discriminative clustering approach for content-based tag recommendation in social bookmarking systems. They grouped posts based on the textual contents of the posts with discriminative clustering. The clustering method was used to build two clustering models whereby the first cluster was based on the tags assigned to posts and the second cluster was based on the content terms of posts. In the case of a new posting, the clustering method generated a ranked list of tags which served as final tag recommendations. If the tagging history is available, then this list is also utilized in the final tag recommendation.

Lu et. al. (2009) proposed a content-based tag recommendation for users to manually and automatically annotate webpages with or without prior tag information. Each webpage shares the tags they own with similar webpages. The similarity metric between sending and receiving webpages is defined as a linear combination of four cosine similarities. The similarity is calculated based on tag information and page content. An entropy-based metric is used to describe tags/terms to represent the annotated document. They represent each document with two vectors, namely a tag vector and a term vector using a vector space model.

There are also many content-based tagging systems with prior tag information consisting of different methods (Zhang et al., 2009; Guan et al., 2009; Wetzker et al., 2010; Rendle & Schmidt-Thieme, 2010). Collaborative tagging approaches are seen in studies by Chen et al. (2008), Koren (2010), Gueye et al. (2014) and Ifada, & Nayak (2015).

We present a content-based approach which automatically generates social tags from a learning resource using Part-Of-Speech Tagging and K-Means Clustering techniques to tag learning resources without prior tag information available in social tagging system.

METHODOLOGIES FOR SOCIAL TAG GENERATION

In this section, we provide a formal description of folksonomy, part-of-speech tagging and k–means clustering algorithm.

Folksonomy

A folksonomy is a system where users can use personal or public tags to annotate online resources such as web pages, videos, podcasts, photos and others. It is also known as collaborative tagging and social tagging. This social tagging system uses these tags to index information, facilitate searches and navigate resources (Wikipedia, 2015).

As depicted in Figure 3, a folksonomy consists of users, tags, documents (resources) and the user-based assignment of tags to resources. A folksonomy can be written as a tuple $F := (U, T, R, Y)$ where U (users), T (tags), and R (documents) are finite sets, and Y is a ternary relation between the three components, $Y \subseteq U \times T \times R$, (Jäschke et al., 2007).

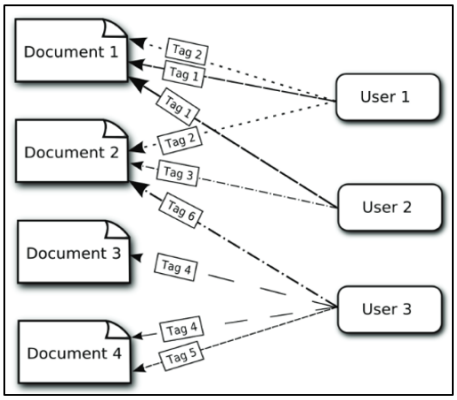

Figure 3. Relations of Tags, Users and Resources (Peters & Stock, 2007)

Part-of-Speech Tagging

Part-of-speech (POS) tagging is applied to transform unstructured text format into a structured text format (Navigli, 2009). Every word in the text is assigned a unique part-of-speech as listed in Table 1. It predicts the part-of-speech even for an unknown word by exploiting the context of the word in a sentence. The POS tagging process is shown in Figure 4 and explicated as below:

1.) Tokenization is a normalization process that splits up the text into a set of words.

2.) Part-of-speech tagging is the process to assign a grammatical category to each word. This process is referred as grammatical tagging as it assigns a single part-of-speech tag to each word and punctuation marker.

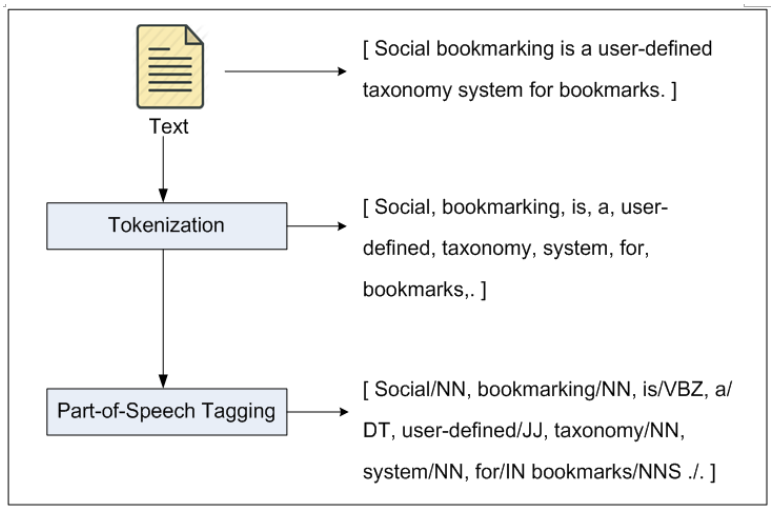

Figure 4. Process of POS Tagger

Table 1
Description for Tags of Part-of-Speech

Tag	Description	Tag	Description
$	dollar	PDT	pre-determiner
``	opening quotation mark	POS	genitive marker
"	closing quotation mark	PRP	pronoun, personal
(	opening parenthesis	PRP$	pronoun, possessive
)	closing parenthesis	RB	adverb
,	comma	RBR	adverb, comparative
--	dash	RBS	adverb, superlative
.	sentence terminator	RP	particle
:	colon or ellipsis	SYM	symbol
CC	conjunction, coordinating	TO	"to" as preposition or infinitive marker
CD	numeral, cardinal	UH	interjection
DT	determiner	VB	verb, base form
EX	existential there	VBD	verb, past tense
FW	foreign word	VBG	verb, present participle or gerund
IN	preposition or conjunction, subordinating	VBN	verb, past participle
JJ	adjective or numeral, ordinal	VBP	verb, present tense, not 3rd person singular
JJR	adjective, comparative	VBZ	verb, present tense, 3rd person singular
JJS	adjective, superlative	WDT	WH-determiner
LS	list item marker	WP	WH-pronoun
MD	modal auxiliary	WP$	WH-pronoun, possessive
NN	noun, common, singular or mass	WRB	Wh-adverb
NNP	noun, proper, singular		
NNPS	noun, proper, plural		
NNS	noun, common, plural		

K-Means Clustering

K-Means clustering is a simple unsupervised clustering technique (Berkhin, 2006). It is used to classify a given data set into a previously specified number of clusters (k). K-means clustering divides a data set to a number of clusters. It is defined as

$$E = \sum_{k=1}^{C} \sum_{x \in Q_k} \|x - c_k\|$$

where C is the number of clusters, x is a data point, and c_k is the centroid of the data points k.

The algorithm of k-means is composed of four steps:

Step 1: Specify the number of clusters, k. Initialize k point randomly as cluster centers.
Step 2: Assign each instance to its closest cluster center using Euclidean distance.

$$Euclidean\ distance: dist(x, \mu) = \sum_{j=i}^{d} (x_j - \mu_j)^2$$

where μ_j is mean of point in x_j.

Step 3: Re-compute the centroid (mean) for each cluster as a new cluster center.

$$mean: \vec{\mu} = \frac{1}{N_C} \sum_{i \in C} \overrightarrow{X_i}$$

Step 4: If the new cluster centers are different from the old cluster centers repeat Step 2 until the cluster centers do not change anymore.

THE SOCIAL TAG GENERATION FRAMEWORK

This section explicates the automatic social tag generation framework as depicted in Figure 5.

The algorithm implementation of the framework comprises the following steps:

Input : A learning resource

Step 1 : HTML Parser
A learning resource obtained online is parsed into unstructured text (unformatted text) using HTML Content Extractor (Alexander, 2015) automatically. All non-text contents such as flash animation, hyperlinks, audios, videos and others are parsed. Meanwhile the unformatted text context is saved into text processing format (.txt) as output for the next process.

Step 2 : Tokenization
The sentences are tokenized into each word (token) prior to the POS tagging process. For example, the text "`This is social bookmarking.`", is tokenized into "`This, is, a, social, bookmarking, .`".

Step 3 : Part-of-Speech Tagging
The tokenized words are assigned with POS tags. The Standford POS English tagger, namely bidirectional-distsim (Toutanova et. al, 2003) is used to perform the POS tagging assignment. For example, the tokens "`This, is, a, social, bookmarking, .`", are POS tagged into "`This_DT is_VBZ a_DT Social_NNP bookmarking_NN ._.`". The structured text is generalized at the end of this process.

Step 4 : Contextual Clustering
K-means clustering in Weka is used to contextualize the structured text in order to reduce the tag generation processing time (Hall et. al., 2009).

Clusters of five are applied in k-means clustering to cluster each word in the structured text. The words are clustered into five clusters according to their attributes.

Step 5 : Keyword Generation
In this process, words that are associated with the unconventional part-of-speech (``, :, ? CD, DT, VBZ, IN, PRP, RBS, VBN, VBP, EX, -RRB-, -LRB-, CC, VBG, MD, VB, WRB, RB, WDT, RP, VBD, RP, WP, JJR, TO, PRP$, POS, RP) in each cluster are eliminated to retain only the words in nouns. Key words (tags) are formed based on the sequence relations of each word in a cluster.

Output : A set of tags (controlled vocabularies).

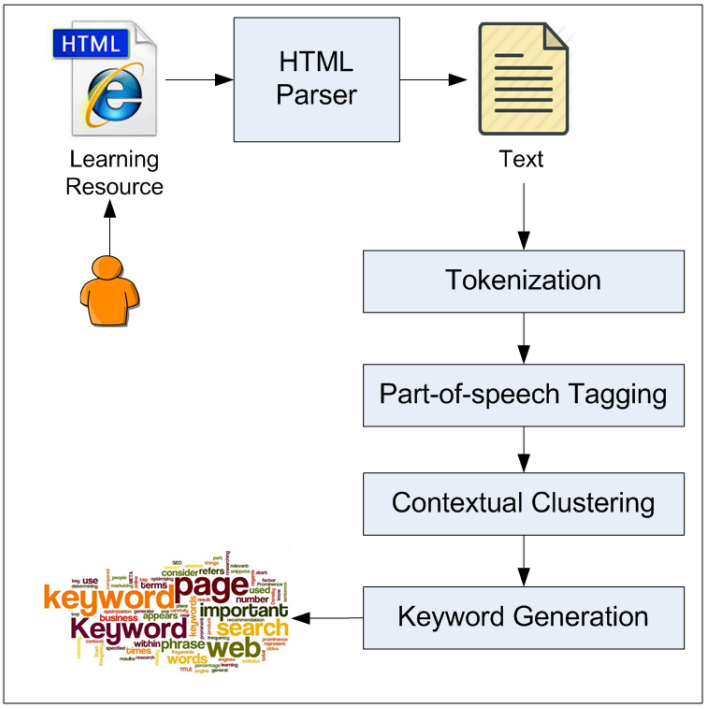

Figure 5. Framework for Automatic Social Tag Generation

SIMULATED EXAMPLE

The learning resource (http://whatis.techtarget.com/definition/social-bookmarking) to be tagged is illustrated in Figure 6. The learning resource is parsed into unstructured text using HTML Parser and saved into text processing format. Each of the words in the file is tokenized and assigned with part-of-speech has resulted 341 tokens as illustrated in Figure 7. K-Mean clustering (Figure 8) is applied to cluster the tokens according to the tokens' attributes. 117 token are yielded after the process of contextual clustering (Figure 9). The process of elimination the unconventional part-of-speech which associated with the words has generated 23 tags

(controlled vocabularies) as shown in Figure 10. The generated tags are the recommended tags for a learner to annotate the learning resource.

DEFINITION

social bookmarking

Like 3 Tweet +1 0 Share Email

Part of the Internet applications glossary:

Social bookmarking is a user-defined taxonomy system for bookmark s. Such a taxonomy is sometimes called a folksonomy and the bookmarks are referred to as tags. Unlike storing bookmarks in a folder on your computer, tagged pages are stored on the Web and can be accessed from any computer. Technorati, a blogging site, describes the system as "The real-time Web, organized by you." Web sites dedicated to social bookmarking, such as Flickr and del.icio.us, provide users with a place to store, categorize, annotate and share favorite Web pages and files.

Here's how you might use del.icio.us: Once you've registered, you can install buttons to your toolbar . If you visit a Web page that you want to save, you click a "tag" button. A window pops up with the URL and page name and optional fields for you to add notes and tags. Tags are single-word descriptors -- this is how social bookmark systems categorize content so that you and other users can find it.

Another button takes you directly to a page with your saved bookmarks and associated tags. If you click on one of the tags you created, you'll be taken to a page listing your saved pages associated with that tag. You can also view all users' content associated with that tag or the most popular examples. The site inbox feature lets you subscribe to content saved with a specific tag or content saved by a specific user or a combination of the two.

When you click a tag or search for a term on del.icio.us, the results include information about how many members have saved each item and any tags that they included for it.

Joshua Schachter started del.icio.us in 2003 as a way to track and share bookmarks. As the service grew and demanded more of his time, Schachter quit his job at Morgan Stanley to devote himself to the site, which now serves hundreds of thousands of members. In December of 2005, he sold the site to Yahoo.

This was last updated in June 2006

Posted by: Margaret Rouse

Figure 6. The Tagged Learning Resource

Index	Token	Tag	Index	Token	Tag	Index	Token	Tag
1	Social	NNP	21	bookmark	NNS	41	the	DT
2	bookmarking	NN	22	are	VBP	42	Web	NN
3	is	VBZ	23	referred	VBN	43	and	CC
4	a	DT	24	to	TO	44	can	MD
5	user-defined	JJ	25	as	IN	45	be	VB
6	taxonomy	NN	26	tags	NNS	46	accessed	VBN
7	system	NN	27	Unlike	IN	47	from	IN
8	for	IN	28	storing	VBG	48	any	DT
9	bookmark	NN	29	bookmark	NNS	49	computer	NN
10	s	NN	30	in	IN	50	Technorat	NNP
11	Such	JJ	31	a	DT	:	:	:
12	a	DT	32	folder	NN	:	:	:
13	taxonomy	NN	33	on	IN	:	:	:
14	is	VBZ	34	your	PRP$	:	:	:
15	sometimes	RB	35	computer	NN	336	he	PRP
16	called	VBN	36	tagged	VBN	337	sold	VBD
17	a	DT	37	pages	NNS	338	the	DT
18	folksonomy	NN	38	are	VBP	339	site	NN
19	and	CC	39	stored	VBN	340	to	TO
20	the	DT	40	on	IN	341	Yahoo	NNP

Figure 7. List of Tokens after POS Tagger

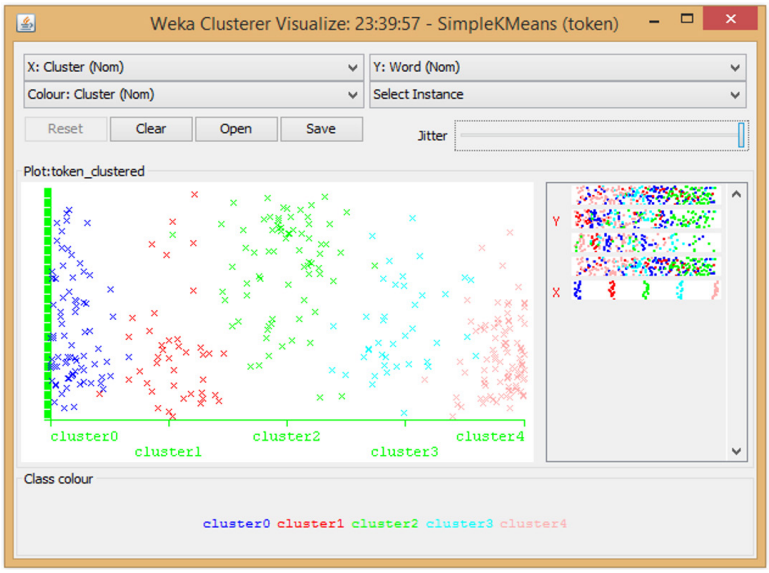

Figure 8. Visualization of Clustered Tokens

Index	Token	Tag	Cluster	Index	Token	Tag	Cluster	Index	Token	Tag	Cluster
12	Social	NNP	cluster1	21	real-time	JJ	cluster1	:	:	:	:
13	bookmarking	NN	cluster1	22	Web	NN	cluster1	:	:	:	:
14	user-defined	JJ	cluster1	23	Web	NN	cluster1	:	:	:	:
15	taxonomy	NN	cluster1	24	sites	NNS	cluster1	:	:	:	:
16	system	NN	cluster1	25	social	JJ	cluster1	102	track	NN	cluster1
17	bookmark	NN	cluster1	26	bookmark	NN	cluster1	103	share	NN	cluster1
18	Such	JJ	cluster1	27	such	JJ	cluster1	104	bookmark	NNS	cluster4
19	taxonomy	NN	cluster1	28	Flickr	NNP	cluster1	105	service	NN	cluster1
20	folksonomy	NN	cluster1	29	del.icio.us	NNP	cluster1	106	time	NN	cluster1
22	tags	NNS	cluster1	30	users	NNS	cluster1	107	Schachter	NNP	cluster4
23	bookmarks	NNS	cluster1	31	place	NN	cluster1	108	job	NN	cluster1
24	folder	NN	cluster1	32	store	NN	cluster1	109	Morgan	NNP	cluster4
25	computer	NN	cluster1	33	categorize	NN	cluster1	110	Stanley	NNP	cluster4
26	pages	NNS	cluster1	34	annotate	NN	cluster1	111	site	NN	cluster1
27	Web	NN	cluster1	35	share	NN	cluster1	112	hundreds	NNS	cluster4
28	computer	NN	cluster1	36	favorite	JJ	cluster1	113	thousands	NNS	cluster4
29	Technorati	NNP	cluster1	37	Web	NN	cluster1	114	members	NNS	cluster4
30	blogging	NN	cluster1	38	pages	NNS	cluster1	115	Decembei	NNP	cluster4
31	site	NN	cluster1	39	files	NNS	cluster1	116	site	NN	cluster1
32	system	NN	cluster1	40	del.icio.us	NN	cluster1	117	Yahoo	NNP	cluster4

Figure 9. List of Tokens after Contextual Clustering and Part-of-Speech Elimination

Tags (Controlled Vacabularies)		
blogging site	Morgan Stanley	site inbox feature
bookmarks	optinal fields	social bookmarking
buttons	other users	systems
computer	page name	tags
content	pages	user-defined taxonomy system
del.icio.us	real-time web	web pages
Joshua Schachter	share favorite web pages	web sites
members	single-word descriptors	

Figure 10. Generated Tags for a Learning Resource Tagging

CONCLUSION AND FUTURE WORK

Tags used by learners to annotate learning resources are often ambiguous, imprecise and overly personalised. Hence this has resulted in uncontrolled vocabularies that cause learning resources retrieval, sharing and reuse to become ineffective. This paper has proposed an automatic tags generation algorithm to generate controlled vocabularies (social tags) from contents of a learning resource. The experimental result has shown the used of part-of-speech and unsupervised clustering techniques in the proposed algorithm has improved the scalability of tag generation from a learning resource. Furthermore, prior knowledge (tag information) is not required in tag generation. For future work, we will investigate a suitable weighting scheme for tag recommendation by incorporating a learner profile.

Tagging a learning resource with the generated controlled vocabularies can appropriately describe the content of the learning resource itself. Subsequently, these learning resources can be shared and reused effectively and efficiently among learners in an e-learning environment. In addition, learning resources navigation and retrieval are more effective with controlled vocabularies annotation.

The algorithm can be applied to generate tags for explicit knowledge organizing and navigating in knowledge management systems. It also can be extended to E-Commerce system to generate tags from product catalogue or description. Product tagging with controlled vocabularies can enhance product searching, recommendation and personalization. On the other hand, the generated tags from a product catalogue can serve as SEO keywords and metadata for the product itself.

REFERENCES

Alexander, B. (2015). *HTML-Content-Extractor*. Retrieved 1 November 2015, from http://search.cpan.org/dist/HTML-Content-Extractor/.

Begelman, G., Keller, P., & Smadja, F. (2006). Automated tag clustering: Improving search and exploration in the tag space. In *Collaborative Web Tagging Workshop at WWW2006.* Edinburgh, Scotland, UK.

Berkhin, P. (2006). A survey of clustering data mining techniques. In Kogan, J., Nicholas, C., & Teboulle, M. (Eds.). *Grouping multidimensional data*. (25-71). Berlin Heidelberg: Springer.

Bischoff, K., Firan, C. S., Nejdl, W., & Paiu, R. (2008). Can all tags be used for search? In *Proceedings of the 17th ACM conference on Information and knowledge management* (193-202). New York: ACM.

Chen, W.Y., Zhang, D., & Chang, E.Y. (2008) Combinational Collaborative Filtering for Personalized Community Recommendation. In *Proceedings of the 14th ACM SIGKDD International Conference on Knowledge Discovery and Data Mining, Las Vegas, 24-27 August 2008* (115-123). New York: ACM. http://dx.doi.org/10.1145/1401890.1401909

De Caro, P., Pini, M. S., & Sambo, F. (2016). A Tag-Based Recommender System. In Menegatti, E., Michael, N., Berns, K., & Yamaguchi, H. (Eds). *Intelligent Autonomous Systems 13* (1049-1061). Cham, Switzerland: Springer International Publishing.

Guan, Z., Bu, J., Mei, Q., Chen, C., & Wang, C. (2009) Personalized Tag Recommendation Using Graph-Based Ranking on Multi-Type Interrelated Objects. In *Proceedings of the 32nd International*

ACM SIGIR Conference on Research and Development in Information Retrieval, New York, 19-23 July 2009 (540-547). New York: ACM. http://dx.doi.org/10.1145/1571941.1572034

Gueye, M., Abdessalem, T., & Naacke, H. (2014). A Parameter-Free Algorithm for an Optimized Tag Recommendation List Size. In *Proceedings of the 8th ACM Conference on Recommender Systems* (233-240). New York: ACM.

Hall, M., Frank, E., Holmes, G., Pfahringer, B., Reutemann, P., & Witten, I. H. (2009). The WEKA data mining software: an update. *ACM SIGKDD explorations newsletter*, *11*(1), 10-18.

Hassan, M. T., Karim, A., Manandhar, S., & Cussens, J. (2009). Discriminative clustering for content-based tag recommendation in social bookmarking systems. *ECML PKDD Discovery Challenge 2009 (DC09)* (85). Retrieved 1 November, 2015, from http://ceur-ws.org/Vol-497

Heymann, P., Koutrika, G., & Garcia-Molina, H. (2008). Can social bookmarking improve web search? In *Proceedings of the 2008 International Conference on Web Search and Data Mining* (195-206). New York: ACM.

Ifada, N. & Nayak, R. (2015) Do-Rank: DCG Optimization for Learning-to-Rank in Tag-Based Item Recommendation Systems. In: Cao, T., Lim, E.-P., Zhou, Z.-H., Ho, T.-B., Cheung, D. & Motoda, H., Eds., *Advances in Knowledge Discovery and Data Mining* (510-521). Berlin Heidelberg: Springer International Publishing. http://dx.doi.org/10.1007/978-3-319-18032-8_40

Jaschke, R., Marinho, L., Hotho, A., Schmidt-Thieme, L., & Stumme, G. (2007). Tag recommendations in folksonomies. In *Knowledge Discovery in Databases: PKDD 2007* (506-514). Berlin Heidelberg: Springer.

Kiu, C. C., & Tsui, E. (2011). TaxoFolk: A hybrid taxonomy–folksonomy structure for knowledge classification and navigation. *Expert Systems with Applications*, *38*(5), 6049-6058.

Kogan, J., Nicholas, C., & Teboulle, M. (Eds.) (2006). *Grouping multidimensional data*. Berlin Heidelberg: Springer.

Koren, Y. (2010) Collaborative Filtering with Temporal Dynamics. *Communications of the ACM* , *53*, 89-97. http://dx.doi.org/10.1145/1721654.1721677

Lau, S. B. Y., Lee, C. S., & Singh, Y. P. (2015). A folksonomy-based lightweight resource annotation metadata schema for personalized hypermedia learning resource delivery. *Interactive Learning Environments*, *23*(1), 79-105.

Lipczak, M. (2008). Tag recommendation for folksonomies oriented towards individual users. In *ECML PKDD Discovery Challenge 2008* (84–95). Retrieved 1, November 2015, from http://www.kde.cs.uni-kassel.de/ws/rsdc08

Lu, Y. T., Yu, S. I., Chang, T. C., & Hsu, J. Y. J. (2009). A Content-Based Method to Enhance Tag Recommendation. *IJCAI 9*, 2064-2069.

Macgregor, G., & McCulloch, E. (2006). Collaborative tagging as a knowledge organisation and resource discovery tool. *Library review*, *55*(5), 291-300.

Navigli, R. (2009). Word sense disambiguation: A survey. *ACM Computing Surveys (CSUR)*, *41*(2), 10.

Peters, I., & Stock, W. G. (2007). Folksonomy and information retrieval. In *Proceedings of the 70th Annual Meeting of the American Society for Information Science and Technology*, *45*, 1510-1542.

Rendle, S. & Schmidt-Thieme, L. (2010) Pairwise Interaction Tensor Factorization for Personalized Tag Recommendation. In *Proceedings of the 3rd ACM International Conference on Web Search and Data Mining, 2010* (81-90). New York: ACM. http://dx.doi.org/10.1145/1718487.1718498

Shepitsen, A., Gemmell, J., Mobasher, B., & Burke, R. (2008). Personalized recommendation in social tagging systems using hierarchical clustering. In *Proceedings of the 2008 ACM conference on Recommender systems* (259-266). New York: ACM.

Sigurbjornsson, B. & Van Zwol, R. (2008). Flickr tag recommendation based on collective knowledge. In *Proceedings of the 17th international conference on World Wide Web*. (327-336). New York: ACM.

Symeonidis, P., Nanopoulos, A., & Manolopoulos, Y. (2008). Tag recommendations based on tensor dimensionality reduction. In *Proceedings of the 2008 ACM conference on Recommender systems* (43-50). New York: ACM.

Tatu, M., Srikanth, M., & D'Silva, T. (2008). Rsdc'08: Tag recommendations using bookmark content. *ECML PKDD discovery challenge*, 96-107.

Toutanova, K., Klein, D., Manning, C. D., & Singer, Y. (2003). Feature-rich part-of-speech tagging with a cyclic dependency network. In *Proceedings of the 2003 Conference of the North American Chapter of the Association for Computational Linguistics on Human Language Technology-Volume 1* (173-180) Stroudsburg PA: Association for Computational Linguistics.

Wei, S., Zheng, X., Chen, D., & Chen, C. (2016). A hybrid approach for movie recommendation via tags and ratings. *Electronic Commerce Research and Applications*. doi: 10.1016/j.elerap.2016.01.003

Wetzker, R., Zimmermann, C., Bauckhage, C., & Albayrak, S. (2010). I Tag, You Tag: Translating Tags for Advanced User Models. In *Proceedings of the 3rd ACM International Conference on Web Search and Data Mining, New York, 2010* (71-80). New York: ACM. http://dx.doi.org/10.1145/1718487.1718497

Wikipedia (2015). Folksonomy. Retrieved 25 March 2016, from https://en.wikipedia.org/wiki/Folksonomy#cite_note-Berlin.2C_B._1992-21

Zhang, N., Zhang, Y., & Tang, J. (2009). A Tag Recommendation System for Folksonomy. In *Proceedings of the 2nd ACM Workshop on Social Web Search and Mining, New York, 2 November 2009* (9-16). New York: ACM.

Zhang, S. & Ge, Y. (2015). Personalized Tag Recommendation Based on Transfer Matrix and Collaborative Filtering. *Journal of Computer and Communications*, *3*(09), 9.

Pertanika J. Sci. & Technol. 24 (2): 507 - 516 (2016)

SCIENCE & TECHNOLOGY

Journal homepage: http://www.pertanika.upm.edu.my/

A Case Study on Utilizing a Mobile Application to Teach Malaysian Governance to International Students

Azizan Yatim

Centre for Pre-U Studies, UCSI Univesity, Sarawak Campus, Lot 2498, Block 16, KCLD, Jalan Tun Jugah, 93350, Sarawak, Malaysia

ABSTRACT

Malaysian Studies is a compulsory course for international undergraduate students in Malaysia. The subject comprises Malaysian history, its governance and administration system. Due to different socio-cultural backgrounds and histories, most, if not all, international students, struggled with this subject. This research project aims to create, implement and evaluate a mobile application (app) as a catalyst for mobile learning (m-learning) for one particular topic of the Malaysian Studies course. The increased use of technology in learning environments has changed instructional approaches by making it more accessible and essentially, more student-centered. Using a design-based research approach, the mobile app is aimed to guide students to write their own notes to assist in deeper understanding of the subject. The mobile app was also reviewed by users to gauge its effectiveness and ease of use. Findings from the tests showed the potential to structure the students' learning from the topic. From the research, there are a few improvements and suggestions that could be implemented for similar future studies and projects.

Keywords: Mobile learning, m-learning, technology-based learning environment, constructivist learning, Malaysian Studies, Malaysian governance components, student engagement, design-based research

INTRODUCTION

This design-based research project investigated how a mobile app could be used as a catalyst for learning. The development involved the analysis, design, development, implementation, and evaluation processes, following what is more popularly known as the ADDIE model (Forest, 2014), which was used as a guide by educators in both the designing and evaluating of their instruction.

In this research project, a mobile app was developed for one of the Malaysian Studies class session in one of the private universities in East Malaysia. An analysis of the learners,

Article history:
Received: 8 December 2015
Accepted: 22 April 2016

E-mail address:
azizan@ucsiuniversity.edu.my (Azizan Yatim)

ISSN: 0128-7680

the topic, potential problems and the appropriate learning theories was conducted before the app's design process. The design process incorporated the findings from the analysis and the app was later developed using the appnotch software. Upon completion, the learners were given full access to the app to use as part of their class activity. The learners were given the freedom to either work together with their course mates or as individual activity using the app as a guide. Online evaluation forms were used to evaluate the app's effectiveness and usability.

RESEARCH SCOPE

The Topic

The topic for the learning environment is "Components of Malaysia's Government System". This topic is part of the *Mata Pelajaran Umum (MPU)* Malaysian Studies course for international students.

In the topic, the students will learn about the fundamentals of Montesquieu's Separation of Powers Doctrine, draw an outline of the Malaysian system of government and finally to be able to understand the roles, limitations and importance of the key figures in Malaysia's administrative system.

This topic was chosen for several reasons. Primarily, it has been the hardest topic for international students to master in previous semesters. Previous students showed that they were not able to see the bigger picture of the topic, more specifically, how the main components are interrelated to each other. Though there has been no known research done in the area, the reason may be the apparent differences in governance systems for the international students. The socio-cultural backgrounds of students studying in foreign countries have an impact on their learning. Mahmud, Amat, Rahman, & Ishak (2010) found that among the three areas of concern - culture, climate and care, the cultural aspects causes the main concern for international students in Malaysia. The cultural part in the research focused on language, values, food and sanitation practices and the cause for the concern is due to their acculturation issues in Malaysia. Academic and social adjustments were also discovered to play an important part in international students' learning and experience in Malaysia (Malaklolunthu & Selan, 2011). Hence, the topic was chosen because the Malaysian governance system is different from the students' own due to their socio-cultural backgrounds.

The next reason for the selection of this topic for this project is due to the difference in the students' needs, wants and expectation in their classes. Alavi & Mansor (2011) conducted a study at Universiti Teknologi Malaysia, which indicated that factors such as boring classes (34.1%), inefficient teaching (39.3%) and curriculum and method of teaching (12%) caused concerns among international students in their studies here. Thus, the use of mobile apps would enable these students to learn at their own pace by guiding them to construct their understanding of the course material. Also, the usage of mobile apps, especially apps created by the instructor themselves, gives a "wow-factor" to the students in their classes, and thus, this is aimed to reduce boredom in classes. Hence, the other reason for the selection of this course is to fulfil the international students' needs and expectations for their course.

The Malaysian Studies and *Bahasa Melayu Komunikasi* course are part of the MPU subjects offered under the new Ministry of Higher Education policy. These subjects, offered

since September 2013 for private higher education institutions, are aimed to immerse, or at least, introduce international students to the Malaysian socio-cultural systems and history. But, international students tend to see these subjects as uninteresting and more importantly, not related to their programs. This is supported in the study by Alavi & Mansor (2011) which discovered that 20% of the international students surveyed from five private higher education institutions, see certain subjects as not related to their programs. Thus, the topic was selected in hopes of making the subject interesting for the students.

To conclude, the topic was chosen as it is among the hardest topic to master in this subject, the differences in the international students' socio-cultural backgrounds and the fact that the subject is seen as not being related to their programs.

The Technology-Based Learning Environment

For this project, the technology-based learning environment is the use of mobile app in the instruction. The app is aimed to guide students to produce their own notes that would further enhance their understanding of the topic. At the end of the class, the students shared their notes and the instructor helped by correcting any incorrect understanding and misconceptions by emphasizing the main points of the topic.

The increased use of technology in learning environments has changed instructional approaches by making it more accessible and essentially, more student-centered. Strommen & Lincoln (as cited in Hannafin & Land, 1997) mentioned that rapid technological development played an integral role in the evolution of student-centered learning environments.

The use of mobile phones in classrooms is the next dimension in the use of technology. It can be said that mobile learning (m-learning) is an extension and the next step for e-learning. Wireless mobile technology empowers learners from all around the world by giving them access to learning materials and information from to enable them to learn anywhere, any time (Ally, 2012). Georgiev, Georgieva, & Smrikarov (2004) defined m-learning as a learning activity that is not limited by geographical constraints by constantly being connected to cable networks by utilizing mobile and portable devices which must be able to connect to other devices that presents educational materials and open up two-way information exchange between the learners and the teacher. Therefore, m-learning emphasizes mobility, portability and accessibility that is absent from traditional and even e-learning platforms.

The use of mobile devices is relatively new in education and studies have been conducted to investigate the potential for m-learning and to develop the framework to implement the technology in classrooms, such as by Alioon & Delialioglu (2015); Motiwalla (2007); Sharples et al. (2005). These studies recommend the best methodologies and practices for m-learning. It is undeniable that there are challenges for the implementation of m-learning (small screen size, keyboards, limited memory, battery usage, application compatibility, multimedia elements' use and high price), but it is getting more popular as continuous advancements are made in information and communication technologies (Georgiev et al., 2004). Thus, there is an emerging potential for further studies and application of m-learning in the future.

For this project, the inclusion of mobile apps may prove useful in the helping the international students manage the differences in culture, the method of teaching and learning

styles as it gives them freedom to learn at their own pace. The multiple capabilities of mobile technology are useful as they support different instructional strategies, provide an efficient delivery of the course and enhance student learning (Ferdousi & Bari, 2015). Thus, mobile devices and apps provide students with options on their learning. Therefore, the use of the mobile app is a new approach for the intended learners for this project.

The Integrated Learning Theory

In creating the app, two learning theories were drawn upon. The learning theory that underpins the app's purpose and application is Constructivism.

Constructivism is a learning theory where the responsibility to learn is from the learners. This is because under this theory, the learners are the knowledge and information builders, or more appropriately, the constructor. Demirel (as cited in Epçaçan, 2014, p. 5106) argued that constructivism is not related to teaching but is more inclined towards and related with information and learning. As further explained by Sjøberg (2010, p.3), "learners construct their knowledge through their interaction with the physical world, collaboratively in social settings in a cultural and linguistic environment". In short, constructivism is a learning theory that is student-centered and applied by putting the learners in the right learning environment to complete specific tasks through social and environmental interaction.

It is due to this "learning empowerment" concept that this learning theory was applied to the mobile app. It is hoped that the theory integration would overcome the challenges faced by the international students. By giving them specific tasks to accomplish and understand the topic, the learners will be able to construct their understanding and ultimately, master the topic. This learning theory provides the theoretical basis for the use of the app, and which drives the app's objective.

The Learners

There were 11 students in this class. The students were all undergraduates taking their Bachelor's Degree program. The students took the Malaysian Studies course during the May-August 2015 semester. The students were from Bangladesh, China, Indonesia, Korea, Pakistan, the Philippines and Uzbekistan.

The students were between 18 to 27 years old and were from Semesters Two and Three. There were 5 male and 6 female students. The levels of understanding on basic governance systems, including those from their respective countries, vary from being knowledgeable to no knowledge at all. This is an important aspect as a good foundation here would provide the basics for their learning on Malaysia's governance system.

MOBILE APPLICATION DESIGN

Learning Theory Integration

To integrate the learning theories mentioned, the mobile app has to be able to include activities which guide the students to create their own knowledge and be able to recreate the bigger picture of the key concepts.

The learners must be guided to seek and form their own understanding about the Malaysian government system. And to be able to do that, the responsibility to produce their notes is now given to the learners. The app guides the international students by first giving them the brief information on the matter and following up with specific questions for the student to answer. The ultimate goal is for them to be able to visualize and create the bigger picture of Malaysia's administrative structure and link the main components in a visual diagram.

App Flowchart

Figure 1 below outlines the app's overall layout.

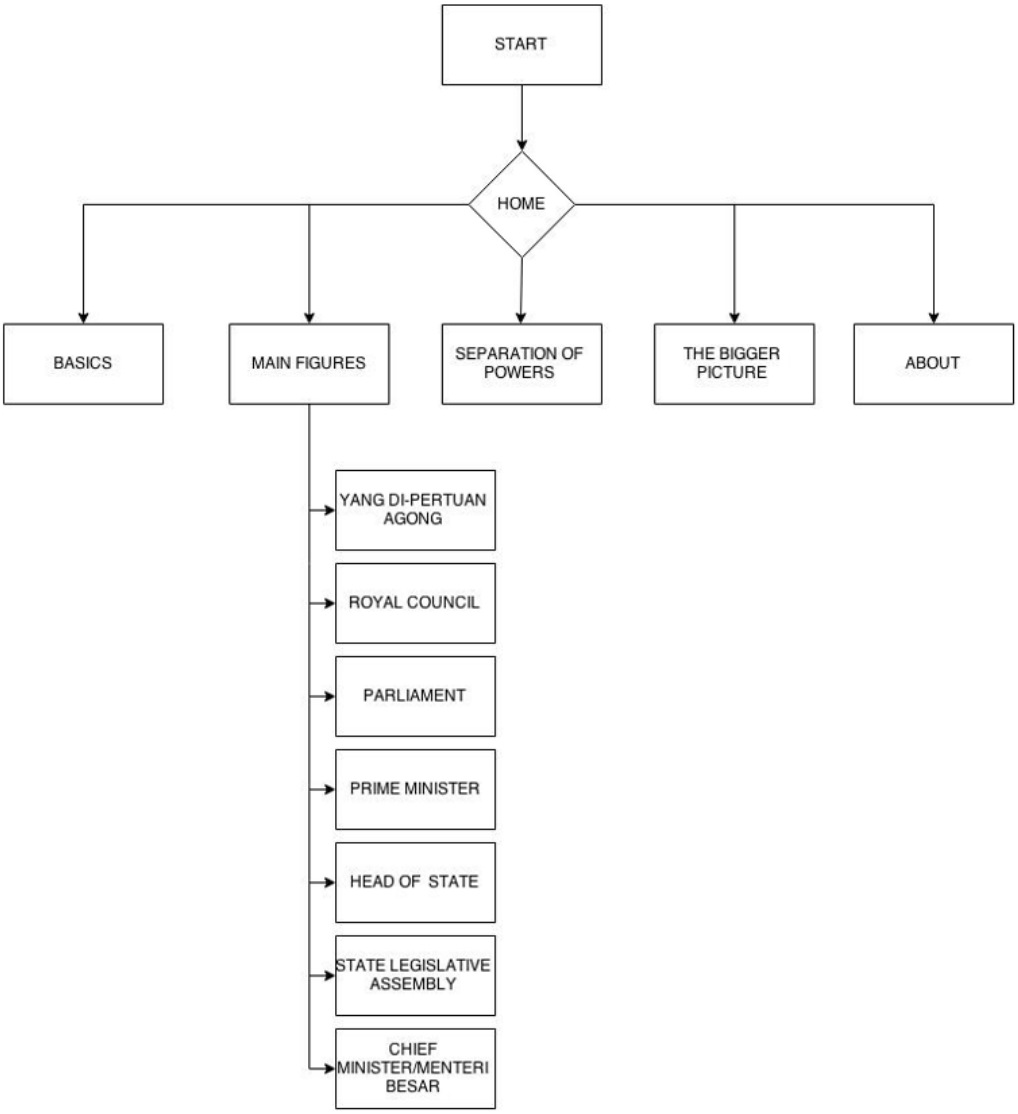

Figure 1. Flowchart of the App's overall layout

Design Process

The design process for the mobile app took into account factors such as content, layout and color that would help with maximizing the learner's usage and experience. Ideas were initially drawn on paper until a practical but user friendly layout was finalized. The ideas were put in appnotch and the completed product proceeded to troubleshooting and beta testing before the implementation. The beta testing was implemented by letting other students and non-students (working adults) try out the app to assess its usability.

The Methodology

The app was used for the Malaysian Studies class. The class was conducted in week two of the semester (12 May 2015) in one of the university's classrooms from 2pm to 5pm.

The students were briefed about the project, which was made part of the class activity. The flow of the class on that day was explained and the activities are listed in Table 1.

The students were given the link to the mobile app for their study, observations were then made by the course instructor, particularly on how they used the app and interactions they made with their peers during the activity. Questions that were asked by the students were also noted to better understand how they had used the mobile app. Instrument-wise; the observations were made using a camera (the students were asked for consent beforehand and their anonymity and privacy were assured) and notes were taken using a notebook.

The class activity was completed when students successfully created the "Visual Note" (seen in Figure 2) and are able to explain the key concepts and components in their own words. The instructor gave some scaffolding to help with the articulation of ideas and correct any misconceptions, as necessary.

Consequently, the students were asked to complete two separate evaluation forms online via the university's Learning Management System (LMS). The first evaluation utilized the 10 item SUS scale instrument, developed by Brooke (1996). The SUS evaluation was utilized for its simple and easy to interpret instrument items and the average score were compared to a score table proposed by Sorflaten (2010). In the second evaluation, the students were given 6 questions (5 multiple choice and 1 open-ended) for some general feedback.

OBSERVATIONS OF THE STUDENTS' APP USAGE

It was found that students used the mobile app in a different manner. Three groups of students worked in groups while three remaining students worked individually. It was observed that the group of three students used the class' main textbooks to get the information and answer the questions posed in the app whilst the other groups used the computer laboratory and even asked some of the senior students (who had completed the subject) for clarifications and explanations.

All of the students used their laptops to search for the answers online. There was active classroom discussion and some interaction with the instructor for some clarification on some of the terms.

No problems emerged with the app use except in one instance. In the first few minutes of the app use, a student had problems with the app layout –but after the explanations were given, the student continued to use the app without any problems.

Table 1
Flow of class activities

Activity	Details
Briefing	Students were briefed on the project and what is to be expected for the class on that day.
App Usage & Class Session	The students are given the link to the mobile app and to go through the activities that is in the app. They are expected to come up with their own visual notes/mind map on the topic (see: "The Bigger Picture" page of the app)
Break	Class Break – 15 minutes
Evaluation	The students went to complete two evaluation using their LMS page: The System Usability Scale (SUS) Evaluation General Feedback
Class Discussion	The instructor discussed the students' findings and they all came up with the bigger picture of the topic.

The Visual Note

At the end of the session, the students discussed their findings with the instructor and together, they constructed their understanding of the topic. Figure 2 below shows the overall lesson and how the main components are linked to each other.

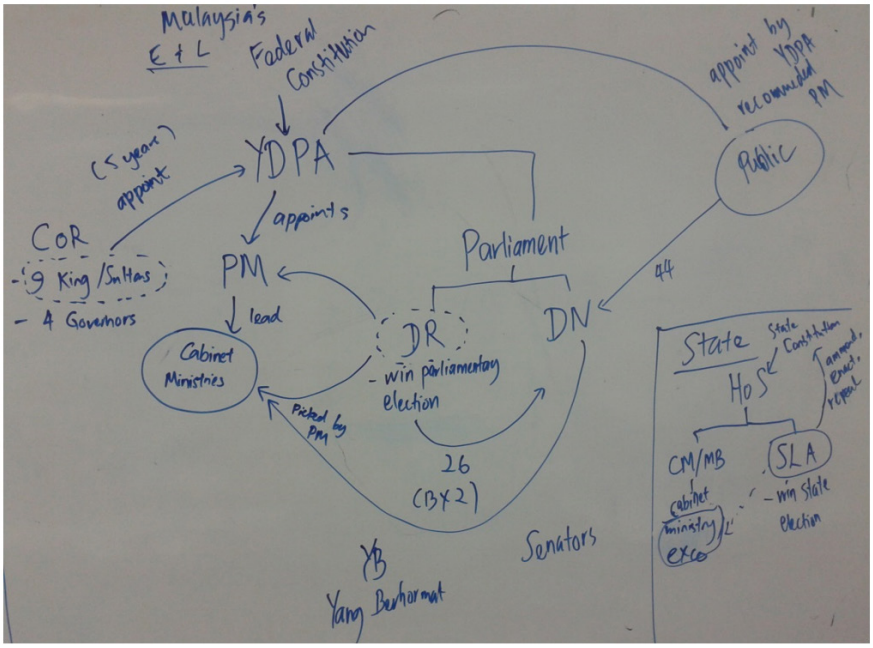

Figure 2. The Class' Mind Map

EVALUATION AND FINDINGS

System Measurement (SUS Evaluation)

To evaluate the app, the SUS Evaluation was used. The results of the SUS measurements are seen in the following table. From the data, the minimum was 47.5 and maximum was 92.5. The average mean for the evaluation was 61.8, which is a D and is marginally acceptable. The SUS Score was obtained drawing from a table by Sorflaten (2010).

It was discovered later that the difference between the min and max score for the SUS evaluation was attributed to two of the students' limited understanding of what was asked in the SUS' 10 item questions. The students shared that though the language was simplified, they couldn't understand the exact context of what was written and in the end, they simply randomly picked the rating for the item.

General Feedback

The students were also given the chance to give their feedback about using the app for the topic. The general feedback was given via the Learning Management System. There were 6 questions for them to answer, 5 multiple choice and 1 open ended.

The feedback was generally positive. 72% of the students saw the app as useful to the class session with 81% finding it as easy to use. 8 students agreed that the app forces them to find information. In terms of app layout, 9 students gave 'Good' and 'Very Good' rating for the app with 2 being neutral, whilst in the context of design and aesthetics, almost 90% of the students gave 'Good' and 'Very Good' ratings whilst only one student gave a 'Neutral' rating. For the open-ended question, the students were asked to provide feedback on the app and only 8 gave their feedback. The feedback, in verbatim, can be seen in Table 2.

Table 2
Student's General Feedback

Student's Feedback	
good enough	It is extremely helpful. It makes understanding easier and learning much more effective.
So far, I think it's very useful for me, can let I am interested in Malaysian studies!	app is convenient, but real lectures are the best!
good	N/a
Nice app...	This app i think is useful somewhat but i think you need to provide more guide line and information for the users. One more thing is good to use this app in laptop or computer because is easy to see and clear...

From the feedback and SUS evaluation, it is clear that there is room for improvement for the ap. These include providing clearer guidelines and information on the usage of the app. The benefits from the students' perspective was the ease of understanding and learning and the increased interest in the subject. Furthermore, the apps' convenience and ability to be used

in laptops and desktop computers was an advantage to the students. For future research, more data need to be collected (especially student's qualitative feedback) to improve the application.

CONCLUSION

The objective of this project was to develop a mobile app that would guide the intended learners (international students) to learn the fundamentals of the Malaysian system of government. As this is a complex topic, even for Malaysian students, the content was made more accessible by utilizing the constructivist learning approach. In addition to that, the app was intended to create variety in learning for the learners, and which would alleviate boredom, at least to some degree.

Based on the results of the SUS evaluation and general feedback, this app does demonstrate the potential to be used for other learning purposes and course evaluation. To conclude, the app did achieve some of its intended objectives and the project could be successful in the future, provided some refinements and tweaks are made in terms of simplifying the layout. Due to the small number of students (a normal occurrence for the course) and considering that this is the first iteration of the research, improvements, better idea implementation, and approaches could be further unearthed with further research on a bigger scale down the line.

REFERENCES

Alavi, M., & Mansor, S. M. S. (2011). Categories of problems among international students in Universiti Teknologi Malaysia. *Procedia - Social and Behavioral Sciences*, *30*, 1581–1587. doi:10.1016/j.sbspro.2011.10.307

Alioon, Y., & Delialioglu, O. (2015). A Frame for the Literature on M-learning. *Procedia - Social and Behavioral Sciences*, *182*, 127–135. doi:10.1016/j.sbspro.2015.04.747

Ally, M. (Ed.). (2012). *Mobile Learning - Transforming the Delivery of Education and Training*. Edmonton: AU PressAtkinson, R., & Shiffrin, R. (1968). Human Memory: A Proposed System and Its Control Processes. In K. Spence & J. Spence (Eds.), *The Psychology of Learning and Motivation (Volume 2)* (pp. 89–195). New York: Academic Press.

Brooke, J. (1996). *SUS: A "Quick And Dirty" Usability Scale*. In P. W. Jordan, B. Thomas, B. A. Weerdmeester, & A. L. McClelland. Usability Evaluation in Industry. London: Taylor and Francis.

Driscoll, M. (2001). *Psychology of Learning for Assessment* (2nd ed.). Boston: Allyn and Bacon.

Epçaçan, C. (2014). Examination of Texts of Secondary School Turkish Schoolbooks in Terms of Constructivism Approach. *Procedia - Social and Behavioral Sciences*, *116*, 5105–5114. doi:10.1016/j.sbspro.2014.01.1082

Ferdousi, B., & Bari, J. (2015). Infusing mobile technology into undergraduate courses for effective learning. *Procedia - Social and Behavioral Sciences*, *176*, 307–311. doi:10.1016/j.sbspro.2015.01.476

Forest, E. (2014). The ADDIE Model: Instructional Design. Retrieved May 15, 2015, from http://educationaltechnology.net/the-addie-model-instructional-design/

Georgiev, T., Georgieva, E., & Smrikarov, A. (2004). M-learning - a New Stage of E-Learning. *International Conference on Computer Systems and Technologies - CompSysTech'2004*, *17*, 1–5. doi:10.1145/1050330.1050437

Hannafin, M., & Land, S. (1997). The foundations and assumptions of technology-enhanced student-centered learning environments. *Instructional Science*, *25*(3), 167–202. Retrieved December 10, 2014, from http://link.springer.com/article/10.1023/A:1002997414652

Lutz, S., & Huitt, W. (2003). Information processing and memory: Theory and applications. *Educational Psychology Interactive*, 1–17. Retrieved October 24, 2014, from http://www.edpsychinteractive.org/papers/infoproc.pdf

Mahmud, Z., Amat, S., Rahman, S., & Ishak, N. M. (2010). Challenges for international students in Malaysia: Culture, climate and care. *Procedia - Social and Behavioral Sciences*, *7*(2), 289–293. doi:10.1016/j.sbspro.2010.10.040

Malaklolunthu, S., & Selan, P. S. (2011). Adjustment problems among international students in Malaysian private higher education institutions. *Procedia - Social and Behavioral Sciences*, *15*, 833–837. doi:10.1016/j.sbspro.2011.03.194

Motiwalla, L. F. (2007). Mobile learning: A framework and evaluation. *Computers & Education*, *49*(3), 581–596. doi:10.1016/j.compedu.2005.10.011

Sharples, M., Taylor, J., & Vavoula, G. (2005). Towards a Theory of Mobile Learning. *Proceedings of mLearn*, *1*(1), 1–9. doi:citeulike-article-id:6652555

Sjøberg, S. (2010). Constructivism and learning. *International Encyclopedia of Education*, 485–490. doi:10.1016/B978-0-08-044894-7.00467-X

Sorflaten, J. (2010). Clean Metrics from Quick and Dirty Assessment: "The SUS." Retrieved May 26, 2015, from http://www.humanfactors.com/newsletters/clean_metrics_from_quick_and_dirty_assessment.asp

Pertanika J. Sci. & Technol. 24 (2): 517 - 530 (2016)

PERTANIKA JOURNALS

SCIENCE & TECHNOLOGY

Journal homepage: http://www.pertanika.upm.edu.my/

An Investigation on Impact of E-Learning Implementation on Change Management in Malaysian Private Higher Education Institutions

Sheiladevi, S.[1]* and Rahman, A.[2]

[1]*Centre of Excellence in Learning and Teaching, UCSI University, 1 Menara Gading, UCSI Heights, 56000 Kuala Lumpur, Malaysia*

[2]*Department of Education Management, Planning and Policy, Faculty of Education, University of Malaya, 50603 Kuala Lumpur, Malaysia*

ABSTRACT

The purpose of this research is to analyse the impact of identified variables to adapt change management due to e-learning implementation in Malaysian private higher education institutions focusing on educators' perspectives. The conceptual framework was modified in combination of various theories from Systemic Change Models and E-learning Cycle Models. A self-administered questionnaire adapted from Siebel 4.0-2 Survey Questionnaires (SSQ) by Hambling, 2010 was the data collection instrument. The sample consisted of educators from private higher education institutions with visions or missions based on e-learning implementation in Malaysia. As per findings, through review of the visions and missions, the selected private higher education institutions integrated teaching and learning, advancement of the knowledge based on e-learning and leadership in service and outreach.

Keywords: Change management, e-learning, vision, mission, private higher education, implementation

INTRODUCTION

E-learning is a teaching and learning method that switches educators' responsibilities from instructors to facilitators (Frye, 2002). This is important because an e-learning based pedagogy requires educators to not only extend their teaching potential, but also to adjust their attitudes (Center of Educational Technology, 2005). This is in line with the National Accreditation Board (NAB), an accreditation agency which supports the uppermost of educational values and the authorisation of courses by private higher education institutions (Ministry of Education, 2010). These institutions were given approved university status by the

Article history:
Received: 8 December 2015
Accepted: 22 April 2016

E-mail addresses:
sheiladevis@ucsiuniversity.edu.my (Sheiladevi, S. and),
aridris@um.edu.my (Rahman, A.)
*Corresponding Author

ISSN: 0128-7680

Malaysian Minister of Higher Education, authorised under the Private Higher Educational Institutions Act 1996. MAPCU (Malaysian Association of Private Colleges and Universities) registered 18 March 1997. They form Malaysia's most prominent group of private higher education institutions with involvement from well established private colleges and universities in Malaysia (Molly, 2005). The Malaysian Association of Private Colleges and Universities is acknowledged by the Ministry of Education, the National Accreditation Board, the Multimedia Development Corporation, the Ministry of Finance, and the Economic Planning Unit of the Prime Minister's Department (Molly, 2005).

The main point of managing an online digital archive is to create and utilise the instructional technology in various ways for accommodating student preferences (Ravet & Layte, 2008). In researchers' views, the important issue to integrating instructional technology is how to accommodate learners with different learning abilities. Clearly, there is a need to look at the educators' strategies and their attitudes to adapt to changes produced by implementing e-learning in learning and teaching. In private higher education institutions, the quality of e-learning is deeply linked to the educators' mindset about their roles (Ridzuan, 2010). They should be able to adjust according to the changes they encounter in diverse teaching environments (Ridzuan, 2010). The Sixth International Conference on adult education, held in Brazil in December 2009 found that many private higher education institutions still rely on professional programmers to set a syllabus that included e-learning, instead of the educators who are the subject experts (Victoria, 2009).

The survey of Zakaria and Iksan (2007) states that with good professional development programmes, the majority of Malaysians believe that to turn our country into a knowledge-based economy, we need to incorporate technology for educational advancement. According to the Malaysia Education Blueprint (2013-2025), the Ministry of Education has identified the need to convert lecturers' careers as the most preferred job by the graduates (Ministry of Education, 2012). Educators' qualities influence students' outcomes (Zakaria & Iksan, 2007). The quality of the education system is only as good as its educators (Ministry of Education, 2012). In short, educators' ability to adapt to change is becoming an issue of dependence in the education system.

PROBLEM STATEMENT

In the National Higher Education Strategic Plan (2010) e-learning has been identified as one of the Critical Agenda Projects (CAPs) and is a National Key Result Area (NKRA) for MOHE (Ministry of Education, 2011). Embi (2011) identified the main aspects of e-learning to be e-learning policies, governance, Learning Management Systems (LMS), training, the development of e-content and the integration of e-learning in teaching and learning. These aspects have exposed a gap in the practice of e-learning that has proved the difficulty of implementing and sustaining e-learning in the Malaysian education system (Embi, 2011). E-learning was not an application that was readily available with the birth of the internet. It came about only almost two decades after the internet was introduced (Alhabshi, 2006). Hence, implementing e-learning is not as easy as it was first thought (Alhabshi, 2006).

Furthermore, the challenges faced by institutions of higher learning in relation to e-learning utilisation (88.9%) were that the academic staff was complacent about the current teaching practices, due to lack of training on how to adapt to the changes in the education system in Malaysia (Hamat, Embi & Sulaiman, 2011). Most lecturers are found to be unfamiliar with e-learning. (Embi, 2011) Therefore, training is often considered the fastest way to deliver instructions (Embi, 2011). "One finds that the diverse array of theoretical perspectives and overwhelming latest application without proper concepts are the reasons for lacking in acceptance of e-learning" (Gene & Weibelzahl, 2007, pp. 42-45). These findings indicated that change is crucial for e-learning implementation in higher learning institutions. However there is a gap in identifying the significant of concepts and theories of e-learning and change management for educators.

In order to encourage change in people to include ICT in the educational and administrative processes, Malaysia has heavily invested in its education plan, resources and infrastructure (Ministry of Education, 2012). The future economic and social well-being of the nation depends critically on the success of adaptation to educational transformation (Ministry of Education, 2007). Universities are being equipped with the latest ICT infrastructures, and educators are being trained to use ICT for education and also administrative purposes (Gene & Weibelzahl, 2007). Since ICT has yet to be seen to be fully embraced by educators, an analysis of how private higher education institutions implement e-learning is deemed necessary (Maznah & Harland, 2012). Therefore this research has only focused on educators from private higher education institutions with an e-learning based vision and mission. Change management was the main area of interest within the field of e-learning implementation. However there has been no study conducted to analyse the relationship between change management and the e-learning focus on educators that emphasizes methodological triangulation by using qualitative and quantitative methods concurrently. To address this gap in methodology, there is a need to conduct a comprehensive study on managing change in status, trends, challenges, and ways to adapt change management and to explore the journey that educators experience during the change process of e-learning implementation in private higher learning institutions.

RESEARCH QUESTION, OBJECTIVE AND HYPHOTHESIS

The objective of this research is to analyse the significant relationship between e-learning implementation and change management in private higher education institutions within Malaysia from the perspectives of educators, thus the following research question has been constructed: Is there a significant relationship between e-learning implementation and change management in private higher education institutions within Malaysia from the perspective of educators? To relate research question and objective of the research the hypothesis of this research has been reviewed as e-learning implementation has no significant effect on change management in private higher education institutions within Malaysia from the perspective of educators.

METHODOLOGY

The research instruments were modified according to the conceptual framework based on theoretical framework. This research matter examined aspects of literature on e-learning and change management to identify a theoretical outline. In this research the survey method, cross sectional study and exploratory method were used as the research strategy to conduct this research in Malaysia's private higher education institutions. This survey method was used because the data obtained was standardized, facilitated comparison and analyzed using quantitative means.

A self-administered questionnaire was chosen as the data collection instrument for the quantitative method and interviews were conducted as the qualitative method. The samples were educators from private higher education institutions with visions or missions based on e-learning implementation in Malaysia. The questionnaire was adapted from the Siebel 4.0-2 Survey Questionnaire (SSQ) by Hambling (2010). The rationale for adapting the ideas of the SSQ was because the research that Hambling conducted used the Systemic Change Model in implementation of the Siebel 4.0-2, an e-learning platform from the perspective of the 'people' who were the users. SSQ was cited by 14 research articles that used Systemic Change Model from the year 2010-2012 (MS Academia, 2013). Besides that, this research questionnaire used the ideas of SSQ with modified variables to suit the conceptual framework and answer the research questions.

For this study, the researcher selected participants from institutions with university status situated in Kuala Lumpur that incorporate e-learning implementation in their vision and mission. Private higher education institutions in Kuala Lumpur were selected as the sample because the majority of the university status private higher education institutions with visions and missions on e-learning were situated in Kuala Lumpur. Besides, technologically advance private universities were also situated in Kuala Lumpur. In line with government ambition to make Malaysia a regional hub for education, higher education in Kuala Lumpur aims at attracting top world institutions with innovative teaching and learning (Ministry of Education Statistic, 2013).

Besides that higher education institutions in Kuala Lumpur are envisioned as leading in teaching and learning facilities with a major contribution to the education sector of the country. There are 37 private universities in Malaysia with total 282928 students studying in Malaysia (Ministry of Education, 2013).

Universities in Malaysia have been shaped with conducive monitoring from the Universities and University Colleges Act 1971 (Ministry of Higher Education, 2012). The number of students and educators was determined by the ratio of 1:13 which means that in total there were 21763 of educators in the year of 2014 (Ministry of Education, 2014). There were nine private higher education institutions with university status that were qualified to participate in this research after analyzing the vision and mission of the institutions. However, only private higher education institutions in Kuala Lumpur with university status that included e-learning implementation in their institute's vision and mission statement were selected. Educators in this research consist of teachers, tutors, instructors and lecturers in the selected private higher education institutions based on their qualifications.

Besides that, Krejcie and Morgan's (1970) model was used because it was an appropriate model to get the sample size and this model has been cited in 394 studies.

CONTENT VALIDITY

Content validity was determined through using scales which were adopted from established empirical studies (Narver et al., 1993; Jaworski & Coupland, 2014). The questionnaire validity and reliability was ascertained by conducting Cronbach alpha. Furthermore, the researcher conducted a pilot test to determine the actual validity in the context of this research.

Moreover, the test was not used for statistical purposes and responses from the pilot test were not included in the research findings. In fact, only a preliminary reliability evaluation was carried out with Cronbach's Coefficient Alpha Reliability analysis.

Additionally, participants were encouraged to be very free with their responses, make suggestions for improvement and delineate any difficulties that they found. After questionnaires were answered by each participant, they were asked for their comments. Comments were solicited on the clarity of the questions and the editing was done in order to simplify the questions. The pilot test results identified ambiguities in the questionnaire items. Problems concerning instructions given for completing the questionnaire were also solved. A final version of the questionnaire was prepared for use in the actual research. The entire commentaries, opinions and implications of the respondents were taken into consideration. The summary results of Cronbach's Alpha stated in Table 1.

Table 1
Summary results of Cronbach's Alpha

	Construct	No. of items	Means	Std-deviation	Cronbach's Alpha
1	Stakeholders involvement	2	75.39	14.76	.8002
2	Systems view	8	45.89	4.67	.9001
3	Evolving mindset	4	59.56	7.87	.8395
4.	Understanding transition	3	64.56	9.87	.8279
5.	System design	8	80.70	14.87	.8007
6.	System evaluation	2	80.66	14.89	.8021
7.	Academic transform	6	53.86	11.54	.7910
8.	Service and satisfaction	10	64.63	9.32	.8153
9.	Ownership control	10	62.83	11.28	.8522

NUMBER OF QUESTIONAIRES DISTRIBUTED, RETURNED AND USABLE

In order to capture the targeted sample size of 381 respondents, 550 survey questionnaires were distributed to private higher education institutions in Kuala Lumpur that have visions and missions on e-learning implementation. A total 493 were returned, representing a response rate of 89.6%. Out of the 493 returned, 487 were found to be usable (98.8%) and 6 questionnaires were rejected due to incomplete responses (1.21%). From this feedback, it was concluded that respondents were willing to give their cooperation in answering the survey questions at their

convenience. This provides evidence that if a survey is monitored and administered properly, much information can be gathered from the respondents.

SKEWNESS AND KURTOSIS OF STUDY VARIABLES

All variables were measured on a five points Likert type scale. The mean scores for all the variables range between 20.23 and 67.54. This indicates that change management variables and e-learning variables are at a moderate level. The standard deviation scores range from 6.03 to 22.67.

The normality distribution of the data, the skewness and kurtosis of each variable were examined. The critical value for both measures of normality has drawn the distribution. The skewness and kurtosis for the nine main variables of this study were examined. By applying the above criteria to the skewness values for each of the study variables, it is shown that none of the variables fall outside the more and less 2.58 range of skewness. Thus, the data for this study is normal with regards to skewness.

Univariate skewness and univariate kurtosis values range from -0.501 to 0.062 and -0.402 to 0.564 respectively. The relatively large value of Mardia's normalized multivariate estimate kurtosis (23.623) shows evidence that the data are slightly not multivariate normal. In order to address the issue of multivariate non-normality, bootstrapping is conducted to assess the stability of parameter estimates and report them more accurately. Within the context of the Structural Equation Model, bootstrapping provides a mechanism for addressing situations where the statistical assumptions of large samples and multivariate normality may not hold (Boon, 2003). In this study the Bollen-Stein bootstrap procedure (Bollen & Scott, 1993) was employed.

It is a modified bootstrap method for the $\chi 2$ goodness of fit statistic which provides means to test if the specified model is correct. In particular, it can be used to correct for the standard error and fit statistic bias that occurs due to non-normal data. It tests the adequacy of the hypothesized model based on the transformation of the sample data such that the model is made to fit the data perfectly. In this study, 1000 bootstrap samples were drawn with replacement from this transformed sample. The Bollen-Stein bootstrap *p*-value is 0.356 (>.05) indicating that there is sufficient evidence to reject the hypothesized model.

Considering the feasibility and statistical significance of all parameter estimates, the substantially good fit of the final model and the lack of any substantial evidence of model misfit, the author concludes that the nine dimensions (ownership control, academic transform, service and satisfaction, stakeholders involvement, system view, evolving mindset, understanding transition, system design and system evaluation) can represent an adequate description of educators' perspectives of change management due to e-learning implementation in private higher education institutions.

The Cronbach's alpha was computed on each of the Likert scale items that were factor loaded into the nine factors. The internal consistency reliability scores ranged from .641 to .854 after removing some items with low corrected item-total correlations value. Reliability is also an indicator of convergent validity (Hair, Black, Babin, Anderson & Tatham., 2006). According to Hair et al., (2006) coefficient alpha is generally an internal measure of reliability as in most practical cases it is only the lower bound on reliability. Hair et al., (2006) also

stated that coefficient alpha remains a commonly applied estimate although it may understate reliability. The rule of thumb for the reliability estimate is that 0.7 or higher suggests good reliability (Hair et al., 2006), and the results indicate that convergent validity exists for the constructs of the study. Variance extraction measures the total amount of variance in the indicators accounted by the variable (Hair et al., 2006). Variance extracts of less than 0.5 indicate that on average, more error remains in the items than the variance explained by the factor structure in the measurement model (Hair et al., 2006). The calculated results of the variance extracted, indicate that the variance extracted for item are below 0.5, however they did not cause concern as it is not uncommon to find estimates below 0.5, even when the reliability is acceptable (Hatcher, 1994).

The results of the construct reliability for the variables examining the dimension of change management due to e-learning implementation showed that the overall alpha that exceed the cut off point of reliability recommended by Nunnally and Berstein (1994), are evolving mindset, academic transform, system view, stakeholders involvement and ownership control with 0.942, 0.952, 0.914, 0.961 and 0.952 respectively. However, the result showed that the construct reliability coefficients for understanding academic transform, service and satisfaction and system design showed 0.864, 0.835 and 0.843 respectively. For system evaluation, the result for construct reliability coefficients showed 0.732. Table 2 revealed the summary of Skewness and Kurtosis.

Table 2
Skewness and Kurtosis for study variables

Study Variables	Skewness	Kurtosis
1) Stakeholders involvement	0.062	-0.627
2) Systems view	-0.130	-0.468
3) Evolving mindset	-0.222	-0.862
4) Understanding transition	-0.306	-0.355
5) System design	-0.100	0.768
6) System evaluation	-0.500	-0.455
7) Academic transform	-0.465	-0.344
8) Service and satisfaction	0.060	-0.643
9) Ownership control	0.041	-0.535

CHARACTERISTICS OF THE RESPONDENTS

Data collected on the demographics of private higher education educators were analyzed using descriptive statistics. Respondents were asked to identify themselves according to five different categories from doctorate degree to diploma and the others. Four levels of professional qualification of educators in the selected private higher education institutions were identified. The findings showed that 244 (50.1%) of the respondents held a Master level degree. In total of 46 (9.5%) of the respondents had a doctoral degree and the remaining 190 (39.1%) respondents had a bachelor degree with six 6 (1.2%) respondents holding a diploma and only one who answered “Other” for their qualification.

More than half of the respondents were lecturers: 265 (54.4%) respondents. This was followed by tutors, 101 (20.7%) respondents and teachers 80 (16.4%) respondents. However, 25 (5.1%) respondents were senior lecturers and only 16 (3.2%) respondents were instructors.

The most respondents, almost one third, (169 or 34.3%) were in the age range between 25-35 years. 97 (20%) respondents were more than 56 years old. These results indicated that slightly fewer educators were in the age range 46-55 and 36-45 which were 94 and 92 respectively. The fewest educators (35 or 7.2%) were in the range of less than 25 years old.

Most of the respondents (398 or 81.7%) were full time educators, compared to part time respondents numbering 80 (16.4%) and under contract who numbered only 9 (1.8%) respondents. None of the respondents was in "other" category of job status.

Most respondents 191 (39.2%) had 2-5 years of experience in the teaching profession. The results indicated that more than one third of the total respondents had teaching experience within five years. 96 (19.7%) respondents had 6-10 years of experience in the teaching profession. 85 respondents had 11-15 years of teaching experience and this number was close to respondents who had 6-10 years of teaching experience. These results also indicated that fewer educators or 66 (13.6%) had less than 1 year of experience. Those with 16-20 years of experience in the teaching profession numbered 46 (9.4%). Furthermore, 3 (0.6%) of educators stated they had teaching experience exceeding 20 years.

CORRELATION ANALYSIS

Pearson's correlation analysis was conducted on all the main constructs as well as between e-learning implementation variables and change management variables. After the measurements were confirmed the correlation analysis was performed to provide preliminary information regarding the associations between the relationships of each dependent variable with independent variables using multilinear regression. The correlation analysis also gives an indication of whether there exist any multicollinearity problems in the data set. In this study, e-learning variables are explained by three separate variables namely academic transformation, ownership control (OC), and service and satisfaction (SS). In order to generate comparable mean scores on e-learning variable for each of the three variables, the weighted average approach was used. The total score for each three variables were divided by numbers of items. Among the studies that used average approach were Albers-Miller and Straughan (2000).

It was an evident that there is not very strong correlation (0.8 and above) between any pairs of the nine variables of this study. One correlation coefficient value ("academic transform" (AT) and "evolving mindset (EM)") was significant at the 0.01 level while the remaining were significant at the 0.05 levels. "Academic transform" also was found to have significant and positive correlation with "understanding transition (UT)" (r=0.449). "Ownership control" was recorded having high correlation with "system view (SV)" (r= 0.481). However, it was recorded as having low and positive correlation with "stakeholders involvement (SI)" (r= 0.276). "Service and satisfaction" recorded high correlation with positive significance with "system evaluation (SE)" (r=0.413) and "system design (SD)" (r=0.383). According to Benny and Feldman (1985), a rule of thumb states that any correlation exceeding a value of 0.8 (a very strong correlation) between independent variables is likely to result in multicollinearity

in the data. The multicollinearity is likely to affect the interpretation of the regression model as the absolute of the correlation coefficients (ranging from -0.088 and 0.449) are lower than the acceptable cut off value of 0.8. Table 3 shows the summary of the correlation coefficient matrix.

Table 3
Correlation coefficient matrix

	Evolving mindset	Academic transform	Understanding transition	Service and satisfaction	System evaluation	System design	Ownership control	Stekeholders involvement	System view
1-Evolving mindset	1								
2-Academic transform	0.412**	1							
3-Understanding transition	0.220**	0.449**	1						
4- Service and satisfaction	0.211**	0.201**	0.297**	1					
5- System evaluation	0.153**	0.287**	0.308**	0.413**	1				
6- System design	0.236**	0.172**	0.279**	0.383**	0.345**	1			
7- Ownership control	0.299**	0.274**	0.371**	0.287**	0.184**	0/254 **	1		
8- Stakeholders involvement	0.231**	0.257**	0.311**	0.434**	0.267**	0.291**	0.276**	1	
9- System view	0.288**	0.361**	0.301**	0.203**	0.282**	0,319**	0.481**	0.258**	1

**p<0.01 level (2-tailed)

RELATIONSHIP BETWEEN E-LEARNING IMPLEMENTATION AND CHANGE MANAGEMENT

Multivariate analysis of variance (MANOVA) was conducted with six dependent and three independent variables. Box's M test was not significant, M=15.16, F (18, 171664) =.865, p>0.001 and so was Levene's test of homogeneity of variance. The non-significance of both tests indicates that the assumptions of homogeneity of variance covariance and homogeneity of variance are tenable.

MANOVA between variables revealed that there were significant differences in the mean scores of all measures of e-learning variables as well as change management variables. Significant differences exist in the mean scores of (SI), $F(2,485)=11.92$, $p<0.001$; (SV), $F(2,485)=10.93$, $p<0.003$; (EM), $F(2,485)= 9.53$, $p<0.001$; (UT), $F(2,485)=7.75$, $p<0.001$; (SD), $F(2,485)= 6.69$, $p<0.001$; (SE), $F(2,485)=10.03$, $p<0.001$. Post hoc test indicated that the mean scores of SI, SV, SD for OC and SS were not significantly different from each other. However, those obtained by AT were different and thus significantly lower than those of their counterparts of OC and SS. On the other hand, EM and UT for AT and SS were not significantly different from each other. However, SE for OC and AT was also not significantly different from each other.

The analysed data revealed that there were significant differences in the mean scores of all measures of e-learning and change management variables.

Significant differences exist in the mean scores of SI, SV, EM, UT, SD, and SE. These findings are consistent with related studies done by Sims (2008). The study found that change management had significant effect with the e-learning implementation. Some scholars like Jung et al. (2011) and Seale (2014) have highlighted that some facets of change, such as a system view, system design and system evaluation were needed for e-learning implementation. The

post hoc test indicated that the mean scores of SI, SV, SD for OC and SS were not significantly different from each other. However, those obtained by AT were significantly lower than those of their counterparts at OC and SS.

A related study conducted in Kuwait by Ali (2008) that examined the phenomenon of resistance to change, in implementing e-learning also found that "academic transform" had a lower significant difference compared to other study variables. The further argued that change was dependent on its conformance to values, attitudes and patterns of behaviour typical of human attitude. Therefore, in order to have high relevance in "academic transform", the change management variables that supported the study variables of "evolving mindset" and "understanding transition" will need to play a role. Thus the educators may have a particular way to adapt to the "academic transform" from the e-learning implementation. The rate of change depends on the change agent. Table 4 reveals the summary results of MANOVA on e-learning variables and change management variables.

Table 4
Results of MANOVA on e-learning variables and change management variables

	Mean			MANOVA		
	OC	AT	SS	*df*	*F*	*p*
SI	4.23	4.62	4.53	2	11.92	.000*
SV	4.13	4.56	4.51	2	10.32	.003*
EM	4.29	4.82	4.11	2	9.53	.000*
UT	4.08	4.57	4.32	2	7.75	.001*
SD	4.27	4.02	4.17	2	6.69	.000*
SE	4.66	4.13	4.22	2	10.03	.000*

*Significant mean effect

CONCLUSION

Overall, the implications of the findings are that educational institutions embrace all kinds of faculty and staff. However some of the educators may simply be opposed to change. This can result from adapted or assumed pedagogical concepts of the past or from a lack of exposure to better ways of doing things, or just being slow to decide. With regards to these barriers to change management due to e-learning implementation among the educators, the human factor is of vital importance and success largely depends on positive and constructive management motivation, educators' creativity, and adaptability to e-learning implementation in the relevant teaching and learning situations. The change management process has been acknowledged by private higher education institutions in Malaysia, as an engaging approach.

The private higher education institutions are showing interest in supporting research and development of new knowledge. This has allowed the researcher to explore the internal systems of the institutions and report the findings. Each finding could add to a greater reservoir of knowledge on change management due to e-learning implementation. Private higher education institution deputy vice chancellors, deans and the decision makers at the top level, e-learning experts and other relevant parties could definitely benefit from the findings that

reflect on experience that improves continuously. This study's findings also allow other higher education institutions to reflect on their counterparts' experiences of change management, due to e-learning implementation, in order that they might emulate them or adapt their practices.

For theoretical implications based on the findings, the model illustrates two types of variables affecting (positively or negatively) the different dimensions of change management due to e-learning. An inspection of the model indicates that age and experience variables, such as years of working experience as a lecturer, years of working in the institution, negatively influence the lecturers' adaptation to e-learning implementation. Findings indicate that younger lecturers show more confidence, and are better in using various new software, tools and programmes in the change management process, as compared to senior lecturers. These factors along with good communication helps determine the understanding of change management due to e-learning implementation. Secondly, "ownership control" has a significant effect on the "system view" when e-learning implementation starts in the institution, and the experiences of educators handling e-learning classes are positively affected, which has not been studied before. This is strengthened by the finding that lecturers with a Master's Degree and who are working full time in the respective institutions, show greater adaptability to change due to e-learning as compared to the other categories of educators. Thirdly, no research has linked the relationship of "service and satisfaction", which is also found to correlate with "system design".

For methodological implications the present study provides a few methodological contributions. In terms of adding to the body of literature, the significance of this study involves the newly developed change management due to e-learning implementation. In this study, the researcher decided to take a weighted average for the variables to represent change management due to e-learning. This is the first implication contributed by this study, as no past studies have conducted such research to develop a measurement of change management. This study departs from most of the previous studies in that it has focused on e-learning implementation and change management separately. Secondly, this study adds to the existing literature on change management due to e-learning implementation. In the newly developed variables constructed was measured using 18 items. Thus, this also provides a significant methodological contribution in terms of scale development for change management variables, due to e-learning implementation constructs. Lastly to date there is no known study investigating change management due to e-learning implementation in terms of significant relationship between change management variables that contribute to e-learning implementation, status, trend, problem, challenges and ways to adapt from the perspective of educators using quantitative methods. Therefore, it is a significant methodological contribution to the body of knowledge in terms of new findings pertaining to change management due to e-learning implementation in private higher education institutions.

In terms of practical implications the present study provides a number of contributions to practice. The first implication of this study is the variables of change management namely "stakeholders involvement", "system view", "evolving mindset", "understanding transition", "system design" and "system evaluation" influence three aspects of e-learning implementation, namely "ownership and control", "academic transform", and "service and satisfaction". This finding will enable educators and e-learning management teams in private higher education institutions, to create a more refined strategy to carry out successful change management.

In addition, this contribution can be discussed further in terms of status and trend, problem and challenges and ways to adapt to change and the journey of e-learning implementation. Leaders and top management of private higher education who integrate teaching and learning, advancement of the knowledge should concentrate in constructing a vision and a mission that relates to educators, teaching and learning.

REFERENCES

Alhabshi, S. O. (2006). E-learning experience in Malaysia. In *Proceedings of the Second International Conference on eLearning for Knowledge-Based Society, UNITAR E-JOURNAL*, *2*(2), 4- 7. Retrieved from http://unitar.edu.my/journal/pdf/013e1/01241/652543241E.pdf Instruction.pdf. 16 May 2015.

Ali, G. E. (2008). Barriers to implementing e-learning: a Kuwaiti case study. *International Journal of Training and Development*, *12*(1), 36-53.

Barrett,T., & Luedecke D. K. (1996). *What Hardware and software are most critical for learning effectively with technology? Education Technology & Society* (32-37). New York: McGraw-Hill Press Publications.

Benny, W. D., & Feldman, S. (1985). *Multiple regression in practice,* Thousand Oaks, CA, Sage Publication.

Bollen, K. A., & Scott, L. (1993).*Testing structural equation models.* Thousand Oaks, CA*:* Sage Publication.

Boon J. (2003). An organisation of learning style theory and constructs. InL. Curr. *Learning style in continuing education*. (Unpublished PhD Dissertation). Canada: Dalhousie University.

Canterucci, J. (1995).*The role of emotions in planning INSET courses for IT.* Unpublished PhD Dissertation, United Kingdom: University of Nottingham.

Canterucci, J. (1998). *Change Project Management SM- The Next Step Transition Management.* New York: The Falmer Press.

Center of Education Technology annual report. (2005). *Ministry of Education Report.* Retrieved from http://unesdoc.unesco.org/images/0022/002297/229719E.pdf Instruction.pdf. 3 October 2015.

Cooper, D. R., & Emory, C. W. (1995). Management research methods. *Journal of International Research*, *17*(1), 4-7.

Cooper, D. R., & Schindler, P.S., (2003).*Business Research Method*, New York: McGraw-Hill Press Publications.

Davis, T. L., Hart, J. A., Russell, J. F., & Sears, J. W. (1989). *Information consolidation within a transaction network.* New York: Springer Publisher.

Dick, W. C., & Carey, L. (2001). *The systematic design of instruction*. Upper Saddle River, NJ: Pearson Education.

Embi, M. A. (2011). *E-learning in Malaysia institutions of higher learning: status, trends and Challenges.* Learning Conference (ICCL). Proceeding, eprint.OUM.

Frye, N. (2002). Gender-based factors in computing enrolments and achievement: Evidence from a study of tertiary students. *Journal of Educational Computing Research*, *5*(4), 409-429.

Gene, C., & Weibelzahl, S. (2007). Usability engineering for the adaptive web. *Journal Adaptive Web*, 742-745.

Hair, J. F. Jr., Black, W. C., Babin, B. J., Anderson R. E., & Tatham, R. L. (2006). *Multivariate Data Analysis,* Upper Saddle River, NJ, Pearson Education International.

Hamat, A., Embi, M. A., & Sulaiman, A. H., (2011). Learning Management Systems in Malaysian Higher Education Institutions. *e-Learning in Malaysian Higher Education Institutions* (30-50). Putrajaya: Jabatan Pengajian Tinggi, Kementerian Pengajian Tinggi publication.

Hambling, M. (2010). Expanding a teacher's knowledge base: A cognitive discomfort in using computers at elementary grade teaching. *Annual Meeting of the National Education, 27*(1), 61-72.

Jaworski, A., & Coupland, N. (2014). *The discourse reader. London:* Routledge Publication.

Jung, I., Wong, T. M., Li, C., Baigaltugs, S., & Belawati, T. (2011). Quality assurance in Asian distance education: Diverse approaches and common culture. *The International Review of Research in Open and Distributed Learning, 12*(6), 63-83.

Krejcie, R.W., & Morgan, D.W. (1970). *Determining sample size for research activities*. ERIC.

Maznah R., & Harland, T. (2012). *The scholarship of teaching and learning: Challenges for Malaysian academic*. Oxford: Taylor & Francis Publication.

Ministry of Education. (2010). *Ministry of Higher Education. Annual Report* Retrieved on 4 November 2015 from http://moe.my/987654321/666/1/Faculty%20Best%20Practices%20Using%20Blended%20Learning%20in%20E-learning%20and%20Face-to Face%20Instruction.pdf.

Ministry of Education. (2011). *Ministry of Higher Education. Annual Report.* Retrieved on 4 November 2015 from http://moe.my /987654321/666/1/Faculty%20Best%20Practices%20Using%20Blended%20Learning%20in%20E-learning%20and%20Face-to-Face%20Instruction.pdf.

Ministry of Education. (2012). *Ministry of Higher Education. Annual Report.* Retrieved on 17 February 2015 from http://moe.my/ 9179373/9qe9/ F%139792/.

Ministry of Education. (2014). *Ministry of Higher Education. Annual Report. Ministry of Higher Education.Annual Report.* Retrieved on 17 February 2015 from http://moe.my/ 9179373/9qe9/ F%139792/.

Ministry of Education. (2007). *National Higher Education Master Plan (2007-2010)*. Retrieved on 3 February 2015 from http://mohe.my/75746352pdf./64bewbb/8ysdfaanfkka%./undxjj.%/pdf.

Ministry of Education Statistic. (2013). Retrieved on 13 June 2015 from https://www.mohe.gov.org/..2r425523/pdf/ergfsge643t/vnjsnvl%20%pdf.

Ministry of Higher Education Report (2012). *National higher education in Malaysia: Balancing benefits and concerns through regulations.* Putrajaya: MOHE annual report publication.

Molly L. (2005). *Restructuring private higher education in Malaysia, Journal of In-service Education, 30*(1)*,* 115-139.

MS Academia, annual report. (2013). *Statistic of Academic Scholars.* Retrieved on 16 March 2015 from *https://www.excemed.org/.../ms-academia-multiple- sclerosis-advanced-c...MS Academic Publication/*.

MS Academia, annual report. (2014). *Statistic of Academic Scholars.* MS Academic Publication.

Narver, J. C., Slater, S. F., Jaworski, B. J., & Kohli, A. K. (1993). Market orientation and the learning Organization. *The Journal of Marketing*, *43*(1), 7-9.

Nunnally, J. L. (1979). Examination of the factor structure of the Ways of Coping Questionnaire with Populations. *Journal of International Research*, *7*(1), 24-27.

Nunnally, J. L., & Bernstein, I. H. (1994).*Psychometric Theory*, New York: McGraw-Hill Publications.

Ravet, S., & Layte, M. (2008). A model of professional development to support technology Integration. *Association for the Advancement of Computing in Education Journal*, *13*(3)*,* 251- 272.

Ridzuan, F. (2010).Thrust into technology: How veteran teachers respond. *Journal of Educational Technology Systems, 30*(1)*,* 85-111.

Seale, K. J. (2014*). E-learning and Disability in Higher Education: Accessibility Research and Practice.* London: Routledge.

Sims, R. (2008). Rethinking (e) learning: A manifesto for connected generations. *Journal of Distance Education*, *29*(2)*,* 153-164.

Van Vught, F. (2008). Mission diversity and reputation in higher education. *Higher Education Policy,21*(2)*,* 151-174.

Victoria, B. O. (2009). The Sixth International Conference on adult education. *Comparative Economics, Rapporteur General report*, (Vol. 22) (45-48). Nigeria: Belium Publication.

Zakaria, E., & Iksan, Z. H., (2007). Promoting cooperative learning in science and mathematics education: A Malaysian perspective. *Journal of Lifelong Learning*, *45,* 62-65.

REFEREES FOR THE PERTANIKA
JOURNAL OF SCIENCE AND TECHNOLOGY

VOL. 24(2) JUL. 2016

The Editorial Board of the Journal of Science and Technology wishes to thank the following for acting as referees for manuscripts published in this issue of JST.

Abdul Rahman Mohd Sam
(UTM, Malaysia)

Amimul Ahsan
(UPM, Malaysia)

Amu Therwath
(University of Paris, France)

Azizah Baharum @ Abdul Aziz
(UTM, Malaysia)

Biswa Mohan Biswal
(KPJ Ipoh Specialist Hospital, Malaysia)

Clemente Michael Wong Vui Ling
(UMS, Malaysia)

Engku Muhammad Nazri Engku Abu Bakar
(UUM, Malaysia)

Gan Seng Neon
(UM, Malaysia)

Geok Yuan Annie Tan
(UM, Malaysia)

Gyo Miyabara
(Osaka University, Japan)

Hamid Yusoff
(UiTM, Malaysia)

Hari Srivastava
(University of Victoria, Canada)

Hasnida Ab Samat
(UPM, Malaysia)

Helmi Norman
(UKM, Malaysia)

Jagannath Korody
(Manipal Institute of Technology, India)

Jimson Mathew
(University of Bristol, UK)

Julie Juliewatty Mohamed
(UMK, Malaysia)

Kazuto Takashima
(Kyushu Institute of Technology, Japan)

Kek Sie Long
(UTHM, Malaysia)

Krishnamurthy Nayak
(Manipal Institute of Technology, India)

Lilia Halim
(UKM, Malaysia)

Mabel Tan Hwee Joo
(UCSI University, Malaysia)

Menaga Ayyappan
(SASTRA University, India)

Mohd Khalid Mohamad Nasir
(UKM, Malaysia)

Nagaraj S Nayak
(Manipal Institute of Technology, India)

Naveen Kumar
(National Institute of Technology, Kurukshetra India)

Ng Choy Peng
(UPNM, Malaysia)

Ravikrian Kadoli
(National Institute of Technology Karnataka, India)

Rizal Zahari
(UPM, Malaysia)

Rosni Abdullah
(USM, Malaysia)

Satish B Shenoy
(Manipal Institute of Technology, India)

Senathipathi Velmurugan
(Central Rice Research Institute, India)

SM Abdul Khader
(Manipal International University, Malaysia)

Srikanth Prabhu
(Manipal Institute of Technology, India)

Suman Kapur
(Birla Institute of Technology and Science, BITS-Pilani, India)

Suphakrit Sopikul
(Mahidol University, Thailand)

Suriati Ghazali
(UMP, Malaysia)

Syazwani Idrus
(UPM, Malaysia)

Vijayaretnam Panchanathan
(Perdana University Graduate School of Medicine, Malaysia)

Virender Ranga
(National Institute of Technology, Kurukshetra India)

Yosphatrachai Kanitpunyacharoen
(Uttaradit Rajabhat University, Thailand)

You Ah Heng
(MMU, Malaysia)

MMU - Multimedia University
UCSI - University College Sedaya International
UiTM - Universiti Teknologi MARA Malaysia
UKM - Universiti Kebangsaan Malaysia
UM - Universiti Malaya
UMK - Universiti Malaysia Kelantan
UMP - Universiti Malaysia Pahang
UMS - Universiti Malaysia Sabah
UPM - Universiti Putra Malaysia
UPNM - Universiti Pertahanan Nasional Malaysia
USM - Universiti Sains Malaysia
UTHM - Universiti Tun Hussein Onn Malaysia
UTM - Universiti Teknologi Malaysia
UUM - Universiti Utara Malaysia

While every effort has been made to include a complete list of referees for the period stated above, however if any name(s) have been omitted unintentionally or spelt incorrectly, please notify the Chief Executive Editor, *Pertanika* Journals at nayan@upm.my.

Any inclusion or exclusion of name(s) on this page does not commit the *Pertanika* Editorial Office, nor the UPM Press or the University to provide any liability for whatsoever reason.

Pertanika Journals

Our goal is to bring high quality research to the widest possible audience

INSTRUCTIONS TO AUTHORS

(Manuscript Preparation & Submission Guidelines)

Revised: August 2015

We aim for excellence, sustained by a responsible and professional approach to journal publishing.
We value and support our authors in the research community.

Please read the Pertanika guidelines and follow these instructions carefully. Manuscripts not adhering to the instructions will be returned for revision without review. The Chief Executive Editor reserves the right to return manuscripts that are not prepared in accordance with these guidelines.

MANUSCRIPT PREPARATION

Manuscript Types

Pertanika accepts submission of mainly **four** types of manuscripts for peer-review.

1. **Regular article**

Regular articles are full-length original empirical investigations, consisting of introduction, materials and methods, results and discussion, conclusions. Original work must provide references and an explanation on research findings that contain new and significant findings.

Size: Generally, these are expected to be between 6 and 12 journal pages (excluding the abstract, references, tables and/or figures), a maximum of 80 references, and an abstract of 100–200 words.

2. **Review article**

These report critical evaluation of materials about current research that has already been published by organizing, integrating, and evaluating previously published materials. It summarizes the status of knowledge and outline future directions of research within the journal scope. Review articles should aim to provide systemic overviews, evaluations and interpretations of research in a given field. Re-analyses as meta-analysis and systemic reviews are encouraged. The manuscript title must start with "Review Article:".

Size: These articles do not have an expected page limit or maximum number of references, should include appropriate figures and/or tables, and an abstract of 100–200 words. Ideally, a review article should be of 7 to 8 printed pages.

3. **Short communications**

They are timely, peer-reviewed and brief. These are suitable for the publication of significant technical advances and may be used to:

(a) report new developments, significant advances and novel aspects of experimental and theoretical methods and techniques which are relevant for scientific investigations within the journal scope;

(b) report/discuss on significant matters of policy and perspective related to the science of the journal, including 'personal' commentary;

(c) disseminate information and data on topical events of significant scientific and/or social interest within the scope of the journal.

The manuscript title must start with "*Brief Communication*:".

Size: These are usually between 2 and 4 journal pages and have a maximum of three figures and/or tables, from 8 to 20 references, and an abstract length not exceeding 100 words. Information must be in short but complete form and it is not intended to publish preliminary results or to be a reduced version of Regular or Rapid Papers.

4. **Others**

Brief reports, case studies, comments, concept papers, Letters to the Editor, and replies on previously published articles may be considered.

PLEASE NOTE: NO EXCEPTIONS WILL BE MADE FOR PAGE LENGTH.

Language Accuracy

Pertanika **emphasizes** on the linguistic accuracy of every manuscript published. Articles must be in **English** and they must be competently written and argued in clear and concise grammatical English. Contributors are strongly advised to have the manuscript checked by a colleague with ample experience in writing English manuscripts or a competent English language editor.

Author(s) **must provide a certificate** confirming that their manuscripts have been adequately edited. A proof from a recognised editing service should be submitted together with the cover letter at the time of submitting a manuscript to Pertanika**. All editing costs must be borne by the author(s)**. This step, taken by authors before submission, will greatly facilitate reviewing, and thus publication if the content is acceptable.

Linguistically hopeless manuscripts will be rejected straightaway (e.g., when the language is so poor that one cannot be sure of what the authors really mean). This process, taken by authors before submission, will greatly facilitate reviewing, and thus publication if the content is acceptable.

MANUSCRIPT FORMAT

The paper should be submitted in one column format with at least 4cm margins and 1.5 line spacing throughout. Authors are advised to use Times New Roman 12-point font and *MS Word* format.

1. Manuscript Structure

Manuscripts in general should be organised in the following order:

Page 1: *Running title*

This page should **only** contain the running title of your paper. The running title is an abbreviated title used as the running head on every page of the manuscript. The running title should not exceed 60 characters, counting letters and spaces.

Page 2: *Author(s) and Corresponding author information.*

This page should contain the **full title** of your paper not exceeding 25 words, with name(s) of all the authors, institutions and corresponding author's name, institution and full address (Street address, telephone number (including extension), hand phone number, and e-mail address) for editorial correspondence. First and corresponding authors must be clearly indicated.

The names of the authors may be abbreviated following the international naming convention. e.g. Salleh, A.B.[1], Tan, S.G[2*]., and Sapuan, S.M[3].

Authors' addresses. Multiple authors with different addresses must indicate their respective addresses separately by superscript numbers:

George Swan[1] and Nayan Kanwal[2]
[1]Department of Biology, Faculty of Science, Duke University, Durham, North Carolina, USA.,
[2]Office of the Deputy Vice Chancellor (R&I), Universiti Putra Malaysia, Serdang, Malaysia.

A **list** of number of **black and white / colour figures and tables** should also be indicated on this page**.** Figures submitted in color will be printed in colour. See *"5. Figures & Photographs"* for details.

Page 3: *Abstract*

This page should **repeat** the **full title** of your paper with only the **Abstract** (the abstract should be less than 250 words for a Regular Paper and up to 100 words for a Short Communication), and **Keywords**.

Keywords: Not more than eight keywords in alphabetical order must be provided to describe the contents of the manuscript.

Page 4: *Introduction*
This page should begin with the **Introduction** of your article and followed by the rest of your paper.

2. *Text*

Regular Papers should be prepared with the headings *Introduction, Materials and Methods, Results and Discussion*, *Conclusions, Acknowledgements, References, and Supplementary data* (if avavailble) in this order.

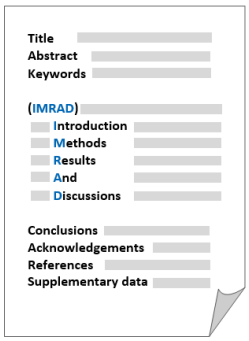

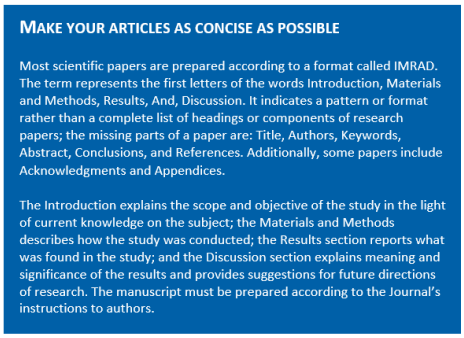

3. *Equations and Formulae*

These must be set up clearly and should be typed double spaced. Numbers identifying equations should be in square brackets and placed on the right margin of the text.

4. *Tables*

All tables should be prepared in a form consistent with recent issues of Pertanika and should be numbered consecutively with Roman numerals. Explanatory material should be given in the table legends and footnotes. Each table should be prepared on a new page, embedded in the manuscript.

When a manuscript is submitted for publication, tables must also be submitted separately as data - .doc, .rtf, Excel or PowerPoint files- because tables submitted as image data cannot be edited for publication and are usually in low-resolution.

5. *Figures & Photographs*

Submit an **original** figure or photograph. Line drawings must be clear, with high black and white contrast. Each figure or photograph should be prepared on a new page, embedded in the manuscript for reviewing to keep the file of the manuscript under 5 MB. These should be numbered consecutively with Roman numerals.

Figures or photographs must also be submitted separately as TIFF, JPEG, or Excel files- because figures or photographs submitted in low-resolution embedded in the manuscript cannot be accepted for publication. For electronic figures, create your figures using applications that are capable of preparing high resolution TIFF files. In general, we require **300 dpi** or higher resolution for **coloured and half-tone artwork**, and **1200 dpi or higher** for **line drawings** are required.

Failure to comply with these specifications will require new figures and delay in publication. **NOTE**: Illustrations may be produced in colour at no extra cost at the discretion of the Publisher; the author could be charged Malaysian Ringgit 50 for each colour page.

6. *References*

References begin on their own page and are listed in alphabetical order by the first author's last name. Only references cited within the text should be included. All references should be in 12-point font and double-spaced.

NOTE: When formatting your references, please follow the **APA reference style** (6th Edition). Ensure that the references are strictly in the journal's prescribed style, failing which your article will **not be accepted for peer-review**. You may refer to the *Publication Manual of the American Psychological Association* for further details (http://www.apastyle.org/).

7. *General Guidelines*

Abbreviations: Define alphabetically, other than abbreviations that can be used without definition. Words or phrases that are abbreviated in the introduction and following text should be written out in full the first time that they appear in the text, with each abbreviated form in parenthesis. Include the common name or scientific name, or both, of animal and plant materials.

Acknowledgements: Individuals and entities that have provided essential support such as research grants and fellowships and other sources of funding should be acknowledged. Contributions that do not involve researching (clerical assistance or personal acknowledgements) should **not** appear in acknowledgements.

Authors' Affiliation: The primary affiliation for each author should be the institution where the majority of their work was done. If an author has subsequently moved to another institution, the current address may also be stated in the footer.

Co-Authors: The commonly accepted guideline for authorship is that one must have substantially contributed to the development of the paper and share accountability for the results. Researchers should decide who will be an author and what order they will be listed depending upon their order of importance to the study. Other contributions should be cited in the manuscript's Acknowledgements.

Copyright Permissions: Authors should seek necessary permissions for quotations, artwork, boxes or tables taken from other publications or from other freely available sources on the Internet before submission to Pertanika. Acknowledgement must be given to the original source in the illustration legend, in a table footnote, or at the end of the quotation.

Footnotes: Current addresses of authors if different from heading may be inserted here.

Page Numbering: Every page of the manuscript, including the title page, references, tables, etc. should be numbered.

Spelling: The journal uses American or British spelling and authors may follow the latest edition of the Oxford Advanced Learner's Dictionary for British spellings.

SUBMISSION OF MANUSCRIPTS

Owing to the volume of manuscripts we receive, we must insist that all submissions be made electronically using the **online submission system ScholarOne™**, a web-based portal by Thomson Reuters. For more information, go to our web page and click "**Online Submission**".

Submission Checklist

1. **MANUSCRIPT**: Ensure your MS has followed the Pertanika style particularly the first four pages as explained earlier. The article should be written in a good academic style and provide an accurate and succinct description of the contents ensuring that grammar and spelling errors have been corrected before submission. It should also not exceed the suggested length.

2. **COVER LETTER**: All submissions must be accompanied by a cover letter detailing what you are submitting. Papers are accepted for publication in the journal on the understanding that the article is **original** and the content has **not been published** or **submitted for publication elsewhere**. This must be stated in the cover letter. Submission of your manuscript will not be

accepted until a signed cover letter *(original pen-to-paper signature)* has been received. The cover letter must also contain an acknowledgement that all authors have contributed significantly, and that all authors are in agreement with the content of the manuscript. The cover letter of the paper should contain (i) the title; (ii) the full names of the authors; (iii) the addresses of the institutions at which the work was carried out together with (iv) the full postal and email address, plus telephone numbers and emails of all the authors. The current address of any author, if different from that where the work was carried out, should be supplied in a footnote.

3. **COPYRIGHT**: Authors publishing the Journal will be asked to sign a copyright form. In signing the form, it is assumed that authors have obtained permission to use any copyrighted or previously published material. All authors must read and agree to the conditions outlined in the form, and must sign the form or agree that the corresponding author can sign on their behalf. Articles cannot be published until a signed form *(original pen-to-paper signature)* has been received.

Please do **not** submit manuscripts to the editor-in-chief or to any other office directly. Any queries must be directed to the **Chief Executive Editor's** office via email to nayan@upm.my.

Visit our Journal's website for more details at http://www.pertanika.upm.edu.my/home.php.

HARDCOPIES OF THE JOURNALS AND OFF PRINTS

Under the Journal's open access initiative, authors can choose to download free material (via PDF link) from any of the journal issues from Pertanika's website. Under "**Browse Journals**" you will see a link, "*Current Issues*" or "*Archives*". Here you will get access to all current and back-issues from 1978 onwards.

The **corresponding author** for all articles will receive one complimentary hardcopy of the journal in which his/her articles is published. In addition, 20 off prints of the full text of their article will also be provided. Additional copies of the journals may be purchased by writing to the Chief Executive Editor.

Why should you publish in *Pertanika*?

BENEFITS TO AUTHORS

PROFILE: Our journals are circulated in large numbers all over Malaysia, and beyond in Southeast Asia. Our circulation covers other overseas countries as well. We ensure that your work reaches the widest possible audience in print and online, through our wide publicity campaigns held frequently, and through our constantly developing electronic initiatives such as Web of Science Author Connect backed by Thomson Reuters.

QUALITY: Our journals' reputation for quality is unsurpassed ensuring that the originality, authority and accuracy of your work are fully recognised. Each manuscript submitted to Pertanika undergoes a rigid originality check. Our double-blind peer refereeing procedures are fair and open, and we aim to help authors develop and improve their scientific work. Pertanika is now over 38 years old; this accumulated knowledge has resulted in our journals being indexed in SCOPUS (Elsevier), **Thomson (ISI) Web of Science™ Core Collection, Emerging Sources Citation Index (ESCI)**, Web of Knowledge [BIOSIS & CAB Abstracts], EBSCO, DOAJ, ERA, AGRICOLA, Google Scholar, ISC, TIB, Journal Guide, Citefactor, Cabell's Directories and MyCite.

AUTHOR SERVICES: We provide a rapid response service to all our authors, with dedicated support staff for each journal, and a point of contact throughout the refereeing and production processes. Our aim is to ensure that the production process is as smooth as possible, is borne out by the high number of authors who prefer to publish with us.

CODE OF ETHICS: Our Journal has adopted a Code of Ethics to ensure that its commitment to integrity is recognized and adhered to by contributors, editors and reviewers. It warns against plagiarism and self-plagiarism, and provides guidelines on authorship, copyright and submission, among others.

PRESS RELEASES: Landmark academic papers that are published in Pertanika journals are converted into press-releases as a unique strategy for increasing visibility of the journal as well as to make major findings accessible to non-specialist readers. These press releases are then featured in the university's UK and Australian based research portal, ResearchSEA, for the perusal of journalists all over the world.

LAG TIME: The elapsed time from submission to publication for the articles averages 3 to 4 months. A decision on acceptance of a manuscript is reached in 3 to 4 months (average 14 weeks).

PERTANIKA JOURNALS

Address your submissions to:
The Chief Executive Editor
Tel: +603 8947 1622
nayan@upm.my

Journal's Profile: www.pertanika.upm.edu.my/

Call for Papers 2017-18

now accepting submissions...

Pertanika invites you to explore frontiers from all key areas of agriculture, science and technology to social sciences and humanities.

Original research and review articles are invited from scholars, scientists, professors, post-docs, and university students who are seeking publishing opportunities for their research papers through the Journal's three titles; JTAS, JST & JSSH. Preference is given to the work on leading and innovative research approaches.

Pertanika is a fast track peer-reviewed and open-access academic journal published by Universiti Putra Malaysia. To date, Pertanika Journals have been indexed by many important databases. Authors may contribute their scientific work by publishing in UPM's hallmark SCOPUS & ISI indexed journals.

Our journals are open access - international journals. Researchers worldwide will have full access to all the articles published online and be able to download them with zero subscription fee.

Pertanika uses online article submission, review and tracking system for quality and quick review processing backed by Thomson Reuter's ScholarOne™. Journals provide rapid publication of research articles through this system.

For details on the Guide to Online Submissions, please visit http://www.pertanika.upm.edu.my/guide_online_submission.php

About the Journal

Pertanika is an international multidisciplinary peer-reviewed leading journal in Malaysia which began publication in 1978. The journal publishes in three different areas — Journal of Tropical Agricultural Science (JTAS); Journal of Science and Technology (JST); and Journal of Social Sciences and Humanities (JSSH). All journals are published in English.

JTAS is devoted to the publication of original papers that serves as a forum for practical approaches to improving quality in issues pertaining to tropical agricultural research- or related fields of study. It is published four times a year in *February, May, August* and *November.*

JST caters for science and engineering research- or related fields of study. It is published twice a year in *January* and *July.*

JSSH deals in research or theories in social sciences and humanities research. It aims to develop as a flagship journal with a focus on emerging issues pertaining to the social and behavioural sciences as well as the humanities, particularly in the Asia Pacific region. It is published four times a year in *March, June, September* and *December.*

An **Award-winning** International-Malaysian Journal **— CREAM AWARD**, MoHE –Sept 2015

Case Studies

Selected Papers from the International Conference on Computational Methods in Engineering and Health Sciences 2015 (ICCMEH 2015)

Selected Papers from the International Conference on Innovations, Shifts and Challenges (ICISC 2015)

Pertanika Journal of Science & Technology
Vol. 24 (2) Jul. 2016

Contents

Pertanika Editorial Office, Journal Division
Office of the Deputy Vice Chancellor (R&I),
1st Floor, IDEA Tower II,
UPM-MTDC Technology Centre
Universiti Putra Malaysia
43400 UPM Serdang
Selangor Darul Ehsan
Malaysia

http://www.pertanika.upm.edu.my/
E-mail: executive_editor.pertanika@upm.my
Tel: +603 8947 1622/1620

PENERBIT UPM PRESS
UNIVERSITI PUTRA MALAYSIA
BERILMU BERBAKTI

http://penerbit.upm.edu.my
E-mail : penerbit@putra.upm.edu.my
Tel : +603 8946 8855/8854
Fax : +603 8941 6172

ISSN 0128-7680
07 >
9 770128 768083